Leibniz-Institut
für Festkörper- und
Werkstoffforschung
Dresden

Annual Report 2008

Contents

Flashback to 2008

The Annual Report of the IFW presents a typical cross section of our scientific activities in the past year, highlighting main results in the first part and giving a somewhat more systematic overview of results obtained in our five Research Areas in its second part. It finally informs on the materialized and personalized output and activities, and on how the IFW is organized. The very first pages of the Annual Report we want to use for a flashback to the institutes life in 2008: highlights, events and important developments beyond scientific results.

In the very beginning of 2008 the cooperation agreement between the Martin Andersen Nexö High School and the IFW Dresden has been signed. The close cooperation results from the project "Teachers into Research" initiated by the IFW and supported by the Saxon Ministry of Cultural Affairs. Within this project physics teachers are released for one year from teaching to work scientifically in a research team at the IFW Dresden. After the first teacher who took part in this program in 2006/2007 returned to Martin Andersen Nexö High School the relation between the IFW and the high school continued and developed into a close partnership manifested now in a cooperation agreement. The IFW supports the high school students in their first steps to scientific work and organizes lab-tours for physics and chemistry school classes.

The IFW Winter School takes place every year in January to foster the scientific communication among IFW groups and to train young scientists in special topics of IFW's Research Program. In 2008 the topical focus was put on magnetism, the largest research area in the IFW's Research Program. The program of the four-day event included tutorial lectures of experts and short contributions of senior and junior scientists as well as some time for skiing and social gathering. All participants agreed that the IFW Winter School is a very useful event to strengthen the internal cooperation and to train the skills of senior and junior scientists.

On March 3, 2008, the IFW invited its partners, friends and sponsors to the Annual Reception. On this occasion Dr. Rudolf Schäfer was awarded the IFW Research Prize for his excellent and internationally renowned work on magnetic microstructures. The Deutsche Bank Junior Award was given to Dr. Karin Leistner for her outstanding PhD thesis on hard-magnetic Iron-Platinum films. A further highlight of this evening was the talk of Dorothee Dzwonnek, General Secretary of the German Research Foundation (DFG), on the excellence in research funding – a topic which refers to the current discussion in German research politics and which was discussed quite vividly.

Signing of the Cooperation Agreement between the IFW and the Nexö High School in presence of the State Minister Steffen Flath (right).

Lab-tour with the speakers of the Annual Reception: in the foreground State Secretary Neverman, in the middle Dorothee Dzwonnek.

Group picture of VIP during the official ceremony to mark the change of office of the Scientific Director.

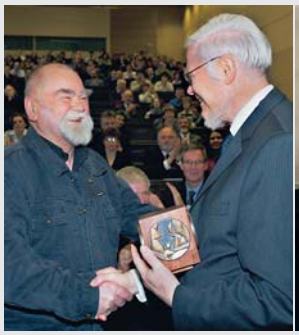


An important event for the IFW in 2008 was the change of the Scientific Director. On April 1, 2008, Prof. Dr. Ludwig Schultz took over the directorship from Prof. Dr. Helmut Eschrig who has been in responsibility for the scientific work of the IFW Dresden during the last 10 years. On the occasion of the official ceremony on April 4 the Saxon Minister of Science and Arts, Dr. Eva-Maria Stange, the Leibniz President Prof. Ernst Th. Rietschel and the Rector of the Dresden University of Technology Prof. Hermann Kokenge appreciated the merits of Helmut Eschrig and congratulated Ludwig Schultz on taking office. The ceremony was accompanied by music of the IFW's chorus and of the IFW's brass band "nanonics". This was a nice opportunity to demonstrate the range of the institute's life in the IFW which reaches far beyond scientific communication.

The IFW as a Leibniz Institute is institutionally funded by the federal government and by the German Länder in equal shares. The justification of this funding has to be affirmed for each institute in intervals of about seven years by an Evaluation Group under a particular Senate Commission of the Leibniz Association. The prerequisite of confirmed funding is high-quality scientific work which meets the demands of the society of the whole country. IFW was visited by the Evaluation Group in April 2007. On 9 July 2008 the Leibniz Senate came to the final statement attesting the IFW a very good, often excellent scientific work, an effective combination of experiment and theory, a very convincing publication output, an excellent networking in the scientific community, a high training performance for young researchers and in the non-academic area and a very good fund raising. The statement of the Leibniz Senate includes eight suggestions and recommendations one of them being the strengthening of chemistry in the IFW.

The IFW participates as a starting member in the science network Sigma 5 (School of Solid State Sciences Saxony) which has a focus on chemistry, especially on materials synthesis and characterization techniques. This recent initiative coordinates and develops a number of matured bilateral cooperations so that the organization does not require supplementary legal constructions or additional administration. The academic school envelops academic teaching activities from undergraduate Bachelor studies up to final postdoctoral lecture qualifications. Thus, the regional cluster goes well beyond a typical graduate school. The aim of high quality and efficiency is tackled by integrating the widespread competences in research and education of all partner institutions. International Summer Schools on selected topics intensify the exchange of scientific expertise within Europe and combine the deepening of professional competence with the acquisition of desirable soft skills. To date, the cluster comprises a total of fourteen participants from the Technical Universities of Dresden and Freiberg as well as from the Leibniz, Fraunhofer and Max Planck Societies.

The present for the parting Scientific Director, Helmut Eschrig, was handed over by the artist Peter Makolies.

Prof. Dr. Ludwig Schultz (left) took over the directorship from Prof. Dr. Helmut Eschrig.

PhD seminar on project management and presentation

Women high school students try the work in a chemical lab during the Autumn School "Theoria cum praxi"

The number of PhD students working at the Institute is about 100 on average. Some of them spend guest stays or fellowships at the IFW and do their examinations at other places. Also the number of diploma and master students doing their theses at the IFW has been increased significantly during the last years resulting in the record number of 23 diploma theses in 2008. The training of students and young scientists is a very important concern of IFW's work. PhD and diploma students are involved in nearly all scientific projects and in the resulting publications. In regular internal PhD seminars and multi-day workshops they not only deepen the knowledge in their special fields but also acquire presentation and management skills. In the result five PhD students won best presentation awards at international conferences in 2008. However the promotion of young people starts not just as students but already in primary and secondary schools. The IFW is quite active in bringing science to school and in making kids excited of things like magnetism and superconductivity. As in the years before the IFW offered ambitious programs for the Girls' Day in April 2008 and for the Summer University in July and August 2008. 13 girls aged 12 to 18 used the excellent opportunity to gain insight into our electronic lab and the working life of a research institute. The experimental lectures of Prof. Schultz enriched events like the Kids' Academy in Görlitz and project days at high schools. In October 2008 the IFW launched a new project to encourage female high-school graduates to decide for a career in natural or engineering sciences – the Autumn Course "Theoria cum praxi" which is supported by the Saxon Ministry of Science and Arts for three years. 36 girls spent 4 days in the institute listening lectures, working in the laboratories and workshops and proving students' working day. Already traditionally, the IFW played also in 2008 an active role in some outstanding public events like Dresden Long Night of Sciences, Highlights of Physics in Halle, ThyssenKrupp Ideas' Park in Stuttgart and the Festival of Sciences in Genoa, Italy. The IFW regularly participates in public events of the TU Dresden like Students' Day and Physics at Saturday. Furthermore the IFW offers guided lab-tours for groups and school classes of which ample use is made.

The IFW is engaged in getting scientific conferences to Dresden and in organizing them. In 2008 IFW scientists were responsible for eight conferences, among them the International Conference on Rapidly Quenched and Metastable Materials (RQ13) and the International Workshops on Physics and Chemistry of FeAs-based Superconductors. 300 material scientists from all over the world came to Dresden in August 2008 for the RQ13 to present and discuss the latest results on metastable materials, quasicrystals, nanometer scale materials and bulk metallic glasses. The "International Workshops on Physics and Chemistry of FeAs-based Superconductors" was organized within a short term in October 2008 in reaction to the tremendous interest raised world-wide in the physics and chemistry of the new family of Fe-based compounds which exhibit superconducting transition temperatures above 50 K. A full list of conferences organized by the IFW in 2008 is given on page 111.

Participants of the Final European Workshop "Strengthening the role of women scientists in Nano-Science"

Autumn School "Theoria cum praxi" for women high school students

Full house and full courtyard in the IFW during the Dresden Long Night of Sciences 2008

Presentation of the superconducting train on the Science Festival in Genoa, Italy




All these conferences demonstrate that Dresden has developed to an attractive place for the scientific community. The IFW as one of the key players in this regional network of university and non-university research institutes takes much effort to improve further the collaboration between Dresden institutes to have a good starting position for the next call in the German excellence initiative.

Large efforts are being made by the IFW to acquire project funding. After some decrease in 2005 and 2006 caused by changes in positions of directors the level of third party funding has raised since 2007. For 2008 it achieves more than 10 Mio. Euro. A large amount of funding was acquired in competitive mode from the DFG and the EU. In particular the grant of a new Emmy Noether Research Group by the DFG for four years was a nice success. The IFW is very successful in initiating EU projects and participating in them. Four of the 26 EU-projects running in 2008 were coordinated by the IFW. Within the Saxon Excellence Initiative the IFW participates in 2 of the 5 programs granted from 2009 on, namely in the European Centre for Emerging Materials and Processes Dresden (ECEMP) and in the program "Functional structure design of new high performance materials".

2008 was again a yielding year with respect to prizes and honors awarded to members of the IFW. A complete list of prizes awarded to members of the IFW is included at the end of this Report. The most prestigious of the prizes won in 2008 by IFW members is the Gottfried-Wilhelm-Leibniz-Prize of the German Research Foundation, which has been awarded to Prof. Dr. Jürgen Eckert. Along with the great prestige of winning, Prof. Eckert is awarded a significant amount of prize money which can be used flexibly for the own research.

So we are looking back to a successful year 2008 in the Institute's development. We are quite aware that this is due to the sustainable network of colleagues and partners in universities, research institutes and industry, both on the regional and the international scale. We thank all of them for constructive cooperation and are looking forward to taking up future challenges together. Special tribute is paid to the members of the Scientific Advisory Board and of the Board of Trustees as well as the funding organizations that continuously support and foster the positive development of the IFW.

Dresden, January 2009

Prof. Ludwig Schultz
Scientific Director

Dipl.-Finw. Rolf Pfrengle
Administrative Director

Presentation of the Research Prizes of IFW Institutes during the first colloquium of the winter term

The Megalloys Team of the IFW was successful in the FutureSax contest and won the 1. Prize in the category technology.

IFW teams took part in various sports competitions, e.g. Dresden Marathon and Dresden Soccer Contest both benefiting from the team spirit and strengthening it.

IFW Summer Day – one example for improving the balance of work and family. In the afternoon all participants met in the courtyard to enjoy several games and a concert together with their families.

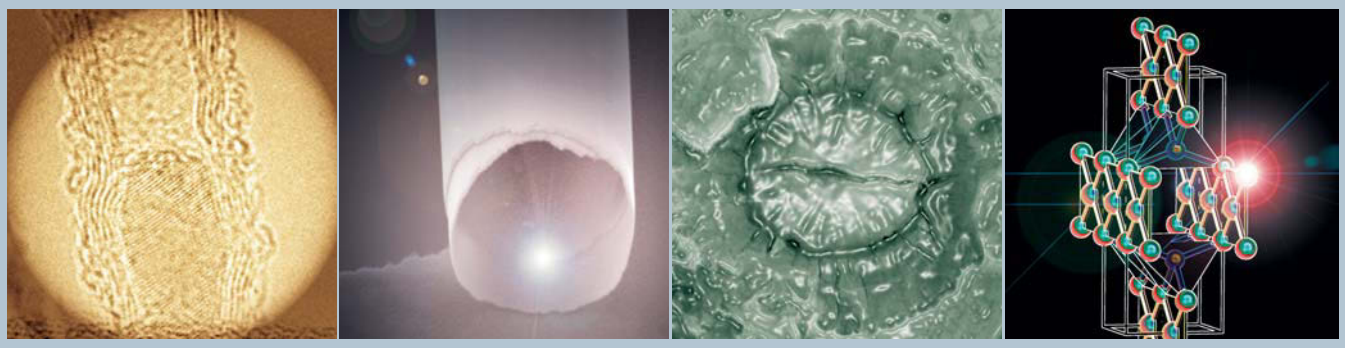

Highlights 2008

Root of a Carbon nanotube on the substrate with elongated catalyst particle

Rolled up AlGaAs/Cr/Pt microtube

Corrosion pit generated on a shot-peened Zr-based bulk metallic glass

Lattice structure of a typical edge-shared chain cuprate: Li_2CuO_2

Highlights

New Fe-based Superconductors

The Iron Age of High-Temperature Superconductivity

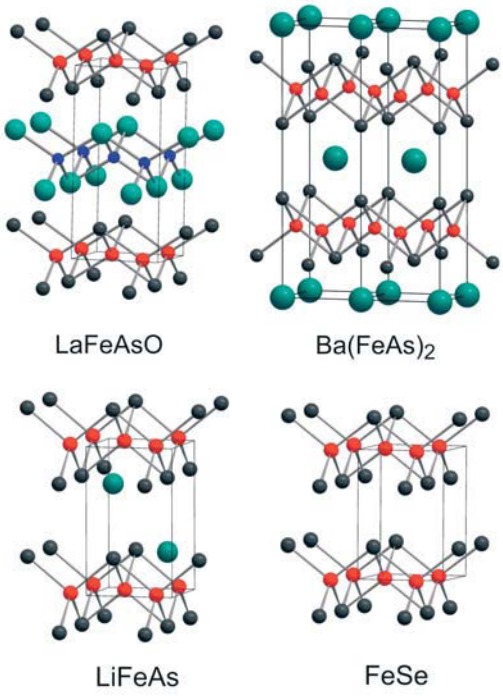

Fig.: Crystal structures of parent compounds of pnictide high temperature superconductors

In February 2008, a paper appeared showing superconductivity in a layered iron arsenide material with a transition temperature (T_c) of 26 K [1]. This discovery has triggered an enormous amount of research activities all over the world. Meanwhile there are more than 500 papers dealing with this new class of high temperature superconductors. At first glance the story looks very similar to that of the cuprates: There are non-superconducting antiferromagnetic parent compounds, as e.g. LaOFeAs, the parent compound of the so-called '1111' structure. The systems become superconducting upon doping, for example by replacing some of the oxygen in LaOFeAs by fluorine. Also the crystal structures of the new superconductors are somehow reminiscent of the cuprates, with layers of FeAs separated by spacer layers, such as LaO, where the dopants are introduced (Fig.). However, looking in more detail on the physical properties reveals pronounced differences between pnictides and cuprates. For example, the parent compounds of the pnictides are not Mott insulators but 'bad metals' with a spin density wave state [2,3]. Moreover, comparing experimental data to DFT calculations suggests that electron correlations are less important in the pnictides. On the other hand, there are good arguments, that the superconductivity in the pnictides can not be explained within the frame of a conventional electron phonon scenario.

Meanwhile there is a whole family of pnictide superconductors. The highest critical temperatures are obtained by substituting La with smaller rare earths, at present the maximum T_c amounts to about 54 K in the Sm based 1111 compound [4]. A simpler class of materials based on the $BaFe_2As_2$ parent compound (the '122' structure, Fig. right) that does not have the LaO spacer layers also superconducts with a comparable T_c [5]. More recently, superconductivity has been discovered in even simpler LiFeAs '111' and FeSe materials [6,7]. The race is therefore on, just as for the cuprates, to discover materials with increasingly higher T_c.

At the IFW, research on the pnictides superconductors started in April 2008 and meanwhile there are more than 20 papers on this topic dealing with (i) the synthesis of bulk materials and thin films, (ii) experimental studies of superconductivity and normal state using a broad spectrum of methods, as well as (iii) theoretical treatments.
Some aspects of this research are introduced in the following.

References

[1] Y. Kamihara, T. Watanabe, M. Hirano und H. Hosono, J. Am. Chem. Soc. **130**, 3296 (2008).
[2] H.-H. Klauss, H. Luetkens, R. Klingeler, C. Hess, F. J. Litterst, M. Kraken, M. M. Korshunov, I. Eremin, S.-L. Drechsler, R. Khasanov, A. Amato, J. Hamann-Borrero, N. Leps, A. Kondrat, G. Behr, J. Werner und B. Büchner, Phys. Rev. Lett. **101**, 077005 (2008).
[3] C. de la Cruz, Q. Huang, J. W. Lynn, J. Li, W. R. II, J. L. Zarestky, H. A. Mook, G. F. Chen, J. L. Luo, N. L. Wang und P. Dai, Nature **453**, 899 (2008).
[4] Z.-A. Ren, W. Lu, J. Yang, W. Yi, X.-L. Shen, Z.-C. Li, G.-C. Che, X.-L. Dong, L.-L. Sun, F. Zhou und Z.-X. Zhao, Chin. Phys. Lett. **25**, 2215 (2008).
[5] M. Rotter, M. Tegel und D. Johrendt, Phys. Rev. Lett. **101**, 107006 (2008).
[6] X. C. Wang, Q. Q. Liu, Y. X. Lv, W. B. Gao, L. X. Yang, R. C. Yu, F. Y. Li und C. Q. Jin, arXiv:0806.4688 (2008).
[7] F.-C. Hsu, J.-Y. Luo, K.-W. Yeh, T.-K. Chen, T.-W. Huang, P. M. Wu, Y.-C. Lee, Y.-L. Huang, Y.-Y. Chu, D.-C. Yan und M.-K. Wu, arXiv:0807.2369 (2008).

Electronic Phase Diagrams of FeAs superconductors

A. Kondrat, J. E. Hamann-Borrero, N. Leps, V. Kataev, A. Narduzzo, J. Werner, G. Behr, R. Klingeler, C. Hess, B. Büchner

Rapidly after the initial publication by Kamihara et al. [1], it was established that, similar as in other unconventional superconductors such as cuprate and heavy fermion compounds, superconductivity emerges from an antiferromagnetic parent state (SDW state) which is present in the non-doped materials [3,8]. In order to elucidate the properties of the parent materials as well as the evolution of the superconducting phase we have performed a detailed study of the magnetic, structural and electric transport properties of LaOFeAs upon fluorine doping through muon spin rotation (μSR), X-ray diffraction, magnetic susceptibility and resistivity measurements [2,9-13].

Fig. 1 presents our results for the undoped material. Measurements of the magnetic order parameter by means of local magnetic probes, i.e. μSR and Mössbauer spectroscopy (Fig. 1c), clearly show the development of the SDW ground state at temperatures lower than $T_{SDW} = 138$ K [2]. The magnetic moment at the Fe sites amounts to 0.3 to 0.4 μ_B which is much smaller than that of localized Fe ions in the high spin state [2,3]. The magnetic transition appears to be coupled with a tetragonal-to-orthorhombic transition which occurs at slightly higher temperature $T_S = 160$ K [3,10,11] as demonstrated by the lattice parameters in Fig. 1d. These two transitions have a strong impact on both the electrical resistivity and the bulk magnetic susceptibility, as can be seen in the top panels of Fig. 1 [2,11]. The resistivity ρ exhibits a maximum at T_S where it starts to decrease upon lowering the temperature. Interestingly, at the onset of long range antiferromagnetic SDW order the drop of the resistivity becomes weaker which is visible through an inflection point in ρ and hence a peak in dρ/dT (right ordinate of Fig. 1a). Both phase transitions are also visible in the static susceptibility $\chi = M/B$ in Fig. 1b. Concomitant with the resistivity drop, the static susceptibility drops at T_S, too, indicating the enhancement of antiferromagnetic correlations at the structural phase transition. This feature is highlighted if the magnetic specific heat is considered which is proportional to $d(\chi T)/dT$ (right ordinate of Fig. 1b). The data exhibit a clear jump in $d(\chi T)/dT$ at T_S. The magnetic specific heat also exhibits an anomaly at T_{SDW} which is similar but much weaker than the one at T_S.

Fig. 2 shows the evolution of the SDW state, i.e. of T_S and T_{SDW}, and the superconducting state of $LaO_{1-x}F_xFeAs$ as measured by XRD, magnetic susceptibility and μSR as a function of the fluorine content x. As can be seen in the figure, the SDW remains the ground state up to a doping level of about 4% fluorine content. Remarkably, the transition temperatures T_S and T_{SDW} are only weakly dopingdependent in this regime. However, the transitions are abruptly suppressed at $x \geq 0.05$ in favour of a superconducting phase with a

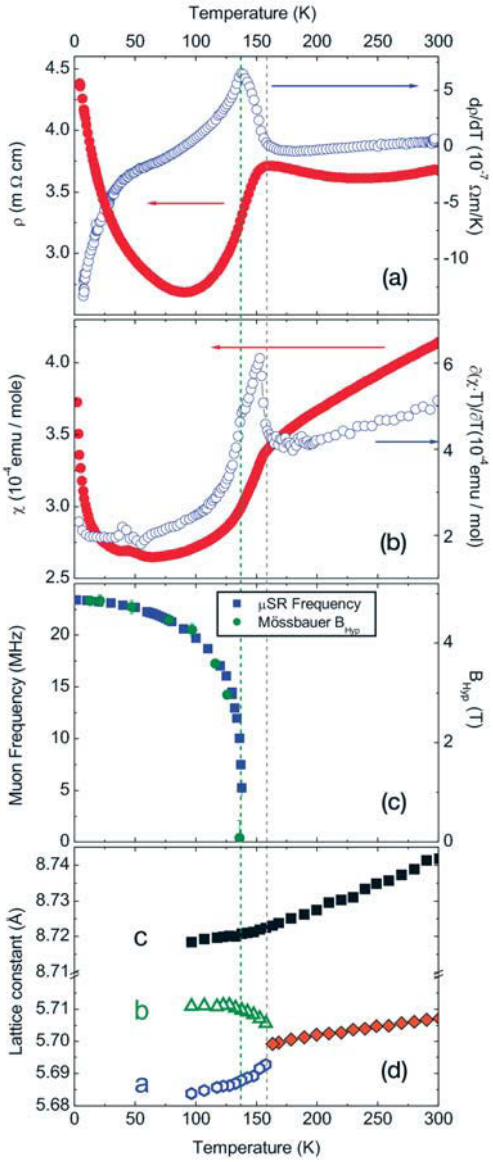

Fig. 1: The temperature dependence of ρ (a), $\chi = M/B$ (b), the muon frequency (c) and the lattice constants (d) of the undoped compound LaOFeAs. Figure (a) and (b) also show the derivative dρ/dT and the magnetic specific heat $d(\chi T)/dT$, respectively. The static susceptibility has been measured in an external magnetic field of B = 1 T. The dashed lines indicate the temperatures of the structural ($T_S \approx 160$ K) and the magnetic ($T_{SDW} \approx 138$ K) transition.

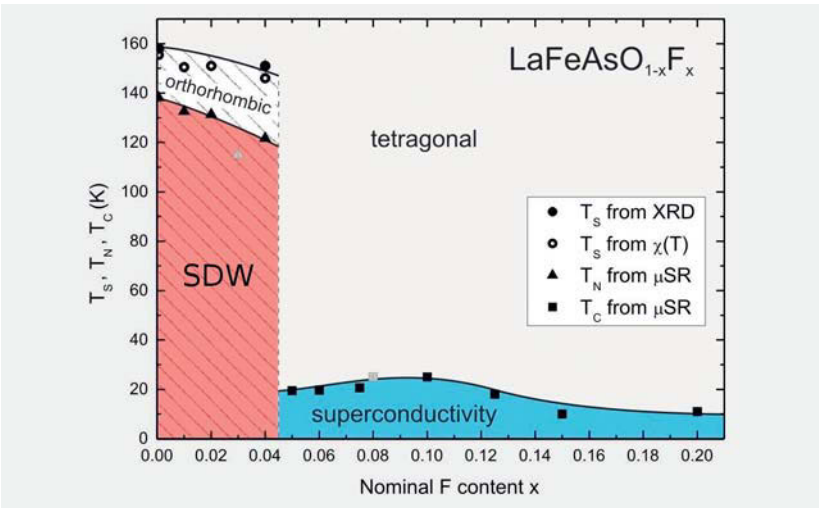

Fig. 2: The doping dependence of the magnetic and superconducting transition temperatures determined from the μSR experiments. Also shown are the tetragonal to orthorhombic structural transition temperatures T_S determined directly from XRD and from susceptibility measurements which show a kink and subsequent strong reduction below T_S. Figure taken from [10].

critical temperature $T_c > 20$ K, i.e. close to the boundary in the phase diagram where superconductivity emerges. Upon increasing the F-doping, T_c increases up to a maximum of $T_c = 26.8$ K at $x = 0.1$ which is followed by a decrease with $T_c \approx 10$ K at $x \geq 0.15$. In the superconducting regime of the phase diagram, i.e. as soon as the orthorhombic distortion and the SDW magnetism is suppressed, μSR reveals a ~100% superconducting volume fraction [9,10]. The first order-like transition between the magnetic and the superconducting ground state between $x = 0.04$ and 0.05 suggests that the key element for superconductivity in this system is the suppression of the orthorhombic distortion together with the static magnetic order rather than the moderate increase of the charge carrier density by the Fluorine doping. It is worth mentioning, that the homogeneous superconducting state which we observed in $LaO_{1-x}F_xFeAs$ appears to be an unique feature, if one compares our results with those for rare earth based isostructural compounds such as $SmO_{1-x}F_xFeAs$ [14,15] or first results on 122 compounds [16,17].

In order to obtain further information about the nature of superconductivity in these materials we have investigated the normal state electrical resistivity ρ and the magnetic susceptibility across the phase diagram.

The analysis of ρ reveals distinct anomalies in the underdoped superconducting doping regime ($0.05 \leq x < 0.1$), which appear as remnants of the anomalies that accompany the structural and magnetic phase transitions of the non-superconducting parent compound. More specifically, ρ(T) is linear at $T \geq 250$ K, but drops below the low-T extrapolation of this linearity. This drop is connected with an inflection point at ~150 K, which can be conveniently extracted from the derivatives dρ/dT [13]. These features remarkably well resemble the pseudogap signatures of underdoped cuprate superconductors [19]. Upon further increasing the F doping level, this feature vanishes, and a transition towards Fermi liquid-like behavior ($\rho \sim T^2$) is observed. This observation is a further similarity to cuprate superconductivity because the normal state of overdoped cuprates exhibits a qualitatively similar ρ(T) [19].

The major findings which can be extracted from the resistivity and its temperature derivative are summarized in the phase diagram shown in Fig. 3. In the underdoped superconducting region ($0.05 \leq x < 0.1$) the signature of the resistivity drop clearly 'survives' despite the suppression of the structural/magnetic transitions and the occurence of superconductivity. These pseudogap features strongly suggest that

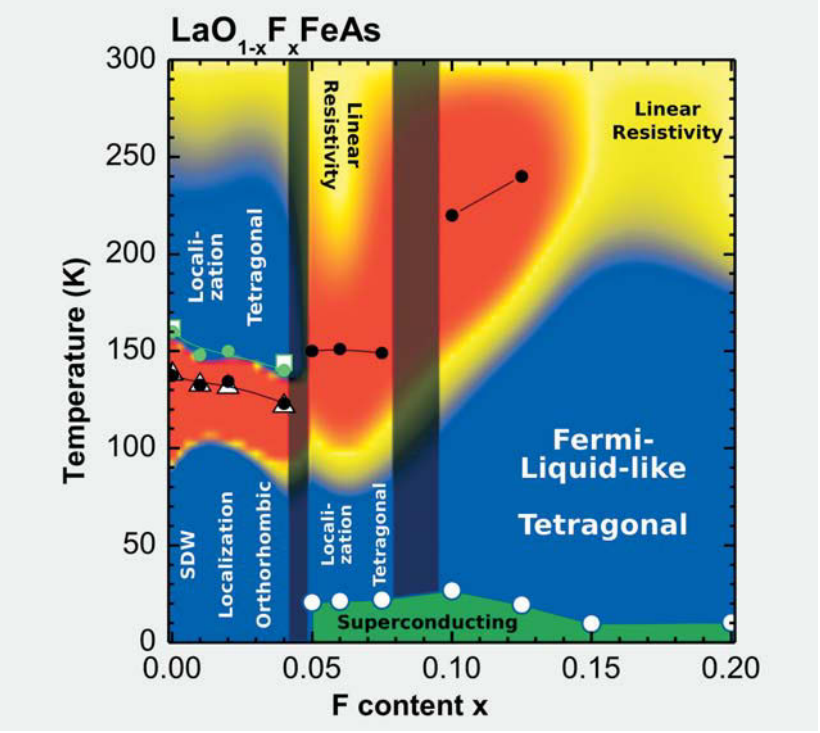

Fig. 3: Phase diagram of $LaO_{1-x}F_xFeAs$ as a function of the doping level x and temperature T, highlighting the unusual temperature dependence of ρ as compared to that of the (approximately) linear ρ(T) at room temperature. The latter gives rise to the yellow areas. The blue regions ($d\rho/dT < d\rho/dT(T=300\,K)$) indicate carrier localization/fluctuation and Fermi liquid-like behavior for $x \leq 0.075$ and $x \geq 0.1$, respectively. Across the whole phase diagram the red areas ($d\rho/dT > d\rho/dT(T=300\,K)$) are centered around the inflection point and mark the signatures of the structural/magnetic transitions ($x \leq 0.04$) and the corresponding remnant feature ($x \geq 0.05$). The dark bars separate the non-superconducting, the underdoped and the overdoped superconducting doping regimes. Apart from data points for the maximum ρ (green bullets), the inflection point (black bullets) the diagram shows also data points for T_c, (open circles), and T_{SDW} (open triangles) and T_S (open squares) from μSR and XRD. Figure taken from [13].

fluctuations connected to the SDW are still present. They apparently lead to a renormalization of the charge carriers, thus playing a major role in the physics of the superconductivity in the system. Intriguingly, in the overdoped region ($x \geq 0.1$) the fluctuation features vanish and Fermi liquid-like behavior becomes increasingly dominating over a large T-range. At this point it is important to note that the high temperature superconductivity in the iron pnictides appears to be intimately correlated with anomalous transport properties in the normal state: The critical temperature T_c is small in the overdoped region where Fermi liquid-like behavior dominates and pseudogap features are weak. On the other hand, true high T_c -superconductivity is found only in the lower doped region of the phase diagram where the resitivity shows pronounced anomalies which are clearly related to the anomalous SDW state of the undoped parent compounds. This important finding is corroborated by resistivity studies on $SmO_{1-x}F_xFeAs$ up to a doping level $x=0.1$. In this doping regime, this material exhibits qualitatively a very similar behavior as the La-based pendant but, interestingly, the pseudogap signatures are more pronounced in $SmO_{1-x}F_xFeAs$ concomitant with a much higher critical temperature T_c [13].

There are also similarities in the normal state static susceptibility of underdoped superconducting ($0.05 \leq x < 0.1$) and SDW ($x \leq 0.04$) materials. As shown in Fig. 1b, for the parent material with $x = 0$ there is a nearly linear increase of χ for $T > T_S$ upon heating the origin of which is not yet clear. Qualitatively, however, such behaviour implies at least locally antiferromagnetic interactions [12]. As seen in Fig. 4a, the susceptibility barely changes upon doping in the SDW state below $x = 0.04$ except for the slight suppression of T_{SDW} and T_S as mentioned above. Surprisingly, neither the magnitude nor the slope of the susceptibility at room temperature strongly change for the superconductors with $0.04 \leq x < 0.1$. This is illustrated by the example of $x = 0.05$ in Fig. 4b. For the overdoped material with $x = 0.125$ (Fig. 4c) there is possibly a slight increase of the slope $d\chi/dT$ at 300 K but again the general features and in particular the increase of χ upon heating is still visible. This normal state susceptibility hence implies possibly local antiferromagnetic interactions in the superconducting regime which might be relevant to the appearance of superconductivity [15].

Based on the qualitative similarities of the physical properties between the La- and Sm-based systems we proposed a generic electronic phase diagram for these new high temperature superconductors which is shown in Fig. 5. It possesses a striking resemblance to the generic phase diagram of cuprate superconductors and that of other unconventional superconductors in the vicinity of a quantum critical point. However, unlike the latter examples, the doping-driven transition from the non-superconducting magnetic ground state to superconductivity appears to be first order-like and/or accompanied by inhomogeneity [16-18].

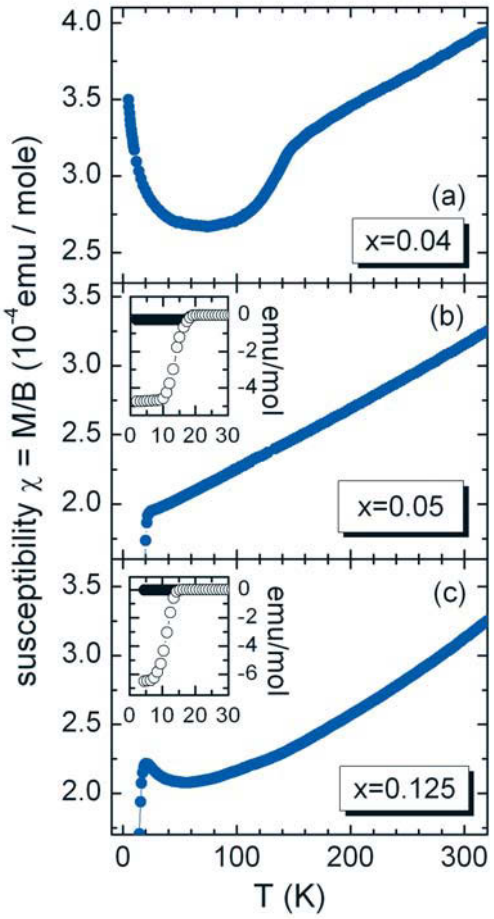

Fig. 4: Static susceptibility $\chi = M/B$ of $LaO_{1-x}F_xFeAs$ with $x = 0.04$, 0.05, and 0.125 measured in an external magnetic field $B = 1T$. For the latter samples, the insets show M/B at $B = 2$ mT in the temperature region of the superconducting transition.

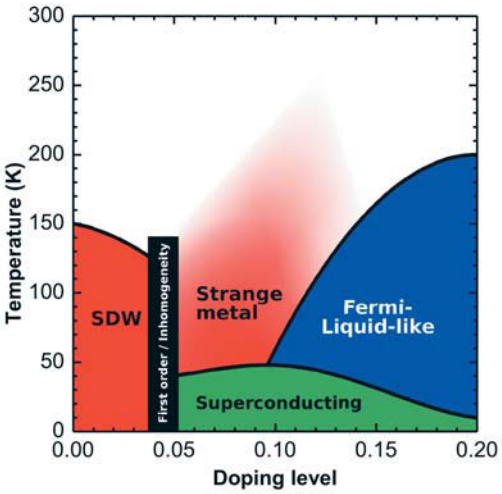

Fig. 5: Schematic phase diagram of FeAs superconductors. The red, green and blue regions indicate the SDW, superconducting and Fermi liquid-like regions, respectively. In the 'strange metal' region unusual temperature dependencies of $\rho(T)$ are observed. The black bar marks the doping-driven transition from the SDW state to superconductivity, which is of first order character and/or accompanied by strong inhomogeneity, i.e., the coexistence of the superconductivity and static magnetism. Figure taken from [13].

References

[1] Y. Kamihara, T. Watanabe, M. Hirano und H. Hosono, J. Am. Chem. Soc. **130**, 3296 (2008).

[2] H.-H. Klauss, H. Luetkens, R. Klingeler, C. 18, F. J. Litterst, M. Kraken, M. M. Korshunov, I. Eremin, S.-L. Drechsler, R. Khasanov, A. Amato, J. Hamann-Borrero, N. Leps, A. Kondrat, G. Behr, J. Werner und B. Büchner, Phys. Rev. Lett. **101**, 077005 (2008).

[3] C. de la Cruz, Q. Huang, J. W. Lynn, J. Li, W. R. II, J. L. Zarestky, H. A. Mook, G. F. Chen, J. L. Luo, N. L. Wang und P. Dai, Nature **453**, 899 (2008).

[4] Z.-A. Ren, W. Lu, J. Yang, W. Yi, X.-L. Shen, Z.-C. Li, G.-C. Che, X.-L. Dong, L.-L. Sun, F. Zhou und Z.-X. Zhao, Chin. Phys. Lett. **25**, 2215 (2008).

[5] M. Rotter, M. Tegel und D. Johrendt, Phys. Rev. Lett. **101**, 107006 (2008).

[6] X. C. Wang, Q. Q. Liu, Y. X. Lv, W. B. Gao, L. X. Yang, R. C. Yu, F. Y. Li und C. Q. Jin, arXiv:0806.4688 (2008).

[7] F.-C. Hsu, J.-Y. Luo, K.-W. Yeh, T.-K. Chen, T.-W. Huang, P. M. Wu, Y.-C. Lee, Y.-L. Huang, Y.-Y. Chu, D.-C. Yan und M.-K. Wu, arXiv:0807.2369 (2008).

[8] M. Rotter, M. Tegel, D. Johrendt, I. Schellenberg, W. Hermes, R. Pöttgen, Phys. Rev. B **78**, 020503 (2008).

[9] H. Luetkens, H.-H. Klauss, R. Khasanov,A. Amato, R. Klingeler, I. Hellmann, N. Leps, A. Kondrat, C. Hess, A. Köhler, G. Behr, J. Werner, and B. Büchner, Phys. Rev. Lett. **101**, 097009 (2008).

[10] H. Luetkens, H.-H. Klauss, M. Kraken, F. J. Litterst, T. Dellmann, R. Klingeler, C. Hess, R. Khasanov, A. Amato, C. Baines, J. Hamann-Borrero, N. Leps, A. Kondrat, G. Behr, J. Werner, B. Büchner, arXiv:0806.3533, Nature Materials (accepted)

[11] A. Kondrat, J. E. Hamann-Borrero, N. Leps, M. Kosmala, O. Schumann, J. Werner, G. Behr, M. Braden, R. Klingeler, B. Büchner, C. Hess, arXiv:0811.4436.

[12] R. Klingeler, N. Leps, I. Hellmann, A. Popa, C. Hess, A. Kondrat, J. Hamann-Borrero, G. Behr, V. Kataev, B. Büchner, arXiv:0808.0708.

[13] C. Hess, A. Kondrat, A. Narduzzo, J. E. Hamann-Borrero, R. Klingeler, J. Werner, G. Behr, B. Büchner, arXiv:0811.1601.

[14] A. J. Drew, F. L. Pratt, T. Lancaster, S. J. Blundell, P. J. Baker, R. H. Liu, G. Wu, X. H. Chen, I. Watanabe, V. K. Malik, A. Dubroka, K. W. Kim, M. Roessle, C. Bernhard, Phys. Rev. Lett. **101**, 097010 (2008).

[15] M. Berciu, I. Elfimov, G.A. Sawatzky, arXiv:0811.0214

[16] A. J. Drew, Ch. Niedermayer, P. J. Baker, F. L. Pratt, S. J. Blundell, T. Lancaster, R. H. Liu, G. Wu, X. H. Chen, I. Watanabe, V. K. Malik, A. Dubroka, M. Roessle, K. W. Kim, C. Baines, C. Bernhard, arXiv:0807.4876.

[17] A. A. Aczel, E. Baggio-Saitovitch, S. L. Budko, P.C. Canfield, J. P. Carlo, G. F. Chen, Pengcheng Dai, T. Goko, W. Z. Hu, G. M. Luke, J. L. Luo, N. Ni, D. R. Sanchez-Candela, F. F. Tafti, N. L. Wang, T. J. Williams, W. Yu, Y. J. Uemura, arXiv:0807.1044.

[18] T. Goko, A. A. Aczel, E. Baggio-Saitovitch, S. L. Bud'ko, P. C. Canfield, J. P. Carlo, G. F. Chen, Pengcheng Dai, A. C. Hamann, W. Z. Hu, H. Kageyama, G. M. Luke, J. L. Luo, B. Nachumi, N. Ni, D. Reznik, D. R. Sanchez-Candela, A. T. Savici, K. J. Sikes, N. L. Wang, C. R. Wiebe, T. J. Williams, T. Yamamoto, W. Yu, Y. J. Uemura, arXiv:0808.1425.

[19] H. Takagi, B. Batlogg, H. L. Kao, J. Kwo, R. J. Cava, J. J. Krajewski, W. F. Peck, Jr., Phys. Rev. Lett. **69**, 2975 (1992).

Cooperation TU Dresden (H.-H. Klauss et al.), Univ. Köln (M. Braden et al.), HZ Berlin (D. Argyriou et al.), TU Braunschweig (F. J. Litterst et al.), PSI Villigen (H. Luetkens et al.).

High-field studies of the upper critical field of strongly disordered arsenic-deficient $LaO_{0.9}F_{0.1}FeAs_{1-\delta}$ superconductors

G. Fuchs, S.-L. Drechsler, N. Kozlova, K. Nenkov, J. Freudenberger, G. Behr, C. Hess, R. Klingeler, B. Büchner, L. Schultz

The upper critical field B_{c2} is a fundamental characteristic quantity whose study as a function of temperature T, its anisotropy, as well as its dependence on the amount of disorder allows important insights into the mechanism and symmetry of the superconducting pairing as well as into the electronic structure of the normal state.

This knowledge is of special interest at the beginning of a new chapter in the study of superconductivity started recently after the discovery of iron based pnictide superconductors with critical transition temperatures T_c up to 57 K. For instance, an observed nearly linear T-dependence in the vicinity of T_c excludes a bipolaronic mechanism [1] or pronounced multiband superconductivity sometimes discussed in the literature (with bands exhibiting significantly different Fermi velocities) of Cooper pairs which would result in a clear positive curvature. Strong disorder is detrimental for unconventional scenarios such as p and d-wave scenarios but helpful for conventional extended s-wave scenarios in order to improve B_{c2}. The latter property is also important for the evaluation of future technical high-field applications. In this context we remind the reader, how an external magnetic field may affect (destroy) Cooper pairs (see Fig. 1). Finally, it may also shad light on the competition and a mutual dependence on superconductivity and magnetism which is probably the most central issue in the field of pnictide superconductors.

We started our high-field studies [2] with a somewhat special polycrystalline $LaO_{0.9}F_{0.1}FeAs_{1-\delta}$ sample. The reduced As content of this sample (with $\delta \sim 0.1$) was obtained by wrapping it in a Ta foil during the annealing procedure. Ta acts as an As getter at high temperatures forming a solid solution of about 9.5 at% As in Ta which leads to an As loss in the pellet. The resisitivity of the arsenic-deficient sample in the normal state at 31 K clearly exceeds that reported for other $LaO_{0.9}F_{0.1}FeAs$ samples which points to a substantial shortening of the mean free path due to the As-deficiency. Nevertheless, this sample exhibits a rather high T_c value of 28.5 K.

The resistance of the arsenic-deficient sample was investigated in magnetic fields up to 60 T. The high-field measurements were performed in the pulsed field facilities of the IFW and the FZ Dresden-Rossendorf. Resistance data vs. applied field are shown in Fig. 2. Gold contacts (100 nm thick) were made by sputtering in order to provide a low contact resistivity and, therefore, to avoid possible heating effects in the high-field measurements. The magnetic field generated by the IFW's pulsed field magnet rises within about 10 ms to its maximum value $B_{max} \leq 50$ T and decreases to zero within the same time. The resistance data shown in Fig. 2 were taken for descending field using $B_{max} = 47$ T. Additionally, resistance data were collected for $B_{max} = 29$ T at several selected temperature.

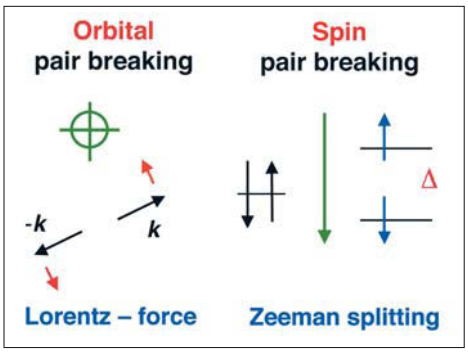

Fig. 1: Schematical view of the magnetic field affecting a Cooper-pair. Pair breaking can occur by the Lorentz force acting via the charge and the momenta on the paired electrons (orbital effect) or by the Zeeman effect aligning the spins of the two electrons with the applied field.

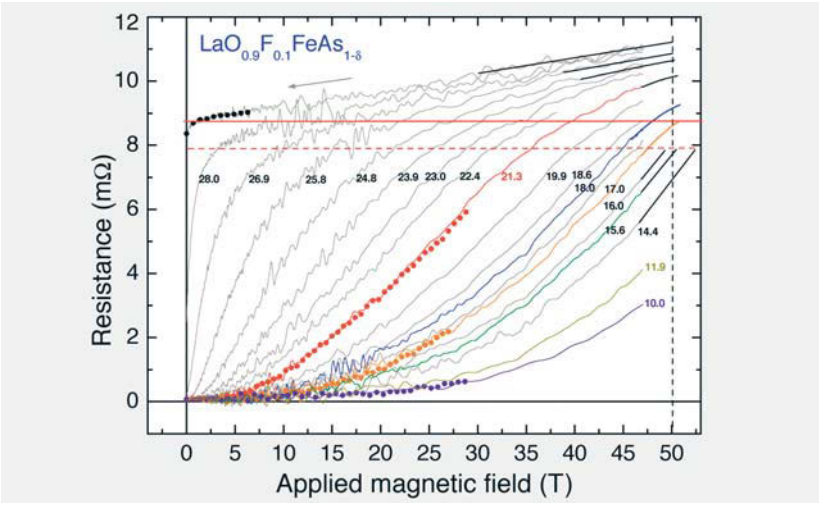

Fig. 2: Field dependence of the resistance at fixed temperature (see legend) measured in pulsed fields. Lines: measurements up to 47 T; symbols: measurements up to 29 T shown for four selected temperatures

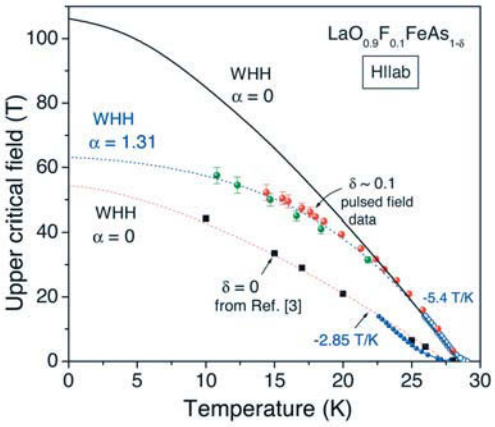

Fig. 3: Upper critical field vs. temperature data for the arsenic-deficient $LaO_{0.9}F_{0.1}FeAs_{1-\delta}$ sample (pulsed field data from IFW (●) and FZD (●)) and two reference samples without As-deficiency (● - our sample, ■ - Ref. [3]). Dotted line: WHH model for $\alpha = 1.31$. Solid and dashed line: WHH model for $\alpha = 0$.

The agreement between resistance data for $B_{max} = 47$ T and 29 T confirms that our data are not affected by sample heating. At high magnetic fields a pronounced broadening of the transition curves is observed. It stems from the large anisotropy of the upper critical field B_{c2}. For polycrystalline samples, only the higher B_{c2}^{ab} (for $H \parallel$ ab) is accessible which is related to those grains oriented with their *ab*-planes along the applied field. B_{c2}^{ab} was determined from the onset of superconductivity defining it at 90% of the resistivity in the normal state (see dashed line in Fig. 2).

The $B_{c2}^{ab}(T)$ curve of our arsenic-deficient sample is shown in Fig. 3 together with $B_{c2}^{ab}(T)$ data reported for a $LaO_{0.9}F_{0.1}FeAs$ reference sample [3]. The $B_{c2}(T)$ data of the arsenic-deficient sample shows a surprisingly steep $dB_{c2}/dT|_{Tc} = -5.4$ T/K which exceeds the slope of $B_{c2}(T)$ of the non-arsenic-deficient sample by more than a factor of 2. This points to strong impurity scattering in the arsenic-deficient sample in accord with its enhanced resistivity at 30 K. For applied fields up to about 30 T, these $B_{c2}(T)$ data can be well described by the standard WHH (Werthamer-Helfand-Hohenberg) model [4] for the orbital $B_{c2}(T)$ which predicts $B_{c2}^*(0) = 0.69\, T_c\, (dB_{c2}/dT) = 106$ T at $T = 0$. However, for applied fields above 30 T or at temperatures below 23 K, increasing deviations from the WHH curve are clearly visible. The flattening of $B_{c2}(T)$ at high fields points to its limitation by the Pauli spin paramagnetism. The paramagnetically limited upper critical field B_{c2}^p at T = 0 is given by the expression

$$B_{c2}^p(0) = B_{c2}^*(0)(1+\alpha^2)^{-0.5} \qquad (1)$$

where the Maki parameter

$$\alpha = \sqrt{2}\, B_{c2}^*(0)/\, B_p(0) \qquad (2)$$

is a measure for the relative strength of orbital and spin pair breaking. The Pauli limiting field B_p characterizing the spin pair breaking is given by

$$B_p(0)\ [\text{Tesla}] = 1.86\, \eta_{eff}(\lambda)\, T_c[\text{K}] \qquad (3)$$

where $\eta_{eff}(\lambda) = (1+\lambda)^{\varepsilon}\, \eta_{\Delta}\, \eta_{Bc2}\, (1-I)$ is a correction to BCS due to *el-boson* and *el-el* interaction (with λ as the *el-boson* coupling constant, I as the Stoner factor and $\varepsilon = 0.5$ or 1). The experimental data for the arsenic-deficient sample can be well described by the WHH model using $\alpha = 1.31$, $B_{c2}^p(0) = 63$ T, $\lambda = 0.5$ and $\eta_{eff} = 2.09$ as shown in Fig. 3.

The observed Pauli-limiting behavior in our arsenic-deficient sample points to an enlarged Pauli-susceptibility compared with cleaner samples [5,6] showing no Pauli-limiting behaviour at the same high fields we have probed. Thus we are confronted with a rather unusual situation in superconductivity not observed so far to the best of our knowledge: Improved superconductivity at high temperature and low-fields and somewhat suppressed superconductivity at high-fields and low temperature. The first observation and the T_c-enhancement can be understood within conventional s-wave superconductivity by enhanced disorder and by a disorder-induced suppression of nested related antiferromagnetism, respectively. The high-field properties strongly suggest an enhanced paramagnetism as the preceding phase to ferromagnetism. In other words, at least in disordered pnictides superconductivity competes with two kinds of magnetism. The elucidation of the microscopic reason of our anomalous high-field properties is of great interest and obviously will be helpful for the understanding of the still unknown pairing mechanism, too. Also in view of future practical applications one has different choices for optimization of their properties in dependence of the requested external field regime.

References

[1] G.A. Sawatzky *et al.* arXiv: 0808.1390
[2] G. Fuchs *et al.* , Phys. Rev. Lett. **101,** 237003 (2008)
[3] F. Hunte *et al.*, Nature **453**, 903 (2008)
[4] N.R. Werthamer et al., Phys. Rev. **147**, 295 (1966)
[5] H. Luetkens *et al.*, Phys. Rev. Lett. **101,** 077005 (2008)
[6] S.-L. Drechsler *et al.*, Phys. Rev. Lett. **101,** 257004 (2008)

Cooperation FZ Dresden-Rossendorf
Funded by DFG

Nuclear Magnetic Resonance Study of the new iron arsenide superconductors

H.-J. Grafe, G. Lang, F. Hammerath, Dalibor Paar, K. Manthey, B. Büchner

Nuclear Magnetic Resonance (NMR) plays a central role in the study of superconducting materials from the time when spin lattice relaxation experiments revealed the presence of a superconducting gap, and proved that the Cooper pairs are a coherent superposition of two particles [1]. Moreover, it revealed that cuprates [2] and heavy fermion superconductors [3] are unconventional superconductors with a d-wave order parameter of the superconducting state. Measurements of the Knight shift in Sr_2RuO_4 identified this compound as one of the rare spin triplet superconductors [4]. For these reasons we started to investigate the new superconductor $LaO_{1-x}F_xFeAs$ by means of NMR immediately after its successful preparation at the IFW, resulting in one of the first experimental works on this compound world wide [5]. Thereby, we turned our attention not only to the superconducting state, but used NMR also to investigate the intriguing normal state properties of $LaO_{1-x}F_xFeAs$ [6].

In the superconducting state, we find that the spin lattice relaxation rate T_1^{-1} exhibits a drop at T_c, with no evidence for a Hebel-Slichter coherence peak. For $T << T_c$, T_1^{-1} varies as T^3, as seen in Fig. 1. This behavior is indicative of line nodes in the superconducting gap function, $\Delta(\boldsymbol{k})$, and contrasts with the exponential behavior $T_1^{-1} \sim \exp(-\Delta/k_BT)$ expected for an isotropic superconducting gap. Nevertheless, these results are also in contrast to other techniques like ARPES and Andreev spectroscopy which find evidence for an isotropic superconducting gap. This discrepancy still needs to be clarified.

In the normal state, we have measured the Knight shift, K_{ab}, with the external magnetic field applied along the *ab* directions for ^{139}La, ^{57}Fe, and ^{75}As. Each shift can be written as the sum of an orbital shift K_{orb}, expected to be temperature independent, and a spin shift K_s, temperature dependent through its proportionality to the local spin susceptibility χ_s. All shifts are plotted in Fig. 2 together with the macroscopic susceptibility, $\chi_{powder} = \chi_s + \chi_{dia} + \chi_W$, where χ_{dia} and χ_W are the temperature independent diamagnetic and Van Vleck susceptibilities, respectively. Through proper scaling and vertical shifting, the four datasets can be made to overlap in the paramagnetic region. The ratio of the scales of the NMR shifts to the scale of χ_{powder} reflects the strength of the hyperfine coupling of each nucleus to the spin susceptibility, with the shifting of the scales necessary to account for the finite temperature independent terms K_{orb} and χ_{dia} and χ_W. Qualitatively, it is remarkable that such general scaling can be obtained, with

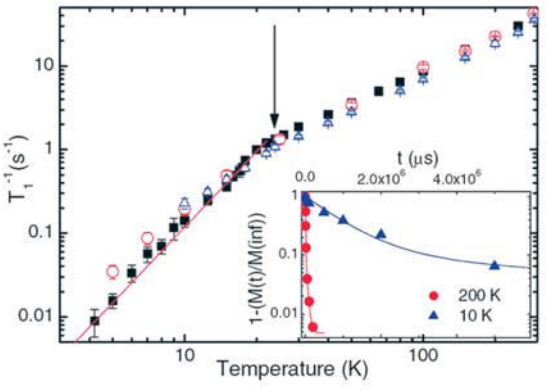

Fig. 1: T_1^{-1} of ^{75}As versus temperature. The arrow indicates T_c = 23.5 K at 7 T, and the solid line indicates $T_1^{-1} \sim T^3$, indicative of line nodes. Open red symbols have been measured on an *ab* oriented sample, open blue triangles for a different field orientation (**H** 41° to *c*, see [5] for further explanation). Inset: Magnetization recovery and fits for two temperatures.

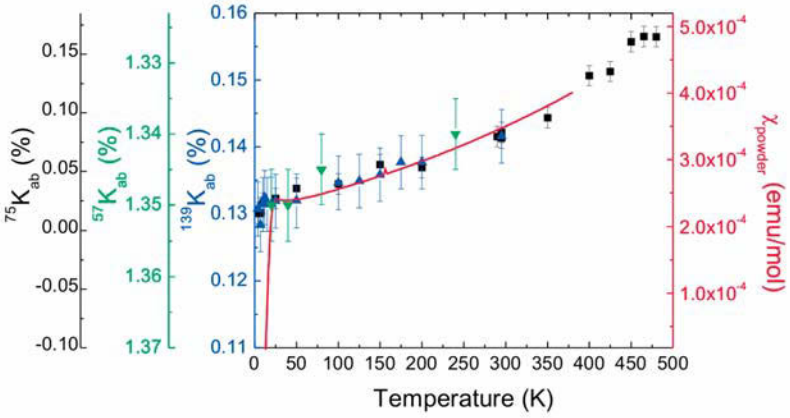

Fig. 2: Knight shift of ^{75}As (black squares), ^{57}Fe (green down-pointing triangles) and ^{139}La (blue triangles), and the macroscopic susceptibility χ_{powder} (solid red line) versus temperature with different vertical scales and origins. Note the reversed scale for ^{57}Fe.

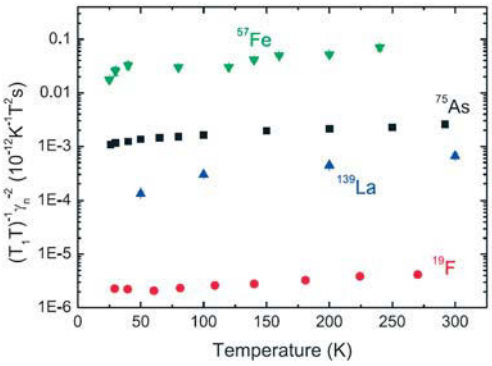

Fig. 3: The temperature dependence of the ^{57}Fe, ^{75}As, ^{139}La, and ^{19}F $(T_1T)^{-1}$ divided by the squared nuclear gyromagnetic ratio for quantitative comparisons. The ^{19}F data is reproduced from Ahilan *et a.l* [7].

an identical temperature dependence. This means that the three nuclei probe the spin susceptibility in a similar way, i.e. the electronic system is likely a single spin liquid. There is no apparent multiband effect which could appear due to selective hyperfine couplings to different bands. In the cuprates, where a single-band modeling of the electronic structure is appropriate, the presence of a single spin component has been shown similarly with copper and oxygen NMR. Quite remarkably, the spin susceptibility decreases with decreasing temperature. Such a progressive suppression of low-energy spin excitations has been ascribed to the existence of a pseudogap in this system. This assumed that the temperature for which the susceptibility would reach a maximum (the pseudogap peak) was significantly higher than the highest studied temperature, i.e., higher than room temperature. However, the present ^{75}As measurements, which constitute the first NMR study at temperatures up to 480 K, still show no signature of a pseudogap peak, thus casting doubt on the true nature of the suppression of excitations.

In contrast to the Knight shift that probes the time averaged or static electronic susceptibility, the spin lattice relaxation rate T_1^{-1} probes the *dynamic* susceptibility $\chi''(\boldsymbol{q},\omega)$ for different wave vectors $\boldsymbol{q}$. Note that different nuclei may be differently coupled to the electronic spin system via the $\boldsymbol{q}$ dependent hyperfine coupling $A_{hf}(\boldsymbol{q})$, e.g. $^{75}A_{hf}(\boldsymbol{q})$ is well-developed at $\boldsymbol{q}=0$ and tends to vanish towards $q=(\pi/a, \pi/a)$, while $^{57}A_{hf}(\boldsymbol{q})$ exhibits an opposite behaviour, tending to low values around $\boldsymbol{q}=0$. T_1^{-1} measurements were performed, with the temperature dependence of $(T_1T)^{-1}$ shown in Fig. 3, including ^{19}F data from Ahilan *et al.* [7] for comparison. A clear result is that the strength of the relaxation correlates with the distance to the iron plane, with values spread over three orders of magnitude at a given temperature, possibly indicating two-dimensional physics. Although the nuclei may be differently coupled to the dynamic spin susceptibility, all nuclei obey the same temperature dependence as seen for the NMR shifts, with roughly homothetic curves. This means that as temperature is decreased, spin excitations are suppressed across all $\boldsymbol{q}$ vectors, with a similar temperature-dependence of the dynamic susceptibility across $\boldsymbol{q}$-space. In other words, while the susceptibility is temperature-dependent, there is no transfer of spectral weight across $\boldsymbol{q}$-space suggesting that the relaxation comes mostly from quasi-particle scattering. Concerning the presence of a pseudogap, the known lack of a peak in the ^{75}As data is confirmed by the ^{57}Fe data. This is revealing in light of the higher sensitivity of Fe and As to respectively the nonferromagnetic ($\boldsymbol{q}\neq0$) and ferromagnetic ($\boldsymbol{q}=0$) fluctuations. Indeed, one may have expected that if present, the pseudogap peak could show up at a lower temperature for $\boldsymbol{q}\neq0$ than for $\boldsymbol{q}=0$, as is the case in the cuprates. In that case, a peak for ^{57}Fe would likely show up at a temperature lower than for ^{75}As, which is not seen here. Therefore, it cannot be ruled out that the physics hiding behind the decrease of low-energy spin excitations are of an entirely different nature than in the cuprates.

References

[1] L. C. Hebel and C. P. Slichter, Phys. Rev. **113**, 1504 (1959)
[2] R. L. Corey *et al.*, Phys. Rev. B **53**, 5907 (1996)
[3] N. J. Curro *et al.*, Nature **434**, 622 (2005)
[4] K. Ishida *et al.*, Nature **396**, 658 (1998)
[5] H.-J. Grafe *et al.*, Phys. Rev. Lett. **101**, 047003 (2008)
[6] H.-J. Grafe *et al.*, arXiv:0811.4508
[7] Ahilan *et al.*, Phys. Rev. B **78**, 100501(R) (2008)

Cooperation N. J. Curro, Department of Physics, University of California, Davis, CA 95616, USA; K. Koch, H. Rosner, Max Planck Institute for Chemical Physics of Solids, Dresden; H.-H. Klauss, IFP, Institut für Festkörperphysik, TU Dresden; F.J. Litterst, Institut für Physik der Kondensierten Materie, TU Braunschweig

Funded by DFG, Forschergruppe 538, Alexander von Humboldt Stiftung

Electronic structure of FeAs-based superconductors from spectroscopic methods

A. Koitzsch, S.-L. Drechsler, T. Kroll, D. S. Inosov, V. B. Zabolotnyy, D. V. Evtushinsky, A. A. Kordyuk, S. V. Borisenko, J. Fink[1)], M. Knupfer, H. Eschrig, G. Behr, J. Werner, M. Grobosch, F. Roth, R. Schuster, K. Koepernik, H. Rosner[2)], B. Büchner

Elucidating the electronic structure of a given material and derive its macroscopic properties from that knowledge is at the core of solid state physics. The most direct way to investigate the electronic structure is by spectroscopic means such as photoemission-, x-ray absorption and optical spectroscopy. Here we apply those techniques to the new FeAs superconductors and obtain deep insight on various important aspects. The picture of a weakly to moderately correlated, density wave prone material emerges with its low energy properties dictated almost exclusively by iron d-levels and an isotropic but band-dependent superconducting order parameter.

The Fe-pnictides show some remarkable analogies to other superconductors with unclear pairing mechanism. Like the cuprates and some heavy fermion superconductors they obey a tetragonal symmetry and bear out two-dimensional aspects in their crystal as well as in their electronic structure. Therefore it seems a natural starting point to ask some of the questions that turned out to be appropriate for the "classical" high temperature superconductors: 1) How strongly are the pnictides correlated? It is well known that the cuprates are categorized as strongly correlated materials, i.e. due to the localized, atomic-like nature of the Cu 3d levels the electrons cannot move independently through the lattice. This directly influences also the magnetic properties of the material. 2) What is the appropriate model for the experimentally observed electronic structure? What interactions have to be taken into account? 3) What role play density waves known to be important for many low dimensional materials and superconductors, and, in fact observed for the parent compounds of the pnictides. 4) What is the symmetry and size of the superconducting order parameter?
In the case of the cuprates some of these questions are iterated again and again on ever deeper levels of sophistication. Answering them in the first place forms a solid basis for advanced studies but not necessarily a solution to any of the central problems.

The special surprise that came with the discovery of high-T_c superconductivity in the pnictides was that they contain iron which was thought to be detrimental to pairing. Moreover band structure calculations suggested early on that iron is by no means an electronically inert part of the crystal lattice but, on the opposite, makes up almost the

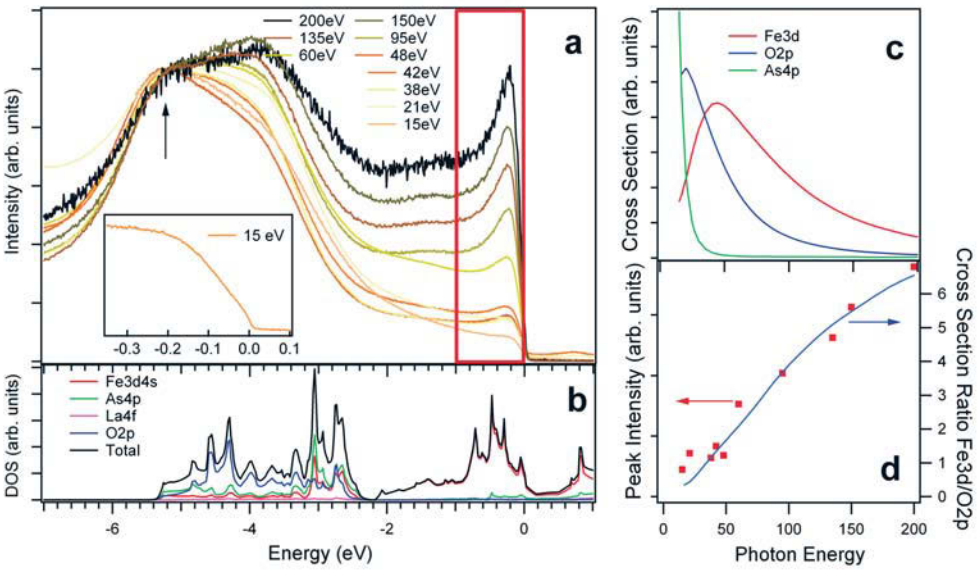

Fig. 1: (a) Photon energy dependent valence band spectra of LaFeAsO. The arrow marks the point of normalization. Inset: Low energy region with Fermi edge. (b) LDA derived orbital resolved density of states. (c) Atomic photoemission cross section for the relevant orbitals. (d) Ratio of the Fe 3d and O 2p cross section from (c) (blue line) compared to experimental values obtained by integrating the low energy peak (red box in (a)).

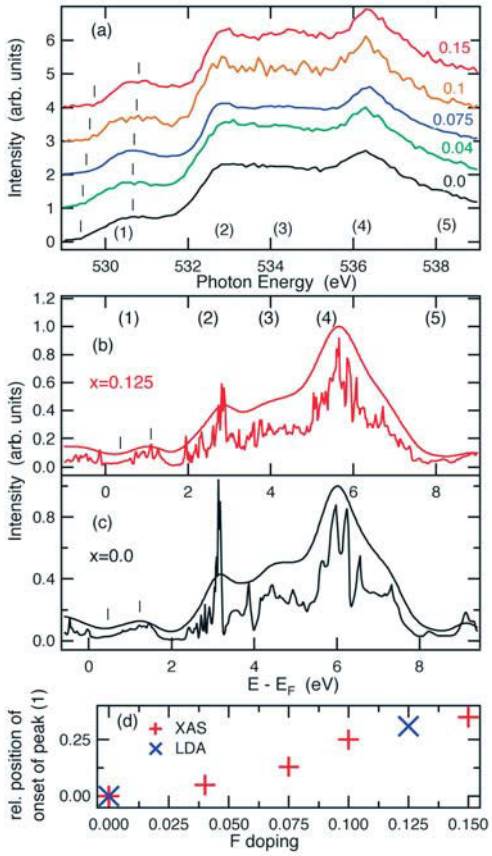

Fig. 2: $LaFeAsO_{1-x}F_x$: (a) doping dependence of XAS O *K*-edge spectra. The spectra have been normalized at 610 eV where they become structure less. (b), (c) Oxygen *p*-projected partial density of states for $x = 0.0$ and $x = 0.125$. (d) Energy shift of the onset of peak (1) as compared to $x = 0.0$ for experimental and theoretical results.

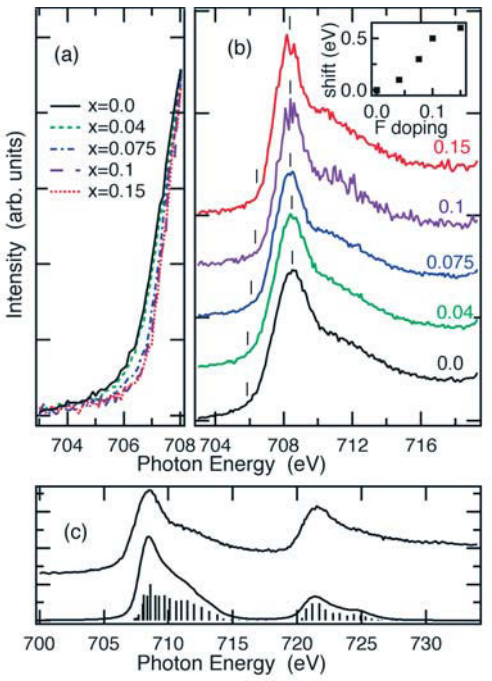

Fig. 3: $LaFeAsO_{1-x}F_x$: doping dependence of the Fe $L_{2,3}$ edge. (a) Blowup of the low-energy side of experimental Fe L_3 edge. For the sake of clarity, the spectra in (a) were shifted in such a way that their maxima match. (b) Experimental L_3 edge for the same doping range. The inset shows the shift of the onset of the main peak in eV relative to $x = 0.0$ as a function of doping x. (c) Comparison of LaFeAsO XAS spectrum with charge-transfer multiplet calculation.

entire density of states in a wide energy window around the chemical potential. To test this specific theoretical prediction and the general applicability of LDA (local density approximation) based band structure theory for the pnictides we performed photoemission experiments, focussing on the valence band [1]. Figure 1 shows the results for polycrystalline nonsuperconducting LaFeAsO samples made in the IFW. Figure 1a presents a compilation of the valence band taken with different photon energies, ranging from $h\nu = 15$ eV to $h\nu = 200$ eV. The valence band consists of a peak at $E = -0.25$ eV, which is followed by a plateau and, centered at $E \approx -5$ eV, a broad peak with at least two shoulders. The relative intensity of all these features are strongly photon energy dependent. In Figure 1b the total and orbital resolved density of states (DOS) as calculated by LDA are depicted. We find at this stage qualitative agreement to experiment. The low energy peak near the Fermi energy (E_F) is reproduced as well as the plateau and the broad peak at higher energies and even the fine structure of the latter finds correspondence in experiment. Theory somewhat underestimates the energy of features. From the reasonable agreement of experiment and LDA already some substantial conclusions can be drawn: It is unlikely that the material is strongly correlated as this would significantly alter the electronic structure from its independent particle shape represented by the LDA. Also the agreement gives credit to the idea that the low energy DOS is due to Fe 3d states, as this is an inherent part of the LDA result. The latter point can be corroborated independently by considering the photon energy dependence of the low energy region highlighted by the red box in the figure. Different orbitals emit electrons with different probability depending on the incoming photon energy. This dependence is shown in Figure 1c and exploited in Figure 1d. Experiment (points) match the expectations from the emission probability (cross section) for Fe 3d orbitals thereby confirming the dominant Fe 3d character of the intensity in the red box.

A complementary method to photoemission spectroscopy is absorption spectroscopy, where it is measured how strongly incoming photons are absorbed by the solid depending on their energy, i.e. the unoccupied states are probed [2]. Figure 2a shows x-ray absorption profiles of $LaFeAsO_{1-x}F_x$ in the energy range of the oxygen K edge. Critical temperatures for $x = 0.075$, 0.1, and 0.15 have been found at $T_c = 22$, 26.8, and 9.9 K, respectively. Figures 2b and 2c present orbital projected oxygen p-DOS for the unoccupied valence band. The overall structure of these LDA derived curves compare well to experiment. The observed peaks (numbered 1 to 5) correspond to hybridization channels of the oxygen to its atomic neighbors in the lattice. Figure 2d compares the onset of peak 1 depending on doping with theory. Generally the peak positions change with doping because the injected charge carriers shift the chemical potential and may change the charge balance of a given specimen in the lattice expressed by the Madelung potential. Here convincing agreement is found between experiment and theory. The results presented in Figure 2 confirm the conclusions from photoemission in Figure 1: As LDA is a good starting point for the description of the electronic structure on the energy scale of the valence band, the material cannot be strongly correlated, or in other words U, the Hubbard repulsion must be smaller than the bandwidth, W. To achieve a more quantitative conclusions about the degree of correlations we performed charge transfer multiplet calculations for the Fe L edge shown in Figure 3. Similarly to the oxygen edge in Figure 2 the line shape hardly depends on doping, nevertheless the peak onset does. It consists of a peak around $h\nu = 709$ eV and a shoulder at higher energies. Figure 3c compares the experimental curve for the undoped compound with the calculation. The calculation takes into account the different multiplets in the initial and final state and possible charge transfer to the ligand atoms (in this case Arsen). Good agreement can be achieved with

a parameter set containing $U \approx 1.5$ eV which is a rather small value for a d-metal and confirms the above conclusions. Within the series REFeAsO (RE = La, Ce, Sm, Gd) we did not find significant changes for different rare earth atoms and temperatures [2].

The degree of photon absorption determines also the reflectivity of a solid and, as low photon energies are concerned, its optical properties. The inspection of normal state room temperature optical data in the frequency region of the screened in-plane plasma frequency $\omega_p = \Omega_p / \sqrt{\varepsilon_\infty}$ allows important insights into the charge dynamics of free carriers whose pairing determines the superconducting condensate below T_c, into the strength of the screening measured by the back ground dielectric constant ε_∞, as well as into the strength of correlations measured by the ratio of the on-site repulsion U at Fe-sites to the total bandwidth W.

Three representative reflectivity spectra for polycrystalline samples of the $LaO_{1-x}F_xFeAs$ –family (La-1111), namely, the undoped nonsuperconducting parent compound LaOFeAs, the optimally fluorine doped system $LaO_{0.9}F_{0.1}FeAs$ with $T_c = 26$ K, and the arsenic deficient $LaO_{0.9}F_{0.1}FeAs_{0.9}$ with $T_c = 28.6$ K all shown in Fig. 4 show a clear signature of a plasma edge we ascribed to $\hbar\omega_p = 0.38$, 0.395, and 0.24 eV, respectively [3]. A relatively large background dielectric constant $\varepsilon_\infty \approx 12$ to 15 has been deduced from both ellipsometry [4] as well as from our reflectivity data on high-quality single crystals of one of the parent compounds of the 122-family $BaFe_2As_2$ [3] where a complete analysis in terms of a DRUDE-LORENTZ model was possible. Such high values of ε_∞ are incompatible with intermediately strong on-site COULOMB interaction ($U \approx 4$ eV within an eight-band HUBBARD model) sometimes suggested in the literature [5]. Using the results for the in-plane optical conductivity obtained within the framework of the dynamical mean-field theory [5] for $U = 4$ eV we obtained $\varepsilon_\infty \approx 5.4$, only (see Fig. 5). Instead, we suggest a significantly smaller value $U \approx 2$ eV [3] in accord with the electron spectroscopy data given above and the high pnictide-polarizability picture proposed in Ref. 6. Thus, our finding points also to a weak correlation regime $U_d / W << 1$ in contrast to Ref. [5].

The empirical unscreened plasma frequency Ω_p compared with LDA-FPLO band structure calculations points to moderate electron-liquid renormalizations of the electron mass by a factor of two. A comparison with the plasma frequency $\tilde{\Omega}_p$ renormalized additionally by electron-boson couplings, disorder effects and the density of the superfluid condensate as derived from the reported extrapolated in-plane penetration depth $\lambda_{ab,L}(0)$ at $T = 0$ taken from μSR-measurements [7] allows us to estimate the corresponding total *electron - boson* coupling constant λ_{tot} within ELIASHBERG theory. As a result we arrive for the optimally doped $LaO_{0.9}F_{0.1}FeAs$ at a weak to intermediately strong *electron - boson* coupling regime with $\lambda_{tot} = \lambda_{el\text{-}ph} + \lambda_{el\text{-}sp} \ldots \approx 0.6 \pm 0.35$ (see Fig. 6), again in accord with the mass renormalization which determines the kink in the dispersion law observed in ARPES measurements for the related $(Ba, K)Fe_2As_2$ -systems, and at a quasi-clean limit regime ($\delta \approx 0.9$). Note that our coupling constant includes both attractive and repulsive couplings on equal footing. It sufficiently exceeds the standard *electron - phonon* coupling $\lambda_{el\text{-}ph} \approx 0.2$ as calculated in Ref. 8. Therefore it becomes clear that either unconventional electron-phonon coupling plays a role here [9] or that the electrons couple to other degrees of freedom of the solid e.g. magnons.

So far we considered the electronic structure on the energy scale of the valence band and of the plasma frequency. Now we like to shift our attention to the low energy excitations in the close vicinity of E_F. The appropriate experimental tool for this is angle-resolved photoemission spectroscopy (ARPES), since it directly mirrors the band structure of the solid. The latter statement rests on the presumption that the electronic structure under consideration is sufficiently two-dimensional, which is indeed the case for the pnictides. Furthermore ARPES can only be performed on single crystals. Here single crystals from the $(Ba, K)Fe_2As_2$ (BKFA) family have been used. Figure 7 presents the Fermi surface of $Ba_{1-x}K_xFe_2As_2$ for two different excitation energies and deploying different polarization conditions for the incoming photon beam [10]. The natural starting point for the inter-

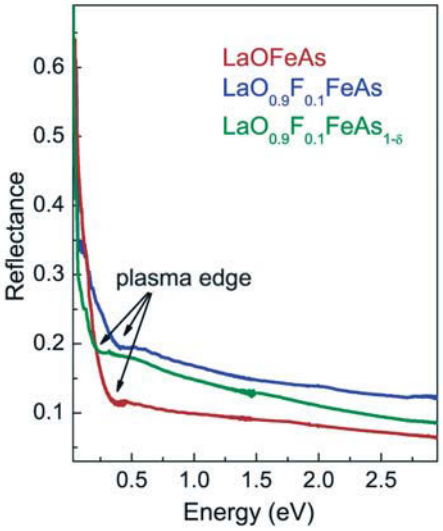

Fig. 4: Reflectance data vs. frequency for three $LaO_{1-x}F_xFeAs$ polycrystalline samples. The plasma edge measuring the screened in-plane plasma frequency $\hbar\omega_p$ is shown by arrows.

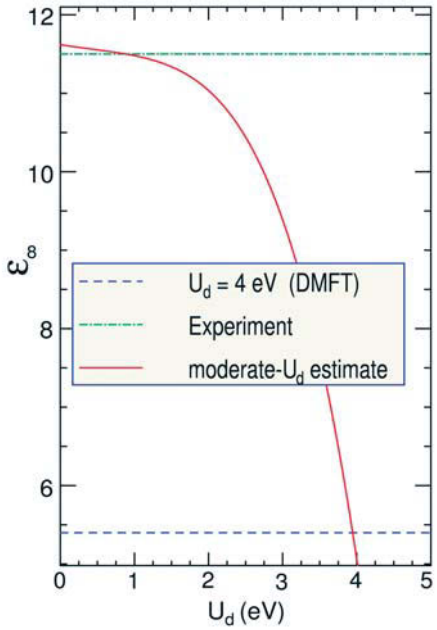

Fig. 5: Schematical behaviour of the back ground dielectric constant ε_∞ vs. COULOMB repulsion U_d on Fe sites.

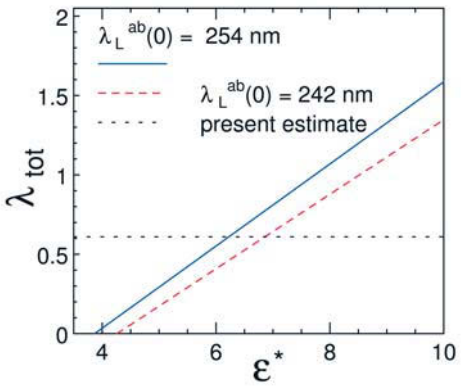

Fig. 6: Strength of the total electron-boson coupling constant λ_{tot} vs. the effective back ground dielectric constant $\varepsilon^* = \varepsilon_\infty / (1+\delta)N$ renormalized by disorder ($\delta \geq 0$) and the relative density of free charge carriers in the superfluid condensate n_s, where $N = n_{tot}/n_s \geq 1$.

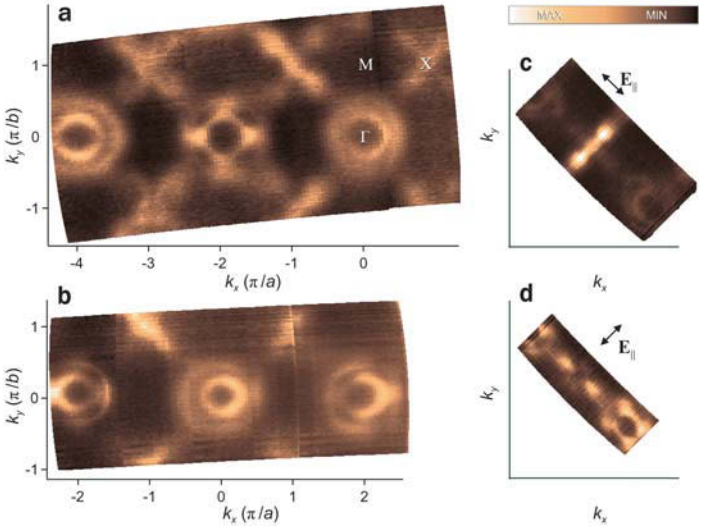

Fig. 7: Fermi surface topology of $Ba_{1-x}K_xFe_2As_2$. The color plots display the photoelectron intensity distribution as a function of quasimomentum k integrated in a small energy window of 15 meV around the Fermi level. (a,b) Fermi Surface maps of $Ba_{1-x}K_xFe_2As_2$ measured using excitation energy $h\nu$ = 80 and 50 eV respectively at T = 14 K. Images (c) and (d), measured with $h\nu$ = 80 eV, demonstrate strong effect of light polarization on the photoemission.

pretation of the data are the band structure calculations which proved successful for the energy scale of the valence band. The band structure calculations predict two concentric hole-like Fermi surface sheets around the Γ-point and two electron-like sheets around the X-point. The two hole-like Fermi surfaces around the Γ-point are indeed observed. However, the Fermi surface around the X-point does not resemble the expected picture at all. Instead of two simple electron pockets a complicated cross-shaped structure is found. Closer scrutiny reveals that this structure consists of a small electron pocket directly at the X-point and the four "blades" are due to hole pockets surrounding it. This substantial disagreement points towards a failure of the underlying assumptions of the band structure calculations. The original solution fulfils a nesting condition: shifting the Γ-Fermi surfaces by a (π,π) vector results in significant overlap with the original electron sheets. Such a situation is unstable, it favors instead a density wave order which reduces the kinetic energy of the electrons. If the band structure is reconstructed by a (π,π) backfolding the Γ and X-point should become equivalent which is not seen in the data. However, here one has to consider the fact that the backscattering potential is weak and also that photoemission matrix element effects may influence the visible intensity distribution at the Fermi surface. Instead, clear traces of the (π,π) order can be found in the data as shown in Figure 8. Fermi surfaces of undoped

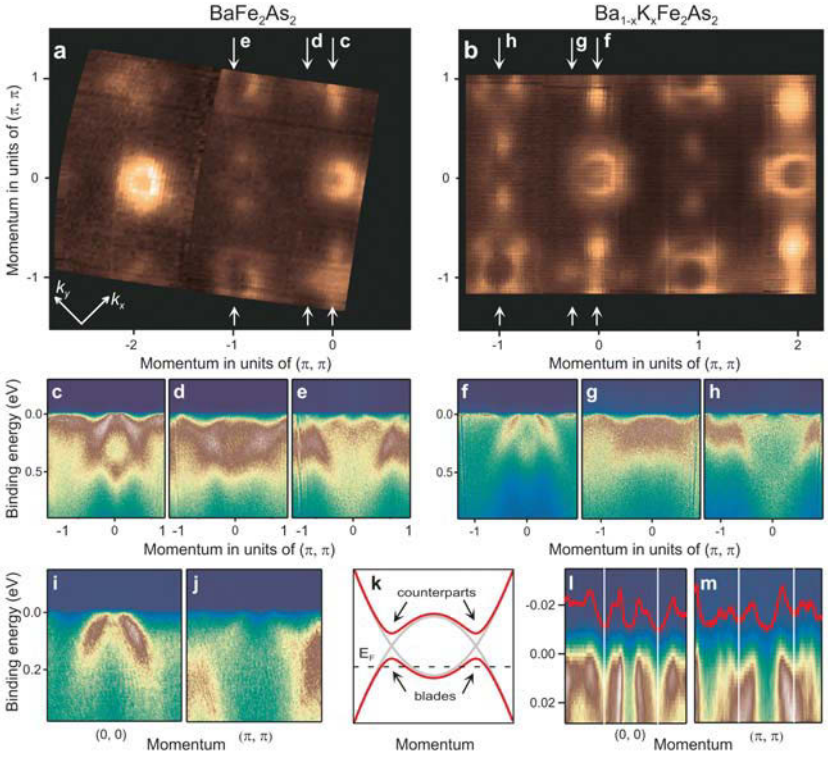

Fig. 8: (a, b) Fermi surface maps for $BaFe_2As_2$ and $Ba_{1-x}K_xFe_2As_2$ respectively, $h\nu$ = 80 eV. (c,d, e), (f, g, h) Several typical energy-momentum cuts. The cuts positions in momentum space are indicated by the arrows in panels (a) and (b). (i, j) Parallel cuts through the electronic structure of $BaFe_2As_2$ set apart by the (π,π) vector. **k**, Simplest model showing the result of folding of single hole- and electron-like bands. (l, m), Parallel cuts through the Γ and X points in electronic structure of $Ba_{1-x}K_xFe_2As_2$ set apart by the (π,π) vector. Red curves are the MDCs integrated within the 8 meV showing the symmetric behavior about the new Brillouin zone boundaries (white lines) due (π,π) folding of the original structure.

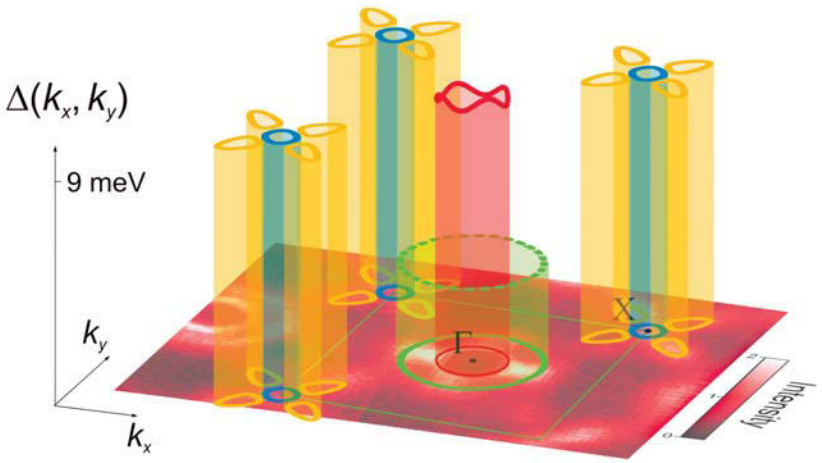

Fig. 9: Momentum dependence of the superconducting gap in $Ba_{1-x}K_xFe_2As_2$ (T_c = 32 K) is shown as a three-dimensional plot with the underlying Fermi surface map for orientation. Green line denotes the boundary of the Brillouin zone.

and doped BKFA are presented together with energy-momentum cuts as indicated in the Fermi surface panels. The important point is that cuts, which are set apart by the (π,π) vector, resemble each other. This is the case for Fig. 8 i + j (undoped) and 8 l + m (doped compound). There is no reason for this similarity without (π,π) order. Fig. 8k shows a sketch of a possible scenario how the backfolding may result in the blade structure around the X-point: intersecting hole and electron-like bands of comparable diameter create a local minimum, which may well form hole pockets somewhat offset from the high symmetry point.

From the temperature dependence of the "blade" structures we find that they persist up to room temperature, i.e. the density wave order sets in above the structural, magnetic and superconducting transitions in the pnictides. Those ARPES data manifest the presence of electronic order of a special kind. It sets in already at high temperatures and is dictated by the nesting instability predicted in the band structure calculations. This electronic order may entail the structural transition at lower temperatures for the undoped compound.

In the superconducting state a gap opens at the Fermi surface. This gap can be directly seen by ARPES as suppression of the photoemission intensity near E_F. However, precise estimation of the gap magnitude requires detailed analysis. Figure 9 shows the extracted gaps for the various Fermi surface sheets. Its value is Δ = 9 meV for the inner Γ-barrel, the X-pocket and the "blades" but significantly lower (Δ < 4 meV) for the outer Γ-barrel. The gap values are almost isotropic in each case indicating s-wave symmetry of the order parameter. This does not, however, exclude the possibility that the order

Fig. 10: Superconducting and non-superconducting constituents of the spectrum. (a) Energy distribution of the intensity, corresponding to superconducting and non-superconducting parts of the spectrum. (b) Second derivatives of the data and fit. Structure of the second derivative confirms presence of superconducting and non-superconducting components. (c) Sketch, illustrating the presence of two different components in the same spectrum.

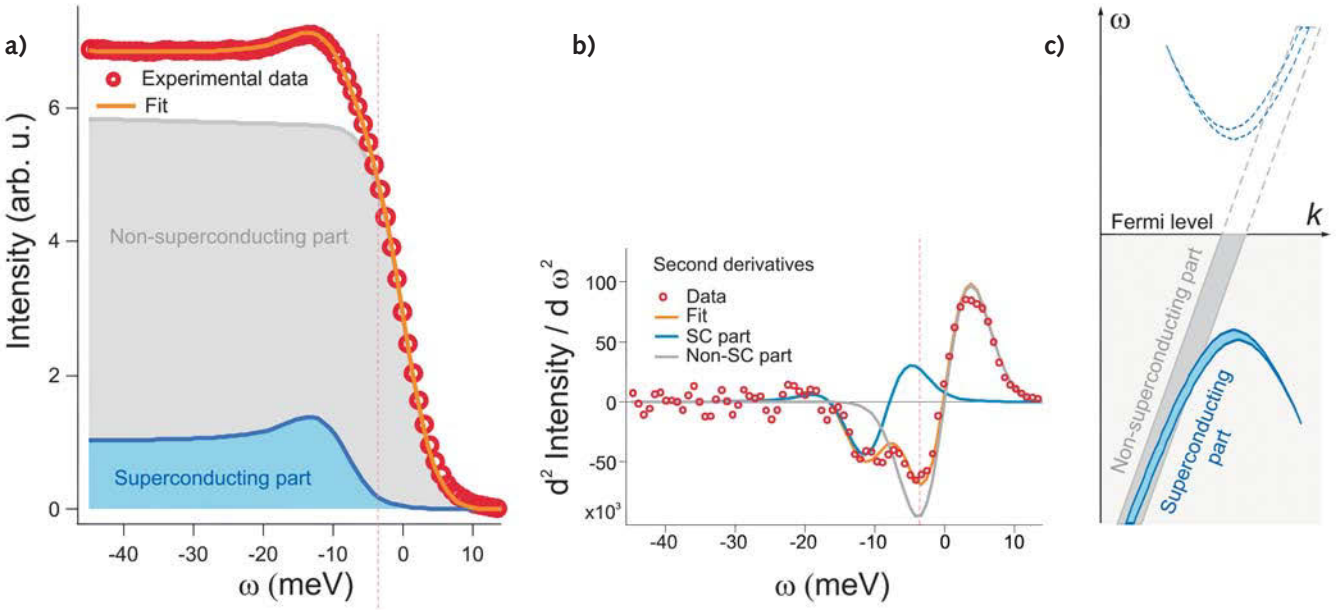

parameter changes sign from one Fermi surface sheet to the other. From the above mentioned fitting procedure an interesting additional conclusion can be drawn. Figure 10 shows an example of the energy distribution of the photoemission intensity in the superconducting state for a certain k-interval [11]. The fit clearly requires a nonsuperconducting component, which is actually more intense than the superconducting one. This is consistent with recent results from neutron scattering and Müon- spectroscopy, where a phase separation in the BKFA family has been observed [12, 13].

The electronic structure of the pnictides holds its own surprises. Contrary to the cuprates those materials are not strongly but on the opposite unusually weakly correlated. The iron states dominate the low energy electronic structure and are, hence responsible for the high superconducting transition temperatures and the other peculiar phase transitions. The Fermi surface shows signatures of a density wave order with a vector (π,π) which sets in already at high temperatures. The consequences of this electronic order need to be investigated in detail. The superconducting order parameter appears isotropic and s-wave like.

We would like to thank R. Hübel, R. Schönfelder, and S. Leger for technical support. Single crystals for ARPES measurements where kindly provided by G. L. Sun, J.-T. Park, D. Haug, V. Hinkov, A. V. Boris, C. T. Lin and B. Keimer. Beamline support is acknowledged for A. Varykhalov and R. Follath. We thank S. Bonhommeau, T. Kachel, H. A. Dürr, A. K. Ariffin, R. Manzke for their contributions to the photoemission and absorption experiments. We received theoretical support from F. M. F. de Groot and A. N. Yaresko.

References

[1] A. Koitzsch et al., Phys. Rev. B **78**, 180506(R) (2008)
[2] T. Kroll et al., Phys. Rev. B **78**, 220502(R) (2008), New Journal of Physics (submitted)
[3] S.-L. Drechsler *et al.,* Phys. Rev. Lett. **101,** 257004 (2008), New Journal of Physics (submitted)
[4] A.V. Boris *et al.,* arXiv: 0806.1732v2 [Phys. Rev. Lett. (to be published)]
[5] K. Haule *et al.*, Phys. Rev. Lett. **100,** 226402 (2008)
[6] G.A. Sawatzky *et al*. arXiv: 0808.1390
[7] H. Luetkens *et al.,* Phys. Rev. Lett. **101,** 077005 (2008)
[8] L. Boeri *et al.,* Phys. Rev. Lett. **101,** 0206403 (2008)
[9] H. Eschrig, arXiv:0804.0186
[10] V. B. Zabolotnyy et al., arXiv: 08082454, Nature *in press*
[11] D. V. Evtushinsky et al., arXiv: 0809.4455, Phys. Rev. B *in press*
[12] T. Goko et al., arXiv: 0808.1425
[13] J. T. Park et al., arXiv: 0811.2224

Cooperation [2)]MPI für Chemische Physik fester Stoffe Dresden, [1)]Helmholtz-Zentrum Berlin, TU Dresden, L.M.-Universität München, MPI für Festkörperforschung Stuttgart, Humboldt Univ. Berlin, Utrecht University, Institut of Metal Physics of National Academy of Sciences of Ukraine

Funded by DFG, Emmy-Noether-Programm, BMBF

Superconductivity in La(O,F)FeAs – Thin film growth and H_{c2} anisotropy

E. Backen, S. Haindl, T. Niemeier, R. Hühne, T. Freudenberg, J. Werner, G. Behr, L. Schultz, B. Holzapfel

In order to obtain a basic understanding of the mechanism of superconductivity in the recently discovered FeAs-based superconductors, single crystalline or at least highly textured samples are essential. Epitaxial thin films would open up the realization of a variety of very important investigations and detailed anisotropy measurements. The preparation of these films, however, is very difficult – due to the high As vapour pressure at elevated temperatures, the high sensitivity of the superconducting properties with regard to stoichiometry of the films and the demanding experimental realization because of the necessary process safety requirements.

Last year we were able to synthesize for the first time biaxial textured La(O,F)FeAs (1111) thin films prepared by pulsed laser deposition (PLD) [1]. The films were deposited at room temperature from stoichiometric targets and subsequently post annealed in evacuated sealed quartz tubes. Due to enhanced scattering of fluorine in the plasma plume during the deposition process, targets with high amounts of fluorine (25%) were used for film growth. Besides the high amount of fluorine in the targets, high vacuum deposition conditions are necessary to obtain the (1111) phase in the films.

Structural characterization reveals a c-axis oriented (00*l*) phase with small amounts of other orientations [(112) and (110)] and impurity phases (LaOF and La_2O_3). A clear four fold symmetry with FWHM values of ~1° can be observed in the (102) pole-figure (Fig. (a)). Our films show a superconducting transition onset at about 11K which is lower than the reported values for high fluorine doping in polycrystalline bulk samples (T_c ~ 26K). This reduced transition onset is probably caused by the loss of fluorine during the deposition process as described above. The presence of minor non-superconducting secondary phases which might segregate at grain boundaries influence the resistance quite strongly indicated by the incomplete and broad transition. Nevertheless, the determination of the H_{c2} anisotropy at different fields and angles was possible and is presented in Fig. (b). Extrapolation of the H_{c2} values to 6 K give an anisotropy ratio of y ~ 7,8.

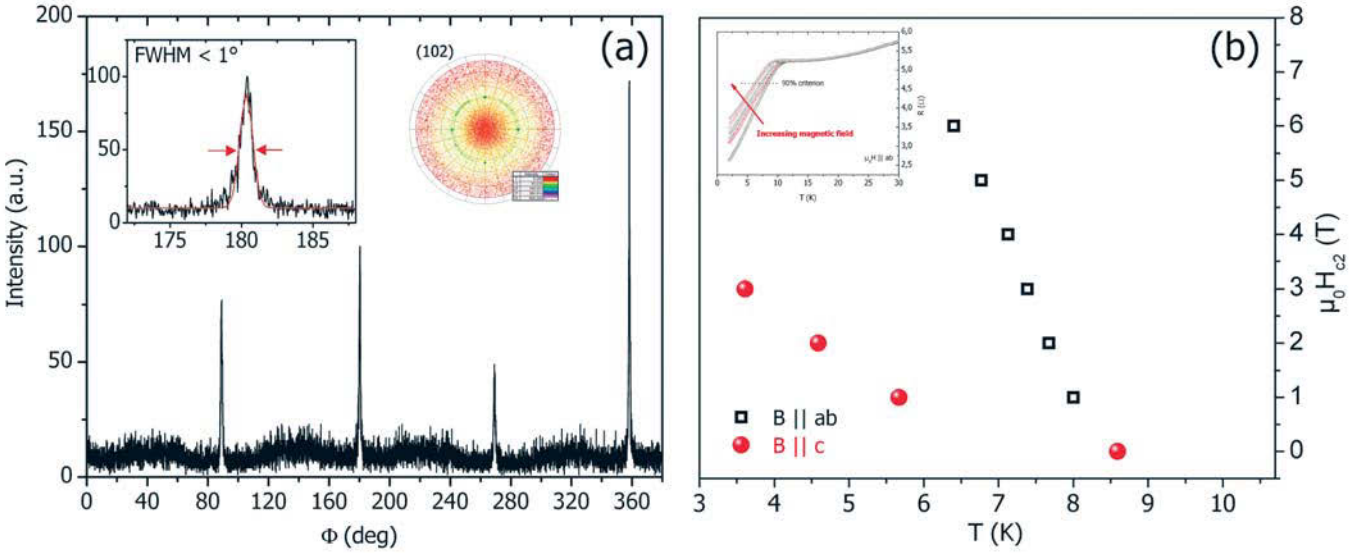

Fig.: Cu Kα (102) phi-scan and pole figure (a) as well as anisotropy characteristics (b) of the superconducting film prepared from a $LaFeAsO_{0.75}F_{0.25}$ target.

References

[1] E. Backen, S. Haindl, T. Niemeier, R. Hühne, T. Freudenberg, J. Werner, G. Behr, L, Schultz and B. Holzapfel: *Supercond. Sci. Technol.* 21 (2008) 122001

Nb/FePt $L1_0$ hybrid thin films

S. Haindl, T. Thersleff, T. Shapoval, Y. W. Lai, J. McCord, L. Schultz, B. Holzapfel

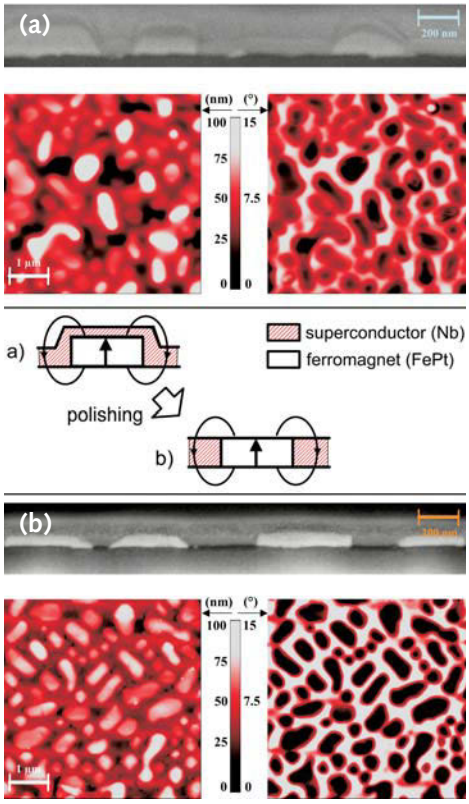

Fig. 1: Cross-sections displayed by a FIB-cut, and AFM (left) as well MFM (right) image of the as-grown (a) and the polished heterostructure (b).

The topic of coexistence of superconductivity and ferromagnetism produced enormous interest among scientists in the last decades. Since it became technically possible to fabricate sub-micron magnetic dots (single or ordered arrays) by employing lithography or shadow mask techniques, the combination of ferromagnets with superconducting thin films yields artificial heterostructures which may lead to new functional devices [1-3]. Usually, the systems found in literature combine soft magnetic materials with superconducting thin films, and typical architectures consist of ferromagnetic dots on top of or covered by an extended superconducting layer [4,5]. A new approach based on the use of highly coercive ferromagnetic materials, like FePt $L1_0$, in combination with conventional superconductors [6], and, by employing new topologies. By means of a nanoscale polishing technique, developed at the IFW (see [7]), a geometrical confinement of the superconducting thin film between ferromagnetic islands has been achieved. In this case the superconducting thin film is multiply connected, and nucleation of superconductivity can only occur between the magnetic islands.

The hybrid heterostructures have been prepared by ultra-high vacuum pulsed laser deposition (UHV-PLD). FePt $L1_0$ islands grow epitaxially on MgO(100) single crystal substrates and are subsequently covered by a Nb thin film. Details of the FePt preparation can be found in [8]. The already mentioned polishing technique developed for thin film surfaces has been employed to obtain the topology of magnetic dots embedded in a multiply connected superconductor. Surface topography (AFM-images), magnetic stray-field distribution (MFM-images) and cross sectional cuts (FIB-SEM) of the heterostructure before and after polishing are shown in Fig. 1.

The superconducting nucleation behavior of Nb/FePt heterostructures has been investigated in detail. The main results consist of the following important observations for the phase boundary $T_C(H)$ when the external magnetic field is applied perpendicular to the thin film surface: 1) the stray-field compensation effect, 2) the control of the phase-boundary by the magnetic stray field of the FePt islands, and 3) evidence of Little-Parks oscillations, which was enhanced by the topology achieved by the polishing procedure.

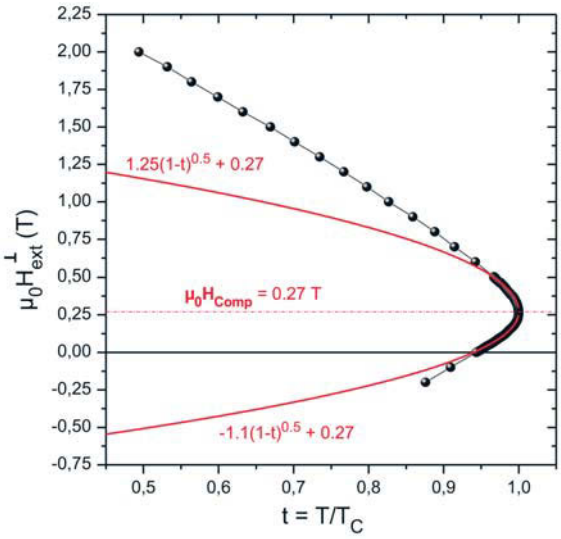

Fig. 2: Phase-boundary of a Nb/FePt thin film heterostructure in an external field perpendicular to the thin film surface. The compensation field is around 0.27 T. Fitting functions and fitting parameters are shown for the in-plane stray-field dominance around the maximum transition temperature.

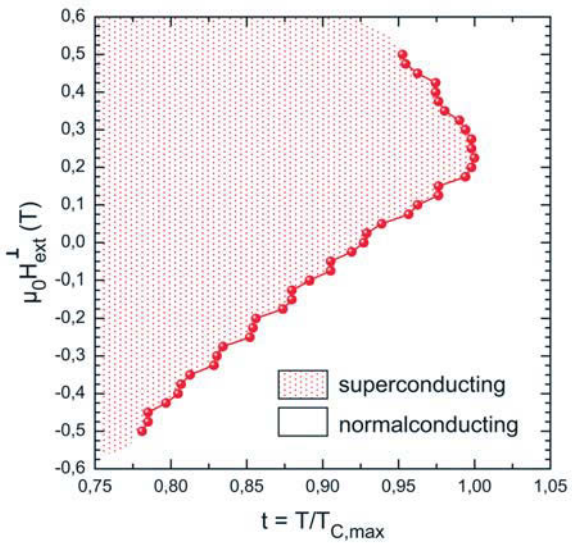

Fig. 3: Oscillatory behavior of the phase boundary for a polished Nb/FePt hybrid sample.

The compensation of the out-of-plane stray-field arising from the FePt islands by an external magnetic field (H_{Comp} applied normal to the sample surface) leads to an enhancement of the critical temperature of the heterostructure and has been described first by M. Lange et al. [9]. Highly coercive FePt $L1_0$ islands demonstrate successfully the ability to tune this effect via the strength of the stray field, which is accompanied by an enormous shift of the superconducting phase in the phase diagram of the hybrid (Fig. 2).
A detailed examination of the shape of the phase boundary (Fig. 2) in the vicinity of the maximum critical temperature shows the typical temperature dependence of a superconductor in parallel field: $H_{c2} - H_{Comp} \sim (1-t)^{0.5}$ with the reduced temperature $t = T/T_C$. This is plausible due to the fact, that at the applied compensation field the out-of-plane stray-field components are cancelled to zero, and a strong influence of in-plane stray-field components becomes crucial.

The oscillatory behavior of the phase boundary, $T_C(H)$, is known to be a manifestation of the fluxoid quantization and referred to as Little-Parks effect [10-12]. Originally observed in a superconducting cylinder, Little-Parks oscillations also appear in mesoscopic samples due to a spatially inhomogeneous order parameter [13]. The heterostructure consists of a superconducting network with a spatially modulated magnetic field pattern and, therefore, can be regarded as a possible application of the Hofstadter problem [14,15], which arises from the formal analogy between the linearized Ginzburg Landau equation and the Schrödinger equation. The oscillations in the phase boundary seen in Fig. 3 may therefore arise from the hopping of whole bundles of vortices.

References

[1] J. I. Martín, M. Vélez, J. Nogués, I. K. Schuller, Phys. Rev. Lett. 79 (1997) 1929
[2] M. Zheng, et. al., Appl. Phys. Lett. 79 (2001) 2606
[3] R. K. Dumas, C.-P. Li, I. V. Roshchin, I. K. Schuller, K. Liu, Phys. Rev. B 75 (2007) 134405
[4] Y. Otani, B. Pannetier, J. P. Nozières, D. Givord, J. Magn. Magn. Mat. 126 (1993) 622
[5] D. J. Morgan, J. B. Ketterson, Phys. Rev. Lett. 80 (1998) 2614
[6] S. Haindl, M. Weisheit, T. Thersleff, L. Schultz, B. Holzapfel, SUST 21 (2008) 045017
[7] T. Shapoval, S. Engel, M. Gründlich, D. Meier, E. Backen, V. Neu, B. Holzapfel, L. Schultz, SUST 21 (2008) 105015
[8] M. Weisheit, L. Schultz, S. Fähler, J. Appl. Phys. 95 (2004) 7489
[9] M. Lange, M. J. Van Bael, V. V. Moshchalkov, Phys. Rev. B 68 (2003) 174522
[10] W. A. Little, R. D. Parks, Phys. Rev. Lett. 9 (1962) 9
[11] R. D. Parks, W. A. Little, Phys. Rev. 133 (1964) A97
[12] M. Tinkham, Phys. Rev. 129 (1963) 2413
[13] V. V. Moshchalkov et al., Physica Scripta T55 (1994) 168
[14] D. R. Hofstadter, Phys. Rev. B 14 (1976) 2239
[15] Y. Iye, E. Kuramochi, M. Hara, A. Endo, S. Katsumoto, Phys. Rev. B 70 (2004) 144524

Cooperation Dept. de Fisica, Univ. Federal de Pernambuco, Recife, Brazil

Funded by SFB 463 (A4)

The optical hallmark of frustration in magnets with small exchange integrals

S.-L. Drechsler, J. Málek[1], S. Nishimoto, R. Kuzian[2], U. Nitzsche, H. Rosner[3], H. Eschrig

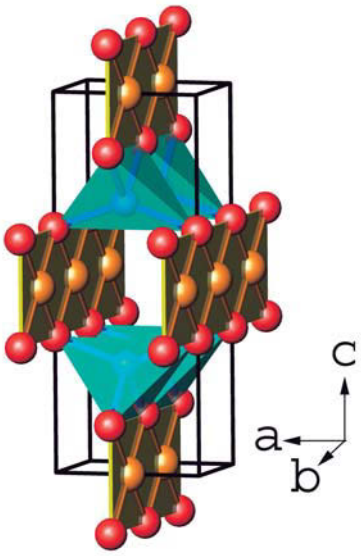

Fig. 1: Lattice structure of a typical edge-shared chain cuprate: Li_2CuO_2 -- Cu: orange balls, O: red balls, Li: centers of the blue tetrahedra. The magnetic moments reside mainly on Cu sites. The main exchange path given by J_1 (NN interaction) and J_2 (NNN interaction) is along the brown CuO_2-chains running along the **b**-axis. The edge-sharing occurs at two O sites in between two NN Cu sites.

It is always a special, intriguing event in science when studies belonging to two, at first glance seemingly almost independent branches of science, come together, in particular, when *high*-energy physics meets *low*-energy physics. Such a situation often provides new insights into complex phenomena and opens new possibilities to resolve long-standing puzzles by giving sharp and clear answers on subtle questions. Here we report on rigorous theoretical predictions [1] concerning the somewhat unexpected interplay of charge response as seen in optical properties at frequencies $\hbar\omega \geq 2$ eV on the one hand with the magnetic nature of the ground state in highly frustrated and strongly correlated edge-shared chain cuprates [2,3] (see Fig. 1) which depends sensitively on the ratio of the main exchange integrals being an order of magnitude smaller (10 to 20 meV), only, on the other hand. As a particular result we arrive at a strongly temperature and magnetic field dependent optical conductivity $\sigma(\omega)$ [see Fig. 2], if the system under consideration is located in the vicinity of a quantum critical point between spiral and ferromagnetic in-chain ordering. Frequently performed measurements at about 300 K can be rather misleading when interpreted in terms of standard calculations being valid for $T = 0$, only.

To illustrate our approach we investigated in detail CuO_2-chains described by Cu_nO_{2n+2} -clusters with $6 \geq n$ by means of exact diagonalizations (ED) at arbitrary temperature T. To exclude artificial finite size effects we studied also longer clusters by means of the density matrix renormalization group technique (DMRG) at $T = 0$ with $16 \geq n$. Both types of calculations we performed in terms of a five-band Cu $3d$ O$2p$ HUBBARD model in order to take into account properly the strong correlation at Cu^{2+} sites bearing mainly the magnetically active $s = 1/2$ quantum spins. Thereby we considered two parameter sets M1 and M2 which differ only slightly each from the other by slightly different Cu-O onsite energies which, however, result in magnetically different ground states with a singlet or low-spin ("spiral-like") ground state for M1 and a high-spin ('ferromagnetic-like") ground state for M2. In case of the spiral set M1 the optical absorption near 2.7 eV strongly decreases with increasing temperature and at room temperature only a weak shoulder does remain as shown in Fig. 2. This absorption corresponds to the excitation of the so-called ZHANG-RICE singlet (ZRS) well-known in the cuprate physics, where a Cu hole is transferred to one of the neighboring CuO_4-plaquettes. There, it will reside mainly on O $2p$ orbitals lowering its energy due to strong antiferromagnetic interaction with the Cu-spin located there. In contrast, for the case described by the ferromagnetic set M2 there is no ZRS excitation at $T = 0$ and instead only a ZHANG-RICE triplet (ZRT) can be excited slightly below 4 eV. At finite temperature some of the excited low

Fig. 2: Temperature dependent optical conductivity at zero magnetic field H = 0 (left and middle). Field effect (right) within the typical energy regions for ZHANG-RICE singlet (ZRS) and ZHANG-RICE triplet (ZRT) excitations for open chain clusters within a low spin spiral-type (M1) and a high-spin ferromagnetic ground state (M2). '$T = \infty$' means $k_BT >> |J_i|$ for any of the exchange integrals, but $\hbar\omega \geq 10^4$ K $>> k_BT$ is still fulfilled.

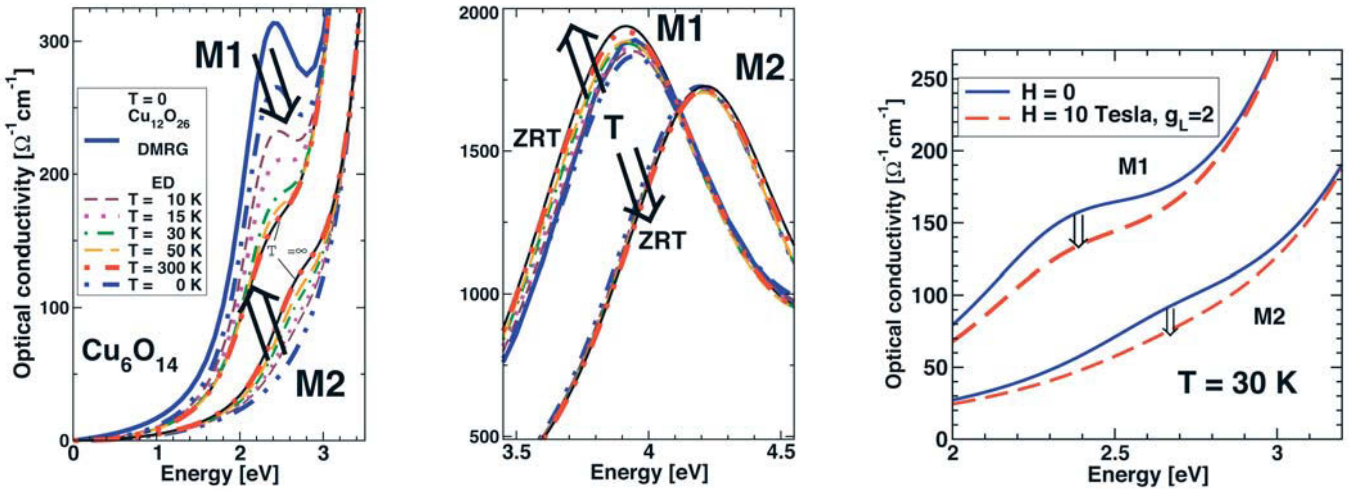

spin-states become thermally populated and a finite probability for the excitation of a ZRS-state does occur. At very high temperature the shape of $\sigma(\omega)$ in the ZRS region become similarly broadened for both ground states in showing only a weak shoulder. Hence, the nature of the ground state can be elucidated only by measurements at sufficiently lower temperatures.

This corresponding *opposite* behavior and the obtained different ground states become more clear mapping our five-band HUBBARD model onto a J_1-J_2 HEISENBERG model where J_1 describes the exchange between nearest neighbors (NN) and J_2 stands for the next-nearest neighbor (NNN) exchange in chain direction. Set M1 corresponds to $\alpha = -J_2/J_1 > \alpha_c = 1/4$ in terms of this projected spin model while the opposite inequality holds for set M2. In other words optical (high-energy) measurements and sufficiently low temperatures allow to discard one of these competing ground states for a real system in the vicinity of the quantum critical point given here approximately by a single parameter α_c.

Since highly frustrated quantum spin systems form one of the hot areas in solid state science, the optical measurements proposed here provide a relatively simple classification of new materials. Anyhow, our method can also be applied to unfrustrated antiferromagnets with unshared "isolated" CuO_4-plaquettes with small exchange integrals $J_1 \equiv J < 300$ K [4]. Here, the measurement of the partially integrated optical conductivity around the ZRS-peak can be used to extract J. However, if its T-dependence doesn't fit that of the NN-spin-spin correlation function of the simple antiferromagnetic spin-1/2 HEISENBERG chain, the presence of other non-negligible contributions such as NNN-exchange, various anisotropic in-chain, or generally of inter-chain exchange interactions can be concluded.

Whereas traditional methods like the spin-wave analysis of inelastic neutron scattering data are only possible in the magnetically ordered phase at low temperature, the proposed temperature dependent optical tool works at higher T and will help to achieve further refinement of the leading exchange interactions in this fascinating class of frustrated highly correlated materials. On the other hand, the precise knowledge of these exchange integrals, especially a relatively large *ferromagnetic* J_1 provides sensitive constraints on the only approximately known intersite COULOMB interactions. This concerns, first of all, the *ferromagnetic* direct Cu-O exchange integral $K_{pd} \approx 80$ meV which we found much more important than the contribution from the famous ferromagnetic HUND's rule coupling (HRC) on the two O orbitals involved at each sharing oxygen. This HRC, however, was the starting point for the celebrated text-book GOODENOUGH-KANAMORI rule for transition metal oxides and halogenides, in particular for cuprates with a nearly 90° Cu-O-Cu bond angle as in the edge-shared chain compounds mentioned above (see Fig. 1).

In addition, also our LSDA+U (local spin density approximation) calculations within density functional theory may benefit from a refinement of J_1 by adjusting the Coulomb repulsion parameter U. Vice versa, having a proper value for U, allows us to predict quantitatively correct other small exchange integrals such as the interchain couplings relevant for the magnetic ordering at low-temperature which are very difficult to extract experimentally or to obtain from other theoretical studies.

References

[1] J. Málek *et al.*, Phys. Rev. B ***78,*** 060508(R) (2008).
[2] S.-L. Drechsler, *et al.*, J. of Mag. & Mag. Mat. **316** (2007) 306, J. Phys.-Cond. **19**, 145230 (2007),
[3] S.-L. Drechsler, *et al.*, Phys. Rev. Lett. **98,** (2007) 077202.
[4] R. Kuzian *et al.*, in preparation.

Cooperation [3]MPI-CPFS Dresden, TU Magdeburg, Univ. Wuppertal, [1]Inst. of Phys. AS-CR, Prague, Czech Rep.; B. Gurion Univ. Beer Sheva, Israel; [2]Inst. f. Probl. of Materials Sciences, Kiev, Ukraine; Inst. f. Low-Temp. Physics & Engineering., Kharkov, Ukraine.
Funded by German-Israeli Foundation (GIF), DFG, Emmy-Noether-Programm

Control of martensitic transition and variant distribution in freestanding epitaxial Ni-Mn-Ga films by magnetic fields

S. Fähler, M. Thomas, O. Heczko, J. Buschbeck, Y. W. Lai, S. Kaufmann, J. McCord, L. Schultz

Structural and microstructural changes during the martensitic transformation from a cubic austenite to a tetragonal martensite phase in freestanding epitaxial Ni-Mn-Ga films are analyzed. It is demonstrated that the low energy input possible by a magnetic field is sufficient to control both, structure and microstructure. The relevant energies for resulting two different actuation modes are compared with the stray field energy of a thin film. When cooling the ferromagnetic film through the martensitic instability, the magneto-static interactions disfavor variants with an out-of-plane easy axis of magnetization and an unequal variant distribution develops. Analogous to a two way shape memory effect, this results in a significant shrinkage of the lateral film area, but does not require any training. Since no external magnetic field is needed for the occurrence of this effect, thermally actuated monolithic microactuators based on magnetic shape memory films are applicable.

Since the discovery of Magnetic Shape Memory (MSM) alloys [1], high strains close to 10 % have been obtained in Ni-Mn-Ga single crystals [2], leading to intense research on new preparation routes as foam [3], fibers [4] and polycrystals [5]. Furthermore, MSM alloys are martensitic as well as ferromagnetic and, through different combinations of these two ferroic properties, several different actuation principles have been identified. One actuation mode uses the coupling of crystal structure and spontaneous magnetization. In a magnetic field, the phase with the higher magnetic moment is energetically favored, allowing a shift of the martensitic transformation temperature T_M [6,7]. As in well trained thermal shape memory alloys, this Magnetically Induced Martensite (MIM) can be used for actuation in the vicinity of the martensitic phase transition temperature [8]. The highest strains, however, are obtained in bulk single crystals within the martensitic state by Magnetically Induced Reorientation (MIR), also called magnetic shape memory effect. For this, the difference in energy, when aligning the magnetization in different crystal directions, has to be considered. This is described by the magnetocrystalline anisotropy energy [9]. This coupling of crystallographic and magnetic directions allows the modification of the martensitic microstructure. A magnetic field can be used to move twin boundaries, connecting neighboring martensitic twin variants, in a way to increase the fraction of those martensitic variants having the energetically favored easy magnetization axis parallel to the external field. This reorientation results in a large length change, as the lattice constants of a martensitic unit cell are different.

Here we develop the energetic models for MIM and MIR in thin films on a phenomenological level. It is shown that for thin MSM films an alternate thermal actuation mode is possible, which requires neither an external field nor training. Thin MSM films are in particular interesting for microactuator applications, as the high strain eliminates the complication of additional levers. Epitaxial films [10, 11] are considered the most promising since the highest strain to date has been obtained in bulk single crystals. Recently, we reported MIR in orthorhombic, epitaxial Ni-Mn-Ga films grown on MgO(100) [12] and $SrTiO_3$(100) [13], although the macroscopic extension was constrained by the substrate. The low blocking stress on the order of MPa reported for MIR [14] requires that, for macroscopic actuation, the films have to be released from the adjacent rigid substrate. Here, we used an approach to obtain freestanding epitaxial films by growing them on water soluble NaCl substrates having the (100) orientation by DC sputtering.

The phase formation in the as-deposited and the freestanding film was analyzed by XRD measurements in the Bragg-Brentano geometry using Co K_α radiation (Fig. 1). With the release from the substrate, the intense and sharp NaCl reflection peak vanishes. The

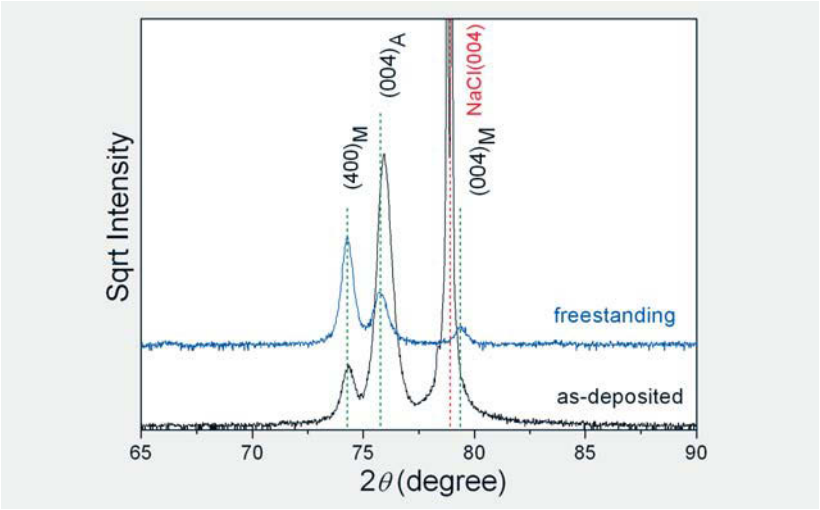

Fig. 1: X-ray measurements in Bragg-Brentano geometry in the as-deposited state (black) and a freestanding film (blue). Reflex positions expected from bulk single crystals for Ni-Mn-Ga (green) and (004) NaCl (red) are marked by dotted lines.

measurements were performed at a temperature of 27°C where the austenite and martensite states coexist. The diffraction pattern can be indexed with one $(004)_A$ austenite reflection ($a_A = 0.583$ nm) and two $(400)_M$, $(004)_M$ reflections of a tetragonal martensite ($a_M = 0.593$ nm, $c_M = 0.560$ nm, $c/a = 0.94$). The obtained values are in good agreement with that of 5M bulk single crystals, where the c-axis is the magnetic easy axis [15]. The observation of only {00l} reflections suggests epitaxial growth which was confirmed by pole figure measurements (not shown).

Dissolving the NaCl substrate in water changes reflex intensities considerably. The decreased intensity of the austenite peak suggests that the volume fraction of the austenite is reduced when the film is released from the substrate. An apparent feature of the free standing state is the low intensity ratio of 0.05 for the $(004)_M/(400)_M$ reflections. This suggests that not all variants occur with the same probability as in stress-free bulk single crystals, but variants with the c-axis pointing out of the sample plane are significantly less probable.

To determine the relative fraction of the in-plane variants and the magneto-crystalline anisotropy, magnetization curves of the freestanding film were measured in the austenite and in the martensite state using a vibration sample magnetometer (VSM) (Fig. 2). In the high temperature austenite phase, the magnetization curve is step-like with low coercivity, which is characteristic for a low magnetocrystalline anisotropy film. When cooling to the martensite state, the shape of the hysteresis loop changes and a significant increase of coercivity is observed. Additionally, the saturation polarization J (at 2 T) increases by about 10% to about 0.7 T. Two distinct slopes in the magnetization curve indicate that the film is in a multivariant state. At low fields, the magnetization change along the magnetically easy [001] axis is indicated by a sharp increase of magnetization with field. With higher external magnetic fields, a lower slope is observed, originating from coherent rotation of magnetization within the variants having their easy axis aligned about perpendicular to the external field. Assuming a superposition of the independent magnetization response from both variants, this allows the determination of the anisotropy field from the sharp change of slope towards saturation [16] to $\mu_0 H_a = 0.58$ T giving a magnetocrystalline anisotropy constant of $K_u = 1.8 \cdot 10^5$ J/m^3. This value directly gives the maximum energy input for MIR, which can be used to overcome the twinning stress of twin boundary movement. This movement reorients variants from their hard axis towards the easy axis (with respect to the magnetic field), which typically results in characteristic jumps within the polarization curve [12, 13]. No indication of such discontinuity and, thus, MIR is observed in our measurements.

Under the assumption of a superposition of easy and hard axis behavior from the magnetization loops, the fraction of variants with their easy axis along the field direction can be estimated by extrapolating the hard axis magnetization loop to zero fields (see

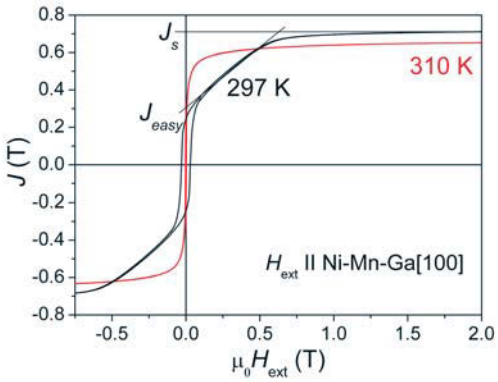

Fig. 2: In-plane magnetization curves of the Ni-Mn-Ga film along a [100] direction. In the martensitic state at room temperature (black) a high magneto-crystalline anisotropy is observed whereas there is a low magneto-crystalline anisotropy in the austenite state (red) at 310 K. The extrapolation to determine the volume fraction of the variants with their easy axis in this direction is sketched.

Fig. 2). A fraction of $J_{easy}/J_S = 0.46$ is obtained. This value is close to 0.5, which is expected when all variants have their easy axis within the film plane and are distributed evenly along both equivalent in-plane directions. This even distribution of variants occurs due to the fourfold substrate symmetry and was confirmed by repeating the in-plane measurement after rotating the sample by 90°. This gives an overall fraction of 2 x 0.46 variants having their easy axis aligned in-plane, leaving a small fraction of 0.08 of variant having their easy axis perpendicular to the film plane.

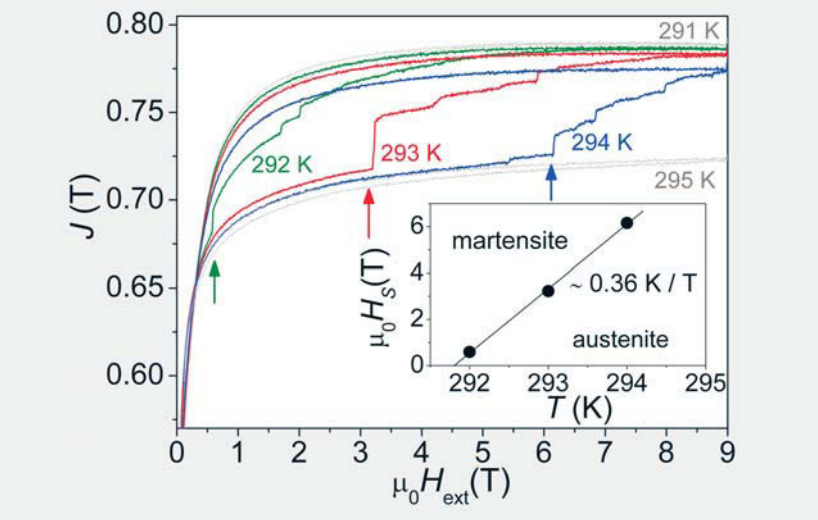

Fig. 3: Details of the polarization curves at high fields measured at different temperatures in the vicinity of the martensitic transformation. The step-like increase in the polarization loops is used to identify the transition field H_S from the austenite to the martensite phase. The inset shows the temperature dependence of this martensitic start field.

The influence of an external field on the martensitic phase transformation is summarized in Fig. 3. A magnetic field stabilizes the martensite phase having a higher magnetization compared to austenite. Hence the 10% increase of saturation polarization of the martensite J_M compared to austenite J_A (Fig. 2) allows to induce the martensitic transformation by a magnetic field. This difference in saturation polarization in addition allows identifying the jumps in magnetization in the vicinity of the martensitic transformation temperature (marked by arrows in Fig. 3) as a Magnetically Induced Martensite (MIM) transition. For each temperature, the transformation starts with a well defined jump at a transition field H_S which is used to construct a field-temperature phase diagram (inset in Fig. 3). From the slope, the shift of the transition temperature in the external magnetic field can be extracted as $dT/dH = 0.36\ K/T$. Following this thermodynamic approach [6], the energy input for MIM at each temperature can be numerically calculated from the measured $J(H)$, which differs for both phases, by $\int_0^{Hs} \Delta J dH$. The energy input required for MIM strongly increases with temperature (e. g. the above integral gives $0.78 \times 10^5\ J/m^3$ at 292 K and $1.92 \times 10^5\ J/m^3$ at 293 K).

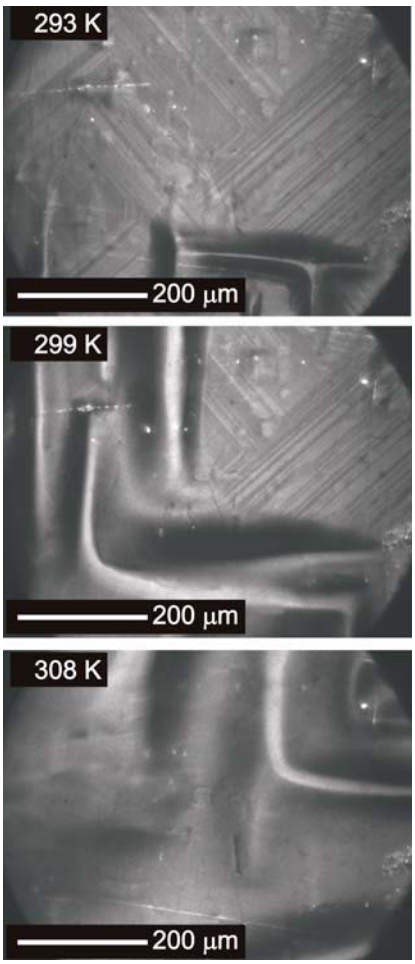

Fig. 4: (a)-(c) Martensitic transformation of the freestanding Ni-Mn-Ga film. The film was heated from 273 K up to 308 K.

The martensitic transformation of the freestanding film was investigated locally using a temperature dependent optical polarization microscopy without the application of an external field. A sequence of the three key images is shown in Fig. 4 a-c. With the transformation to austenite, the twinned microstructure gradually disappears and the film buckles even more. At 308 K, the transformation is finished, which is in agreement with the temperature dependent magnetization measurements presented before. During the cooling procedure, thermal hysteresis requires cooling to 289 K in order to obtain a fully martensitic state. The twin pattern is similar but not identical to the variant distribution at the beginning of the heating-cooling cycle. The observed film's mechanical contraction when transforming into the martensitic state is due to the non-equal distribution of variants, with a low fraction of c-variants having their short c-axis aligned perpendicular to the film plane. This direction is energetically unfavorable, as c-variants have their easy magnetization axis perpendicular to the substrate, resulting in an unfavorable increase of magnetostatic energy compared to variants with their easy axis in-plane. The upper limit of the magnetic stray field energy can be estimated for a

single c-variant and single domain state by $1/2 \times 1/\mu_0 \times J_S^2 = 1.9 \times 10^5\ J/m^3$[9]. The formation of magnetic multi-domain states might further reduce the energy of the system. From domain theory [17], a possible reduction of total energy to 0.5×10^5 J/m^3 is calculated. In addition, MSM films can adapt their variant distribution, a degree of freedom not possible in regular magnetic films with a perpendicularly aligned anisotropy axis. There is no stray field energy at all when variants with a perpendicular c-axis are absent. For this case, the shrinkage can be derived from the differences in lattice parameters. As an upper limit for the relative length change, one obtains $\Delta l/l = 1 - 1/2(a_M + c_M)/a_A = 1.1\,\%$, a significant higher value than the length change of 0.2 % calculated from the different volume of austenite and martensite.

In conclusion, the relevant energies for two different actuation modes of MSM alloys had been analyzed. Contrary to bulk, these films exhibit an unequal variant distribution after cooling through the martensitic instability though no external field is applied. A low fraction of variants with the c-axis perpendicular to the film plane is observed by XRD, magnetometry and polarized optical microscopy. Due to its stray field energy, this variant orientation is energetically unfavorable, resulting in a film contraction when transforming to the martensite. This behavior is similar to a two-way shape memory effect but can be obtained without any mechanical training, which is difficult to achieve for monolithic microsystem. Hence this effect will allow for further miniaturisation of thermally activated MSM microactuators to the sub micron scale.

References

[1] K. Ullakko et al., Appl. Phys. Lett. **69(13)** (1996) 1966
[2] A. Sozinov et al. Appl. Phys. Lett. **80(10)** (2002) 1746
[3] Y. Boonyongmaneerat et al., Phys. Rev. Lett. **99** (2007) 247201
[4] N. Scheerbaum et al., New J. of Phys. **10** (2008) 073002
[5] U. Gaitzsch et al., Acta Mat. (2008) in press.
[6] A. N. Vasil'ev et al., Physics Uspekhi **46(6)** (2003) 559
[7] A. A. Cherechukin et al., Phys. Lett. A **291** (2001) 175
[8] R. Kainuma et al., Nature **439** (2006) 957
[9] R. C. O'Handley, *Modern Magnetic Materials* (John Wiley & Sons, Inc, New York, 2000).
[10] J. W. Dong et al., Appl. Phys. Lett. **75(10)** (1999) 1443
[11] G. Jakob et al., Phys. Rev. B **76(17)** (2007) 174407
[12] M. Thomas et al., New J. Phys. **10** (2008) 023040
[13] O. Heczko et al., Appl. Phys. Lett. **92** (2008) 072502
[14] H.E. Karaca et al., Acta. Mater. **54(1)** (2006) 233
[15] N. Lanska et al., J. Appl. Phys. **95** (2004) 8074
[16] O. Heczko et al., J. Appl. Phys. **91** (2002) 8228
[17] A. Hubert and S. Schäfer, *Magnetic Domains*

Cooperation Academy of Science, Prague

Funded by DFG (SPP1239, www.MagneticShape.de)

Atomically resolved surface diffusion during inter-particle sintering

U. Wiesenhütter, D. Pohl, E. Mohn, B. Rellinghaus, L. Schultz

The electron-beam induced sintering of FePt nanoparticles from the gas phase is investigated by delocalisation-free HR-TEM in a newly installed aberration-corrected microscope. The obtained HR-TEM images provide evidence for the assumption that the mechanism essential for the inter-particle coalescence is surface diffusion of atoms. The material transport along the particle surface towards the newly forming sintering neck can be followed on the atomic level.

The thermodynamic equilibrium crystal structure of nanoparticles is known to depend significantly on the particle size. This is due to the fact that upon decreasing the particle size, the surface-to-volume ratio and in turn the significance of the *surface* free energy for the total energy of the particle is increased. As a consequence, many materials that assume face-centered cubic (fcc) structures in their bulk form, become multiply twinned icosahedra or decahedra terminated by low-energy (111) facets upon reducing their size into the nanometer regime (see, e.g., [1-2]).

Besides this change in the ground state properties of nanoparticles with respect to their bulk counterparts, kinetic aspects are often equally important. E.g., nanoparticles grown by gas-phase based techniques grow by both (homogeneous) condensation and subsequent inter-particle collisions and coalescence, i.e., sintering. Hence, in order to fully understand and control the particle growth process and in turn the particles' physical properties, a thorough understanding of the sintering mechanisms involved in the growth process is mandatory. Recent investigations on the in-flight sintering of metallic nanoparticles from the gas phase have revealed activation energies E_A associated with the inter-particle coalescence which clearly indicate that surface and/or grain boundary diffusion is the relevant mechanism in the sintering of "air-born", i.e., free particles. For Ni nanoparticles this energy was determined from transmission electron microscopy (TEM) studies to be $E_A = 0.62$ eV/atom which is in good agreement with the mean activation energy for surface diffusion in Ni [3]. Similar results are obtained for gas-phase prepared stoichiometric FePt nanoparticles [4] and recently for intermetallic CuAu particles in post-deposition annealing experiments [5]. The hereby implied scenario of inter-particle sintering via surface diffusion as schematically illustrated in Fig.1 is corroborated by theoretical investigations utilizing molecular dynamics simulations.

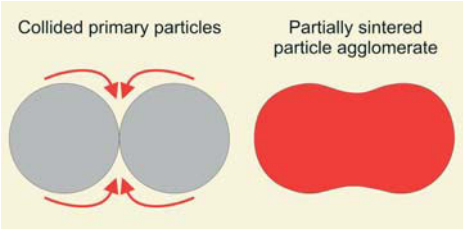

Fig. 1: Schematic representation of the sintering of two spherical particles. Surface diffusion provides the mandatory materials flow from the primary particles (left) into to the sintering neck of the forming particle agglomerate (right).

Although these experimental findings provide clear - though indirect - indications for surface diffusion as the essential sintering mechanism, *direct* experimental proof for the relevance of this mechanism is still lacking. One of the major obstacles in providing such evidence, e.g. by high resolution TEM (HR-TEM), arises from the fact that conventional HR-TEM does not allow for delocalisation-free imaging of individual atoms or atomic columns. As a consequence, atomically resolved imaging of interfaces and surfaces requires the acquisition of focus series which, however, are time consuming and thus do not provide the required temporal resolution for diffusion studies. This contrast delocalisation inherent to previous generation transmission electron microscopes arises from the aberrations introduced by their electromagnetic lenses. We have therefore used a recently installed *FEI Titan^3 80-300* microscope equipped with a monochromator and a so-called C_S corrector (*CEOS GmbH, Heidelberg*) to study the inter-particle sintering of deposited FePt nanoparticles. The corrector element allows for a compensation of the major lens aberrations (up to 3rd order aberrations). E.g., the coefficient of the most influential spherical aberration, C_S or C_3, can be reduced by three orders of

magnitude with respect to values achievable in an uncorrected microscope [6-7]. This way, the contrast delocalisation can be reduced to values basically within the diameter of a single atomic column.

FePt nanoparticles were prepared by inert gas condensation and subsequent in-flight optical heating [8]. Unlike in colloidal chemistry based preparation methods where the particles are to be terminated by organic molecules for steric separation, gas-phase based preparation provides the advantage that the particle surfaces remain uncovered and clean – a mandatory prerequisite to be fulfilled in order to study surface-related phenomena. The particles are deposited onto commercially available 10 nm thin amorphous carbon films supported by copper grids (commercial TEM grids).

Fig. 2 shows two adjacent FePt particles both of which are icosahedra with one of their 2-fold symmetry axes close to parallel to the incident electron beam. During the exposure to the imaging electron beam the particles are moderately heated and as a consequence, inter-particle coalescence is stimulated within the microscope. Starting with the image in Fig. 2, a series of five subsequent HRTEM images was acquired. Fig. 3 shows enlarged details of a section of the right particle which is close to the inter-particle connection as marked with a dashed white square in Fig. 2. Owing to the actual adjustment of the defocus and C_S the atoms (or atomic columns) appear dark in these images. In order to guide the eyes of the reader to the very particle surface, the less interesting central part of the particle is covered with a white shade. The time elapsed after taking the first image (cf. Fig. 2) is denoted in each individual micrograph. In the first 50 seconds, atoms on top of the right particle facet are successively shuffled to the left in order to firstly complete the previously incomplete surface atomic layer (on the left facet). Once being completed, all but the right corner atom (marked with a yellow circle in the image at t = 66 s) in this layer of surface atoms have reached the highest possible coordination and thus a low-energy configuration. Consequently, as can be seen from a comparison of the images obtained at t = 66 s and t = 84 s, this corner atom is the first to leave the layer in order to continue the sintering process. It is to be emphasised here that all materials transport observed is directed towards the newly forming sintering neck between the primary particles, i.e., towards the left of the detail images.

These results thus precisely confirm the picture of inter-particle coalescence via surface diffusion in close resemblance to the classical picture of coalescing spherical droplets. Contrasting this picture is the fact that the general assumption of surface-diffusion mediated materials transport towards the sintering neck also holds for highly facetted solid crystalline particles. It should be mentioned here that although surface atoms may exhibit a (reduced) coordination which differs from the bulk or particle core, surface melting which is also discussed as a possible sintering mechanism was never observed for this case of electron bean induced coalescence.

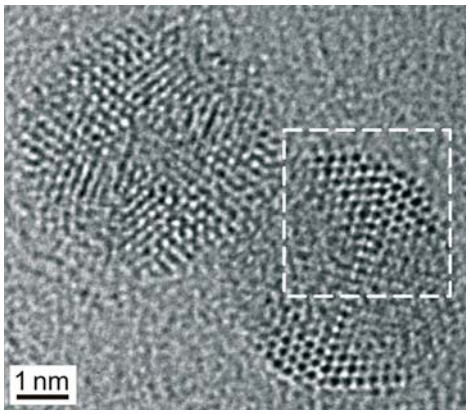

Fig. 2: Delocalisation-free HR-TEM micrograph showing two adjacent icosahedral FePt nanoparticles supported by a thin amorphous amorphous carbon film.

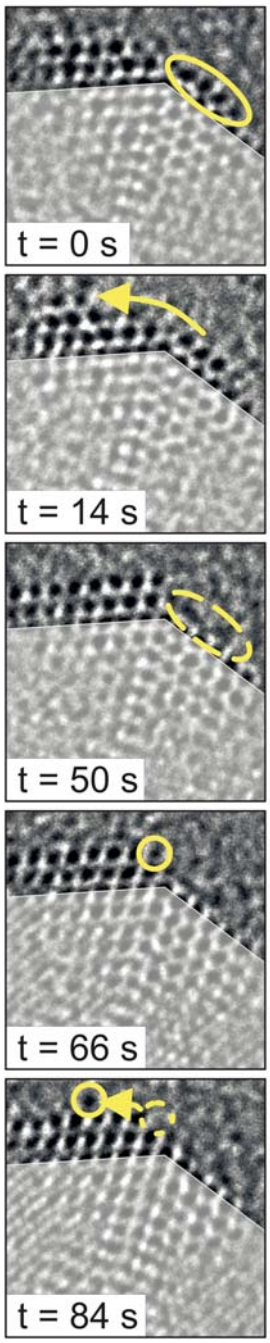

Fig. 3: Enlarged detail views of the section marked with a dashed white square in Fig. 2 at different times. The transparent white areas cover all but the surface region of the right FePt icosahedron. The yellow ovals and arrows indicate the material transport on the atomic level.

References

[1] S. Stappert el al., J. Cryst. Growth 252 (2003) 440.
[2] T.T. Järvi et al., Europhys. Lett. (2009), in print.
[3] S. Tsyganov et al., Phys. Rev. B 75 (2007) 045421.
[4] S. Stappert, PhD thesis, Gerhard-Mercator-Universität Duisburg, 2003.
[5] D. Pohl et al., unpublished (2008).
[6] M. Haider et al., Nature 392 (1998) 768.
[7] S. Uhlemann et al., Ultramicroscopy 72 (1998) 109.
[8] B. Rellinghaus et al., IEEE Trans. Magn. 42 (2006) 3048.

Exploring the role of oxygen in carbon nanotube growth

M. H. Rümmeli, F. Schäffel, M. Bystrejewski, R. Schönfelder, A. Bachmatiuk, T. Gemming, R. Rellinghaus, L. Schultz, B. Büchner

The continued success of anything digital depends critically on the swift improvement in chip density. However physical constraints require new approaches to those currently employed. Carbon nanotubes show significant promise as an alternative, which once we are able to "tune" will offer the opportunity to build fantastically small devices. However, the realisation of this promise requires a significant improvement in understanding and controlling the growth of carbon nanotubes at the atomic level.

The multifaceted promise that carbon nanotubes (CNT) bring is enormous, potentially offering entirely new tools and capabilities. However, in order to fully exploit their potential an improved understanding of their nucleation and growth mechanisms is required. Due to the success of catalyst particles for CNT formation, most investigations on their synthesis focus primarily on the catalyst particles. Generally, it is argued that transition metals are required as catalysts for CNT nucleation ***and*** growth. *In situ* HREM studies confirm this can occur for various transition metals. In the case of chemical vapor deposition (CVD) it is also argued that these catalysts are catalytically active in the decomposition of the hydrocarbon feedstock. However, there are an ever-increasing number of works that show this picture is incomplete. For example, studies have shown the potential of various novel metallic catalysts whilst others show CNT formation from non-metal catalysts. Notably, in many studies, oxygen appears to play an important role in CNT growth. In laser ablation it has been shown that oxygen activates metals as catalysts for CNT synthesis and recent CVD studies confirm oxygen-based activation for non-standard metal catalysts by heating in air prior to synthesis. The preheating air treatment is also key to the CVD synthesis of CNT using semiconductor catalyst particles. In the case of semiconducting particles for the synthesis of CNT on SiC at high temperatures, CNT are only obtained with nominal amounts of oxygen in high vacuum. Oxygen chemically bound to CNT is shown to be involved in the growth process. Further, metal free templated synthesis of CNT is also possible when using porous Al_2O_3 structures. CNT can even be synthesized without catalyst particles in oxy-fuel flames when sufficient oxygen is provided. In addition, oxides typically used as catalyst supports in CNT based CVD synthesis can themselves form graphitic carbon layers.

Here at the IFW we are conducting studies to better comprehend the role of oxygen in carbon nanotubes synthesis. We do this using various synthesis routes, namely laser evaporation and supported catalyst CVD. In each case, hints, that oxygen and/or oxides play a key role seem to surface from the data.

We begin with an original study in laser evaporation in which nominal amounts of water vapour are introduced into the reaction. The use of steam can efficiently etch amorphous carbon and open the ends of single and multi-walled carbon nanotubes. A well-known example of its use is the synthesis route developed by Hata et al. [1]. They demonstrated that small additions of water vapor (50-290 ppm) to the buffer gas during the chemical vapor deposition (CVD) of supported catalysts yields super-dense and vertically aligned ultra-long SWNTs. They claim this technique leads to SWNTs purities above 99%. This type of approach can eliminate the need for post-synthesis processing. However, SWNTs fabricated via CVD tend to posses higher structural disorder, large diameter distributions and usually include a fraction of multi-walled carbon nanotubes (MWNTs) as compared to floating catalyst techniques such as the high-pressure carbon monoxide (HiPCO) process or laser evaporation. Detailed TEM studies for all laser ablated samples showed the samples to be comprised of SWNTs bundles, catalyst particles and amorphous carbon. The amount of amorphous carbon was seen to decrease with increasing water content. Although the data suggests that the presence of water in the

laser ablation reaction reduces amorphous C species, caution should be exercised as TEM studies only monitor picogram quantities of the samples. Hence, we conducted additional studies. The absorption spectra of SWNTs typically contains 3 prominent peaks from interband transitions. The first and most intense pair, from semiconducting tubes, are termed the S_{11} and S_{22} transitions. The third, M_{11}, stems from metallic SWNTs. The peak widths correspond to the sample diameter distribution and can be used to determine the mean diameter. We did not observe any shift in any of the peaks with increasing water content (Figure 1a). The mean diameter as determined from the most prominent peak, S_{11}, was 1.26 nm +/- 0.01 nm after correction for exciton effects. The interband peaks sit on a background originating from the π plasmon from carbon species, namely, SWNTs and carbonaceous impurities (Figure 1a - inset). Hence, comparison of the SWNTs interband peaks with the background provides a measure of the purity. Figure 1a highlights the relative increase in yield for two water contents, 3 ppm and 1227 ppm.

Figure 1b shows the quantitative changes in purity (SWNTs relative to amorphous carbon) determined from the areas of the S_{11} peak after normalization and strapping the background. The data shows a non-linear behavior; the relative SWNTs yield increase decays with increasing water content so that by 700 ppm the improved yield is stable. Changes are also observed in the Raman spectroscopic data. The presence of the radial breathing modes in the spectra verifies that the structures are SWNTs (Figure 2a). The diameters in resonance for these samples using the expression $\omega = 223/d_t + 10$ correspond to diameters between 1.18 and 1.27 nm in good agreement with the OAS data. At higher frequencies the D (disorder) mode and G (graphitic) modes are observed. The G peaks (1565-1595 cm^{-1}) arise from (tangential) C-C stretching in the graphene plane and in these samples they are clearly separated which is also a characteristic of SWNTs. Often the quality of SWNTs is defined as a measure of the G/D ratio, since it is argued the intensity of the D mode is activated by defects in the tubes. In these trials the G/D ratio is seen to rapidly improve with small increases of water vapor after which little further improvement is obtained (at ca. 50 ppm). This improved crystallinity shows that the role of water is more than simply the removal of amorphous carbon. The improved G/D ratio (almost 100%), even with very small amounts of H_2O, does not occur in tandem with the reduction of amorphous carbon as shown in the OAS data. Hence, whilst a reduction in amorphous species might contribute to a reduced D mode, the observed difference between the Raman and OAS data highlights a previously undisclosed role for H_2O enhanced SWNTs synthesis.

The Raman spectroscopic data shows a dramatic increase in the G/D ratio for only small quantities of water (up to 50 ppm), after which little further improvement is obtained. The enhanced crystallinity suggests an improved growth process in the reaction. Previous studies of ours in which the role of oxygen and hygrogen where explored in laser evaporation show that both oxygen and hydrogen can activate catalysts, viz. they promote nanotube growth. The role of H in this presented study is probably weak, since H can etch the SWNTs themselves and so increase the D mode. This is contrary to our observations and points to oxygen activating the catalysts [2].

Another study in which catalysts supported on oxides showed the tops of the nanotubes to have capped ends. The roots, despite persistent HREM investigations, showed no CNT roots ***on*** catalyst particles. Indeed, the consistent observation of elongated catalyst particles in the CNT core at an open end or further up the tube, suggest growth occurs on the substrate itself [3].

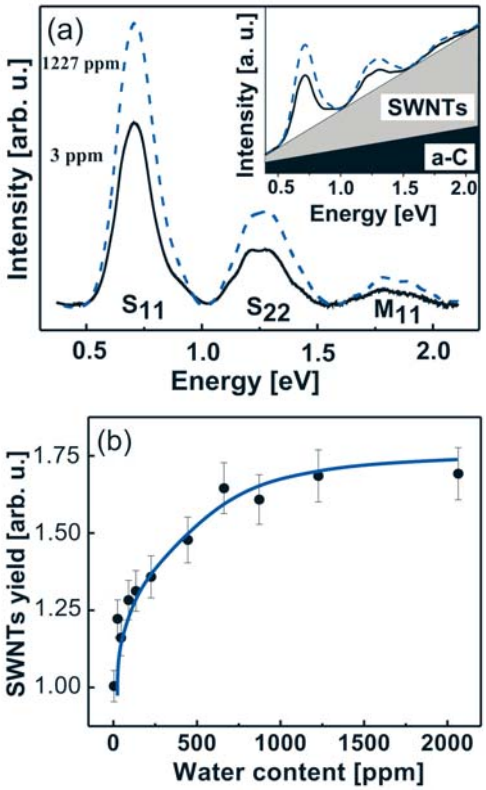

Fig. 1: Panel a: normalized and strapped electronic spectra from SWNTs; *black curve* 3 ppm H_2O, *blue curve* 1227 ppm H_2O. ***Inset:*** normalized electronic spectra sitting on plasmon tail. **Panel b:** SWNTs yield versus H_2O content in laser evaporation reaction. (curve is to guide the eye).

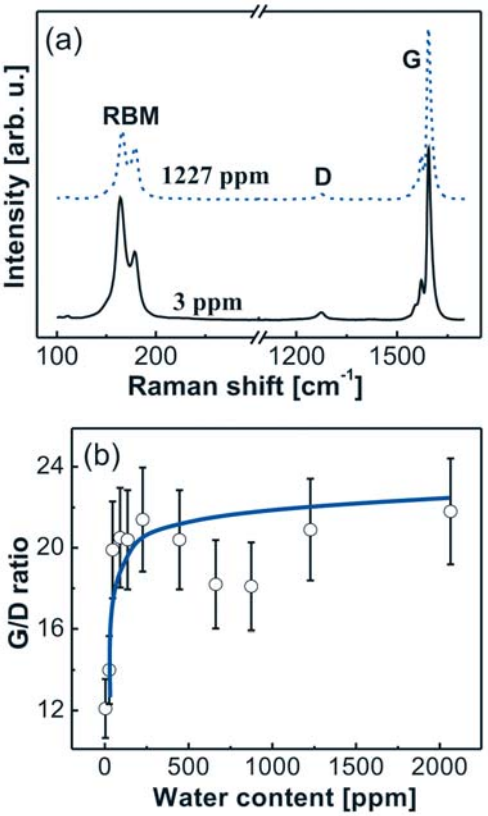

Fig. 2: Panel a: Raman spectra from SWNTs; *black curve* 3 ppm H_2O, *blue curve* 1227 ppm H_2O. ***Inset:*** expanded D modes after normalization to G mode. **Panel b:** G/D ratio versus H_2O content in laser evaporation reaction. (curve is to guide the eye)

This concept is radically different to that in which the catalyst both nucleates and grows CNT and in which the supports role is limited to merely stabilizing the catalyst particle. A catalytically active role by the support in the growth of CNT can also explain the success of oxidizers (H_2O or O_2) in enhancing the growth of substrate based CVD synthesis of CNT. Generally, it is argued that growth enhancement is due to the etching of amorphous carbon species via OH radicals, which helps prevent poisoning of the catalyst particles. Such poisoning of catalyst particles has not been demonstrated and has recently been questioned by Reilly and Whitten [4]. They also point out the contradiction in the argument that an amorphous carbon coating on the catalyst particle halts growth, yet these catalyst particles are able to grow nanotubes (ordered carbon) or even carbon nanofibers (disordered carbon). If however, the oxygen species at the surface of the support are directly involved in the growth of the CNT, then it becomes crucial to maintain oxygen surface species, which will be depleted by hydrogen in the CVD reaction. Inclusion of a supplementary oxidizer in the CVD reaction effectively prevents passivation of the catalytically active oxide (support) surface by re-supplying oxygen. The importance of surface hydroxide groups and surface oxygen in heterogeneous catalysis is well known, as is the catalytic graphitization of carbon by oxides.

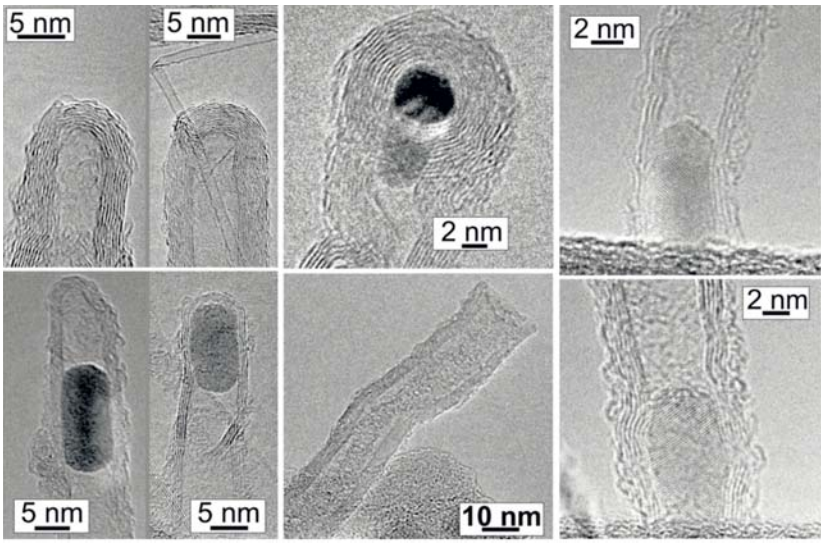

Fig. 3: TEM micrographs of the CNT ends: CNT capped ends with encapsulated (elongated) catalyst particle. CNT ends with compressed catalyst particle within the tube core. Open CNT tubes without catalyst. Root of CNT on the substrate with elongated catalyst particle in the tube core.

Various other studies also indicate an oxygen role in catalyst activation. For example, CVD studies have shown oxygen-based activation of both metallic and non-metallic catalysts, XPS studies on CNT grown from SiC show O chemically bound to C, catalyst free growth of CNT can be obtained in oxy-fuel flames, and oxygen from oxides can also be involved with CNT growth. Importantly, studies with oxygen containing gases show oxygen accelerates graphitization. We postulate that oxygen (and possibly hydrogen) play a role in the growth of the CNT by promoting the graphitisation of carbon at the root of a growing tube. On-going studies are continuing to investigate the growth of carbon nanotubes.

References

[1] Hata K.; Futaba D.N.; Mizuno, K.; Namai, T.; Yumura, M.; Iijima, S. *Science* 2004, *306*, 1362.
[2] Bystrzejewski M. et al., *Chem. Mater.*, 2008, *20*, 6586
[3] Rümmeli M.H. et al., *J. Am. Chem. Soc.*, 2007, *129*, 15773
[4] Reilly, P. T. A.; Whitten, W. B. *Carbon* 2006, *44*, 1653.

Collaboration Oxford Univ., UK; London Metropolitan Univ., UK; Sczcecin Univ., Poland; Warsaw Univ., Poland; Vienna Univ., Austria; US Air Force Research Lab., Ohio, USA; Fisk Univ., Tennessee, USA.
Funded by DFG, EU, Cusanuswerk

A carbon-wrapped nanoscaled thermometer for temperature control in biological environment

A. U. B. Wolter, A. Vyalikh, R. Klingeler, H.-J. Grafe, D. Haase, S. Hampel, M. Ritschel, A. Leonhardt, B. Büchner

One promising field of nanotechnology concerns the diagnostic and therapeutic usage of nanoparticles at the cellular level. One example is the nanoscaled thermometer based on NMR-active material encapsulated in carbon nanotubes. Here, strongly temperature dependent NMR parameters of the filling are exploited for spectroscopic in-situ temperature control. Since many alkali and cuprous halides are known to show pronounced temperature dependencies of NMR parameters, carbon nanotubes have been filled with CuI and the NMR frequency shift and spin-lattice relaxation time were investigated at different temperatures. The experimental data indicate pronounced temperature dependencies of the NMR parameters, thereby giving a proof-of-concept that functionalized carbon nanotubes can be employed for contactless thermometry in biomedical applications.

Promising potential alternatives in cancer therapies emerge from the large field of nanotechnology based on tailored nanosized biocompatible devices, which can be transferred into cells. One therapeutic approach is the so-called "magnetic fluid hyperthermia" (MFH) [1], which applies the fact that a cancer cell-killing effect is caused when a temperature above 41-42 °C is maintained in the target volume. In MFH selective heating of cancerous tissues is achieved by accumulating biofunctionalized superparamagnetic nanoparticles in the tumor followed by their inductive heating caused by the application of an alternating magnetic field. Then, in such a hyperthermia approach accurate control of the tissue temperature is mandatory. Currently, in clinical trials temperature is controlled by a clinician's intervention by placing thermocouples or fiberoptical thermometers into the tumor. As an alternative approach magnetic resonance (MR) thermometry based on a temperature dependent proton resonance frequency shift of the water molecule provides a continuous local non-invasive temperature control in addition to a good spatial localization directly at the cellular level, as e.g. in laser-induced interstitial or ultrasound thermotherapy. However, large doses of unshielded magnets which are present in nanoparticle-based hyperthermia introduce magnetic field inhomogeneities that reduce contrastivity based on the proton relaxation-weighted image and thus prevent proton-based MR thermometry.

Instead, a novel way for contactless thermometry on the cellular level seems to be advantageous, i.e., using a nanoscaled thermometer consisting of a carbon nanotube (CNT) and a filling material with strongly temperature dependent nuclear magnetic resonance (NMR) parameters like the spin-lattice or the spin-spin relaxation, resonance frequency, dipolar or scalar couplings, and electrical quadrupole couplings at 310-350 K. This way, temperature detection is possible with a high accuracy (< 0.1 K) even in more challenging situations with e.g. ferromagnetic particles nearby. Here, the use of carbon nanotubes as nanocontainers has exceptional advantages for biomedical applications. First, due to the protecting stable carbon shell the temperature sensor is protected from oxidation. Second, the outer shell of CNT can be chemically modified, e.g., with cancer-specific binding agents in order to enable attachment to a target tissue. Pantarotto *et al.* demonstrated that the functionalized CNT can cross the cell membrane and accumulate in the cytoplasm or reach the nucleus without being toxic for the cell. [2] Finally, the container feature of CNT might, in principle, allow simultaneous filling of CNT with a temperature sensor and another probe such as a ferromagnet (=heater) or a (chemo-)therapeutic agent like carboplatin [3], thereby combining different functionalities in one kind of CNT (Fig. 1).

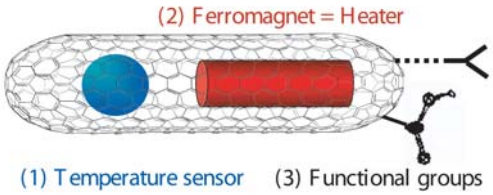

Fig. 1: Sketch of a filled carbon nanotube serving as a nanoscaled thermometer for medical applications. (1) A material with a strongly temperature dependent nuclear magnetic resonance (NMR) signal. (2) An additional filling material for further functionalities, e.g., a ferromagnet for heating by means of applied alternating current (AC) magnetic fields. (3) Functionalization of the outer shell for biocompatibility. [4]

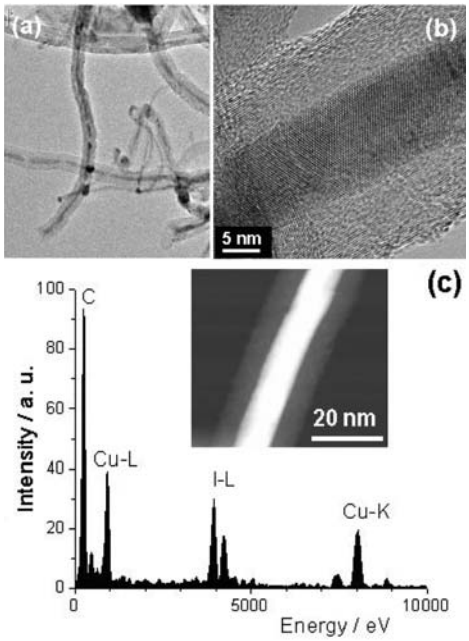

Fig. 2: Characterization of cuprous-iodide-filled carbon nanotubes. (a) Transmission electron microscopy image of the partial filled carbon nanotube. (b) High resolution transmission electron microscopy image indicates single crystallinity of encapsulated material. (c) Local electron diffraction X-ray analysis identifies filling material as cuprous iodide. [4]

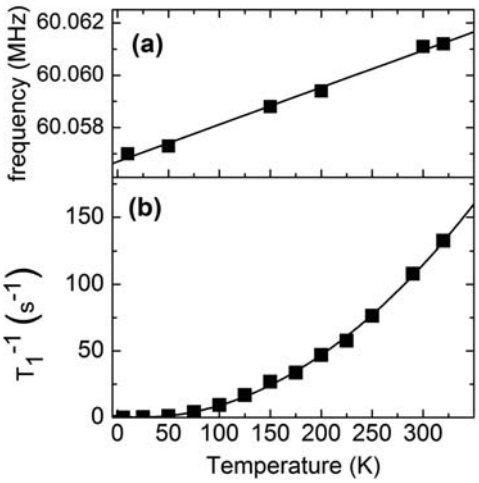

Fig. 3: Temperature dependencies of ^{127}I nuclear magnetic resonance parameters measured on cuprous-iodide-filled carbon nanotubes.
(a) Nuclear magnetic resonance frequency.
(b) Nuclear spin-lattice relaxation rate. The symbols represent the experimental data. The solid lines are the fits (see text). [4]

We have synthesized multi-walled carbon nanotubes by the fix bed method based on the procedure proposed in Ref. [5]. Pristine CNT consist of 10 to 40 carbon layers with the inner diameter of CNT varying from 5 to 20 nm and the typical tube length from 10-30 µm. Since many alkali and cuprous halides are known to show pronounced temperature dependencies of NMR parameters, we chose cuprous iodide (CuI) as a filling agent for such a nanothermometer. For filling with CuI the CNT were opened using a three-step procedure consisting of thermal and acidic treatment. The opened CNT were put in a silica glass ampoule together with CuI in excess and heated at 600°C for 24 h. At this temperature CuI is completely sublimated and transported into the opened CNT thanks to the capillarity effect. The resultant material was examined by transmission electron microscopy (Fig. 2a-b), X-ray diffraction analysis and energy dispersive X-ray analysis (Fig. 2c) and identified as CNT filled to 80 % with single crystalline cuprous iodide.

The NMR measurements were done on powdered material in an external magnetic field of 7.05 T. Although both ^{63}Cu and ^{127}I nuclear isotopes possess a quadrupole moment, in cuprous iodide copper and iodine atoms each are surrounded tetrahedrally by four atoms of the opposite kind. This leads to a vanishing quadrupolar coupling and a single resonance line for each isotope. The temperature dependencies of different NMR parameters (e.g. resonance frequency ν and spin-lattice relaxation rate $1/T_1$) were investigated for ^{63}Cu and ^{127}I. While the overall temperature dependencies for the NMR parameters follow a similar qualitative behavior for the signals from the cation and the anion, the absolute change per temperature interval has shown to be much smaller for the cation site providing a lower accuracy in temperature determination. Hence, in the following only results for the ^{127}I nucleus will be shown and discussed.

From the analysis of the ^{127}I-NMR spectra an increase of the resonance frequency with temperature has been deduced (Fig. 3a), which is most likely caused by variations in the orbital overlap due to an increase of vibrational amplitudes with temperature and lattice dilatation. The data are well fitted with a linear function, but a relative small slope of this function leads to an error of 15 K in temperature determination.

On the other hand, much more promising results have been obtained for the ^{127}I spin-lattice relaxation rate T_1^{-1} (Fig. 3b). The T_1^{-1} dependence is found to be in very good agreement with a quadratic law that is expected for a Raman two-phonon quadrupolar process. [6] This behavior is observed over the entire temperature range implying no contributions from impurities which might appear at low temperatures and from ionic diffusion which might be observed in the high temperature range. This is consistent with the view that the spin-lattice relaxation is driven by a quadrupolar mechanism, which at a first glance might appear to be unusual, since CuI crystallizes in the zinc blende structure. However, time-dependent quadrupolar interactions can arise from time-dependent distortions of the nuclear environment by the lattice vibrational modes, although in a perfect crystal of CuI no static, secular interaction between the nuclear electric quadrupole moment and the crystalline electric field gradient are expected. The ^{127}I experimental data are well fitted with the quadratic function $T_1^{-1} = a + b \cdot T + c \cdot T^2$, where fitting coefficients are $a = 1$, $b = (7 \pm 1) \times 10^{-2}$ and $c = (1.49 \pm 0.05) \times 10^{-3}$. Here, the mean squared errors of the fitting coefficients provide an estimate for the accuracy in temperature determination for the CuI-CNT nanothermometer, resulting in a temperature accuracy of 2 K in the range of biological interest (i.e. 290-320 K). This is a promising result and a good starting point to look for further filling materials in order to increase the accuracy of temperature determination. Possible candidates should be found within the group of metallic and/or magnetic materials usually exhibiting a highly dynamic behavior as well as a strongly temperature dependent susceptibility.

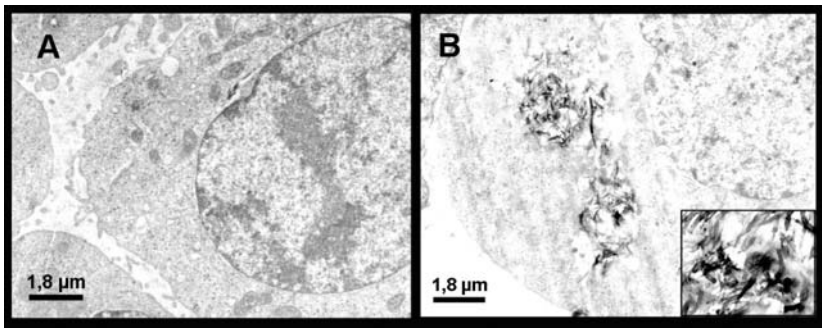

Fig. 4: Transmission electron microscopy images of the EJ28 human bladder cancer cells (a) before the treatment and (b) after the treatment with multi-walled carbon nanotubes. The cellular internalization of multi-walled carbon nanotubes, which were dispersed by human serum albumin, is observed. [4]

Since such a carbon-wrapped nanothermometer is aimed for biomedical applications at the cellular level, it is crucial to demonstrate that the functionalized CNT can penetrate through the cell membrane and enter the cell. As a first step, in the present work the uptake of empty multi-walled CNT used as template for filling has been investigated in a tumor cell culture. Fig. 4 shows the cellular internalization of these CNT (100 µg/ml) dispersed by human serum albumin in EJ28 bladder cancer cells. Then, it is most reasonable to assume that CuI-CNT should also be uptaken in the cells and thus can serve as intracellular thermometers in biological systems.

References

[1] A. Jordan, et al., J. Magn. Magn. Mat. 201, 413-419 (1999).
[2] D. Pantarotto, et al., Chem. Commun. 1, 16-17 (2004).
[3] S. Hampel, et al., Nanomedicine 3, 175-182 (2008); R. Klingeler, et al., Int. J. Hyperthermia 24, 496-505 (2008).
[4] A. Vyalikh, et al., Nanomedicine 3, 321-327 (2008).
[5] E. Flahaut, et al., J. Mater. Chem. 10, 249-252 (2000).
[6] A. Abragam, In Principles of Nuclear Magnetism, ed. Oxford University Press (1961).

Cooperation TU Dresden, Szczecin University of Technology

Funded by DFG, EU (Marie-Curie RTN CARBIO)

Effect of surface finishing and of mechanically induced defects on the corrosion of bulk metallic glasses

A. Gebert, P. F. Gostin, M. Johne, E. Mund, H. Klauss, U. Kühn, J. Eckert, L. Schultz

The kind of surface finishing and mechanical loading can remarkably influence the corrosion resistance of Zr-based bulk metallic glass specimen. Fine-polishing procedures were found to sensitize the surface for chloride attack leading to pitting corrosion. Mechanically induced physical defects like shear bands, cracks or craters are preferred initiation points for pitting. These influencing factors on the corrosion behaviour of bulk metallic glasses will have to be carefully considered for applications.

Multicomponent Zr-based alloys are presently the most prominent bulk metallic glasses (BMG's). Due to their unique mechanical properties, i.e. high yield strength, high elastic strain limit and low Young's modulus, these BMG's are very attractive for applications under high mechanical load, e.g. as small parts of sportive goods, automobiles, portable electronic devices or pressure sensors as well as devices for MEMS or surgical tools [1,2]. Those particular applications require a precise final shaping and surface finishing of the BMG parts on the micron and submicron scale. On one hand BMG's offer the advantage of near net-shape castability. However, often cast parts have to be machined and surface finished in terms of cutting, mechanical grinding and polishing. Moreover, periodically applied mechanical stresses can induce shear band formation leading to fracture of the material. Shot-peening is a conventional technique which was recently firstly employed for BMG's [3]. The controlled introduction of compressive surface stresses results in multiple shear band formation and in consequence, enhanced plasticity is achieved.

High corrosion resistance under application-relevant conditions is a decisive criterion for the commercialisation of new materials. BMG's have been subjected to numerous fundamental corrosion studies [4,5]. Zr-based glasses exhibit excellent passivity in chloride-free aqueous solutions in a very wide pH-value range. This is mainly due to the strong tendency of the valve metal components, e.g. Zr, Al, Ti or Nb, to form barrier-type passive films on the alloy surface. However, a high susceptibility for chloride-induced pitting and a low re-passivation ability was detected. This was attributed to the existence of crystalline inclusions in cast samples, which act as pitting initiation points. But so far mostly neglected aspects are that the kind of surface finishing and defects generated by severe mechanical load can have remarkable effects on the corrosion reactivity of the BMG's. This was in the focus of recent detailed studies. The $Zr_{59}Ti_3Cu_{20}Al_{10}Ni_8$ alloy with

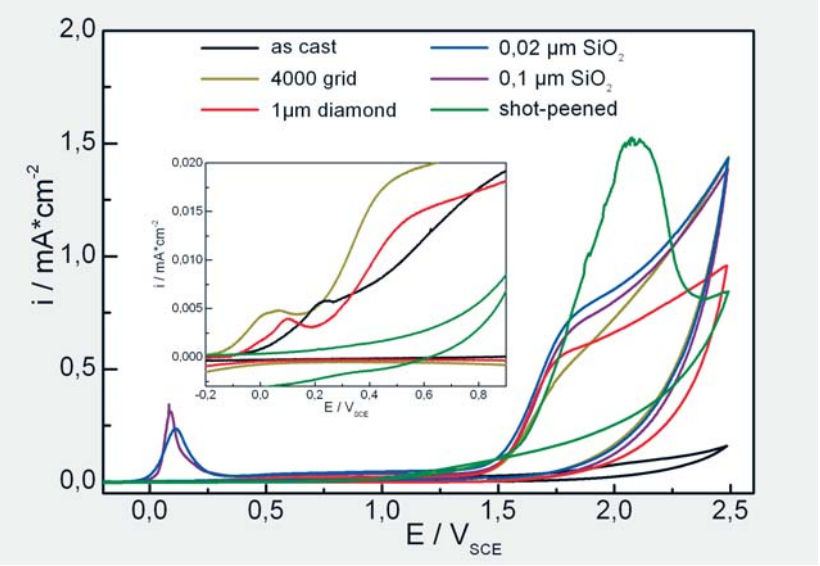

Fig. 1: Cyclic anodic polarization of a Zr-based BMG after different surface finishings recorded in 0.01 M Na_2SO_4 solution; treatment-dependent Cu oxidation at > 0 V

very high glass-forming ability was chosen as example case, for which basic corrosion mechanisms were already known.

The state of surface finishing of a Zr-based bulk metallic glass can decisively determine its reactivity in aqueous solutions. Figure 1 shows anodic cyclic polarization curves recorded on the cross-sectional area of a cast bulk sample after cutting and different finishing procedures. Similar as for an as-cast surface, after mechanical grinding with SiC paper down to grid 4000 and after additional fine polishing with 1 µm diamond suspension the alloy surface is spontaneously passive, i.e. the anodic current density remains generally very low. Also after severe mechanical surface degradation by shot-peening the glassy alloy stabilizes in a passive state, Cu oxidation is completely suppressed and additional pronounced oxidation of Zr and other valve metal components occurs at potentials above 1.5 V. The passive state is related with the growth of very thin non-permeable films mainly composed of Zr- and Al- oxides. But this goes along with an enrichment of metallic Cu in the close metal/oxide interface-near region. In contrast, fine polishing of the BMG surface using SiO_2 suspensions leads to a mirror-like finish, but also increases its environmental reactivity. With beginning anodic polarization at potentials above 0 V a significant oxidation peak occurs indicating a preferred Cu oxidation before a passive state is attained. This is a similar trend as observed for chemically etched alloy surfaces and indicates that this kind of suspension polish is not only a mechanical treatment but comprises also chemical reactions leading to Cu enrichment at the glassy alloy surface. This modification in the surface finishing state has also remarkable consequences for the pitting susceptibility of the alloy. Figure 2 shows linear anodic polarization curves recorded for the glassy $Zr_{59}Ti_3Cu_{20}Al_{10}Ni_8$ alloy in chloride-containing solution. While the mechanically ground (4000 grid) sample surface remains stable passive in the whole anodic regime, the diamond fine-polished sample exhibits under these polarization conditions a slightly higher corrosion current density and a weakly pronounced anodic active peak before a passive state it reached. At this slightly more reactive surface a chloride-induced passive layer breakdown, which initiates the pitting process, occurs at ~ 0.5 V. The steep rise of the current density indicates a very rapid pit growth. An even stronger increase of the chloride susceptibility is obtained after fine-polishing with SiO_2 suspension. The anodic active peak, which is mainly related with the Cu oxidation is clearly pronounced and this selective surface oxidation process results in an early passive film breakthrough at ~ 0.2 V. In summary, these studies demonstrated that fine-polishing procedures of Zr-based glassy alloy samples may be necessary for certain applications, but have a detrimental effect on the corrosion resistance of these new materials.

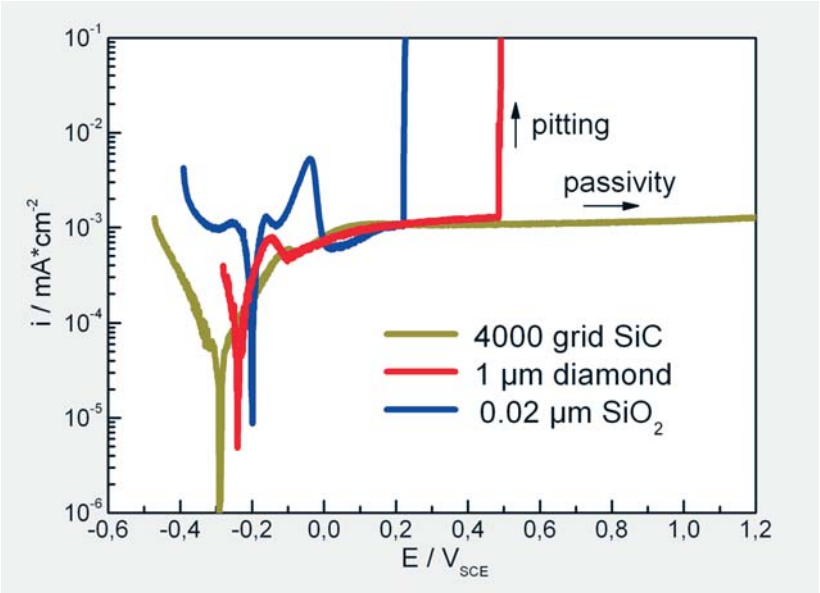

Fig. 2: Linear anodic polarization of a Zr-based BMG in 0.01 M NaCl solution

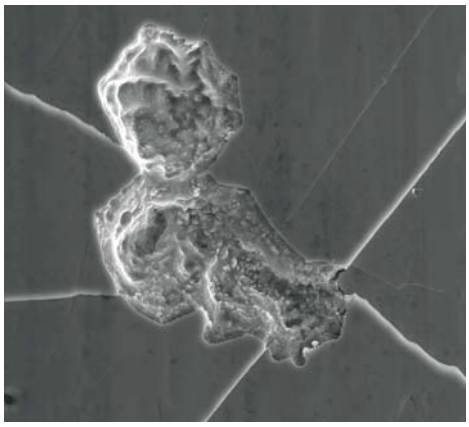

Fig. 3: SEM images of corrosion pits generated on a shear band crossing of a predeformed Zr-based BMG sample

Under high mechanical load bulk metallic glasses exhibit at room temperature an inhomogeneous deformation behaviour, i.e. a high stress level is localized in only very thin shear bands that are visible as lines at a deformed sample surface. Those shear bands can be regarded as physical surface defects of the homogeneous glassy phase and they are obviously electrochemically active higher energetic surface sites. Figure 3 shows corrosion pits generated on a cast sample that was pre-deformed to the maximum stress level and then immersed in acidic chloride solution. Under compressive stress numerous shear bands formed and chloride attack resulting in pit initiation occurred preferentially along those shear bands and on shear band crossings. These sites represent local spots of elevated topography of the otherwise rather smooth surface and of higher stress concentration of the otherwise relaxed glassy state. Furthermore, the shear band formation is related with rupture of the natively formed thin passive layer. That may explain their attractiveness for chloride ions. On the opposite it was also demonstrated that pre-corrosion has a significant effect on the room temperature deformation behaviour of Zr-based BMG's. A general trend was observed that presence of corrosion pits on compression test samples reduces the maximum achievable strength level and many shear bands were found to be pinned to corrosion pits. Obviously these pits are weak points at the sample surface that ease the shear band formation.

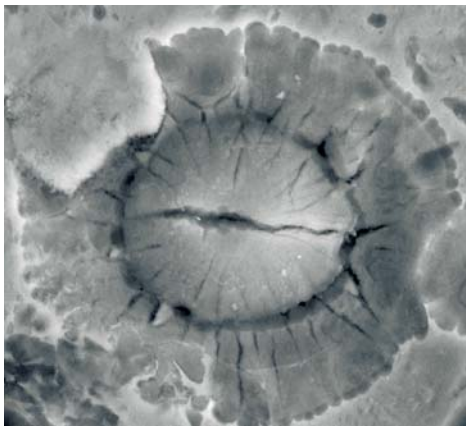

Fig. 4: SEM image of a corrosion pit generated on a shot-peened Zr-based BMG sample

The compressive stress applied to the glassy alloy surface by shot-peening leads not only to shear band formation, but severely damages the surface in terms of cracks, crevices, craters and even vein-like patterns that are typically known from fracture surfaces of BMG's and which origin from flaked off pieces. Also this treatment sensitizes the surface and reduces the pitting resistance. Figure 4 shows a typical morphology of a pit generated on a shot-peened BMG surface. Starting from a crevice the pit propagates spherically into the glassy phase. Due to the residual stress state of the shot peened surface the pit growth is accompanied by formation of manifold small cracks propagating into pit growth direction.

In summary, the kind of surface finishing and mechanical loading can remarkably influence the corrosion behaviour of Zr-based bulk metallic glass specimen. Fine-polishing procedures were found to sensitize the surface for chloride attack. Mechanically induced physical defects like shear bands, cracks or craters are preferred initiation points for pitting. These new aspects will have to be carefully considered for BMG applications.

References

[1] A. Inoue, X.M. Wang, W. Zhang, Rev. Adv. Mater. Sci. 18 (2008) 1
[2] A. Inoue, N. Nishiyama, MRS Bulletin, August (2007) 651
[3] Y. Zhang, W.H. Wang, A.L. Greer, Nature Materials 5 (2006) 857
[4] J. R. Scully, A. Gebert, J.H. Payer, J. Mater. Res. 22 (2007) 302
[5] A. Gebert, V. Haehnel, E.S. Park, D.H. Kim, L. Schultz, Electrochim. Acta 53 (2008) 3403

Cooperation Univ. of Cambridge, UK; TU Dresden

Funded by EU (RTN "Ductile BMG Composites")

Self-propelled Microjets at Low Reynolds Numbers

A. A. Solovev, Y. F. Mei, S. Harazim, C. Deneke, G. S. Huang, O. G. Schmidt

We demonstrate microjet engines with diameters of several micrometers, which are prepared by rolled-up nanotechnology and consist of metallic Ti/Fe/Co/Pt or semiconductor/metallic InGaAs/Cr/Pt microtubes from stacked nanomembranes. In presence of an integrated catalytic platinum layer as an inner wall, hydrogen peroxide can be decomposed into oxygen and water inside the tube, thrusting out microbubbles at one end of the tube and driving it towards the opposite direction. Such microengines can reach high speeds up to ~2100 µm/second (60 body length per second) and their motions can be partially controlled by remote magnetic fileds, which are directly visualized by long microbubble tails resembling those of biological systems.

Development of autonomous micro-/nanoengines is of great interst for emerging technologies like delivery of drugs,[1] self assembly of functional micro-structures,[2] cargo functionality,[3] and its integration into microfluidics.[4] Because at low Reynolds numbers high viscosity and surface tension of liquids are encountered,[5] many efforts have been devoted to control motion at the microscale involving both biological and artificially designed micromotors. For example, bacterial "micro-horses" as transporters,[6] catalytic bimetallic nanomotors,[7] and artificial flagella to support cell motions.[8] have been suggested as potential candidates to realize synthetic biological life on the micro-/ and nanoscale. In recent years catalytic nanomotors have been engineered, since such micro-/nanoscale devices offer universality and high power for motions through fluids at low Reynolds numbers. Here we demonstrate self-propelled microjet engines made of rolled-up microtubes integrating magnetic and catalytic layers.[9-10] In comparison to previous work,[3-4] there are several physical effects simultaneously observed in microtubes, such as fluid capillary micro-pumping, catalytic reaction and the ejection of reaction products (i.e. microbubbles) from the tube end.

Recent progress in the field of catalytic micro/nanoengines suggests two main different mechanisms for engine acceleration. The first one deals with electrophoresis: electrons transferred in bimetallic junctions induce motions of protons within the Debye length and cause fluid pumping, which in turn transfers momentum to the nanoengine. The other explanation relies on gas production at the interface to a catalytic material. Our experiments clearly reveal the occurrence of microbubbles expelled from one tube end, which push the engine into the opposite direction. Each bubble thrusting out causes a descrete step-like motion of the microjet[10]. The microjet's velocity can be roughly described as a product of microbubble radius and ejection frequency. The recoiled bubbles form fascinating tails at the tube ends, which allos us to trace back the microjet trajectory. Such long tails are commonly oberved in biology. For instance, *listeria* moves around by ejecting actin comet tails, and the discrete step size of the movement is equal to the actin monomer length.[11]

Our catalytic microjets are formed from pre-stressed thin films prepared by electron beam angular deposition of metals on patterned sacrificial polymer or semiconductor layers.[9-10] Thin films consisting of Ti/Fe/Au/Pt, Ti/Fe/Co/Pt or hybrid metal/semiconductors (InGaAs/Cr/Pt) roll up into microtubes by selectively etching away a sacrificial buffer layer. Pt is used as the catalyst in the tubular microstructure, and the Fe or Co functional layer is used for magnetic control of the microjet motions. Figure 1 sketches a self-propelled microjet in motion. The visible tail consists of expelled oxygen microbubbles, which push the tube into the opposite direction. Figure 2a displays a scanning electron microscopy image of a microjet with a tubular wall consisting of 6 nm AlGaAs, 5 nm Cr, and 5 nm Pt.

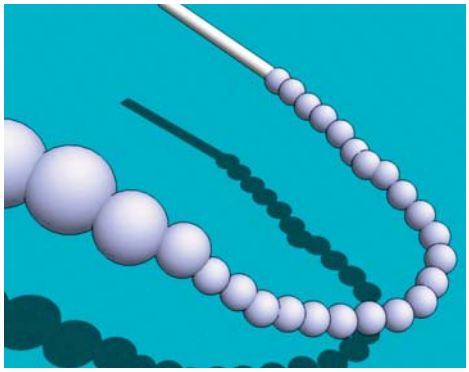

Fig. 1: Schematic diagram showing a self-propelled microjet in an aqueous solution of hydrogen peroxide.

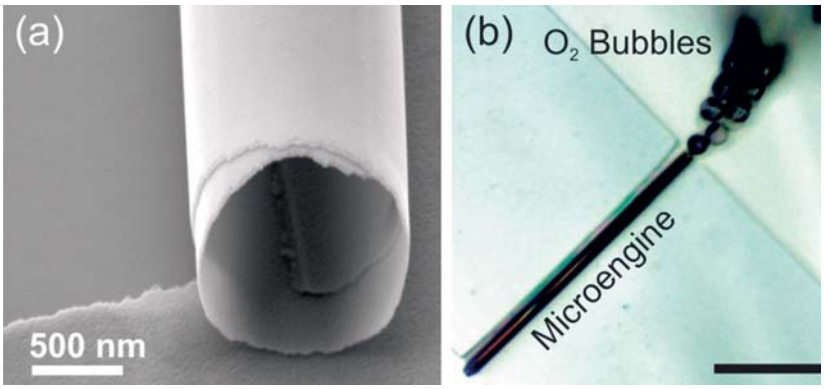

Fig. 2: (a) Scanning electron microscopy image of a rolled up AlGaAs/Cr/Pt microtube, with layer thicknesses of 6 nm (AlGaAs), 5 nm (Cr), and 5 nm (Pt). (b) Optical microscopy image of a working microengine fixed on a substrate. Scale bar in (b) corresponds to 20 µm.

If microtubes, still fixed to the substrate, are immersed in hydrogen peroxide aqueous solution (3–30%), oxygen microbubbles are generated from the tube openings as shown in Fig. 2b. These stationary but chemically active tube structures might find applications as fully integrative on-chip reactors to provide energy in a nanofactory. For a free tube in a H_2O_2 solution, the expelled bubbles can drive the microtubes. Since both ends of the microtube are not necessarily symmetric, bubbles are usually released from one tube end, only, at a certain angle with respect to tube axis. Figure 3 illustrates a wide variety of different microjet trajectories during autonomous motions in a fluid containing hydrogen peroxide. Trajectories can be divided into 3 groups: (a) straight, (b) circular, and (c) spirals. Motion in a straight line is the simplest and the requirement is that the vector of the driving force is parallel to the tube axis. For circular trajectories (see Fig. 3b), bubbles are released from the tubular end at certain angles, which creates torque, causing the microjet to rotate clockwise or counterclockwise. Trajectories similar to those illustrated in Fig. 3 have been discussed in a detailed kinematic picture for *listeria monocytogenes*.[11]

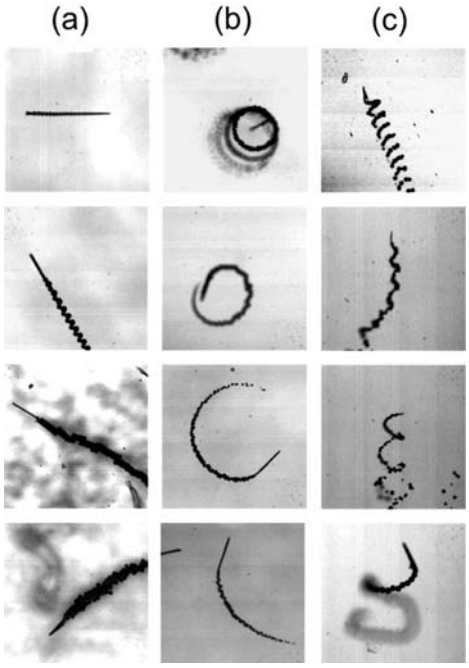

Fig. 3: Trajectories observed during autonomous motions of microjets, consisting of (a) straight lines with multiple and single-tail bubble tails (from right to left), (b) motion in circles with different diameters, and (c) spiral motions. Image sizes are 420 µm x 420 µm.

Full control over microengine motions is required especially for integration in Lab-on-a-Chip applications. We have therefore investigated the motion of our microjets in external rotating magnetic fields. For the sake of simplicity, we have chosen microengines which otherwise move in straight lines. When a rotating field is applied, microjets start to become localized (confined) in circular trajectories. Figure 4a (black circle) shows experimental data points of the localization radius as a function of the rotating

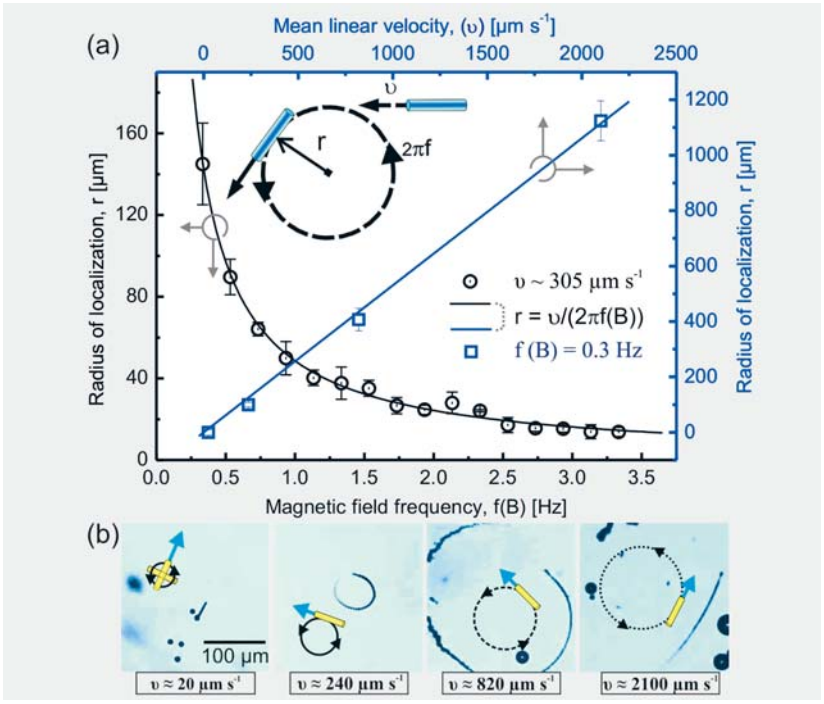

Fig. 4: Magnetic control of microjets which self propel in straight trajectories. (a) Localization radius as a function of rotating magnetic field frequency at a constant linear velocity (circles) and dependence of localization radius on the mean linear velocity at a constant frequency of rotating magnetic field (squares). The solid lines are calculated values. (b) Experimental video frames of moving microjets at different speeds but with constant rotating magnetic field, corresponding to the data points (squares) shown in (a). Yellow drawings represent microjets with a direction of motion indicated by a blue arrow. Black circles with arrows schematically show the applied rotating magnetic field. Scale bar is 100 µm.

frequency of the magnetic field. The microjet has a constant average velocity of 305 μm/s. Blue squares in Fig. 4a and frames in Fig. 4b show experimental results of the localization radius as a function of the linear velocity applying a constant rotating magnetic field with a frequency of 0.3 Hz. Kinematically, the localization radius (r) can be described as a function of the linear velocity υ and the frequency f_B as $r = \upsilon/(2\pi f_B)$. Using the average value of the linear velocity (305 μm/s) and substituting values of magnetic field frequencies in the range of 0.3–3.3 Hz, the calculation can well-describe the experimental points in Fig. 4(a). As expected, the localization radius depends linearly on the velocity for a constant magnetic field as drawn by the blue line in Fig. 4(a). However, at higher magnetic field frequencies the microjets start to hit their own tails (i.e. bubbles), which causes fluctuations in their linear and angular velocities. Interestingly, these results mimic the behavior of magnetotactic bacteria in rotating magnetic fields. Such bacteria contain nanomagnets and navigate by using the relatively week magnetic field of the Earth.[12]

In conclusion, we have demonstrated microjet engines moving at high speeds up to 2 mm/s (60 body lengths per second), which is among the fastest autonomous motions known in both biological and synthetic microengines. The trajectories of the microjets are well-visualized by expelled bubble tails. We can remotely control the motion of the microjets by applying external magnetic field. Our results pave the way towards potential applications of micro-/nanoengines in Lab-on-a-Chip and nanomedicine technologies.

Acknowledgements We are grateful for experimental help and discussions by Elliot J. Smith, Jens I. Mönch, Cornelia Krien, Ronny Engelhard and Emica Coric.

References

[1] R. N. Cohen, M. J. Rashkin, X. Wen, and F. C. Szoka, Jr: Drug Discovery Today, Technologies 2 (1) (2005), 111–118.
[2] J. R. Link, and M. J. Sailor: PNAS. 100 (2003), 10607–10610.
[3] S. Sandararajan, P. E. Lammert, A. W. Zudans, V. H. Crespi, and A. Sen: Nano Lett. 8 (5) (2008), 1271–1276.
[4] J. Burdick, R. Laocharoensuk, P. Wheat, J. Posner, and J. Wang: JACS, 130 (2008), 8164.
[5] E. M. Purcell, American J. Phys. 45 (1977), 3–11.
[6] B. Behkam, M. Sitti, App. Phys. Lett. 90 (2007), 023902-023904.
[7] W. F. Paxton, K. C. Kistler, C. C. Olmeda, A. Sen, S. K. St. Angelo, Y. Cao, T. E. Mallouk, P. E. Lammert, V. H. Crespi: J. Am. Chem. Soc. 126 (41) (2004), 13424–31.
[8] R. Dreyfus, J. Baudry, M. L. Roper, M. Fermigier, H. A. Stone and J. Bibette: Nature 437 (2005), 862–865.
[9] O. G. Schmidt and K. Eberl: Nature 410 (2001) 168.
[10] Y. Mei, G. Huang, A. A. Solovev, E. Bermudez Urena, I. Mönch, F. Ding, T. Reindl, R. K. Y. Fu, P. K. Chu, and O. G. Schmidt: Adv. Mat. 20 (21) (2008), 4085–4090.
[11] V. B. Shenoy, D. T. Tambe, A. Prasad, and J.A. Theriot: PNAS. 104 (20) (2007), 8229–8234.
[12] K. Erglis, Q. Wen, V. Ose, A. Zeltins, A. Sharipo, P. A. Janmey, and A. Cebers: Biophys. J. 93 (2007), 1402–1412.

CdTe quantum dots as single photon sources

H. S. Lee, M. Benyoucef, J. Gabel, F. Ding, T. W. Kim, H. L. Park, A. Rastelli, O. G. Schmidt

Triggered single-photon emission from a single CdTe/ZnTe quantum dot (QD) grown on Si(001) substrate is demonstrated for the first time. Power-dependent and polarization-dependent microphotoluminescence (μ-PL) measurements are performed to identify the neutral exciton (X), the biexciton (XX), and the charged excitons (CX, and CX') in single QDs. The emission wavelength of QDs can be tuned in a wide spectral range (more than 8 meV) using a focused laser beam. A nearly perfect single-photon emission from the X line is preserved even after the energy tuning.

Introduction. Recent experiments have shown that self-assembled quantum dots (QDs) are good candidates for the production of triggered single photons [1-3], indistinguishable photons, and entangled photon pairs. II-VI QDs are interesting due to their large excitonic binding energies, short radiative lifetimes, and the strong Coulomb interaction which make them very attractive for single photon generation and quantum optical experiments. The short lifetime could also allow operation at high repetition rates. From the technological point of view it would be desirable to obtain single-photons on demand from single quantum dots grown on conventional Si(001) substrates. The integration of classical optoelectronic devices on Si is a long standing dream and keeps being a formidable challenge, as it is usually difficult to grow direct bandgap compound semiconductors on Si. Planar structures with QDs have been grown on Si, but single-photon emission has not been reported so far.

Experimental Details. The studied sample was grown by molecular beam epitaxy (MBE) and atomic layer epitaxy (ALE) on a Si(001) substrate and consists of a single CdTe QD layer (with dot density of about $3 \times 10^{10} cm^{-2}$) embedded in ZnTe barriers. The Si(001) substrate was etched in a mixture of NH_4F and HF (7:1) at room temperature for 1 min and rinsed in de-ionized water prior to the growth. A 900 nm ZnTe buffer layer was first grown on Si(001) substrate at 320°C using MBE, followed by 2.5 monolayers CdTe grown at the same temperature using ALE. The CdTe QDs were then capped with 100 nm ZnTe using MBE. For the laser heating experiment a part of the sample was coated with 200 nm SiO_2 using electron beam evaporation. For photoluminescence (PL) measurements the sample is mounted in a helium flow cryostat. A microscope objective ($NA = 0.5$) is used to focus a frequency-doubled Nd:YVO4 continuous wave (cw) laser with an excitation wavelength of 532 nm for PL and laser processing or a frequency doubled Ti-sapphire laser operating at 450 nm (pulse width of ~2 ps and repetition frequency of 76.2 MHz) for photon correlation measurements.

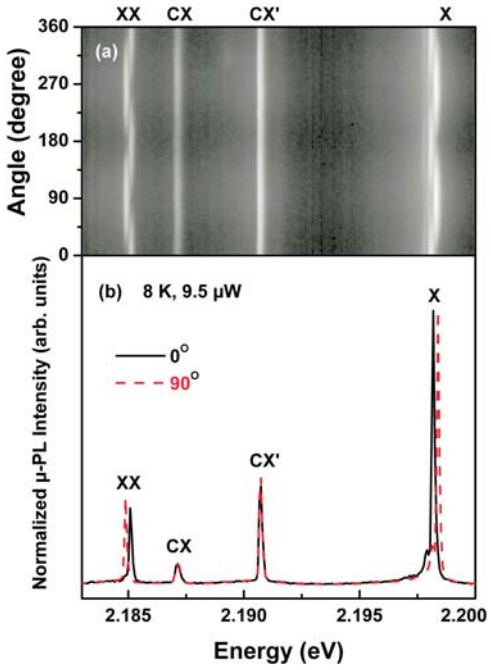

Fig. 1: (a) Gray-scale coded μ-photoluminescence intensity for the exciton (X), the biexciton (XX), and the charged excitons (CX and CX') as a function of linear polarization angle. (b) Normalized μ-Photoluminescence spectra at 0° and 90° polarization angle.

Results and Discussion. Figure 1(a) shows the grayscale coded μ-PL intensity of the emission of a single QD as a function of linear polarization angle and emission energy. Figure 1(b) shows normalized μ-PL spectra taken at 0° and 90° polarization angle. The lines labeled with X and XX split with the same magnitude (~ 200 μeV) but opposite sign. They are therefore attributed to neutral exciton and biexciton recombination where the splitting is due to electron-hole exchange interaction (fine structure splitting, FSS) [4]. On the other hand, since singly charged excitons in their ground states contain two same carriers forming a singlet, we expect no splitting for trions [5]. For this reason we can attribute the CX and CX' lines to the two oppositely charged trions. The biexciton binding energy (13.1 meV) measured in a single CdTe/ZnTe QD is enhanced as compared to that typical for III-V quantum dots (of the order of about 4 meV). This result agrees well with the stronger electron-hole correlation in II-VI quantum dots, which leads to large binding energies for XX.

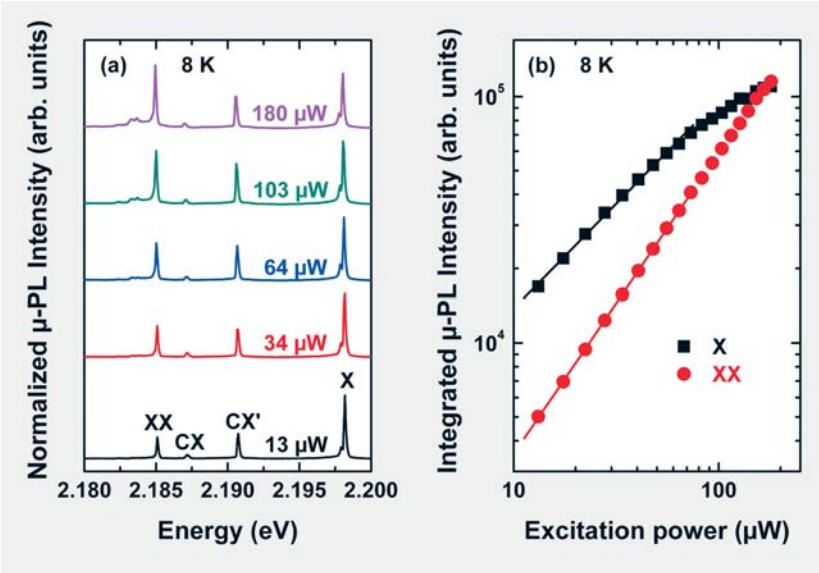

Fig. 2: (a) Micro-photoluminescence spectra of a single QD at 8 K for different excitation powers. (b) The integrated intensity of the emission lines of the exciton (X) and the biexciton (XX) plotted as a function of the excitation power.

In order to further confirm the X and XX lines, we performed power-dependent μ-PL measurements of the emitted light. Figure 2(a) shows the μ-PL spectra of a single QD at 8 K for different excitation power values and Fig. 2(b) the integrated intensity of the X and XX emission lines plotted as a function of the excitation power. The solid rectangles and circles represent X and XX lines, respectively. With increasing excitation power, the intensity of the XX line increases faster than that of the X line. Since the initial state for biexciton creation is an exciton, the biexciton population grows faster with excitation power than that of the exciton [6]. The observed evolution of the spectrum with the increase of the excitation power allows clear assignment of the X line and the XX line to the optically active exciton and biexciton, respectively.

To demonstrate triggered single-photon generation, we measured the second-order correlation function $g^{(2)}(\tau)$ under pulsed excitation. Fig. 3 shows the measured unnormalized correlation function $n(\tau)$ under pulsed excitation for the X emission of a single QD before and after energy tuning by laser heating (see below) and the corresponding PL spectra. All displayed measurements were performed at low excitation power to prevent blue-shift of the QD emission lines. The measured $n(\tau)$ consists of series of correlation peaks separated by the repetition period 13.12 ns. As expected, in the case of coherent source (pulsed laser) all peak areas are identical (see Fig.3 (a)) showing Poisson distributed statistics. In contrast to the mode-locked laser, the central peak at $\tau = 0$ ns of the QD X emission is significantly suppressed, an unambiguous signature of a single-photon source. For perfect single photon emission the central peak is absent indicating the generation of only one photon per pulse. For the investigated QD, a practically perfect single photon emission is observed. The value of the second order correlation $g^{(2)}(0)$ is about 0.14 for the central peak which does not reach its theoretical value of zero due to the presence of a weak uncorrelated background.

A problem related to the use of self-assembled QDs as independent sources for indistinguishable single-photons is, that such QDs emit at different wavelengths due to unavoidable fluctuations in size/shape/composition during the fabrication processes. Therefore, it is important to find strategies to accurately tune the emission of single QDs into resonance ideally within the lifetime-limited dephasing time. As discussed below, using laser heating, we first blue-shift the X line, and then measure the autocorrelation again using the pulsed laser. Interestingly, the single photon emission from the same dot after laser processing is preserved (Fig. 3(c)).

Figure 4 demonstrates that the focused laser beam used for μ-PL spectroscopy can also be used to controllably blue-shift the emission of a single CdTe/ZnTe QD. At low laser power (here 50 μW) we collect μ-PL spectra; at high laser powers (here up to 18 mW) we

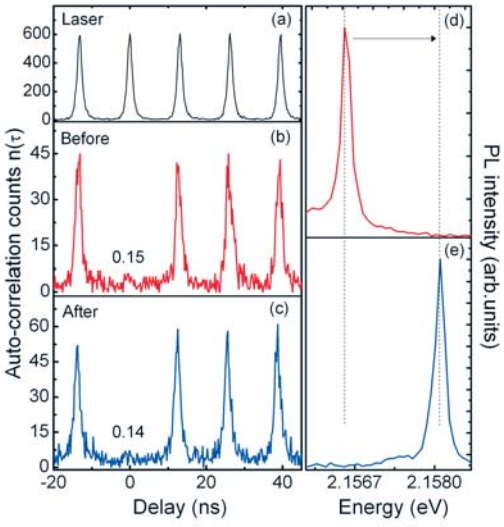

Fig. 3: Photon correlation measurements of: (a) Pulsed laser, (b) and (c) the X line from a single CdTe QD in a sample coated with 200 nm SiO_2 before and after laser heating. (d) and (e) the corresponding PL spectra before and after energy tuning by laser heating.

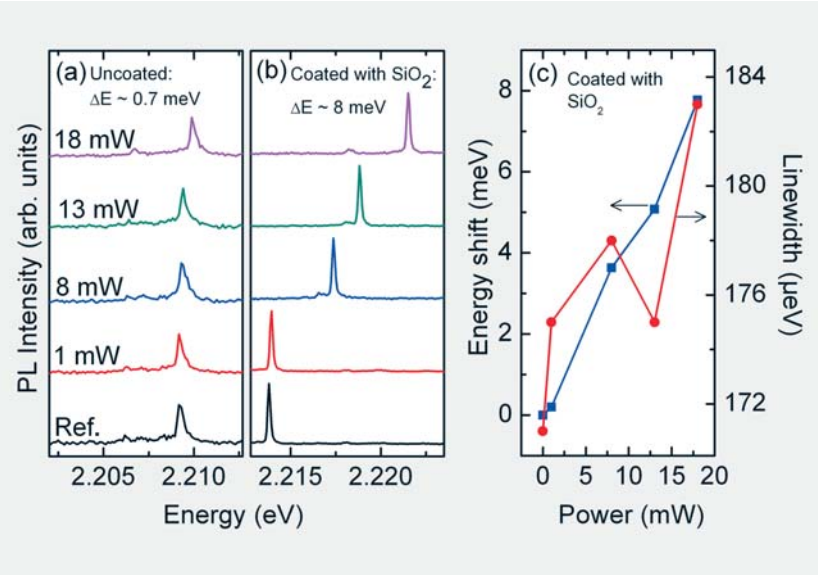

Fig. 4: PL spectra of a CdTe QD annealed several times at different laser powers and collected at 50 μW from: (a) as-grown sample and (b) sample coated with 200 nm SiO2 (c) Peak position and linewidth of exciton as a function of heating powers from the coated sample.

heat the structure and promote structural changes producing a blue-shift of the emission. Figure 4(a) and (b) compare the emission behavior for two different QDs in the as-grown sample (Fig. 4(a)) and in the same sample, but coated with a 200 nm thick SiO_2 layer (Fig. 4(b)). After each heating step (of 5 s duration), the excitonic X line is gradually blue-shifted. Fig. 4(c) illustrates the X peak position and the linewidth as a function of heating power from the SiO_2 coated sample. At a laser power of 18 mW, we obtain a maximum energy shift of about 8 meV for the sample coated with SiO_2 (Fig. 4(c)). In contrast to this, only a small shift is observed for the QD in the uncoated sample (0.7 meV). The linewidth remains almost constant at reasonably low heating powers up to 13 mW and then increases gradually for the investigated QDs suggesting that no significant damage is produced by the laser heating. The single photon emission from the same dot after "laser processing" is preserved (see Fig. 3(c)).

Conclusions. We have investigated the optical properties of single CdTe/ZnTe QD grown on Si (100) substrates by using MBE and ALE. From polarization-dependent and power-dependent μ-PL spectra, we unambiguously identified the exciton and biexciton (X and XX) lines. Two additional lines (CX and CX') with no measurable fine structure splitting were attributed to single charged excitons. We have demonstrated that such dots can be used as triggered single-photon sources and we have presented a method to tune the emission energy in a large spectral range. These results indicate that it may become feasible to fabricate indistinguishable single-photon sources.

References

[1] J. M. Gérard et al. J. Lightwave Technol. 17 (1999) 2089
[2] P. Michler et al. Science 290 (2000) 2282
[3] M. Benyoucef et al. J. Appl. Phys 97 (2005) 023101.
[4] M. Bayer et al. Phys. Rev. Lett. 82 (1999) 1748
[5] B. Patton et al. Phys. Rev. B 68 (2003) 125316
[6] K. Brunner et al. Phys. Rev. Lett. 73 (1994) 1138

Cooperation Yonsei Univ., Hanyang Univ.

Reversibly straining ferroic oxide films

K. Dörr, M. D. Biegalski, O. Bilani-Zeneli, K. Boldyreva, M. C. Dekker, R. B. Gangineni, A. Herklotz, J.-W. Kim, K. Nenkov, A. D. Rata, L. Schultz, H. M. Christen

The biaxial strain present in thin films substantially alters electronic properties of strongly correlated oxide films. We have developed a novel method that is more versatile than mechanical bending for the direct measurement of strain-dependent film properties. Ferroelectric and ferromagnetic oxides grown epitaxially on pseudocubic piezoelectric substrates of PMN-PT have been structurally characterized in reversibly varied biaxial strain states using x-ray diffraction methods. The strain effects on ferroelectric polarization, magnetization and electrical resistance have been directly measured for some selected oxide perovskite materials such as multiferroic $BiFeO_3$, manganites and cobaltites.

Lattice strain is universally present in thin films. Correlated oxide materials with ferroelectric, ferromagnetic or multiferroic orders are extraordinarily sensitive towards strain [1]. For example, efficient coupling of two-phase multiferroics composed of a magnetic and a ferroelectric component is achieved via elastic strain at interfaces [2,3]. Until now, effects of strain have typically been studied by comparing sets of films grown onto substrates with different lattice-mismatch or with different thicknesses. However, inherent variations in defect structure and composition between different films make such comparisons difficult. We have developed a novel method to measure the effects of strain on oxide thin film properties [2]. The method utilizes epitaxial oxide film growth of the material under study directly onto piezoelectric substrates. Electrical actuation of the piezoelectric substrate is employed to provide uniform and reversible strain to thin-film materials while keeping their defect structure and composition unchanged.

Here, piezoelectric substrates of pseudocubic PMN-PT ($0.72Pb(Mg_{1/3}Nb_{2/3})O_3$-$0.28\,PbTiO_3$ (001)) [2] were utilized to exert uniform and reversible strain to single-crystal epitaxial perovskite films. An electric field applied across the crystal significantly changes the lattice parameter of the PMN-PT crystal, as measured using 4-circle x-ray diffraction. Our work shows that the biaxial strain is fully transferred to epitaxial films, regardless of defects and buffer layers.

Using this method, strains in excess of 0.2% are readily achieved, and are remarkably linear with the applied voltage (Fig. 1). Additionally, the strain achieved for a given voltage is essentially temperature-independent (from 80K to room temperature), enabling temperature-dependent strain-effect measurements. In-plane and out-of-plane lattice parameters can be determined (Fig. 1), from which the Poisson ratio of the material can be derived directly. Note that the close-to-cubic structure with in-plane angular distortions below 0.1° for the chosen composition of PMN-PT provides sufficiently uniform film strain irrespective of the actual ferroelectric domain structure [4].

Next to the measurement of mechanical properties, the technique was demonstrated to measure the effects of strain on the ferroelectric behaviour of $BiFeO_3$ thin films [5] (Fig. 2), the only known single-phase room-temperature multiferroic. The results on strain-dependent polarization show a remarkable agreement with predictions [6], whereas the large strain effect on the switching (coercive) field is uniquely observed. As coercivity is a property that strongly depends on defects and microstructure, reversible measurements are capable of providing otherwise inaccessible insight into the strain influence.

Magnetic oxides such as perovskite manganites and cobaltites $La_{1-x}A_xMO_3$ (M = Mn or Co; A = non-trivalent doping element) have been epitaxially grown on PMN-PT in order to evaluate the strain-dependent magnetization and electrical conductivity. For manganites known for their colossal magnetoresistance and spin-polarized conduction band, an unusual sensitivity of the ferromagnetic Curie temperature (T_C) on biaxial

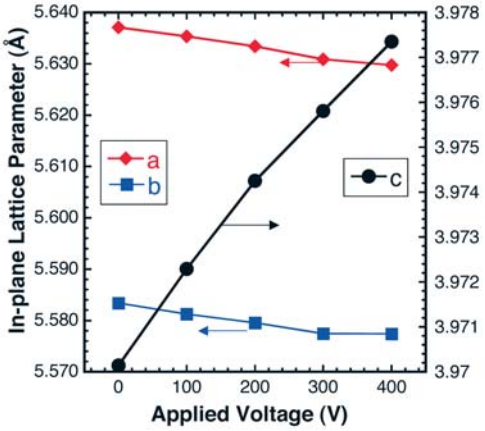

Fig.1: Strain-dependent monoclinic lattice parameters of a $BiFeO_3$ (200 nm) film on PMN-PT(001) as a function of applied voltage to the substrate. The change in lattice parameters is roughly linear.

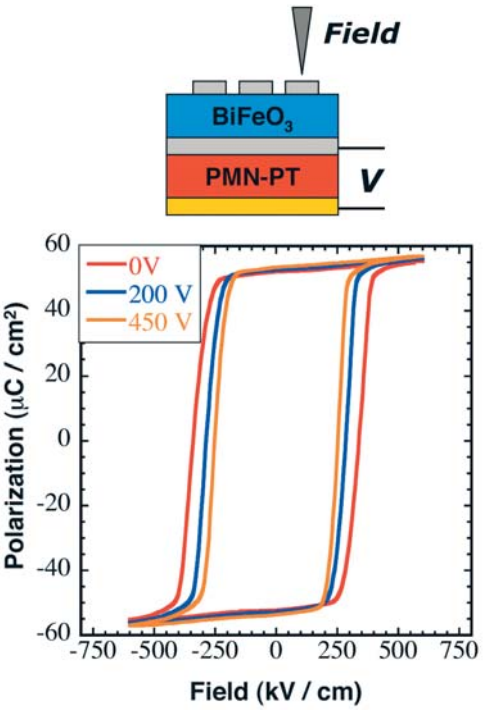

Fig. 2: Top: sample scheme. Bottom: strain-dependent ferroelectric polarization of a $BiFeO_3$ film grown on PMN-PT(001) with a $La_{0.8}Sr_{0.2}MnO_3$ bottom electrode. The voltage of 450 V causes a biaxial in-plane compression of 0.15%.

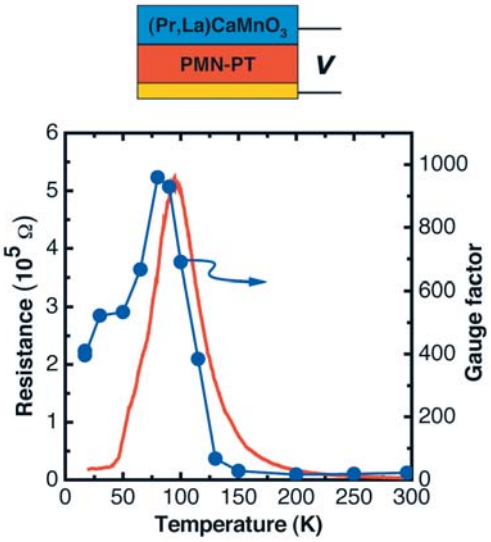

Fig. 3: Top: sample scheme. The resistance is measured using a four-point method (not shown). Bottom: electrical resistance and resistive gauge factor (resistance change per strain change, both in percent) of a magnetic $Pr_{0.28}La_{0.42}Ca_{0.3}MnO_3$ (100 nm) film on PMN-PT(001).

strain exceeding 190 K/% has been found [2]. This can be exploited for strain control of the magnetization, as demonstrated in successful approaches for two-phase multiferroics [2, 3]. Of particular interest is the strain response of electrical transport, since it is rather impossible to extract this information from a comparison of various films due to the impact of microstructure. In recent decades, semiconductors have been checked in a search for large elastoresistance that is the strain-induced resistance (R) change exploited, for instance, in force microscopy tips. Ferromagnetic manganite films have been discovered to show a resistive gauge factor (relative R change per strain change) beyond 400 comparable to the most sensitive piezoresistive semiconductors. Manganites in a phase-separated magnetic state even reveal gauge factors up to 1000 close to the metal-insulator transition (Fig. 3) [7]. Similarly, a huge strain response of the conductivity of a ferromagnetic cobaltite has been observed [8]. These results underline the extraordinary impact of strain on the electronic band structure of correlated oxide thin films.

Summarizing, the straightforward method of applying reversible strain from a piezoelectric substrate provides a general and valuable technique to study the effects of strain on a great variety of material properties. The technique is applicable not only for epitaxial oxide thin films, but for a wide range of materials including metastable materials and nanostructured films. The distinct advantage of this technique over others is that inherent trends in material properties can be extracted directly from single samples. The biaxial film strain is provided as an *in-situ* variable parameter during experiments.

References

[1] K.J. Choi et al., Science 306 (2004) 1005
[2] C. Thiele et al., Phys. Rev. B 75 (2007) 054408
[3] W. Eerenstein et al., Nature Mat. 6 (2007) 348
[4] O. Bilani-Zeneli et al., J. Appl. Phys. 104 (2008) 054108
[5] D. H. Kim et al, Appl. Phys. Lett. 92 (2008) 012911
[6] H. W. Jang et al., Phys. Rev. Lett. 101 (2008) 107602
[7] M. C. Dekker et al., submitted
[8] A. D. Rata et al, Phys. Rev. Lett. 100 (2008) 076401

Cooperation Oak Ridge National Laboratory (Center for Nanophase Materials Sciences), MPI für Mikrostrukturphysik Halle

Funded by DFG, IMPRS, DAAD, US Department of Energy (Division of Scientific User Facilities)

Immediate technological impact

New Crystal Growth Furnace for Floating Zone Melting Under High Gas Pressure

D. Lindackers, S. Ziller, F. Fischer, G. Behr

The opportunity of floating zone crystal growth under high pressure and well defined gases and gas mixtures provides a completely new potential for single crystal growth of new of oxides and other compounds with volatile components.

In early 2008 the IFW single crystal laboratory was enriched by a new apparatus for floating zone melting which has been completely engineered, designed and assembled in house. Its operational parameters are setting new benchmarks regarding variability in material classes, ease of use and reliability in long term operation. Due to the unique performance requirements on the new apparatus quite a number of its major components have to be developed prior to the successful assembly of the prototype. Thus the working title *Smart Floating Zone – SFZ* furnace became official in house and is going to be used further.

The technological basics were derived from a setup reported by Balbashov et al. [1]. Here a vertical floating zone is heated by the radiation of a single, polychromatic light source which is imaged to the process area in an arrangement of two vertically mounted ellipsoid mirrors. The optical setup and details of the crystal growth chamber are depicted in Fig. 1.

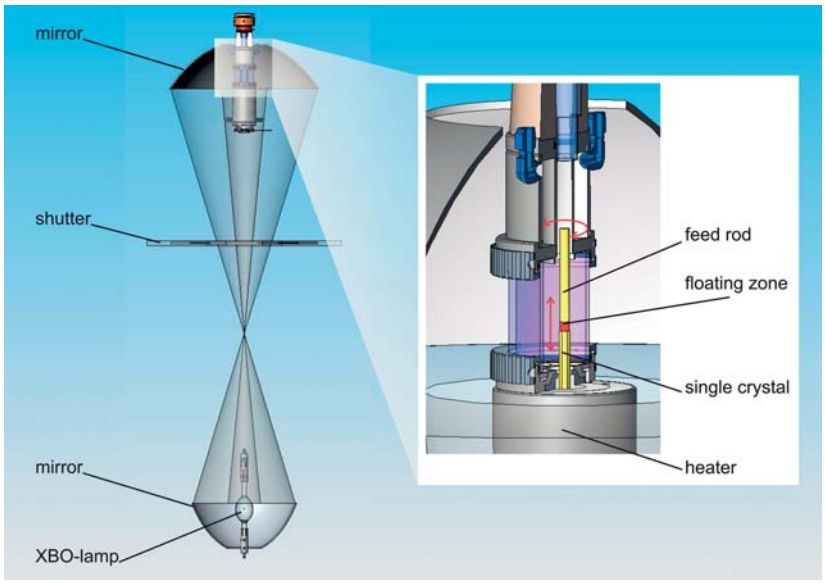

Fig. 1: Optical setup of SFZ furnace with scheme of single crystal growth (highlighted insert)

Single crystal growth proceeds by vertical movement (here shown downwards) of the feed rod through the melting zone and finally the growing crystal out of it. By tuning the electrical power of the XBO xenon short arc lamp and varying the shutter orifice the process temperature can be controlled to some extend.
The advantage of this heating method is the broad variability in terms of melting temperatures, applicable temperature profiles/gradients and, in contrast to inductively heated floating zone furnaces, being independent of the samples electrical properties. Due to the fact that the method is well established for many years in single crystal preparation at the IFW, its benefits are well known just as its limits. Thus the motivation to develop a new floating zone furnace was to have an optimized apparatus available facilitating new experimental conditions and possibilities on single crystal preparation. By which means this goal has been achieved is reported as follows.

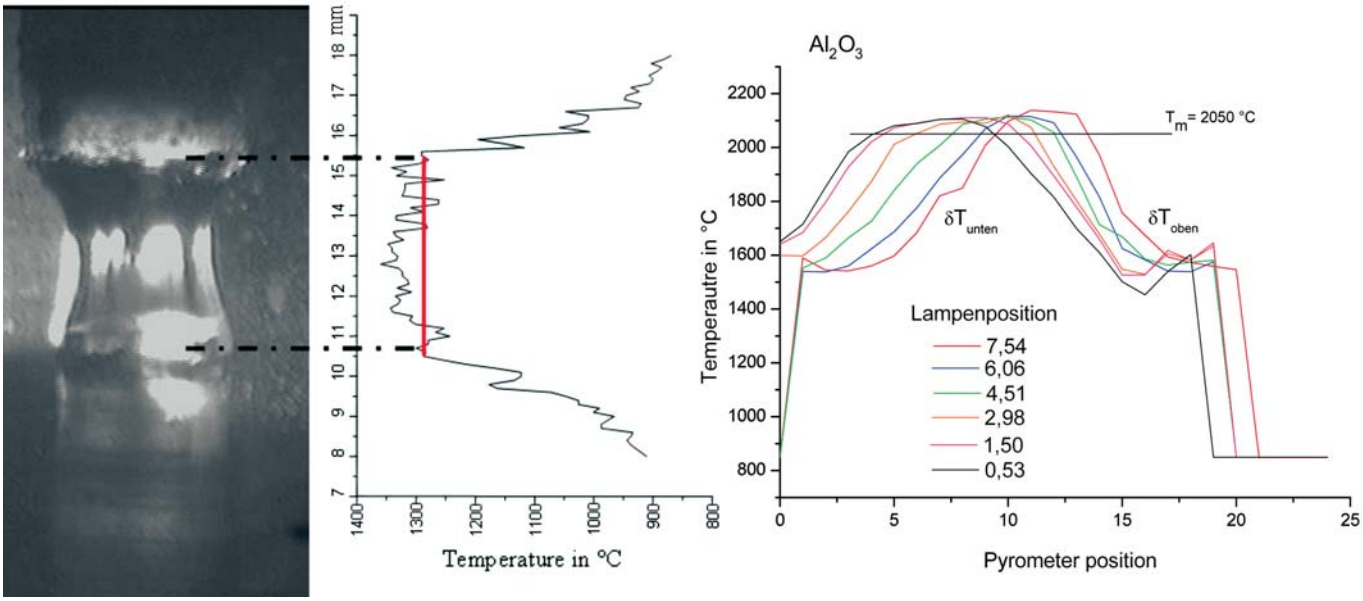

Fig. 2: *in-situ* measurements of the floating zone temperature

In order to optimize the floating zone process - in particular the irradiation profile formation into the melting zone - the optical parameters were analyzed and recalculated in detail [2]. In close cooperation with Fraunhofer Institute für Optik und Feinmechanik in Jena the final mirror geometries were developed ready for manufacturing and application. In the *SFZ* furnace the mirror distance to each other, the position of the XBO lamp in the bottom mirror and the position of the molten zone relatively to the upper mirror can be adjusted easily by separate precision linear drives. This new feature controls the imaging of the xenon arc on the sample surface by focusing, specific defocusing and by varying the angle of incidence, thus influencing the irradiation profile on the floating zone. The effect of each adjustment can be monitored by *in-situ* temperature measurements along the vertical axis [3], which has been realized in the *SFZ* furnace for the first time. The left side of Fig. 2 shows a typical photograph of a floating zone together with a temperature profile which was obtained by moving the temperature probe (ratio pyrometer) parallel to the rod axis. The diagram on the right side indicates the changes in the profile by varying the lamp position relatively to the bottom mirror in a range of approx. 70 mm along the optical axis. The lamp can be positioned by a motorized drive without interrupting the crystal growth process. The light distribution and subsequently the shape of the temperature profiles are very sensitive to this parameter, so that the growth process can be tailored and controlled by tuning the optical setup.

In order to minimize thermal stress on the single crystal right after leaving the floating zone, a resistance heater which is installed in a short distance to the upper mirrors focal point is available (Fig. 1, right). The heater is designed for max. 1100 °C.

In addition to the re-engineering of the thermo-optical process a particular feature of the *SFZ* furnace is its opportunity to vary the process gas pressure from 10^{-3} mbar to 150 bars. In addition to the operation under vacuum conditions the crystal growth chamber can be pressurized with a well defined atmosphere which properties can be varied from oxidizing (e.g. pure O_2) via neutral to reducing conditions. Reactive gases which interfere with the melt during the growth process can also be introduced. Except the oxygen line each feed gas can be lead through a purifying device reducing the oxygen tension to less than 10^{-16} ppm. Finally a highly sophisticated gas control system allows the application of mixtures under static as well as flow conditions within the entire pressure range.

According to the extreme pressure and flow conditions combined with the inherent requirements of light heated floating zone processes, quite a number of key components in the *SFZ* furnace had to be newly developed and designed. In this list the outstanding

subassemblies are the two pulling drives which have to perform the feed rod transfer through the melt into the single crystal under continuous rotation. Due to the flexibility in use of the *SFZ* furnace the linear velocity has to be variable from 0.01 mm/h to 2000 mm/h and the rotation from 0 to 150 rpm. Once adjusted both movements have to be applied smoothly and highly accurate into the growth process and to be maintained during the entire linear travel of 150 mm. Additionally the pulling drives have to cope with the forces caused by the differential pressure of 150 bars and they have to provide tightness under high pressure and vacuum. In order to comply with the requirements listed above the pulling drives were designed as depicted in Fig. 3.

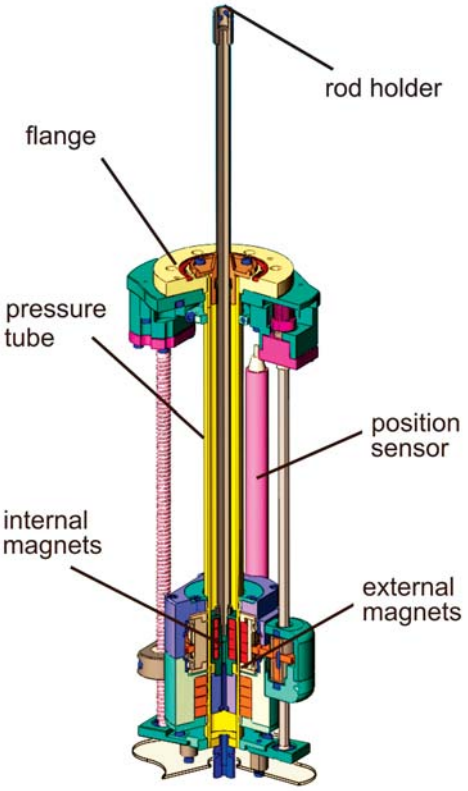

Fig. 3: Design of the new pulling drives

The rod holder performs the movement of the feed rod and single crystal inside the pressurized growth chamber. In order to avoid any slip-stick jerking the design is totally waiving brush seals. Tightness is provided by the flange and the pressure tube which is guiding the rod movement at the same time. The outer gear box generates linear travel and rotation of an external magnet assembly. By magnetic coupling this movement is transferred to a system of internal magnets and finally to the rod holder. A number of tests have proven the accuracy and lack of hysteresis of this device, ensuring the availability of a major component for crystal growth experiments with floating zone under high gas pressure.

The entire set of experimental parameters such as linear and rotational movements of the pulling drives, gas mixture, flow and gas pressure, lamp position and irradiation power are controlled by a programmable logic controller, PLC. This system is also part of the safety system managing the relevant interlocks according to the hazard potentials of high pressure, heat and intense radiation. Passive safety is implemented by covering the optical system as well as the growth chamber against unexpected burst of pressurized items. Fig. 4 shows a photograph of the *SFZ* furnace as it is installed in the IFW.

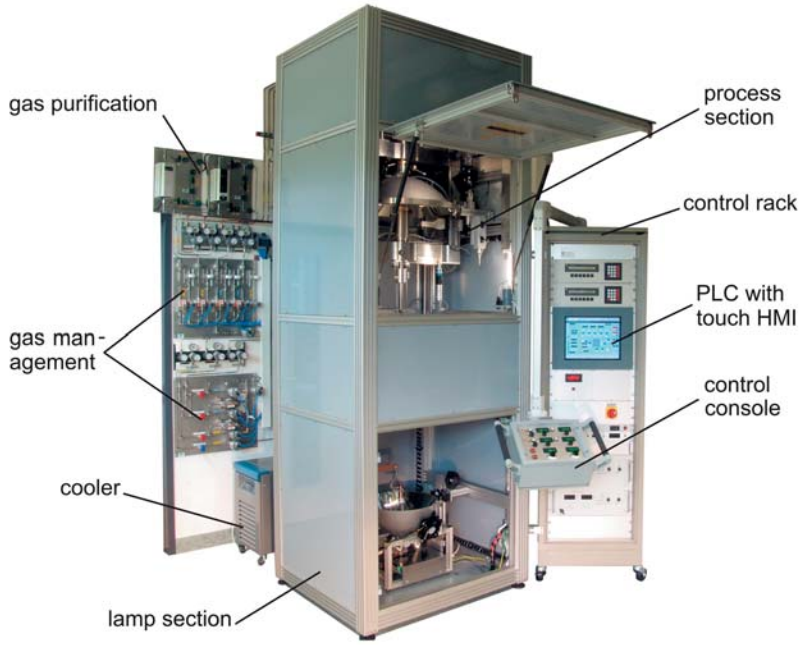

Fig. 4: *SFC* furnace as installed in the IFW crystal growth laboratory

In 2008 hundreds of hours in operation have proven reproducibility and long term stability of growth conditions in the *SFZ* furnace.

References

[1] A.M. Balbashov, S.K. Egorov, J. Crystal Growth 52 (1981), 498-504
[2] D. Souptel, W. Löser, G. Behr, J. Crystal Growth 300 (2007), 538-550
[3] G. Behr, R. Voigtländer, A. Horst, R. Morgner, F. Fischer: Verfahren zur pyrometrischen Messung der Temperatur des Schmelzgutes in Einkristallzüchtungsanlagen. Patent DE 10 2006 019 807 B3 2007.08.23

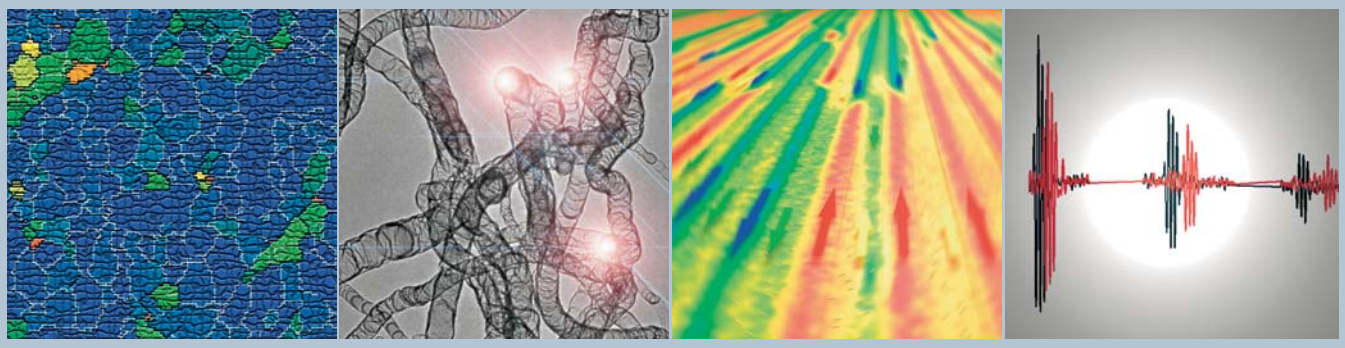

Reports from Research Areas

Ni substrates as templates for YBCO coated conductors

Multi wall Carbon nanotubes with bamboo-like structure

Distribution of magnetization in a Ni-Fe film with local ion implantation of Cr

Ultrasonic pulse-echo patterns for $Sr_3NbGa_3Si_2O_{14}$ single crystal

Research Area 1
Superconductivity and superconductors

Charge-Transfer Excitons In Underdoped $Ca_{2-x}Na_xCuO_2Cl_2$

R. Schuster, M. Knupfer, J. Fink, B. Büchner

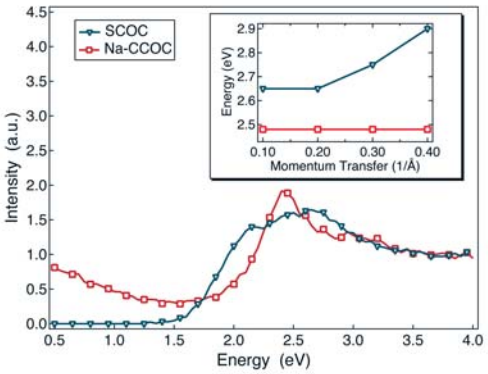

Fig.: The EELS intensity for $Sr_2CuO_2Cl_2$ (SCOC) and $Ca_{1.95}Na_{0.05}CuO_2Cl_2$ (Na-CCOC) parallel to the Cu-O bonds. There is a clear redistribution of the spectral weight between 2…3 eV upon doping. The inset shows how the maximum of the intensity disperses for higher momentum transfers in the case of SCOC whereas the feature in the Na-CCOC spectra is strongly localized.

The low-lying electronic excitations in the high-temperature superconducting cuprates correspond to the transition of electrons from oxygen to copper. The result of such a charge transfer is an electron-hole pair, referred to as charge-transfer exciton (CTE) in the following, similar to an exciton in conventional semiconductors. The dynamics, in particular the band-structure, of these entities allows do draw conclusions about their interference with the antiferromagnetic order on the copper sites and the doping induced charge carriers in the CuO-plane. To this end we performed Electron Energy-Loss Spectroscopy (EELS) on $Ca_{2-x}Na_xCuO_2Cl_2$ and we found remarkable changes compared to the undoped parent compound $Sr_2CuO_2Cl_2$. The figure summarizes the most important modifications: (i) the spectral weight in the relevant energy scale of the CT processes (2…3 eV) is considerably redistributed and, even more importantly, (ii) the bandwidth of the CTE which amounts to several hundred meV in the undoped case breaks down completely already for 5% doping. Depending on the residual strength of the (due to the screening) reduced Coulomb attraction which tends to bind the CTE, different scenarios may be realized. If the doping still allows the formation of bound excitons the strongly fluctuating magnetic background will prohibit a coherent motion of the CTE. If, however, the particle and the hole are independent from each other, then their motion will produce frustrated spins that will confine both of them to a small area within the CuO-plane. In either case our data provide another striking example for the complexity of the excitations in underdoped cuprates.

Cooperation Department of Advanced Materials Science Tokyo; Inst. Chem. Res. Kyoto
Funded by DFG

Local study of vortex pinning in superconducting thin films

T. Shapoval, S. Haindl, J. Engelmann, E. Backen, C. Bran, D. Meier, S. Vock, B. Holzapfel, U. Wolff, V. Neu, L. Schultz

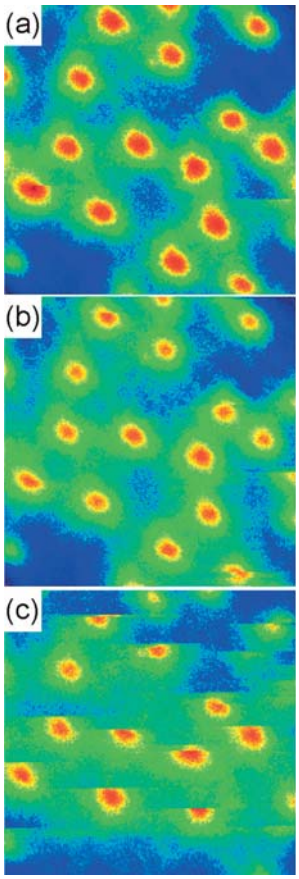

Fig.: Vortex imaging in NbN field cooled in -2mT at (a) 50 % T_c, (b) 62 % T_c and (c) 75 % T_c Scanning area: 4 x 4 μm^2

The interpretation of intrinsic pinning mechanisms, the search for artificial defects with high pinning potential, and commensurable pinning effects by ordered arrays of defects initiated a large variety of studies, which are today an important topic in basic research as well as in application-based engineering. So far, a challenging task for local imaging techniques such as low temperature magnetic force microscopy (LT-MFM) is to correlate the position of superconducting vortices with microstructural defects. Since the surface roughness (droplets, precipitates) poses a severe problem to the scanning tip, a polishing technique for thin films has been developed [1].
As an example, the temperature dependence of the vortex distribution in a 100 nm thick polished NbN film was imaged after field cooling. At 50 % T_c the vortices are organized in a slightly disordered Abrikosov lattice and are pinned by intrinsic defects (Fig. a). Decreased contrast of the vortex profile at a higher temperature corresponds to the temperature dependence of the penetration length (Fig. b). At 75 % T_c the depinning of vortices by the scanned MFM tip is visualized (Fig. c). Thus, the pinning force on the intrinsic defects at this temperature is equal to the magneto-static interaction force between the MFM tip and the vortex. It allows a local estimation of the pinning potential and its comparison with an average value obtained from global magnetization measurements.

Other activities of the MFM group cover investigation of domains in complex magnetic multilayers (Co/CoO and [Co/Pt]/Ru), study of flux distribution in superconducting materials ($YBa_2Cu_3O_{7-\delta}$ [2], $Ba_{1-x}K_xFe_2As_2$ [3]), as well as interpretation of the pinning mechanism in SC/FM hybrid structures (Py/Nb).

[1] T. Shapoval *et. al.* SUST **21**, 105015 (2008)
[2] T. Shapoval *et. al.* Phys. C. **460–462,** 732–733 (2007)
[3] J. T. Park *et. al. arXiv:0811.2224* (2008)

Cooperation LLN Grenoble, Hitachi GST San José, MPI Festkörperforschung Stuttgart, Univ. of Illinois at Chicago
Funded by EU (HIPERCHEM), SFB 463 (A4), IMPRS

MgB_2 – bulk, powder, tapes

W. Häßler, M. Herrmann, A. Kario, C. Rodig, J. Scheiter, K. Schröder, M. Schubert, G. Fuchs, W. Gruner, C. Mickel, K. Nenkov, B. Holzapfel, L. Schultz

In the last years we have developed a nanocrystalline MgB_2 precursor powder prepared by mechanical alloying. Hot pressed bulk samples and powder-in-tube-tapes based on this precursor powder are characterized by high critical current densities j_c due to the small primary grain size and therefore a high number of grain boundaries. By carbon doping of this precursor powder the critical fields and currents can be enhanced further, so monofilamentary tapes with upper critical fields of 32 T at 4.2 K and j_c-values of 10 kA/cm^2 at 16 T and 4.2 K could be obtained.

In the last year our work was focused on the preparation of long length multifilamentary wires. Therefor the deformation technique of the wires with a Monel/Nb double sheath was upgraded. Several wires with a length of more than 100 m using undoped powder were prepared by swaging and drawing (j_c > 10 kA/cm^2 at B < 8 T). In cooperation with Bruker's Advanced Supercon Business our successful research results will now be transferred towards industrial MgB_2 wire production. A potential market for MgB_2 wire is seen in 'dry' MRI and energy research magnets operating without liquid helium at temperatures above 10 K.

For another topic commercial *ex situ* powder was milled to improve grain boundary pinning by smaller grain sizes. At bulk samples improved critical fields and critical current densities were measured. Microstructural investigations at monofilamentary tapes show a better densification of the filaments using milled powder. The irreversibility field of these tapes was improved but it is still lower than in comparison to mechanical alloyed in-situ powder.

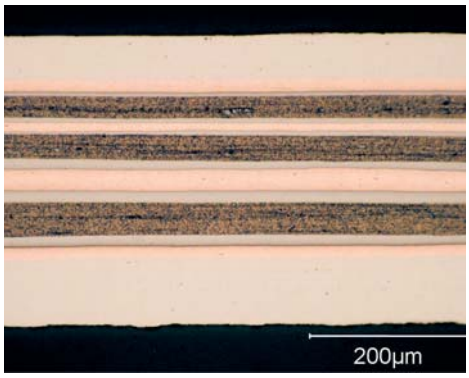

Fig.: Longitudinal section of a multifilamentary MgB_2 wire with Monel/Nb-sheath

Cooperation Bruker EAS GmbH Hanau, Institute of Electrical Engineering Bratislava, FZ Karlsruhe
Funded by EU, EAS Bruker GmbH

YBCO coated conductor architectures

B. Holzapfel, R. Hühne, J. Eickemeyer, A. Güth, C. Rodig, H. Klauß, K. Güth, R. Kaltofen, T. Thersleff, A. Kirchner, T. Freudenberg, S. Engel, L. Schultz

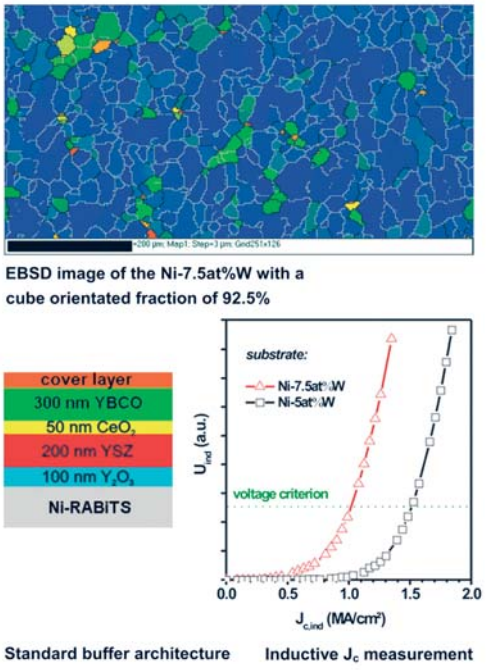

Fig.: Newly developed highly textured Ni-7.5at%W substrates as templates for YBCO coated conductors [1].

The preparation of coated conductor architectures for high-performance superconducting tapes based on YBCO films was continued last year in the framework of an IFW project. A major focus was on the realisation of improved textured metal substrates showing reduced ferromagnetism at 77 K and higher mechanical strength compared to the standard Ni-5at%W tape. A major breakthrough was achieved with the successful preparation of highly textured Ni-7.5at%W tapes. Specific homogenisation and stress relief treatments were implemented in the process to get a cube orientated fraction of more than 92 % [1]. An optimised coated conductor architecture was prepared on these substrates using pulsed laser deposition resulting in YBCO layers with an in-plane alignment of about 8.5° and a critical current density of about 1 MA/cm^2 (see fig.).
A fully electrically conducting buffer architecture was developed based on highly textured TiN layers prepared by ion-beam assisted pulsed laser deposition (IBAD). For the first time, an amorphous Ta-Ni was successfully used directly on electropolished Hastelloy tapes as new metallic seed layer for the IBAD-TiN process [2]. An in-plane alignment below 10° was achieved for the prepared TiN layer in this case. An additional Au/Ir/Nb:$SrTiO_3$ buffer layer architecture was grown on the biaxially textured TiN layers having an epitaxial relationship to the nitride layer. Finally, YBCO was deposited on the buffered substrate showing an in-plane alignment of about 7° and a superconducting transition temperature of 88 K [3].

[1] J. Eickemeyer et al., Supercond. Sci. Technol. 21 (2008) 105012.
[2] R. Hühne et al., J. Phys. D : Appl. Phys. 41 (2008) 245404.
[3] K. Güth et al., IEEE Appl. Supercond. 19 (2009) accepted.

Cooperations evico GmbH, Univ. Cambridge, IIT Madras, Los Alamos National Lab., Zenergy GmbH, Nexans Superconductors GmbH, ICMAB Barcelona, Shanghai Univ.
Funded by BMBF, EU, DAAD

Improved flux pinning in bulk Gd-Ba-Cu-O/Ag superconductors by a quasi beads-milling technique

K. Iida, G. Fuchs, K. Nenkov, G. Krabbes, G. Behr, B. Holzapfel, L. Schultz

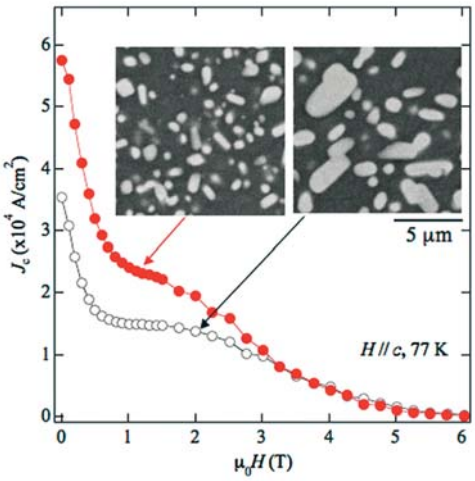

Fig. Beads-milling technique is significantly effective in modifying the sample microstructures. As a result, superconducting properties in low field regime are, in particular, improved.

Unlike (LRE)$Ba_2Cu_3O_{7-y}$ ((LRE)-123, where LRE is a light rare earth element or Y) type thin films, incorporation of nano-sized second phase particles such as $(LRE)_2BaCuO_5$ ((LRE)-211) in the superconducting matrix is one of the most challenging issues in the bulk superconductors. Final size of (LRE)-211 particles in the (LRE)-123 matrix (i.e. after melt-processing) has been determined by its initial size. Hence we have tried to reduce the initial size of Gd-211 particles by a quasi beads-milling technique. Commercial Gd-211 powders were planetary-milled for 45 min in acetone using ZrO_2 beads of 1 mm diameter with a maximum centrifugal acceleration of 15 G. As a result, small Gd-211 particles were successfully embedded in the Gd-123 superconducting matrix as shown in the inset of the figure, which led to a high performance of J_c-B characteristics (see figure). A single grain Gd-Ba-Cu-O/Ag bulk superconductor 26 mm in diameter employing fine Gd-211 particles can trap a significant large field of about 1.1 T at liquid nitrogen temperature, whereas the corresponding value of the standard sample shows only 0.9 T. These results are very promising and encourage us to further improve the superconducting properties by a combination of the current technique and chemical doping technique.

Research Area 2
Magnetism and magnetic materials

Field dependence of magnetic entropy change

M.D. Kuz'min, M. Richter, A.M. Tishin[1]

The emerging room-temperature magnetic refrigeration technology requires materials producing a large entropy change $|\Delta S|$ when exposed to a moderate magnetic field (~2T). Ferromagnets with $T_C \approx 300$ K are best suited for the purpose, since their $|\Delta S|$ reaches a maximum near room temperature. The maximum value of the magnetic entropy change $|\Delta S|_{max}$ depends on the applied magnetic field, the form of this dependence not being firmly established. A well-known fact, however, is that the mean-field prediction, $\Delta S_{max} \propto H^{2/3}$, is not fulfilled. In a recent Letter [1] we demonstrate that, besides the term in $H^{2/3}$, $|\Delta S|_{max}$ must contain a small negative term independent of H. Spatial inhomogeneity of real ferromagnetic materials is shown to be the origin of the off-set term, whose magnitude proves proportional to the width of the distribution of local Curie points. The predicted field dependence of $|\Delta S|_{max}$ is in agreement with available experimental data (see Figure).

[1] M.D. Kuz'min, M. Richter, and A.M. Tishin, J. Magn. Magn. Mater. **321**, L1 (2008).
[2] K. Ahn, A.O. Pecharsky, K.A. Gschneidner, Jr., and V.K. Pecharsky, J. Appl. Phys. **97**, 063901 (2004).
[3] J.D. Zou, B.G. Shen, and J.R. Sun, Chin. Phys. **16**, 3843 (2007).

Cooperation [1]Moscow State Univ., Russia
Funded by DFG, Project RI 932/4-1.

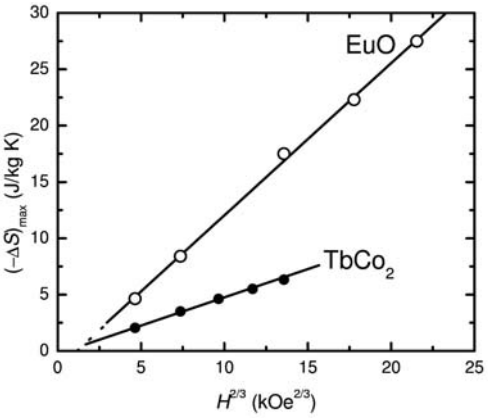

Fig.: The maximum entropy change plotted against $H^{2/3}$. The experimental data are from Refs. [2] (EuO) and [3] ($TbCo_2$).

Magnetoresistance in spin-valve structures with organic spacer layers

J. Schumann, H. Vinzelberg, D. Elefant, K. Dürr, J. Thomas, B. Büchner

Giant magnetoresistance effects in organic spin-valves have been realized as layered (La,Sr)MnO_3 (LSMO)-based junctions with tris-(8,hydroxyquinoline) aluminum (Alq_3)-spacer and ferromagnetic top layers. The experimental work was focused on the understanding of the transport behavior in this type of magnetic switching elements. The device preparation was carried out in an ultra high vacuum chamber equipped with a mask changer by evaporation and sputtering on $SrTiO_3$ substrates with LSMO stripes deposited by pulsed laser deposition. The field and temperature dependences of the magnetoresistance of the prepared elements are studied. Spin-valve effects at 4.2 K have been observed in a broad resistance interval from 50 Ω to MΩ-range, however, without systematic dependence on spacer layer thickness and device area. In some samples, the magnetoresistance (MR) changes sign as a function of the bias voltage. The observed similarity in the bias voltages dependences of the MR in comparison with conventional magnetic tunnel junctions with oxide barriers suggests a description of the found effects within the classical tunneling concept. The proposed model implies the realization of the transport via local Co chains embedded in the Alq_3 layer and spin dependent tunneling over barriers at the interface Co grains/Alq_3/LSMO. The existence of conducting Co chains within the organics is supported by transmission electron microscopic/electron energy loss spectroscopic studies on cross section samples from analogous layer stacks.

Cooperation TU Dresden, Inst. für Angewandte Photophysik

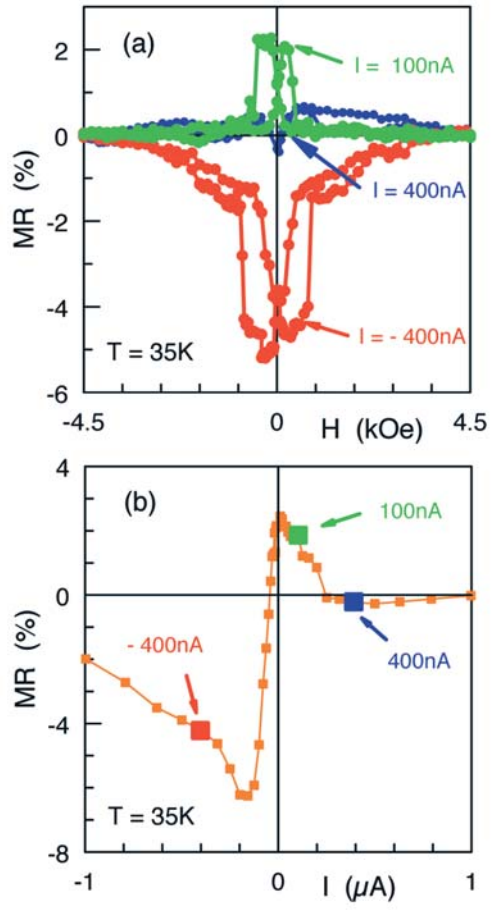

Fig.: Current dependence of the MR of LSMO(100 nm)/Alq_3(150 nm)/Co(10 nm)/Al(10 nm) layer stacks at 35 K. (a) MR(H) at different current and (b) MR(I) with the values of (a) at constant current.

Electrochemical deposition in superimposed magnetic fields

M. Uhlemann, J. Koza, X. Yang, K. Hennig, A. Gebert, K. Tschulik, C. Mickel, L. Schultz

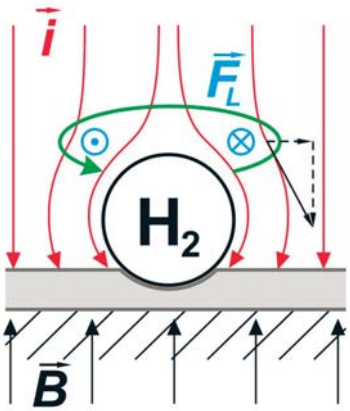

Fig.: Schematic model of the magnetic field influence on the HER

The effect of a magnetic field superimposed with perpendicular orientation relative to the electrode surface on the hydrogen evolution reaction (HER) during metal deposition has been systematically investigated and a model has been proposed. It was found that desorption of hydrogen is enhanced in a magnetic field and a drastically reduced bubble size has been proven by shadowgraph experiments. The origin of the phenomenon is seen in a special type of a micro-MHD effect. An azimuthally directed Lorentz force arises due to the fact that the current distribution is distorted around the hydrogen bubble which creates a swirling flow and provokes an additional pulling force at the liquid-gas interface. This force together with a modified buoyancy force due to changes in the concentration boundary layer is probably the main mechanisms for the accelerated bubble desorption.

Nucleation studies for Fe deposition on polycrystalline Au (111) have been carried out in applied magnetic fields for different configurations relative to the electrode surface. Independent on an applied magnetic field the deposition starts with a 2D layer-by-layer growth followed by a 3D nucleation and growth process. Without magnetic field the nucleation is progressive, the nucleation rate is constant, and the number of active sites is increased with the applied potential. In magnetic fields parallel to the electrode the nucleation proceeds via an instantaneous mode. The nucleation and growth process were analysed based on models developed by Heerman and Tarallo. The hydrodynamic origin of the observed effects was confirmed.

First investigations on electrodeposition in superimposed magnetic field gradients aim at tailored and structured deposits based on overlapping magnetically induced forces.

Cooperation TU Dresden, FZ Dresden-Rossendorf, Univ. Reims, High Magnetic Field Lab. Grenoble, AGH Univ. of Science and Technology, Krakov
Funded by DFG (SFB 609)

Hybrid soft-magnetic films with novel functionality created by magnetic property patterning

J. McCord, C. Hamann, N. Martin, I. Mönch, R. Kaltofen, T. Gemming, R. Schäfer, L. Schultz

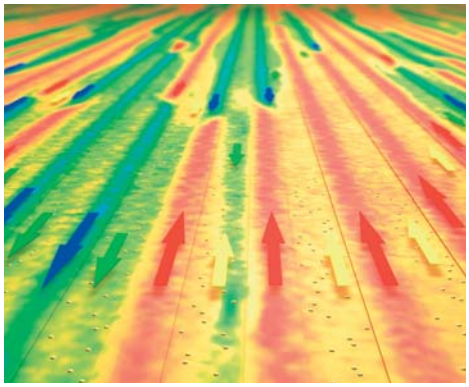

Fig.: Distribution of magnetization of a magnetically hybrid film with laterally modulated saturation polarization generated by local ion implantation of chromium into the initial nickel-iron film.

Methods allowing the tailoring and custom design of soft-magnetic thin film properties are crucial for achieving magnetic devices with improved functionalities. A fundamentally new type of "hybrid materials" is currently investigated, which is created by lateral modulation of the intrinsic magnetic properties on a micrometer scale by means of ion implantation or local oxidation. The films exhibit static and dynamic properties different from regular thin film samples. Intriguing magnetic domain configurations and magnetization reversal features, as for example a lateral exchange spring effect caused by compressed 180° domain walls of adjustable high density, are observed. The physical origin of all these novel structure properties is the intricate interplay between exchange coupling and magneto-static effects, which open new opportunities to tailor overall magnetic thin film properties. The combination with magnetic multi-layers or pre-patterned magnetic elements will result in thin film magnetic structures with custom functionality.

Cooperation FZ Dresden-Rossendorf, Univ. Bochum, Univ. Kiel, Univ. Kassel
Funded by DFG (DFG MC 9/7-1).

Strained epitaxial Nd-Fe-B films by mechanical elongation

A. R. Kwon, S. Fähler, V. Neu, V. Matias[1], J. Hänisch, R. Hühne, B. Holzapfel, T. Schied, M. Seifert, F. Fleischhauer, L. Schultz

While $Nd_2Fe_{14}B$ is already used in high performance bulk magnets, thin films are interesting for applications such as microactuators, motors and magnetic recording. For technological applications, well textured $Nd_2Fe_{14}B$ films are available [1,2]. Nd-Fe-B has very high magnetocrystalline anisotropy, therefore, magnetoelastic anisotropy is usually neglected. However, under large external stress, especially the spin reorientation transition at low temperature should be affected. Here a new approach to study the influence of strain on the intrinsic properties of $Nd_2Fe_{14}B$ under uniaxial stress is presented.
Hastelloy, which has high ductility, is used as a substrate to realize strain of up to 4% by conventional mechanical elongation of the full layer stack. In order to guarantee epitaxial growth on this polycrystalline substrate, in a first step in-plane textured MgO(001) had been deposited by ion beam assisted deposition (IBAD). In a next step Mo buffer and Nd-Fe-B are deposited at 450 °C by pulsed laser deposition. Mo grows epitaxially with a (001) orientation and Nd-Fe-B films possess the desired (00l) out-of-plane orientation. Unlikely on Cr/Ta buffer, which have a single epitaxial relation to the substrate, films on Mo grow with 3 epitaxial variants which results in equivalent in-plane anisotropy (Fig.).
Elongation breaks the in-plane symmetry compared to the as-deposited state, resulting in an elliptical shape of the cone opening during spin reorientation up to a strain value of about 2% (Fig. (c)), whereas the spin reorientation temperature does not change significantly. With higher strain (4%) cracking and partial delamination of the film occurred. By this novel and versatile approach it is possible to study the influence of large strain on the anisotropic properties of various materials as the used MgO (001) layer is a common template for epitaxial growth.
Other activities in permanent magnet films concern hard/soft magnetic bilayers of Fe-Pd and exchange coupling in epitaxial $RECo_5$ multilayers.

[1] A. R. Kwon, V. Neu, L. Schultz, S. Fähler , J. Appl. Phys. **101**, 09K506 (2007)
[2] A. R. Kwon, S. Fähler, V. Neu, L. Schultz, J. Magn. Magn. Mater. **302** 252 (2006)

Cooperation TU Dresden, [1)] Los Alamos National Laboratory
Funded by SFB 463 B20

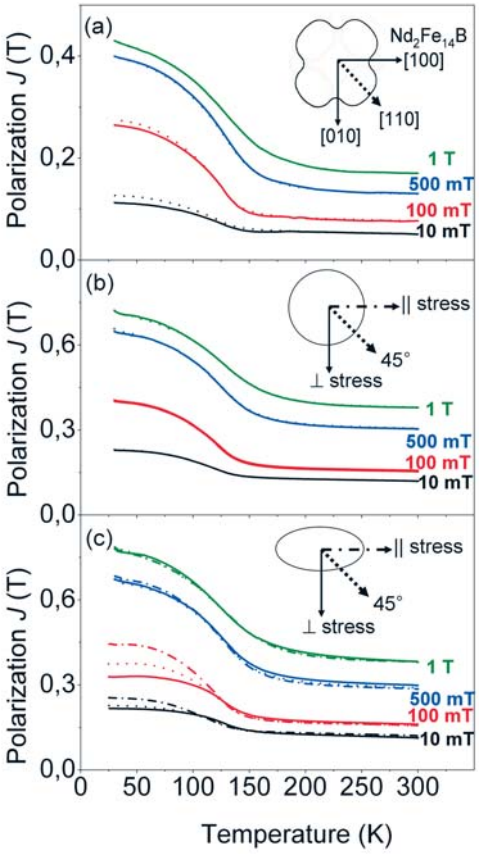

Fig.: Spin reorientation transition in $Nd_2Fe_{14}B$. Temperature dependent magnetic polarization *J* is shown for Nd-Fe-B films grown epitaxially on a combined Cr/Ta buffer on MgO single crystal (a), and grown on a Hastelloy/IBAD-MgO substrate in the as-deposited state (b) as well as after 2 % elongation (c). Measurements have been performed in different in-plane directions and with different field. The sketch in each part illustrates the respective in-plane anisotropy.

Effect of magnetic fields on corrosion

R. Sueptitz, J. Koza, M. Uhlemann, A. Gebert, L. Schultz

NdFeB hard magnets are widely spread in application due to their excellent magnetic properties. However, their poor environmental stability is a critical factor mainly arising from their multiphase structure and the high reactivity of their constituents. In order to improve these materials an understanding of the effect of influencing factors, e.g. of magnetic fields, on their corrosion processes is indispensible. Two magnetically induced forces can act in an electrolyte. The Lorentz force leads to convection and the field gradient force pulls paramagnetic ions into electrode regions of high flux density. All partial corrosion reactions can be influenced by these forces. Therefore anodic dissolution and cathodic reduction reactions are fundamentally investigated by using single phase electrodes and the obtained knowledge will be applied to multiphase systems. The influence of magnetic fields of varying strength and relative orientation to a cylindrical iron electrode was studied. It was found that a field applied parallel leads to an enhanced dissolution due to the Lorentz force driven electrolyte convection. A magnetic field applied perpendicular leads to large flux densities in front of the electrode due

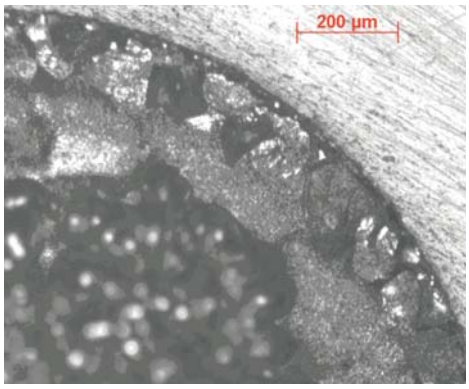

Fig.: Localized corrosion of an iron cylinder in sulphuric acid under influence of a magnetic field (B = 0.3 T) applied parallel to the cylinder axis

to the ferromagnetic nature of iron. Iron ions are collected by the magnetic field gradient force at the rim of the electrode, where the flux density reaches its maximum. This hampers locally its dissolution. The overall corrosion reaction is inhibited by the magnetic field influence in this configuration and the dissolution is localized leading to pit-like material damage in regions of low surface flux density (Fig.).

Cooperation TU Dresden, FZ Dresden-Rossendorf
Funded by DFG, SFB 609

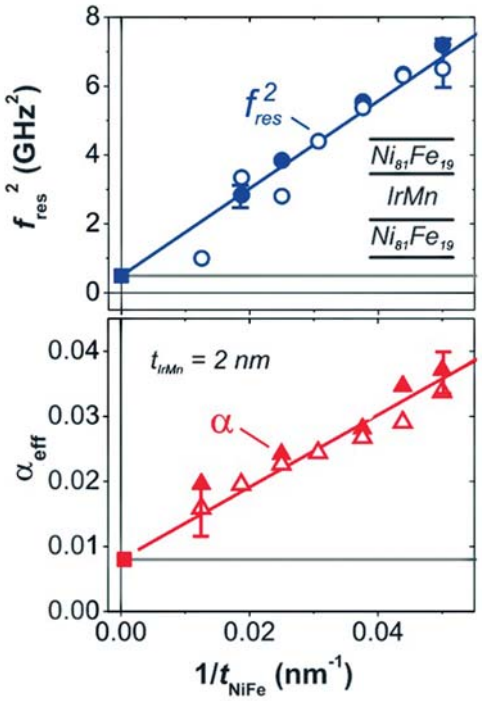

Fig.: Dependence of the precessional frequency square f_{res}^2 and effective damping parameter α_{eff} on reciprocal $Ni_{81}Fe_{19}$-thickness $1/t_{NiFe}$ for $Ni_{81}Fe_{19}/Ir_{19}Mn_{81}$ (2 nm)/$Ni_{81}Fe_{19}$ sandwich structures.

Tuning of magnetization dynamics of coupled ferromagnetic thin films by ultrathin antiferromagnetic layers

J. McCord, R. Kaltofen, L. Schultz, O.G. Schmidt

The existence of mixed magnetic anisotropies and a systematic modification of the dynamic damping parameter in ferromagnet/antiferromagnet polycrystalline thin film systems as a function of antiferromagnetic layer thickness are demonstrated. Based on this findings it is shown that independent of the occurence of exchange bias, using ultra-thin antiferromagnet layers, a controlled adjustment of static and dynamic magnetic properties of ferromagnetic thin films is possible. Due to the combined increase of precessional frequency and effective damping parameter, a significant reduction in magnetic settling time is realized. Simple relations based on the assumption of an interfacial antiferromagnetic layer contribution are derived to describe and predict the change in magnetization dynamics. The experimental findings are of great importance from a fundamental point of view and are significant for various applications based on ferromagnetic thin film technology. The addition of thin antiferromagnetic layers in contact to ferromagnetic thin films facilitates for controlled alteration of magnetic properties beyond the established manipulation of the intrinsic ferromagnetic material properties.

Electrodeposition of magnetic nanowires: Correlation of magnetic properties with deposition conditions and morphology

V. Hähnel, M.S. Khatri, A.K. Srivastav, I. Dobosz, J. Koza, K.L. Rabah, C. Mickel, K. Hennig, S. Neitsch, M. Uhlemann, S. Fähler, H. Schlörb, L. Schultz

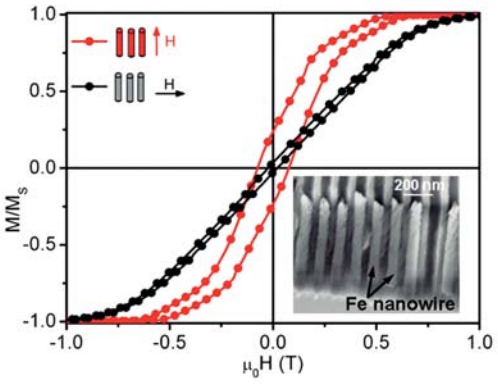

Fig.: Hysteresis loop and SEM cross sectional view of electrodeposited Fe nanowires

Periodic arrays of magnetic nanowires deposited in self-organised nanoporous templates have recently attracted much attention in fundamental and applied research. Scientific interest focuses on these low dimensional nanostructures, as significant changes in terms of chemical and physical properties compared to bulk material are expected. Application potential of these nanostructures ranges from high-density magnetic recording, nanoelectrodes to sensors. Materials under investigation are metals like Ni, Co, Fe, soft-magnetic CoFe and hard-magnetic FePt and CoPt alloys. Our studies aim at correlating morphology, structure and magnetic properties with deposition parameters, e.g. deposition potential and time, as well as electrolyte composition and concentration and to study the influence of external magnetic fields.

As an example Fe nanowires with bcc structure and a coherence length in the order of magnitude of the pore diameter have been deposited using DC voltages between -0.95 and -1.15 V_{SCE} into a nanoporous aluminum oxide membrane with 70 nm pore diameter. Low Fe^{2+} concentration results in a rough surface morphology and discontinuous nanowires. Increasing the Fe^{2+}-concentration and especially adding H_3BO_3 leads to a

smoother wire surface and less defects. By adjusting the deposition time the wire length was varied up to 10 µm. With increasing length it is observed that the axis perpendicular to the wire axis becomes the magnetically hard axis due to shape anisotropy. In addition, for long wires having a smooth surface morphology two different slopes are observed in magnetisation curves measured along the wire (Fig.). Since this behaviour is not expected for isolated wires, this indicates magnetostatic interactions favouring an antiferromagnetic alignment of neighbouring wires.

Cooperation AGH Univ. of Science and Technology Krakow, Poland;
Univ. de Reims, France; IIT Kanpur, India
Funded by DFG, DAAD, SMWK

Bubbles in magnetic multilayers and Skyrmion lattices in chiral magnets

C. Bran, N.S. Kiselev, A.B. Butenko, A.A. Leonov, U. Wolff, A. N. Bogdanov, V. Neu, U.K. Rößler

Localized states in magnetics can be realized, and have been used for data storage, as bubble domains that are stabilized by an external field in magnetic films with strong perpendicular anisotropy. Recently, there is new interest in perpendicular media for data storage in the form of antiferromagnetically coupled multilayers with strong out-of-plane anisotropy. These systems display magnetic stripes or antiferromagnetic ground states and a rich variety of unusual domain and defect states [1]. Experimentally we have observed bubbles in $[(Co/Pt)_8/Co/Ru]_{18}$ by magnetic force microscopy on the scale of several ten nanometers (Fig.). A detailed comparison with theoretical calculations within a micromagnetic model, in particular quantitative agreement of parameters as the strip-out and collapse instability fields between experiment and theory, has been achieved. The topology of a bubble domain in a film is that of a Skyrmion. As predicted earlier, such localized states can be stabilized on the nanometer scale in magnetics under the influence of chiral Dzyaloshinskii-Moriya couplings. Skyrmions may form thermodynamically stable states that compete with helical or collinear ground states. Our new theoretical calculations show that symmetry breaking uniaxial distortions in conjunction with magnetic fields induce stable magnetic Skyrmion lattices in cubic chiral magnets like MnSi. Skyrmion lattices, which are magnetic analogues of Abrikosov lattices in superconductors, could similarly be stabilized in magnetic film systems, e.g., in soft chiral magnetic films under influence of an exchange-bias from a highly anisotropic antiferromagnetic or ferromagnetic substrate near the magnetic ordering temperature.
[1] N. S. Kiselev et al. Appl. Phys. Lett. **93,** 162502 (2008).

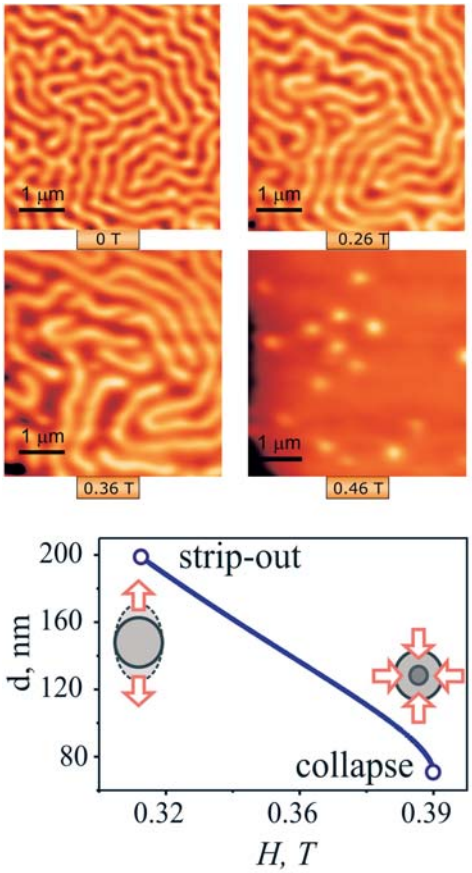

Fig.: Progression from stripe to bubble domains in $[(Co/Pt)_8/Co/Ru]_{18}$ as a function of a perpendicular magnetic field. In a field range between 0.38 T and 0.47 T the solution of the micromagnetic equations leads to stable bubble domains, in agreement with the experiment.

Cooperation Hitachi Global Storage Technologies, San Jose Research Center, USA
Donetsk Institute for Physics and Technology, Ukraine
Funded by DFG (SPP1239, A8)

Crystal growth of intermetallics and oxides with volatile elements

G. Behr, W. Löser, N. Wizent, P. Ribeiro, C.D. Cao, F. Lipps, I. Hellmann, R. Klingeler, V. Kataev, D. Lindackers, F. Fischer, N. Sato, B. Büchner

A unique floating zone crystal growth method for refractory intermetallics and oxides containing volatile elements such as Li, Cu, Sm, Tm and Eu has been installed at the IFW Dresden. Radiation heating in a vertical double-ellipsoid optical configuration enables a compact growth chamber and the application of high pressures up to 15 MPa of various atmospheres (Ar, He, N_2, H_2, O_2). A high pressure of Ar up to 5 MPa utilized in

crystal growth of intermetallic compounds with melting temperatures 1733°C (Tm_2PdSi_3), 1422°C (Eu_2CuSi_3), 1255°C ($EuCu_2Si_2$), which exceed those of some of their constituents, can sluggish the evaporation from the molten zone. The compounds exhibit interesting properties like incommensurate magnetic ordering or mixed valence behavior. For oxide crystals a well controlled oxygen partial pressure must be applied, which strongly affects the thermodynamic stability of valence states of the cationic components at melting temperature. Elevated Ar gas pressure (4 MPa) has been applied in crystal growth of $LiMnPO_4$ (Fig.) to avoid Li_2O vaporization and the oxidation of Mn^{2+} to Mn^{3+}.

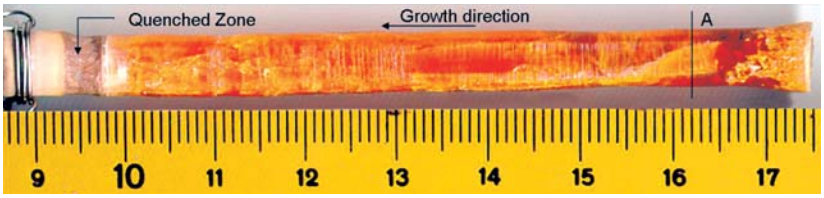

Fig.: $LiMnPO_4$ crystal grown with 10 mm/h at 4 MPa Ar. The growth direction and the quenched last zone are indicated.

The oxygen pressure can directly affect on the thermodynamic equilibrium and the solidification mode of oxides. Elevated oxygen pressure of 3.5 to 5.5 MPa brings the incongruent melting CuO closer to the congruent melting, enabled higher growth rates up to 10 mm/h and improved the crystal perfection. For incongruent melting oxides a vast difference in the oxygen content at the oxide/melt interface may arise because the metal ions change their valence. By diluting oxygen with Ar the partial pressure in an Ar/O_2 mixture was reduced, which prevented the formation of gas bubbles at the melting interface in FZ crystal growth of $CaCu_2O_3$.

Cooperation TU Dresden, NPU Xi'an, RWTH Aachen, Toyota Motor Europe
Funded by DFG, AvH, Toyota Motors

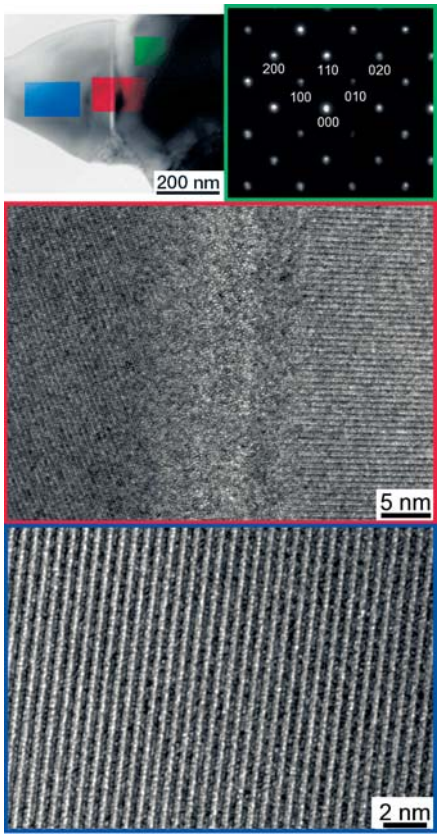

Fig.: TEM images of a grain boundary in a Dy-free NdFeB sintered magnet in the fully annealed state. Top left: bright field image showing the location of the high resolution images. Red frame: high resolution image showing lattice fringes of the two grains and amorphous material in the grain boundary. Green frame: selected area diffraction (SAD) pattern of the right hand grain, tilted to the [001] zone axis. Blue frame: high resolution image of the left $Nd_2Fe_{14}B$ grain.

Permanent Magnets

O. Gutfleisch, J. Thielsch, T. Woodcock, K. Güth, J. Lyubina,
M. Kuz'min, R. Schäfer, K.-H. Müller, L. Schultz

Phenomena related to the fundamentals, processing and applications of high performance permanent magnet materials are being explored. This includes the determination of intrinsic magnetic properties, investigation of high pulsed magnetic field-induced phase transitions, detailed microstructural and micromagnetic analysis as well as the development of novel processing routes. The engineering of internal interfaces on a (sub-)nano scale is aimed at improved temperature stability of the magnet for HEVs (hybrid electric vehicles) applications. Nanostructured (Nd,Pr)FeB-based magnets are optimized in terms of their energy density by either inducing a texture via Hydrogenation Disproportionation Desorption Recombination (HDDR) process or hot deformation or enhancing the remanence via magnetic exchange-coupling. Uni-polar magnetized PrFeB-type ring magnets have been developed for low temperature applications such as frictionless superconducting bearings. Highly-ordered FePt $L1_0$ -type magnets and thick sputtered and highly textured NdFeB-type and SmCo-type films are prepared for MEMS applications. Sm_2Co_{17}-type magnets have been developed for high temperature applications of up to 500°C by tailoring the microchemistry of a multiphase nanostructure.

Cooperation TU Dresden; FZ Dresden-Rossendorf; CNRS Grenoble (F); Toyota Motor Corporation; Tohoku Univ. Sendai, Japan; Univ. of Texas, USA; TU Vienna (Austria); Vacuumschmelze GmbH (D); National Institute of Materials Science, Tsukuba, Japan
Funded by SFB463 (DFG), Toyota, Hans L. Merkle Stiftung, Bosch, Aichi-Steel

Magnetocaloric Materials

O. Gutfleisch, J. Lyubina, M. Kuzmin, J. Liu, M. Richter

Magnetic refrigeration offers a solid state alternative to standard gas compression-based cooling that would simultaneously eliminate the need for harmful refrigerant gases and reduce energy requirements and hence carbon dioxide emissions. About ten years have passed since the discovery of a giant magnetocaloric effect in $Gd_5(Si,Ge)_4$, the magnetic refrigerant that re-ignited interest in magnetic cooling around room temperature. Since then a number of alternative, complex magnetic refrigerants have emerged, resulting in a field that is novel and exciting not only for fundamental research but also for new applications.

Our research focus is on adjusting critical material parameters such as the magnetic and thermal hysteresis properties, the time-dependency of magnetostructural transitions as well as the tailoring of operating temperature and required magnetic fields. The search for novel material systems, nano-architectures and processing routes and the assessment of engineering properties such as thermal conductivity, mechanical and chemical stability are also the subject of our work. Systems of interest are the La-series alloy compounds, some transition-metal-based compounds, especially MnFePGe, as well as Heusler alloys.

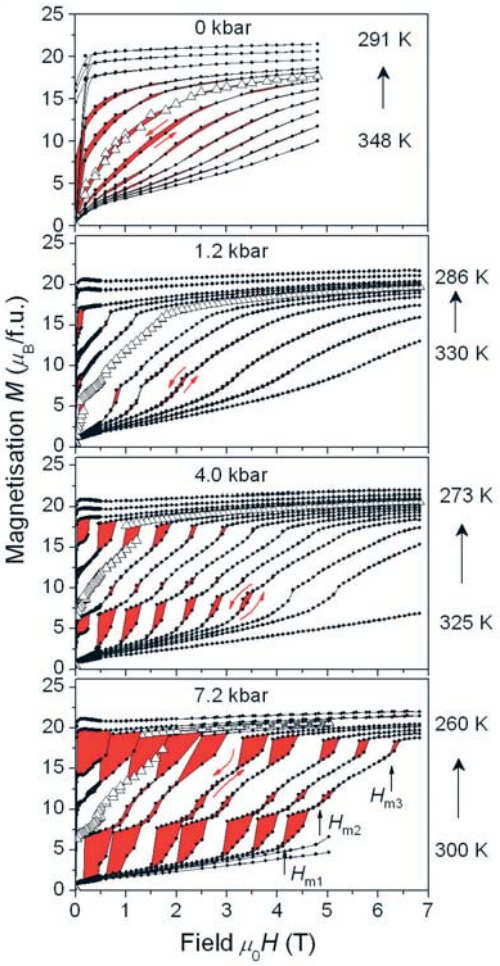

Fig.: Magnetisation isotherms in the vicinity of the Curie temperature T_c at various pressures for $LaFe_{11.57}Si_{1.43}H_{1.64}$. Arrows indicate the direction of temperature and magnetic field change. Open triangles mark magnetisation curves at T_c. H_{mi} indicates the critical field for the i^{th} metamagnetic transition (*Phys. Rev. Lett. 101, 177203 (2008)*).

Cooperation Univ. of Cambridge, UK; Imperial College London, UK; Vacuumschmelze Hanau, D; Istituto Nazionale di Ricerca Metrologica Torino, I; Univ. de Barcelona, E; Univ. de Zaragoza, E

Funded by DFG, EU (Solid State Energy Efficient Cooling - SSEEC)

Research Area 3
Molecular nanostructures and molecular solids

Simultaneous and separate growth of nitrogen- doped single- and multi-walled carbon nanotubes

A. Leonhardt, V. Khavrus, E. M. M. Ibrahim, S. Hampel, S. Oswald, Ch. Täschner, B. Büchner

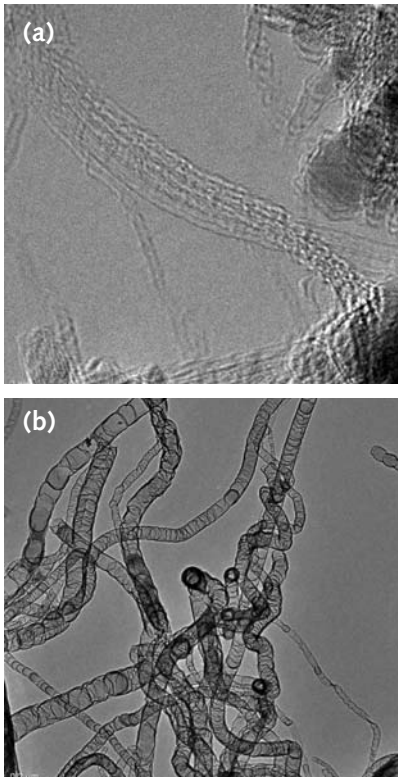

Fig.: Simultaneously and separately deposited SWCNTs and MWCNTs doped with nitrogen: Bundles of SWCNTs, deposited on cooled finger (a) MWCNTs with typical bamboo-like structure caused by nitrogen doping (b)

Synthesis of single- and multi-walled carbon nanotubes (SW- and MWCNTs), simultaneously and separately, is not only an attractive goal for the research but also for the industrial production. Here, the used method is based on the decomposition of a vapor consisting of acetonitrile (CH_3CN) and ferrocene ($Fe(C_5H_5)_2$) at a temperature of 900°C and a pressure of 6 bar in a horizontal tube-reactor. A water-cooled finger is located in the cold zone of the reactor. The gas mixture is injected by using a nozzle-system, described in detail [1]. After the deposition process MWCNTs are located in the hot zone on the wall of the reactor-tube while SWCNTs are concentrated on the cooled finger. The proportion between SW- and MWCNTs is dependent on the carbon/iron ratio in the gas feedstock. Carbon-rich gas mixtures lead to a high yield of aligned MWCNTs on the reactor wall. Lower ratios show more SWCNTs which are grown in the gas phase in the hot zone of reactor and deposit mainly on the cooled finger. Using of acetonitrile results in producing nitrogen-doped SWCNTs and MWCNTs, XPS- measurements show that nitrogen is bound to the graphene layers as pyrrole- and pyridine-type for SWCNTs and as quaternary nitrogen for MWCNTs. The MWCNTs have the typical bamboo-like structure (see Fig.). For a future application this production has some advantages. First, the method is well-scalable and with optimal conditions produces separately SWCNTs and MWCNTs. Second, the synthesis operates with cheap and easily accessible organic precursors, third, the both types of carbon nanotubes are nitrogen- doped.

[1] Barreiro, A. et al. J. Phys. Chem. B 2006, 110, 20973-20977

Cooperations L.V. Pisarzhevsky Inst. of Physical Chemistry, National Academy of Sciences of Ukraine, Kiev; Sohag Univ., Egypt
Funded by DFG, SMWK

Iron-carbide nanowires inside carbon nanotubes

T. Mühl, U. Weissker, M. Löffler, F. Wolny, M. Lutz, N. Scheerbaum, R. Klingeler, A. Leonhardt, B. Büchner

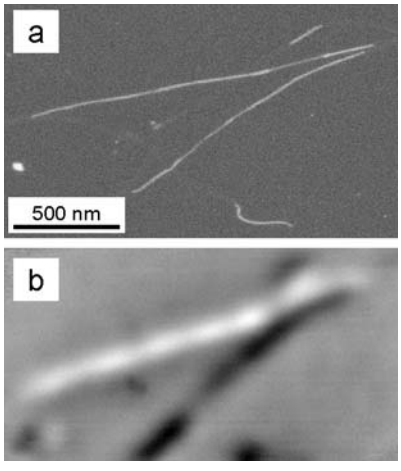

Fig.: Two long iron-carbide nanowires. (a) SEM image using a backscattered electron detector, (b) MFM image. The magnetization direction is perpendicular to the nanowire axis.

Single crystal iron-carbide nanowires contained in multi-walled carbon nanotubes have been prepared by aerosol-based thermal chemical vapor deposition. As a precursor, ferrocene dissolved in 1,2-dichlorobenzene was used. TEM and EBSD measurements reveal that the crystallographic 010 axis of the orthorhombic Fe_3C nanowires is usually aligned parallel to the nanotube axis (Fe_3C lattice parameters: a = 0.4526 nm, b = 0.5087 nm and c = 0.6744 nm). Despite the high aspect ratio of the Fe_3C nanowires, MFM measurements show a magnetization of the single domain nanowires perpendicular to the wire axis. This is explained by the magnetic behavior being dominated by the magnetocrystalline anisotropy contribution, leading to an easy axis along the 001 axis, which is in agreement with the structural results. Nevertheless, the substantial shape anisotropy contribution may control the magnetization reversal of elongated iron-carbide nanowires.

Energy level alignment and interactions at contacts for spin injection into organic semiconductors

M. Grobosch, R. B. Gangineni, K. Dörr, M. Knupfer

The energy level alignment at interfaces between $La_{0.7}Sr_{0.3}MnO_3$ (LSMO) and two archetype organic semiconductors, copper-phthalocyanine (CuPc) and α-sexithiophene (α-6T) has been studied by combined X-ray photoelectron spectroscopy (XPS) and Ultraviolet photoelectron spectroscopy (UPS). LSMO is a ferromagnetic metal and can be used to inject spin-polarized current into organic semiconductors. Thin films of this material have been grown using pulsed laser deposition. Prior to the deposition of the organic semiconductors the LSMO has been cleaned by either an ex-situ treatment only, or by annealing in an oxygen atmosphere. The former results in surfaces that are covered by a thin contamination layer while the latter yields atomically clean surfaces. All interfaces are characterized by a rather large interface dipole and substantial charge injection barriers. Moreover, at the interfaces between clean $La_{0.7}Sr_{0.3}MnO_3$ and the two organic semiconductors there is a chemical reaction resulting in a partial oxidation of the organic molecules. At such interfaces the energy level alignment considerably depends on the LSMO cleaning procedure prior the deposition, i.e. whether there is still a contamination layer present.
For details see: M. Grobosch *et al.*, Appl. Phys. Lett. **92**, 023302 (2008).

Funded by DFG, Project No. KN 393/5.

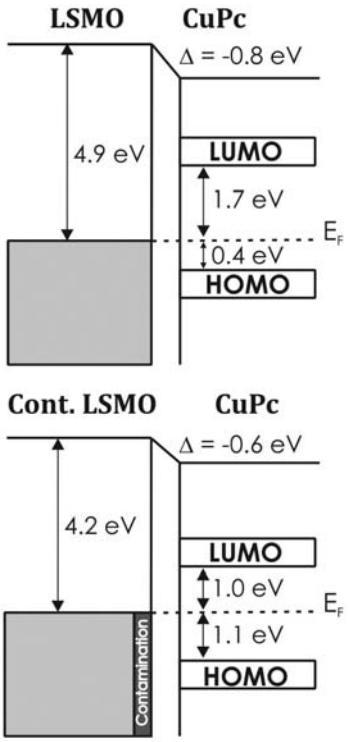

Fig.: Top: Schematic energy level diagram of the clean CuPc/LSMO interface.
Below: Schematic energy level diagram of the contaminated interface between $La_{0.7}Sr_{0.3}MnO_3$ and the organic semiconductor CuPc.

Spin and orbital ground state of Co in Co-phthalocyanine

T. Kroll, V.Yu. Aristov[1], O.V. Molodtsova, Yu.A. Ossipyan[1], D.V. Vyalikh[2], B. Büchner, M. Knupfer

The 3*d* orbital ground state of transition metal ions that are incorporated in a molecular matrix determines the total spin of the transition metal ion as well as the spin anisotropy, and thus the essential magnetic properties of the corresponding molecule. However, there is little known to date on the exact 3*d* ground state of many molecular systems including quite complex molecular magnets as well as relatively simple systems such as for instance cobalt-phthalocyanine (CoPc). For the latter, there are contradictory theoretical predictions with respect to the occupation of the various Co 3*d* electronic levels. We demonstrate that polarization dependent soft X-ray absorption

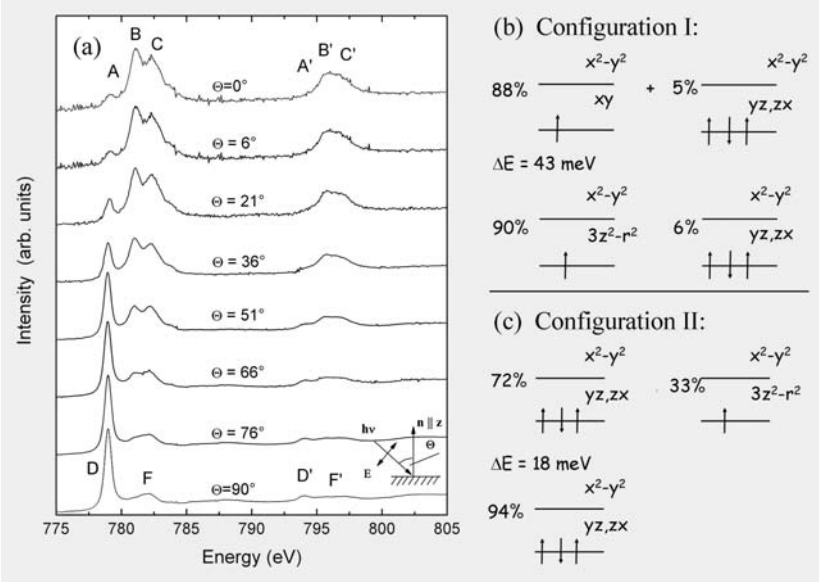

Fig.: (a): Polarization dependent NEXAFS data of flat lying CoPc molecules on a single crystal Au substrate. The z-axis of the molecules points in the direction of the surface normal n. (b) and (c): A sketch of the electronic structure as calculated for the configurations I and II. Only the two highest energy levels are shown, since the lower ones are fully occupied. Furthermore, the electronic configuration of the lowest and first excited state is shown and the energy separation between them.

spectroscopy (Co *L* edge, see Figure) in combination with atomic full multiplet calculations of the spectra is able to unravel valuable information on the spin and orbital ground state of the transition metal ion in CoPc. Our results reveal a complex electronic structure of the ground state that is temperature dependent and emphasize the importance of taking 3*d* correlation effects properly into account (see Figure). From our calculations we find two possible configurations that lead to very similar absorption spectra. Both solutions show a small energy gap between the lowest and first excited state which leads to a temperature dependent behaviour that will be investigated in further experiments.

Cooperation [1]Institute of Solid State Physics, Russian Academy of Sciences, Chernogolovka, Russia, [2]TU Dresden
Funded by SMWK, DFG (SFB 463), RFBR (grant number 08-02-1170).

Huge magnetic anisotropy of transition-metal dimers

D. Fritsch, K. Koepernik, M. Richter, H. Eschrig

Dimers are the smallest chemical objects that may show magnetic anisotropy. Some transition-metal dimers have a considerable barrier against re-orientation of their magnetization [1], the so-called magnetic anisotropy energy (MAE). The height of this barrier is important for technological applications. It determines, e.g., the stability of information stored in magnetic memory devices. We estimated the MAE of all 3d and 4d transition metal dimers by means of relativistic density functional calculations [2]. Our approach was based on a full-potential local-orbital method (FPLO) in a four-component Dirac-Kohn-Sham implementation. Orbital polarization corrections [3] to the local density approximation were employed. Spin multiplicity and bond length (Figure), harmonic vibrational frequency, spin- and orbital magnetic moment, and MAE of the dimers were evaluated and compared with available experimental and theoretical data. We found exceptionally high values of MAE, close to 0.2 eV, for four particular dimers: Fe_2, Co_2, Ni_2, and Rh_2. This value is 3-5 orders of magnitude larger than the related bulk MAE. Technological application would require to embed the dimers in a medium without deteriorating their magnetic behavior.

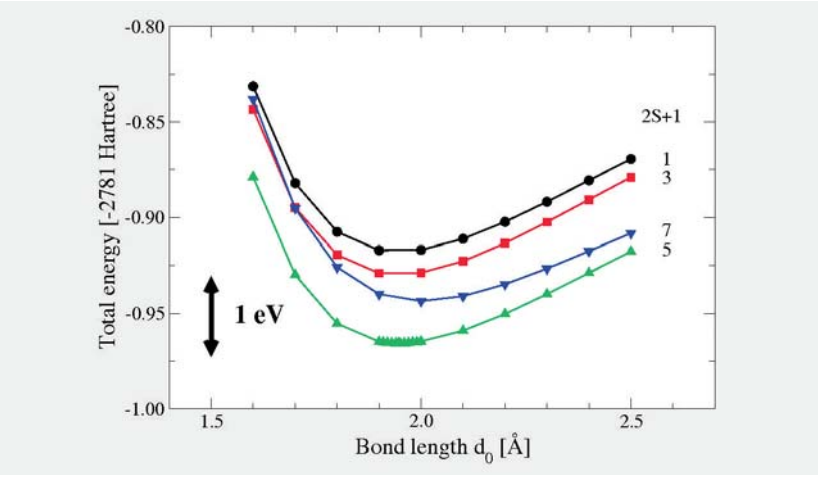

Fig.: Total energy vs. bond length of Co_2 for different spin multiplicities 2S+1 (scalar relativistic calculation).

[1] T.O. Strandberg et al. Nature Materials **6** (2007) 648; L. Fernández-Seivane and J. Ferrer, Phys. Rev. Lett. **99** (2007) 183401.
[2] D. Fritsch et al. J. Comp. Chem. **29** (2008) 2210 (invited contrib.); http://arxiv.org/abs/0804.1233.
[3] O. Eriksson et al. Phys. Rev. B **41** (1990) R7311; H. Eschrig et al. Europhys. Lett. **72** (2005) 611.

Funded by DFG, SPP 1145.

Research Area 4
Metastable alloys

Corrosion behaviour of bulk amorphous steel

F. Gostin, U. Siegel, C. Mickel, S. Baunack, A. Gebert, U. Kühn, J. Eckert, L. Schultz

Fe-based bulk metallic glasses have a high potential for industrial applications due to relatively low production costs and unique properties, e.g. very high strength. Recently it was shown that minor additions of Y or lanthanides significantly improve their glass-forming ability. These newly developed alloys were named "bulk amorphous steels". The most prominent of these alloys is $(Fe_{44.3}Cr_5Co_5Mo_{12.8}Mn_{11.2}C_{15.8}B_{5.9})_{98.5}Y_{1.5}$ with maximum sample thickness of 12 mm - this was subjected to fundamental corrosion studies. The free corrosion behaviour and the anodic passivation ability of the bulk glassy alloy were analysed by means of electrochemical polarization measurements which were performed in aqueous solutions with pH values in the interval 0.3-14. Corrosion current densities were found to be very low in the entire studied pH interval compared with commercial grade steels, e.g. X210Cr12 steel and with the crystalline counterpart alloy. The glassy alloy exhibits high dissolution rates upon anodic polarization in very acidic environments, but with increasing pH values it tends to form passive layers showing the highest protective effect at pH 11. Auger electron spectroscopy studies revealed that the passive layers consist mainly of Fe and Cr oxides. A strong variation of the passive layer structure and composition with the pH value was detected.

Cooperation TU Dresden, Univ. Politehnica Bucarest

Martensitic transformation in Cu-Zr-based alloys

S. Pauly, U. Kühn, J. Freudenberger, N. Mattern, J. Eckert

The discovery of metallic glasses with casting dimensions up to several centimetres allows for the determination of the mechanical properties of these so-called bulk metallic glasses (BMGs). High yield stresses and relatively low Young's moduli are inherent in BMGs. However, a major drawback is the limited plasticity in many alloy systems as they are prone to catastrophic failure. In order to improve the macroscopic deformability composite materials have been developed consisting of a crystalline phase embedded in an amorphous matrix. Particularly interesting under this aspect are Cu-Zr-based alloys as they can be quenched into a glassy structure. Furthermore, proper adjustment of the alloy composition as well as cooling rate permits the targeted precipitation of the B2 CuZr phase in a glassy matrix. The B2 CuZr phase can undergo a reversible martensitic transformation (MT) into a B19′ phase similar to the NiTi system. This strongly affects the mechanical properties as will be shown.

Cu-Zr-Ti and Cu-Zr-Al BMG composites were produced by copper mould suction casting, plastically deformed by cold rolling and investigated in synchrotron radiation. The transformation from the B2 phase to the B19′ could be proved while the transformation depends on the degree of plastic deformation. This MT has a pronounced effect on the deformation behaviour of these alloys under compressive stress as depicted in the figure. The higher the volume fraction of B2 CuZr (curve b) the lower the yield stress and the more distinct the work hardening behaviour, which reminds of a TRIP (transformation-induced plasticity) effect. The large plastic strain up to 15% is attributed to the composite microstructure shown in the inset of the figure. In this way the mechanical properties of the composites can be tailored.

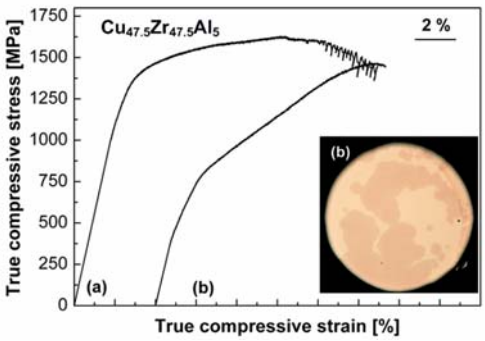

Fig.: Stress-strain curves under compressive loading of a $Cu_{47.5}Zr_{47.5}Al_5$ BMG composite. The B2 CuZr phase is embedded in an amorphous matrix as shown in the inset. Sample (a) contains approximately 30 vol.% crystals and sample (b) approximately 50 vol.%.

Funded by EU (RTN Ductile BMG Composites); Global Research Laboratory Program of the Korean Ministry of Education, Science and Technology

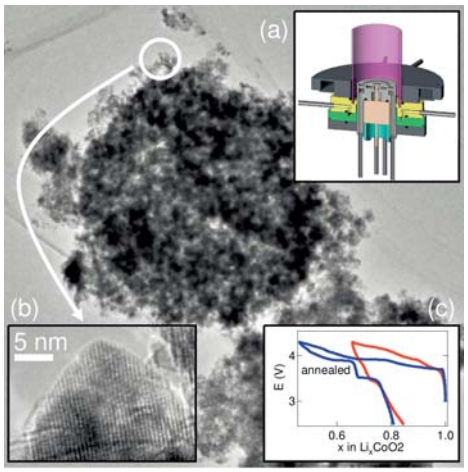

Fig.: TEM figure of the powder synthesized by ultrasonic spray-pyrolysis. Inset (a) shows the sketch of the insertion head, (b) the magnification of a well crystalline grain, and (c) the first cycle of a cell using the as synthesized and the annealed powder, respectively.

Nanocrystalline $LiCoO_2$ prepared by microwave assisted spray pyrolysis

K. Nikolowski, H. Ehrenberg, R. Buckan, H. Wiggers, R. Theissmann, R. Voigtländer, D. Lindackers, J. Eckert

Since their commercialization in the 1990ies nowadays lithium-ion batteries attract much attention, as they will be introduced as power supply for hybrid electrical vehicles in near future. In order to provide the high currents needed for this kind of application, small particles with short diffusion paths are beneficial. Here we report the synthesis of $LiCoO_2$ particles in the nanometre scale by microwave assisted spray pyrolysis.
The injection head for the ultrasonic spray pyrolysis setup was realised in house (see inset in the figure) fitting to the setup at University Duisburg-Essen. To prepare the particles an aqueous solution of lithium and cobalt nitrate was nebulised, carried into the reaction chamber and pyrolysed by a microwave assisted plasma. TEM analysis shows that the particles are well crystalline and their size is in the range of 5-10 nm. The electrochemical performance was evaluated in test cells. The as synthesized material shows a rather poor capacity, but an additional thermal treatment at rather mild conditions (500 °C, 1 h) improves it significantly. The electrochemical curve shows the features which are characteristic for $LiCoO_2$.

Cooperation Univ. Duisburg-Essen
Funded by DFG, SFB 595, PAK 177

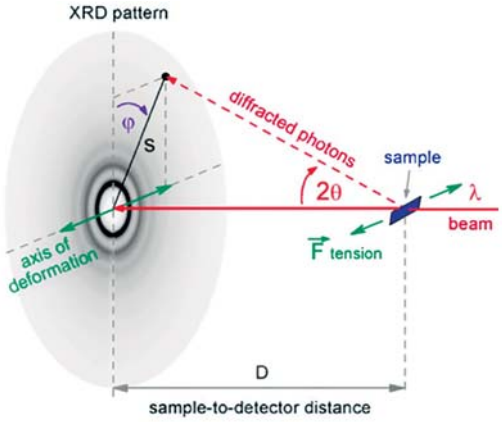

Fig. 1: Schematic setup of the in situ tensile test in hard x-rays.

Strain distribution in bulk metallic glasses

M. Stoica, S. Pauly, J. Das, N. Mattern, J. Eckert

The macroscopic elastic strain can be determined relatively easily with the help of strain gauges during deformation tests. However, in order to get access to the atomic-scale strain tensor in situ tensile or compression tests in synchrotron radiation have to be performed. The experimental setup is schematically shown in Fig. 1. The sample is strained within the beam and the scattered photons are collected on a 2D image plate. The diffraction pattern is consecutively sectioned into 36 slices with an opening angle of 10°. Each slice is integrated and thus a 1D data set is obtained. The first scattering maximum of each slice is fitted with a Gaussian curve. The strain can be obtained from the shift of the first maximum in reciprocal space with respect to its original position; q is the scattering vector:

$$\varepsilon_i(\varphi_i, \sigma) = \frac{q(\varphi_i, 0) - q(\varphi_i, \sigma)}{q(\varphi_i, \sigma)} \qquad \text{(eq. 1)}$$

The atomic-scale strain is plotted as a function of the angle φ for the different stress levels (Fig. 2). The data is fitted by the following equation:

$$\varepsilon_\varphi = \varepsilon_{11}\sin^2(\varphi) - \gamma_{12}\sin(\varphi)\cos(\varphi) + \varepsilon_{22}\cos^2(\varphi) \qquad \text{(eq. 2)}$$

The strain along the loading axis (ε_{11}) and perpendicular to it (ε_{22}) are obtained, giving additionally the Poisson's ratio $\nu = -\varepsilon_{22}/\varepsilon_{11}$. The elastic properties determined by these diffraction experiments only correspond to the first atomic shell. Instead, ultrasonic sound velocity measurements give values averaged over all atomic shells. A comparison of the data obtained from both techniques suggests an interesting correlation. In ductile bulk metallic glasses the first atomic shell behaves in a different way than the macroscopic material indicating local fluctuations of the elastic properties. Yet, when the glass fails directly after yielding the elastic properties of the first atomic shell correspond quite well to the averaged values.

Funded by EU (RTN Ductile BMG Composites)

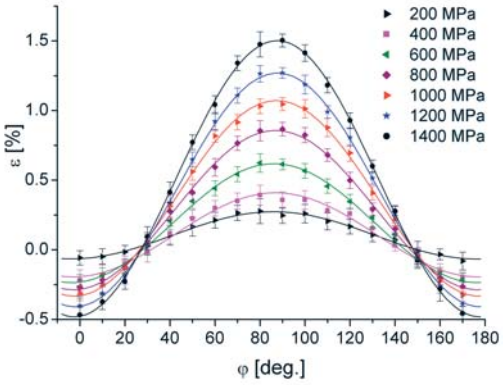

Fig. 2: Fit of the strain at different stress levels according to eq. 2.

Metal matrix composites reinforced with complex metallic alloys

S. Scudino, M. Sakaliyska, K.B. Surreddi, F. Ali, U. Kühn, M. Stoica, N. Mattern, H. Ehrenberg, J. Eckert

Within recent years, complex metallic alloys (CMAs) have been attracting much attention ranging from scientific curiosity about their complex structure to technological aspects of preparation and potential applications. Complex metallic alloys display several interesting properties, such as good corrosion resistance and high-temperature strength, however, they are brittle at room temperature in the single-phase form, which limits their use in engineering applications. A way to improve the room temperature ductility is the development of a heterogeneous microstructure combining a soft metallic matrix with second-phase CMA particles. The CMA particles act as strength-bearing component, while the metallic matrix supplies ductility. In this project, metal matrix composites (MMCs) containing high-strength CMA particles are produced by powder metallurgy and the resulting microstructure and mechanical properties are studied in detail. The results indicate that CMA reinforcing particles are very effective for improving the mechanical properties of the metal matrix, revealing that the properties can be tuned within a wide range of strength and ductility as a function of size and volume fraction of the reinforcement.

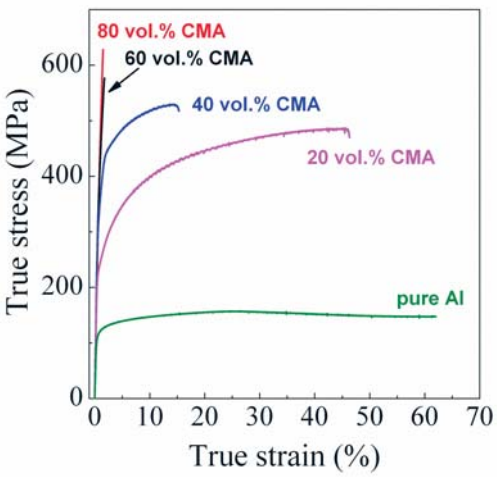

Fig.: Room temperature compression stress-strain curves for the metal matrix composites reinforced with different amounts of CMA particles.

Cooperation FZ Jülich; MPI Dresden; Univ. Frankfurt; Sejong Univ., Seoul/Korea; Univ. Torino, Italy; CNRS Grenoble, France; Slovak Univ. of Technology, Trnava, Slovak Republic

Funded by EU (NoE CMA).

Cluster materials with competing properties

J. Paillier, C. Mickel, A. Gebert, M. Uhlemann, L. Schultz, U. Kühn

Controlled hydrogenation generating nano-sized clusters may be a suitable way to improve the mechanical properties of bulk glassy alloys. Hydrogen absorption performed electrochemically at room temperature alters the structure of glassy alloys, e.g. $Zr_{59}Ti_3Cu_{20}Al_{10}Ni_8$, due to various affinities of the components to hydrogen. Alloy samples with limited hydrogen content remain their global amorphous structure but can exhibit local inhomogeneities, i.e. crystalline regions that are Cu-rich clusters (~ 12 nm) and/or $ZrH_{\sim 1.7}$ hydride (~ 6 nm). These clusters tend to be organised in larger "superstructures" on a scale of one to several hundred nanometers. Hydrogen-induced structural changes are more impacted by the absorption conditions, i.e. by the current density (j), than by the absorbed hydrogen content (see figure).

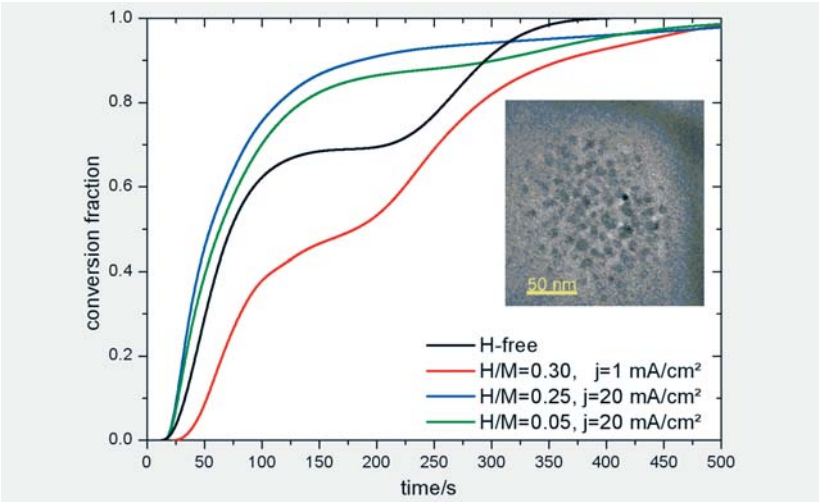

Fig.: Influence of H-content and charging conditions on the primary crystallisation process of a $Zr_{59}Ti_3Cu_{20}Al_{10}Ni_8$ glassy alloy. The plot shows the evolution of the crystallized fraction with time during isothermal (725K) DSC experiments; inset: HR-TEM picture of a nanocrystalline Cu-rich region

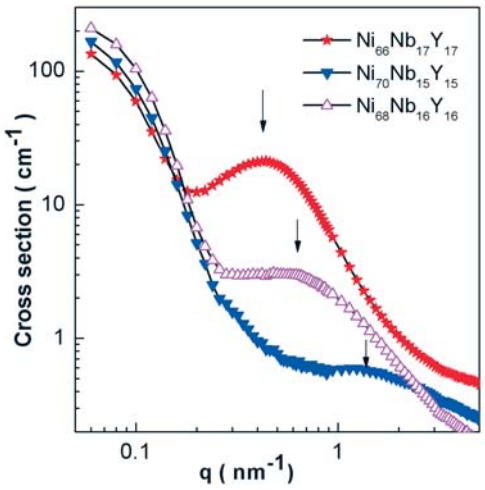

Fig. a): Small Angle X-ray Scattering curves $d\sigma/d\Omega(q)$ of Ni-Nb-Y metallic glasses – the positions of maxima at $q = q_{max}$ correspond to different fluctuation length ζ between 5 and 12 nm.

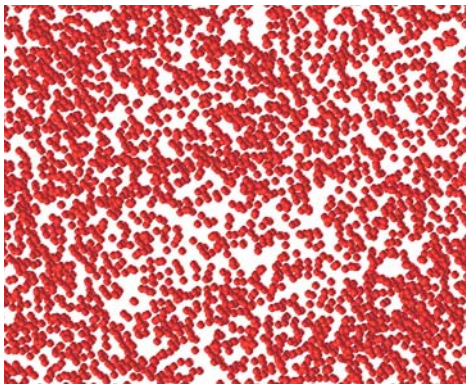

Fig. b): Spatial distribution of Y-atoms of rapidly quenched $Ni_{68}Nb_{16}Y_{16}$ metallic glass by Atom Probe Tomography (edge size is 20 nm x 20 nm, thickness c = 5 nm), fluctuation length of Y atomic density is about 10 nm.

Spinodal decomposition of Ni-Nb-Y metallic glasses

N. Mattern, B. Schwarz, T. Gemming, U. Kühn, J. Eckert

The ternary alloy system Ni-Nb-Y exhibits a miscibility gap in the liquid in accordance with the strong positive enthalpy of mixing between Nb and Y [1]. The liquid-liquid phase separation was explored to prepare new phase-separated Ni-Nb-Y glasses by rapid quenching of the melt. The temperature dependence of the critical temperature of liquid-liquid phase separation T_C determines essentially the structure formation and consequently the obtained microstructures. For Ni contents < 60 at.% ($T_C > T_{liquidus}$), coarsened hierarchical microstructures of two-phase glasses are obtained [2]. For higher Ni contents > 60 at.% ($T_C < T_{liquidus}$), early stages of decomposition can be prepared with correlation lengths in the nanometer-scale. The observed fluctuation lengths range from 5 to 12 nm depending on the actual composition of the glass as determined by small angle X-ray scattering (SAXS) [3]. The occurrence of the maximum in the SAXS curves in Figure a) is related to the high density of electron density fluctuations with a dominant correlation length ζ. The shift of the maximum's position from $q_{max} = 0.5$ to 1.2 nm^{-1} indicates a reduction of ζ with increasing Ni content from $\zeta = 12$ nm for $Ni_{66}Nb_{17}Y_{17}$, and $\zeta = 8$ nm for $Ni_{68}Nb_{16}Y_{16}$, to $\zeta = 5$ nm for $Ni_{70}Nb_{15}Y_{15}$ metallic glass. In situ SAXS measurements at elevated temperatures give evidence for the spinodal character of the decomposition. Annealing the $Ni_{70}Nb_{15}Y_{15}$ glass in the supercooled liquid leads to an increase of the amplitude of the concentration fluctuations, however, the wavelength stays unchanged [3]. The heterogeneous microstructure of rapidly quenched $Ni_{68}Nb_{16}Y_{16}$ alloy was confirmed by 3-D Atom Probe Tomography. A Y atom map is shown in Figure b of a selected volume with lengths a = 20 nm, b = 20 nm, and c = 5 nm, viewed parallel to the c-direction. Concentration fluctuations, i.e. regions with alternating higher respectively lower Y- density, on a ~ 5 - 10 nm lengthscale are clearly visible. The opposed Nb and Y concentrations indicate the existence of Nb- and Y-enriched Ni-clusters in the phase separated glass.

[1] N. Mattern, M. Zinkevich, W. Loeser, G. Behr, J. Acker, J. Phase Equilibria and Diffusion 29 (2008) Nr. 2, 141-155

[2] N. Mattern, T. Gemming, G. Goerigk, J. Eckert, Scripta Materialia 57 (2007) Nr. 1, 29-32

[3] N. Mattern, G. Goerigk, U. Vainio, M.K. Miller, T. Gemming, J. Eckert, Acta Materialia 57 (2009) 902-907

Cooperation Yonsei University Seoul, Oak Ridge National Laboratory (SHaRE program), FZ Jülich, HASYLAB@DESY, MPI Stuttgart

Funded by Leibniz-Society Pakt für Forschung 2008

New Hydrides

O. Gutfleisch, C. Rongeat, I. Llamas-Jansa, B. Gebel, M. Herrich, L. Dunsch, S. Oswald, A. Teresiak, M. Uhlemann, A. Gebert, L. Schultz

Human development has caused a depletion of natural energy resources and climate changes with non-predictable consequences. New energy concepts are required for the future of our industrial society. The only known energy carrier with a high energy density and no emission of greenhouse gas is hydrogen.

Research of solid-state storage of hydrogen - for e.g. zero-emission vehicle propulsion and other mobile applications – is pursued by exploring functional complex hydrides such as alanates, borohydrides and nitride based amides and imides. These materials offer several advantages over conventional metal hydrides provided one or more of the

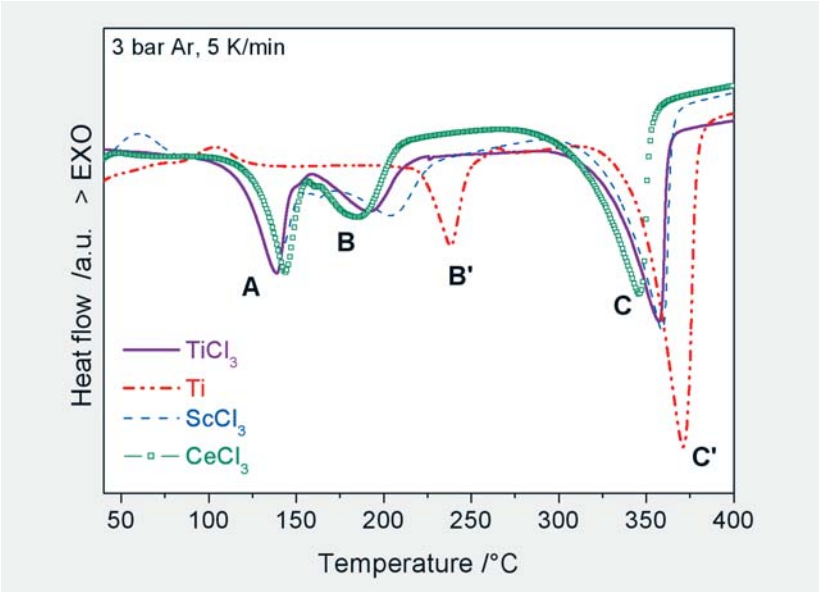

Fig.: DSC traces for as-milled NaH + Al + 4 mol% dopant (3 bar Ar, 5 K min^{-1}) yielding $NaAlH_4$: $TiCl_3$ (—), Ti (–·–·–), $ScCl_3$ (– –) and $CeCl_3$ (▫). The features are related to the three steps of $NaAlH_4$ decomposition: (A) $NaAlH_4$ to Na_3AlH_6, (B) Na_3AlH_6 to NaH and (C) NaH to Na + H_2.

following limitations: a) unfavourable thermodynamics (high temperatures to release hydrogen), b) poor kinetics (low rates of hydrogen release and uptake), c) decomposition pathways involving the release of undesirable by-products (e.g. ammonia), and/or d) an inability to reabsorb hydrogen at modest temperatures and pressures (i.e. "irreversibility") can be overcome.

Our work includes the thermodynamic and kinetic characterisation with high-pressure differential scanning calorimetry, gravimetric and pressure-composition-temperature analysis as well as the study of hydrogen dynamics using in-situ XPS, XRD and Raman in order to understand details of the complex sequence of transformations, to identify intermediate reaction products and rate determining steps in complex hydrides and reactive hydride composites. Novel processing techniques such as high hydrogen pressure reactive milling and high pressure annealing are used in order to identify new materials with high reversible hydrogen contents.

Cooperation EMPA, CH; GKSS Research Centre Geesthacht; FZ Karlsruhe; Univ. of Amsterdam, Netherlands; Univ. of Birmingham, UK; Univ. of Rome "La Sapienza", Italy; Interdisciplinary Nanoscience Center, Univ. of Aarhus, DK
Funded by EU IP (NESSHY), HGF (FuncHy), EU RTN (COSY)

Research Area 5
Stress-driven architectures and phenomena

3D composition profiles of single quantum dots determined by scanning-probe-microscopy based nanotomography

A. Rastelli, M. Stoffel, T. Merdzhanova, O. G. Schmidt

Strain-driven self-assembly provides a straightforward route to fabricate coherent, defect-free semiconductor "quantum dots" (QDs). During epitaxial growth, the deposited material intermixes with the substrate material, leading to the formation of alloyed islands. A precise knowledge of the material distribution in these islands/QDs is important for predicting the electronic and optical properties of novel QD-based devices. We have developed a new method to quantitatively determine the three-dimensional (3D) composition profiles of single QDs and have applied it to SiGe islands grown on Si(001) substrate. The method is based on scanning probe microscopy imaging of the same surface area after successive etching steps in a composition-selective chemical solution. By using an accurate calibration of the etching rate as a function of Ge content and dedicated software algorithms, the 3D composition profiles are reconstructed from the etching sequence. Compared to other existing methods, this "nanotomography" approach offers the possibility of mapping the 3D composition of individual QDs and to gather information on the composition of many islands at the same time.

A. Rastelli et al. Nano Letters, **8,** 1404 (2008).

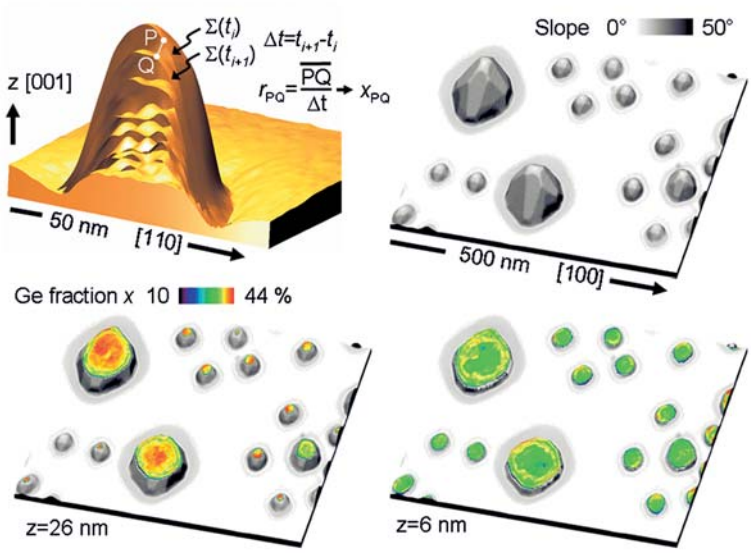

Fig.: Top left: example of sequence of AFM images (3D view) of a SiGe/Si(001) island taken after successive etching steps in a $NH_4OH:H_2O_2$ solution. The distance between subsequent surfaces $\Sigma(t_i)$ measured after an etching time t_i is used to determine the local etching rate r. Based on etching rate calibration the local composition x is then calculated from r. Top righ: AFM image of an ensemble of islands prior to etching. Bottom: examples of horizontal cross-cuts at height z (with respect to the substrate) showing the Ge content inside the islands.

Cooperation Max-Planck-Institut für Festkörperforschung Stuttgart, ESRF Grenoble (France)

From radial hybrid superlattices to planar multilayers

Ch. Deneke, T. Zander*, Ch. Mickel, B. Rellinghaus, O. G. Schmidt

*Max-Planck-Institut für Festkörperforschung

Since the first proposal of semiconductor superlattices (SL), such heterostructures have attracted overwhelming interest over the past 30 years due to their electronic, optical or opto-electronic properties. Over recent years, an approach to realize radial hybrid superlattices (RSL) by the release and roll-up of strained layers has been established. However, for certain device applications, a planar structure of such a hybrid superlattice would be more suitable. Here, the fabrication of a planar metal/semiconductor superlattice (MeSSL) by compressing a RSL into a planar SL is illustrated.

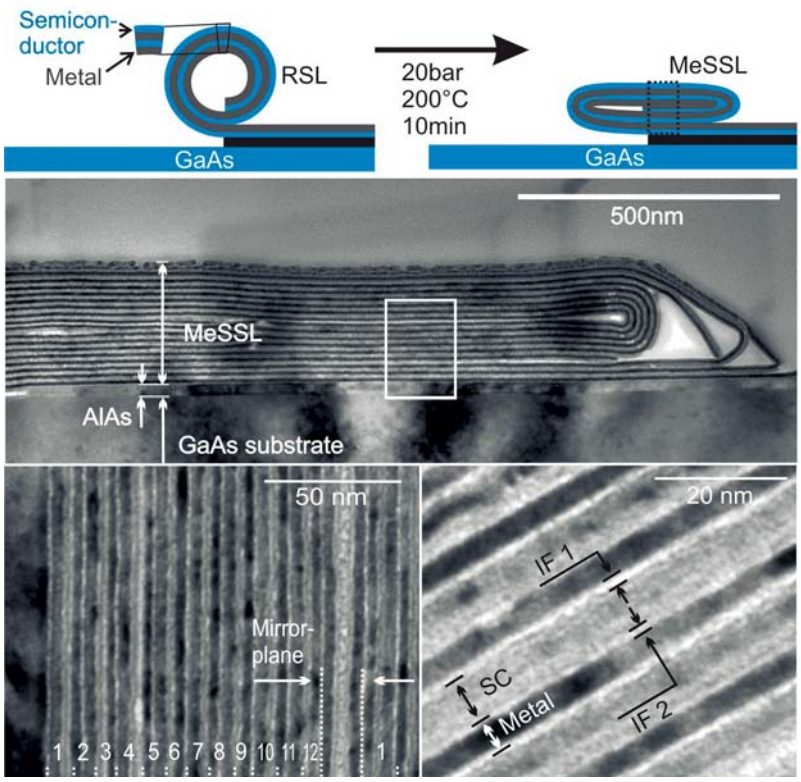

Fig.: Top row illustrates the fabrication of a planar hybrid multilayer stack by compression of a radial hybrid superlattice. Next two rows show a collection of TEM images to illustrate the obtained planar hybrid superlattice by pressing a rolled-up semiconductor/metal tube.

The figure illustrates the approach, and a collection of transmission electron microscopy (TEM) images is shown to exemplify and characterize the resulting layer stacks. A TEM image of a focus ion beam prepared MeSSL cross-section is shown in the middle row of the figure. Besides the superlattice like multilayer stack that formed by pressing a rolled-up semiconductor/metal tube, the AlAs sacrificial layer needed to release the layer from the GaAs substrate can be recognized. The bottom row displays high magnification images of the MeSSL (area marked in Fig. above). The lower half of the MeSSL together with the MeSSL mirror plane is seen. The MeSSL consists of 24 periods created by 12 rotations of the original RSL. The mirror plane arises from a reversal of the layer sequence and has a thickness of two periods of the MeSSL. A single period of the MeSSL is depicted in the high magnification TEM image in the lower row (right side) illustrating the semiconductor and metal layers forming the MeSSL as well as the new interfaces (IF1 and IF2) developing during the pressing of the RSL.

Tunable microtube resonators

G. S. Huang, Y. F. Mei, S. Kiravittaya, V. A. Bolaños Quiñones,
F. Ding, M. Benyoucef, A. Rastelli, O. G. Schmidt

Recently, optical resonators have gained considerable interest because of their applications in opto-electronics and integrated optics. An exact tailoring of the resonant modes is of importance from the viewpoints of fundamental researches and practical applications, which can be feasible and demonstrated by using rolled-up nanotechnology.

In this work, tunable microtube resonators have been fabricated by releasing pre-stressed circular SiO/SiO_2 nanomembranes, where the rotations vary with the distance from the middle of the tube (see the optical microscope image of an ordered microtube array in the inset of the figure.). Interestingly, the photoluminescence (PL) spectra from these microtubes exhibit modulations in intensity. Finite-difference time-domain (FDTD) simulation reveals that the modulation is caused by optical resonant modes from light circulating and interfering in the tube wall.

A series of PL spectra were collected along the microtube axis, and the evolution of the relative intensity of a resonant mode (~1.95 eV; $M = 30$) is displayed in blue triangles.

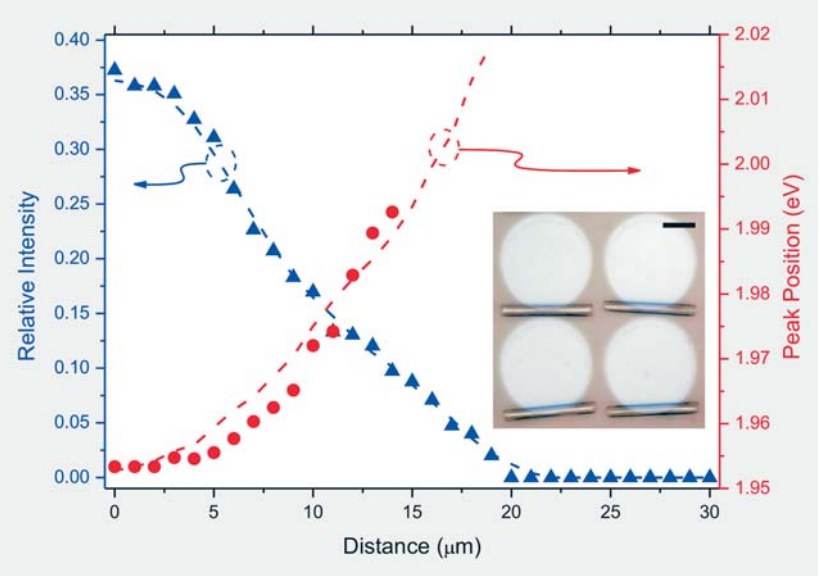

Fig.: Blue triangles show the relative intensity of a mode (azimuthal number $M = 29$) as a function of the distance from the middle of the tube. The blue dashed line is a guide to the eye. The red circles display the experimental result of peak position ($M = 29$) as a function of distance. The result from FDTD simulation is given as red dashed line. The inset shows an optical microscope image of an ordered microtube array formed on circular patterns (scale bar: 20 μm).

The relative intensity reaches a maximal value at the middle of the microtube with maximum rotations. Whereas, at the regions near the ends of the microtube, the thinner tube wall weakens the light confinement and the resonant modes can no longer be observed. In addition to the evolution of the relative intensity, the structure of the microtube has significant influence on the mode positions. The resonant modes shift continuously to higher energy when moving from the middle to the end of the microtube (red circles). To understand this shift qualitatively, we can consider the cross section of a microtube as a circular waveguide. The decrease of the rotations/tube wall thickness shortens the path of the light circulating around the circle, leading to a decrease of the effective refractive index. As a consequence, the modes should move to shorter wavelength/higher energy. The shift quantitatively calculated by FDTD simulation (red dashed lines) fits the experiment result very well.

High temperature properties of SNGS and STGS single crystals

A. Sotnikov, H. Schmidt, K. Suschke, M. Weihnacht

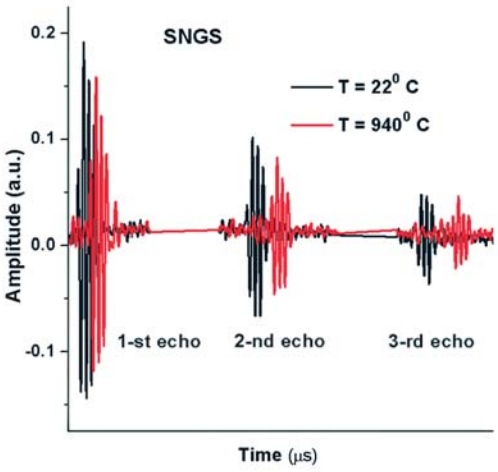

Fig.: Ultrasonic pulse-echo patterns for SNGS single crystal at 22°C (black line) and 940°C (red line). Excitation and receiving of the ultrasonic pulses were done via piezoelectric effect of the crystal without additional transducer.

SNGS ($Sr_3NbGa_3Si_2O_{14}$) and STGS ($Sr_3TaGa_3Si_2O_{14}$) trigonal single crystals which belong to the langasite ($La_3Ga_2Ge_4O_{14}$) crystal family are of considerable interest as very promising materials for both bulk- and surface acoustic wave devices and high temperature sensors. This is due to a combination of relatively large piezoelectric coefficients, moderate dielectric constant, small acoustic loss and absence of any phase transition up to crystals melting points of about 1400°C.

Piezoelectric, elastic and dielectric properties of SNGS and STGS single crystals have been investigated in the temperature range from 22°C up to 940°C using ultrasonic pulse-echo- and resonance methods. Temperature dependences of the dielectric constant ε_{11}, the piezoelectric stress constant e_{11} as well as elastic constants C_{11} and C_{66} have been obtained for the first time in this very wide temperature range. Rather strong piezoelectric response of both investigated materials keeps at least up to 940°C (see Fig.). We did not find any changes of crystal properties after several heating-cooling cycles in the temperature range from 22°C to 940°C. The experimental results show that SNGS and STGS crystals are promising materials for acoustic wave sensor applications at elevated temperatures.

Cooperation TU Bergakademie Freiberg
Funded by DFG, BMBF (InnoProfile)

Tuning magnetic properties by roll-up of Au/Co/Au films into microtubes

C. Müller, M. S. Khatri, C. Deneke, S. Fähler, Y. Mei, E. Bermúdez Ureña, O. G. Schmidt

Tubular structures are of much interest due to a low influence of edge roughness and their minimal stray field resulting in uniform and reproducible switching characteristics. These properties make them attractive for several applications, e.g. hard disk devices [1] or high-sensitivity sensors [2]. In order to obtain aligned arrays of magnetic microtubes, Au(4 nm)/Co(5 – 25 nm)/Au(4 nm) polycrystalline films were fabricated by tilted deposition on pre-structured sacrificial layers (photoresist) and rolled-up by selectively dissolving the photoresist. Depending on the total layer thickness, the pattern size and the deposition conditions the diameter for the obtained microtubes could be adjusted between 2 and 11 µm. The magnetization properties are strongly affected by the roll-up process. In addition to a modified shape anisotropy, the magnetostrictive anisotropy due to the stress release is reversed (see figure). We found that the easy axis of magnetization (along 90°) is induced by the external uniaxial stress. It corresponds to a more compressive stress along 90° compared to the 0° direction. After the roll-up process the easy axis of magnetization is aligned along 0°, corresponding to the direction of compressive stress.

Moreover, low temperature measurements support the presence of significant exchange bias (up to 24 mT) for the rolled-up structures presumably due to the exchange coupling at Co/CoO interfaces.

[1] M. Kläui et al., Appl. Phys. Lett. 78 (2001) 3268.
[2] M. C. K. Wiltshire et al., Phys. Rev. Lett. 291 (2001) 849.

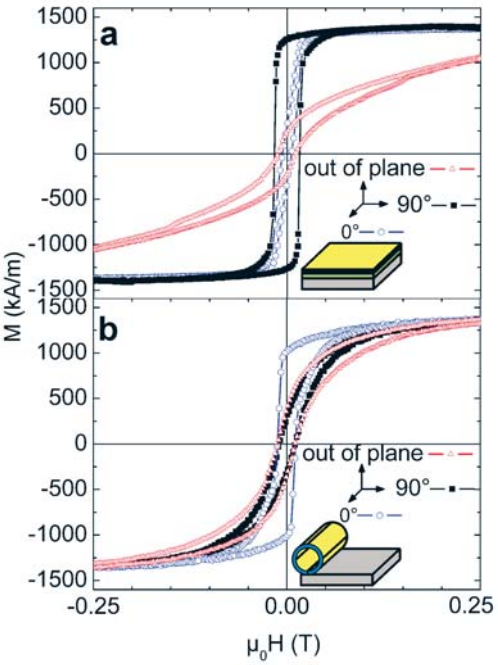

Fig.: VSM hysteresis loops obtained from a) the film array and b) the corresponding tube array. The film consists of 4 nm Au/ 10 nm Co/ 4 nm Au layers. The insets show the directions of the applied field.

Structure and properties of Hafniumoxide-based high-k dielectric layers

J. Gluch, S. Menzel, J. Thomas

The atomic layer deposition (ALD) has a high industrial potential for the next generations of complementary metal-oxide-semiconductor memory technology. Its ability to grow high dielectric constant materials with highly conformal, homogeneous, and atomically accurate films on flat and high-aspect ratio structures in an ultrathin range is subject of this project.

The dielectric properties of yttrium stabilized hafnium oxide (Hf-Y-O) thin films have been evaluated with respect to their crystalline structure. The films with a thickness of few nanometres show different structure depending on thickness, deposition temperature and yttrium content. High quality films could be deposited at 300°C in a tube flow ALD chamber with a halide Hafnium precursor ($HfCl_4$) and a metal organic Yttrium precursor ($(CpCH_3)_3Y$). Water was used as oxygen source. The films with thickness of 10 nm are amorphous in the as-deposited state and fully crystalline after thermal treatment at 400°C. Hereby, the Yttrium stabilizes the desired cubic Hafnium oxide phase. After thermal treatment the crystal size is in the range of film thickness. The crystalline structure directly correlates with the dielectric properties. A maximum dielectric constant with ~80% higher κ value in comparison to that of the pure Hafnium oxide films (κ = 16) was observed for an Yttrium content of ~ 6.2 at%. However, the leakage current does increase linearly with the Yttrium content.

In summary it is shown that the addition of Yttrium to the ultrathin HfO_2 ALD films can successful stabilize the cubic phase and, therefore, may contribute to efficiency of future integrated memory applications.

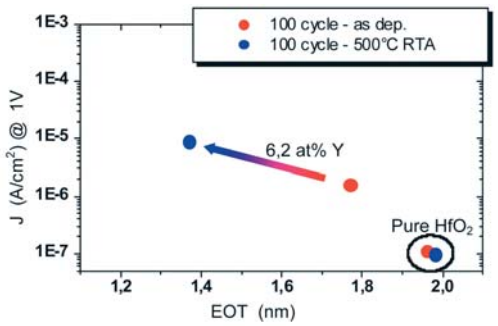

Fig.: Dependency of the leakage current J over dielectric constant represented as equivalent oxide thickness (EOT). The stabilisation of the high-κ phase after the thermal treatment at 500°C results in significantly enhanced dielectric properties with only minor increase in the leakage current. The values for pure HfO_2 do not show such a dramatic change.

Cooperation TU Dresden, Qimonda AG, Fraunhofer CNT, NamLAB gGmbH
Funded by BMBF (01M3171A, SOHAR)

A new interdigital transducer for remote surface acoustic waves (SAW) sensors

G. Martin, S. Biryukov, B. Steiner (1), B. Wall (1)

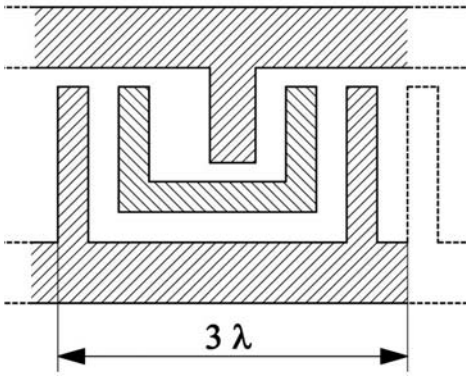

Fig.: Schematic view of a SPUDT cell structure suited for remote SAW sensors on $YZLiNbO_3$.

Remote SAW sensors are very important for the transmission of data from locations which are difficult in access. Such a sensor includes an interdigital transducer (IDT) and at least one reflector on a piezoelectric substrate. The time delay of the waves from the IDT to the reflectors and back to the IDT is the sensitive quantity. The sensor interacts with a transmitting / receiving unit. The goal is to increase the range of that unit for constant power. As a consequence, the IDT is required to radiate a SAW power as high as possible to the reflectors. This is achieved by using single phase unidirectional transducers (SPUDT). As an additional requirement the finger electrodes are to be not narrower than $\lambda/4$ (λ = wavelength) in order to be able to produce sensors up to 2.4 GHz by means of the available technology. The SPUDTs should not essentially be longer than 20λ. In order to obtain a sufficient directivity in spite of the short SPUDT length the reflection factor has to be as large as possible. The figure shows a SPUDT cell type suited for Y cut, Z propagating $LiNbO_3$ ($YZLiNbO_3$). The normalized Al layer thickness, h_{Al}/λ, is intended to be 7.5%. The length amounts to 3λ. The reflection factor per λ is found to be 5.9% what is a very large value. As shown by the figure, the cell includes floating electrodes beside electrodes with a given potential. The floating electrodes are favourable to achieve high reflection factors on high-coupling substrates like $YZLiNbO_3$.The structure is asymmetric resulting in the radiation of different SAW power to the right and left direction. All the electrode fingers and the gaps between them are wider than $\lambda/4$.

Cooperation Vectron International GmbH & Co, KG, Teltow (1)
Funded by Vectron International GmbH & Co, KG, Teltow

Development of SiO_2 layers for SAW microfluidics

A. Winkler, S. Menzel, H. Schmidt, J. Eckert

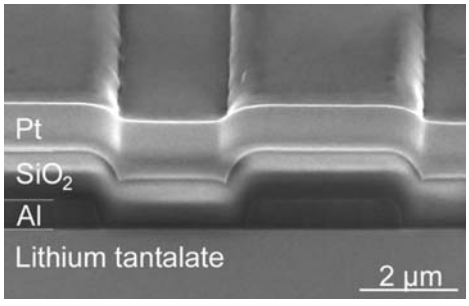

Fig.: FIB Cross-section of an IDT-finger structure with 500 nm thick Al-electrodes on piezoelectric Lithium tantalate, covered with 830 nm sputtered SiO_2

Surface acoustic wave microfluidics, i.e. the surface acoustic wave (SAW) driven actuation of small fluid volumes and the sensing of fluid properties using SAW is a relatively young and interdisciplinary field of research. Due to several reasons the covering of such microfluidic devices with a SiO_2 layer is beneficial: (1) electrical and mechanical passivation of the interdigital transducers (IDTs), (2) bio-/chemical compatibility and modifiability of SiO_2, (3) compensation of temperature-induced operation frequency shift of the SAW device. Additionally, the complete encapsulation of the IDT can generally improve power durability and lifetime of SAW devices, especially of SAW actuators.

We developed high-quality ("SAW-grade") SiO_2 thin films deposited by means of reactive RF magnetron sputtering from SiO_2-target on different piezoelectric substrates. Film characterization was carried out using atomic force microscopy, laser-pulse acoustic measurement, glow-discharge optical emission spectroscopy, variable angle ellipsometry, and x-ray photoelectron spectroscopy. The amorphous SiO_2 films show a high Young's modulus ($E_{SiO2,film}$ = 70...72 GPa), low RMS roughness (R_{RMS} < 0.5 nm), low SiO content (< 3 %) and high growth rates (> 30 nm/min). The edge covering of the films is excellent for finger electrode heights up to 500 nm (Fig.). The as-deposited films are applicable for novel SAW microfluidic devices like sensors or actuators, which will be developed in the IFW Dresden.

Cooperation TU Dresden, Creavac GmbH Dresden, SAW Components Dresden GmbH

Publications 2008 (update: Jan. 15, 2009)

Journal Papers

1) J. Acker, A. Henssge, Chemical analysis of acidic silicon etch solutions: II. Determination of HNO3, HF, and H2SiF6 by ion chromatography, Talanta 72 (2007), S. 1540-1545.
2) G. Allison, S. Spasov, A. Patane, L. Eaves, N.V. Kozlova, J. Freudenberger, M. Hopkinson, G. Hill, Electron effective mass and Si-donor binding energy in GaAs1-xNx probed by a high magnetic field, Physical Review B 77 (2008) Nr. 12, S. 125210/1-6.
3) V.Y. Aristov, O.V. Molodtsova, V.V. Maslyuk, D.V. Vyalikh, V.M. Zhilin, Y.A. Ossipyan, T. Bredow, I. Mertig, M. Knupfer, Electronic structure of the organic semiconductor copper phthalocyanine: Experiment and theory, The Journal of Chemical Physics 128 (2008) Nr. 3, S. 34703/1-6.
4) V. Arpiainen, V. Zalobotnyy, A.A. Kordyuk, S.V. Borisenko, M. Lindroos, Angular dependence of circular dichroism in Pb-doped and pristine Bi2Sr2CaCu2O8+delta, Physical Review B 77 (2008) Nr. 2, S. 24520/1-6.
5) M.E. Arroyo-deDompablo, R. Dominko, J.M. Gallardo-Amores, L. Dupont, G. Mali, H. Ehrenberg, J. Jamnik, E. Moran, On the energetic stability and electrochemistry of Li2MnSiO4 polymorphs, Chemistry of Materials 20 (2008), S. 5574-5584.
6) E. Arushanov, K.G. Lisunov, H. Vinzelberg, G. Behr, J. Schumann, O.G. Schmidt, Hopping conductivity in Mn-doped BETA_FeSi2 single crystals, Journal of Applied Physics 104 (2008) Nr. 5, S. 53720/1-6.
7) P. Atkinson, S. Kiravittaya, M. Benyoucef, A. Rastelli, O.G. Schmidt, Site-controlled growth and luminescence of InAs quantum dots using in situ Ga-assisted deoxidation of patterned substrates, Applied Physics Letters 93 (2008) Nr. 10, S. 101908/1-3.
8) P. Atkinson, O.G. Schmidt, S.P. Bremner, D.A. Ritchie, Formation and ordering of epitaxial quantum dots, Comptes Rendus Physique 9 (2008), S. 788-803.
9) P. Ayala, A. Grueneis, D. Grimm, C. Kramberger, R. Engelhard, M. Ruemmeli, J. Schumann, R. Kaltofen, B. Buechner, C. Schaman, H. Kuzmany, T. Gemming, A. Barreiro, T. Pichler, Cyclohexane triggers staged growth of pure and vertically aligned single wall carbon nanotubes, Chemical Physics Letters 454 (2008) Nr. 4-6, S. 332-336.
10) P. Ayala, W. Plank, A. Grueneis, E.I. Kauppinen, M.H. Ruemmeli, H. Kuzmany, T. Pichler, A one step approach to B-doped single-walled carbon nanotubes, Journal of Materials Chemistry 18 (2008), S. 5676-5681.
11) P. Ayala, M.H. Ruemmeli, T. Gemming, E. Kauppinen, H. Kuzmany, T. Pichler, CVD growth of single-walled B-doped carbon nanotubes, Physica Status Solidi B 245 (2008) Nr. 10, S. 1935-1938.
12) P. Ayala, A. Grueneis, C. Kramberger, M.H. Ruemmeli, I.G. Solorzano, F.L. Freire jr., T. Pichler, Effects of the reaction atmosphere composition on the synthesis of single and multiwalled nitrogen-doped nanotubes, The Journal of Chemical Physics 127 (2007) Nr. 18, S. 184709/1-6.
13) A. Bachmatiuk, R.J. Kalenczuk, M.H. Ruemmeli, T. Gemming, E. Borowiak-Palen, Preparation of ultra-large-scale catalysts for catalytic vapour deposition of carbon nanotubes, Materials Science-Poland 26 (2008) Nr. 1, S. 105-111.
14) E. Backen, S. Haindl, T. Niemeier, R. Huehne, T. Freudenberg, J. Werner, G. Behr, L. Schultz, B. Holzapfel, Growth and anisotropy of La(O, F)FeAs thin films deposited by pulsed laser deposition, Superconductor Science and Technology 21 (2008) Nr. 12, S. 122001/1-4.
15) N. Balchev, K. Nenkov, G. Mihova, B. Kunev, J. Pirov, Magnetic and superconducting properties of RuSr2Sm1.4Ce0.6Cu2O10- delta samples, Journal of Superconductivity and Novel Magnetism 21 (2008) Nr. 6, S. 365-369.
16) N. Balchev, K. Nenkov, G. Mihova, B. Kunev, J. Pirov, Structure, superconducting and magnetotransport properties of Ru1-xSnxSr2Gd1.4Ce0.6Cu2Oy (0=x=0.1), Journal of Physics / Condensed Matter 20 (2008) Nr. 32, S. 325203/1-8.
17) N. Balchev, K. Nenkov, G. Mihova, B. Kunev, J. Pirov, D.A. Dimitrov, Magnetic and superconducting properties of MoSr2HoCu2O8-delta, Journal of Optoelectronics and Advanced Materials 10 (2008) Nr. 10, S. 2757-2761.
18) T.A. Baser, M. Bostrom, M. Stoica, A.R. Yavari, M. Baricco, Analysis of melting and solidification behaviour of glass-forming alloys by synchrotron radiation, Advanced Engineering Materials 9 (2007) Nr. 6, S. 492-495.
19) J. Bednarcik, J. Kovac, S. Roth, J. Fuezer, P. Kollar, L.K. Varga, H. Franz, The soft magnetic properties and temperature stability of Co-Fe-Zr-B metallic glasses, Acta Physica Polonica A 113 (2008) Nr. 1, S. 83-86.
20) J. Bednarcik, K. Saksl, R. Nicula, S. Roth, H. Franz, Influence of cryomilling on structure of CoFeZrB alloy, Journal of Non-Crystalline Solids 354 (2008) Nr. 47-51, S. 5117-5119.
21) J. Bednarcik, S. Venkataraman, O. Khvostikova, H. Franz, D.J. Sordelet, J. Eckert, Microstructural changes induced by thermal treatment in Cu47Ti33Zr11Ni8Si1 metallic glass, Materials Science and Engineering A 498 (2008) Nr. 1-2, S. 335-340.
22) G. Behr, W. Loeser, D. Souptel, G. Fuchs, I. Mazilu, C. Cao, A. Koehler, L. Schultz, B. Buechner, Crystal growth of rare earth-transition metal borocarbides and silicides, Journal of Crystal Growth 310 (2008) Nr. 7-9, S. 2268-2276.
23) M. Benyoucef, S. Kiravittaya, Y.F. Mei, A. Rastelli, O.G. Schmidt, Strongly coupled semiconductor microcavities: A route to couple artificial atoms over micrometric distances, Physical Review B 77 (2008) Nr. 3, S. 35108/1-5.

24) B. Bergk, V. Petzold, H., Drechsler, S.-L., Bartkowiak, M., Ignatchik, O. Rosner, A.D. Bianchi, I. Sheikin, P.C., Wosnitza, J. Canfield, Anisotropic multiband many-body interactions in LuNi2B2C, Physical Review Letters 100 (2008) Nr. 25, S. 257004/1-4.

25) A. Bernardi, S. Kiravittaya, A. Rastelli, R. Songmuang, D.J. Thurmer, M. Benyoucef, O.G. Schmidt, On-chip Si/SiOx microtube refractometer, Applied Physics Letters 93 (2008) Nr. 9, S. 94106/1-3.

26) M.S. Bhuvaneswari, N.N. Bramnik, D. Ensling, H. Ehrenberg, W. Jaegermann, Synthesis and characterization of Carbon Nano Fiber/LiFePO4 composites for Li-ion batteries, Journal of Power Sources 180 (2008) Nr. 1, S. 553-560.

27) O. Bilani-Zeneli, A.D. Rata, A. Herklotz, O. Mieth, L.M. Eng, L. Schultz, M.D. Biegalski, H.M. Christen, K. Doerr, SrTiO3 on piezoelectric PMN-PT(001) for application of variable strain, Journal of Applied Physics 104 (2008) Nr. 5, S. 54108/1-5.

28) A.G. Birdwell, C.L. Littler, R. Glosser, M. Rebien, W. Henrion, P. Strauss, G. Behr, Evidence for an indirect gap in beta -FeSi2 epilayers by photoreflectance spectroscopy, Applied Physics Letters 92 (2008) Nr. 21, S. 211901/1-3.

29) A.R. Biris, D. Lupu, A. Grueneis, P. Ayala, M.H. Ruemmeli, T. Pichler, Z. Li, Y. Xu, I. Misan, E. Dervishi, A.S. Biris, High-Quality double-walled carbon nanotubes grown by a cold-walled radio frequency chemical vapor deposition process, Chemistry of Materials 20 (2008), S. 3466-3472.

30) A. Boehm, S. Roth, G. Naumann, W.-G. Drossel, R. Neugebauer, Analysis of structural and functional properties of Ni50Mn30Ga20 after plastic deformation, Materials Science and Engineering A 481-482 (2008), S. 266-270.

31) S.V. Borisenko, A.A. Kordyuk, A.N. Yaresko, V.B. Zabolotnyy, D.S. Inosov, R. Schuster, B. Buechner, R. Weber, R. Follath, L. Patthey, H. Berger, Pseudogap and charge density waves in two dimensions, Physical Review Letters 100 (2008) Nr. 19, S. 196402/1-4.

32) E. Borowiak-Palen, A. Bachmatiuk, M.H. Ruemmeli, T. Gemming, M. Kruszynska, R.J. Kalenczuk, Modifying CVD synthesised carbon nanotubes via the carbon feed rate, Physica E 40 (2008), S. 2227-2230.

33) A. Bourgeois, A.A. Aligia, T. Kroll, M.D. Nunez-Regueiro, Quasiparticle dispersion near the Fermi surface in NaxCoO2, Physica C 460-462 (2007), S. 497-498.

34) N.N. Bramnik, H. Ehrenberg, Precursor-based synthesis and electrochemical performance of LiMnPO4, Journal of Alloys and Compounds 464 (2008) Nr. 1-2, S. 259-264.

35) N.N. Bramnik, K. Nikolowski, D.M. Trots, H. Ehrenberg, Thermal stability of LiCoPO4 cathodes, Electrochemical and Solid-State Letters 11 (2008) Nr. 6, S. A89-A93.

36) J. Buschbeck, O. Heczko, A. Ludwig, S. Faehler, L. Schultz, Magnetic properties of epitaxial Fe–Pd films measured at elevated temperatures, Journal of Applied Physics 103 (2008) Nr. 7, S. 7B334/1-3.

37) J. Buschbeck, I. Opahle, S. Faehler, L. Schultz, M. Richter, Magnetic properties of Fe-Pd magnetic shape memory alloys: Density functional calculations and epitaxial films, Physical Review B 77 (2008) Nr. 17, S. 174421/1-8.

38) M. Bystrzejewski, A. Huczko, H. Lange, P. Baranowski, W. Kaszuwara, S. Cudzilo, E. Kowalska, M.H. Ruemmeli, T. Gemming, Carbon-encapsulated magnetic nanoparticles spontaneously formed by thermolysis route, Fullerenes, Nanotubes and Carbon Nanostructures 16 (2008) Nr. 4, S. 217-230.

39) M. Bystrzejewski, A. Huczko, H. Lange, W.W. Plotczyk, R. Stankiewicz, T. Pichler, T. Gemming, M.H. Ruemmeli, A continuous synthesis of carbon nanotubes by dc thermal plasma jet, Applied Physics A 91 (2008) Nr. 2, S. 223-228.

40) M. Bystrzejewski, H. Lange, A. Huczko, P. Baranowski, H.-W. Huebers, T. Gemming, T. Pichler, B. Buechner, M.H. Ruemmeli, One-step catalyst-free generation of carbon nanospheres via laser-induced pyrolysis of anthracene, Journal of Solid State Chemistry 181 (2008), S. 2796-2803.

41) M. Bystrzejewski, M.H. Ruemmeli, H. Lange, A. Huczko, P. Baranowski, T. Gemming, T. Pichler, Single-walled carbon nanotubes synthesis: A direct comparison of laser ablation and carbon arc routes, Journal of Nanoscience and Nanotechnology 8 (2008) Nr. 11, S. 1-9.

42) M. Bystrzejewski, R. Schoenfelder, G. Cuniberti, H. Lange, A. Huczko, T. Gemming, T. Pichler, B. Buechner, M. Ruemmeli, Exposing multiple roles of H2O in high-temperature enhanced carbon nanotube synthesis, Chemistry of Materials 20 (2008), S. 6586-6588.

43) C.D. Cao, R. Klingeler, N. Leps, H. Vinzelberg, V. Kataev, F. Muranyi, N. Tristan, A. Teresiak, S. Zhou, W. Loeser, G. Behr, B. Buechner, Interplay between Kondo-like behavior and short-range antiferromagnetism in EuCu2Si2 single crystals, Physical Review B 78 (2008) Nr. 6, S. 64409/1-6.

44) F. Cavallo, W. Sigle, O.G. Schmidt, Controlled fabrication of Cr/Si and Cr/SiGe tubes tethered to insulator substrates, Journal of Applied Physics 103 (2008) Nr. 11, S. 116103/1-3.

45) F. Cavallo, R. Songmuang, O.G. Schmidt, Fabrication and electrical characterization of Si-based rolled-up microtubes, Applied Physics Letters 93 (2008) Nr. 14, S. 143113/1-3.

46) J. Cech, M. Kalbac, S.A. Curran, D. Zhang, U. Dettlaff-Weglikowska, L. Dunsch, S. Yang, S. Roth, HRTEM and EELS investigation of functionalized carbon nanotubes, Physica E 37 (2007) Nr. 1-2, S. 109-114.

47) T. Chanier, I. Opahle, M. Sargolzaei, R. Hayn, M. Lannoo, Magnetic state around cation vacancies in II–VI semiconductors, Physical Review Letters 100 (2008) Nr. 2, S. 26405/1-3.

48) Y. Chen, Y. Mei, A. Malachias, J.I. Moench, R. Kaltofen, O.G. Schmidt, Photoresist-buffer-enhanced antiferromagnetic coupling and the giant magnetoresistance effect of Co/Cu multilayers, Journal of Physics: Condensed Matter 20 (2008) Nr. 45, S. 452202/1-5.

49) Y.-F. Chen, Y. Mei, R. Kaltofen, J.I. Moench, J. Schumann, J. Freudenberger, H.-J. Klauss, O.G. Schmidt, Towards flexible magnetoelectronics: Buffer-enhanced and mechanically tunable GMR of Co/Cu multilayers on plastic substrates, Advanced Materials 20 (2008) Nr. 17, S. 3224-3228.

50) K.-Y. Choi, P. Lemmens, D. Heydhausen, G. Guentherodt, C. Baumann, R. Klingeler, P. Reutler, B. Buechner, Anomalous orbital dynamics in LaSrMnO4 observed by Raman spectroscopy, Physical Review B 77 (2008) Nr. 6, S. 64415/1-5.

51) L. Ciric, K. Pierzchala, A. Sienkiewicz, A. Magrez, B. Nafradi, D. Alexander, J. Warner, H. Shinohara, M.H. Ruemmeli, T. Pichler, G.A.D. Briggs, L. Forro, La@C82 as a spin-active filling of SWCNTs: ESR study of magnetic and photophysical properties , Physica Status Solidi B 245 (2008) Nr. 10, S. 2042-2046.

52) M. Coll, J. Gazquez, F. Sandiumenge, T. Puig, X. Obradors, J.P. Espinos, R. Huehne, Nanostructural control in solution-derived epitaxial Ce1-xGdxO2-y films, Nanotechnology 19 (2008) Nr. 39, S. 395601/1-7.

53) T.A. Coombs, Z. Hong, X. Zhu, G. Krabbes, A novel heat engine for magnetizing superconductors, Superconductor Science and Technology 21 (2008) Nr. 3, S. 34001-34007.

54) P.M.F.J. Costa, D. Golberg, M. Mitome, S. Hampel, A. Leonhardt, B. Buechner, Y. Bando, Stepwise current-Driven release of attogram quantities of copper iodide encapsulated in carbon nanotubes, Nanoletters 8 (2008) Nr. 10, S. 3120-3125.

55) S. Costa, E. Borowiak-Palen, A. Bachmatiuk, M.H. Ruemmeli, T. Gemming, R.J. Kalenczuk, Iron filled carbon nanostructures from different precursors, Energy Conversion and Management 49 (2008) Nr. 9, S. 2483-2486.

56) J. Cwik, T. Palewski, K. Nenkov, G.S. Burkhanov, O.D. Chistyakov, J. Klamut, J. Warchulska, The effect of substitution of La for Tb on some physical properties of Tb1-xLaxNi2 solid solutions, Journal of Alloys and Compounds 460 (2008) Nr. 1-2, S. 41-46.

57) A.N. Darinskii, M. Weihnacht, Acoustic waves guided by a fluid layer on a piezoelectric substrate, Journal of Applied Physics 104 (2008) Nr. 5, S. 54904/1-9.

58) J. Das, F. Ettingshausen, J. Eckert, Ti-base nanoeutectic-hexagonal structured (D019) dendrite composite, Scripta Materialia 58 (2008) Nr. 8, S. 631-634.

59) Y. Das, K.B. Kim, Z.-F. Zhang, G. He, C. Mueller, J. Eckert, Deformation and fracture of Ti-base nanostructured composite, International Journal of Materials Research (Zeitschrift fuer Metallkunde) 99 (2008) Nr. 9, S. 985-990.

60) C. Deneke, J. Schumann, R. Engelhard, J. Thomas, W. Sigle, U. Zschieschang, H. Klauk, A. Chuvilin, O.G. Schmidt, Fabrication of radial superlattices based on different hybrid materials, Physica Status Solidi C 5 (2008) Nr. 9, S. 2704-2708.

61) C. Dietrich, R. Hertel, M. Huber, D. Weiss, R. Schaefer, J. Zweck, Influence of perpendicular magnetic fields on the domain structure of permalloy microstructures grown on thin membranes, Physical Review B 77 (2008) Nr. 17, S. 174427/1-8.

62) S.-L. Drechsler, M. Grobosch, K. Koepernik, G. Behr, A. Koehler, J. Werner, A. Kondrat, N. Leps, C. Hess, R. Klingeler, R. Schuster, B. Buechner, M. Knupfer, Optical study of La00.9F0.1FeAs: Evidence for a weakly coupled superconducting state, Physical Review Letters 101 (2008) Nr. 25, S. 257004/1-4.

63) C. Duhamel, J. Das, S. Pauly, K.S. Lee, J. Eckert, Deformation behavior and fractographic features of ductile Cu47Zr47Al6 bulk metallic glass, Reviews on Advanced Materials Science 18 (2008) Nr. 5, S. 527-533.

64) L. Dunsch, News from the world of endohedral fullerene, Nachrichten aus der Chemie 55 (2007) Nr. 5, S. 503-506.

65) J. Eckert, M. Calin, P. Yu, L.C. Zhang, S. Scudino, C. Duhamel, Al-based alloys containing amorphous and nanostructured phases, Reviews on Advanced Materials Science 18 (2008) Nr. 2, S. 169-172.

66) J. Eckert, J. Das, W. Xu, R. Theissmann, Nanoscale mechanism and intrinsic structure related deformation of Ti-alloys, Materials Science and Engineering A 493 (2008) Nr. 1-2, S. 71-78.

67) T. Edler, J. Buschbeck, C. Mickel, S. Faehler, S.G. Mayr, Mechanisms of stress generation and relaxation during pulsed laser deposition of epitaxial Fe–Pd magnetic shape memory alloy films on MgO, New Journal of Physics 10 (2008), S. 63007/1-11.

68) V.V. Efimova, M.V. Voronov, V. Hoffmann, J. Eckert, Electrical properties of pulsed glow discharge: two new aspects, Publications of the Astronomical Observatory of Belgrade 84 (2008), S. 369-373.

69) J. Eickemeyer, A. Gueth, B. Holzapfel, Elongated grains in cube textured nickel substrate tapes and flat wires, Superconductor Science and Technology 21 (2008) Nr. 3, S. 34007/1-4.

70) J. Eickemeyer, R. Huehne, A. Gueth, C. Rodig, H. Klauss, B. Holzapfel, Textured Ni–7.5 at.% W substrate tapes for YBCO-coated conductors, Superconductor Science and Technology 21 (2008) Nr. 10, S. 105012/1-7.

71) J. Eickemeyer, M. Falter, A. Gueth, Shear crack formation in cold drawing of magnesium and cobalt wires, International Journal of Applied Mechanics and Engineering 12 (2007) Nr. 4, S. 1173-1179.

72) E. Einarsson, H. Shiozawa, C. Kramberger, M.H. Ruemmeli, A. Grueneis, T. Pichler, S. Maruyama, Revealing the small-bundle internal structure of vertically aligned single-walled carbon nanotube films, The Journal of Physical Chemistry C 111 (2007) Nr. 48, S. 17861-17864.

73) D. Elefant, R. Schaefer, J. Thomas, H. Vinzelberg, C.M. Schneider, Competition of spin-flip and spin-flop dominated processes in magnetic multilayers: Magnetization reversal, magnetotransport, and domain structure in the NiFe/Cu system, Physical Review B 77 (2008) Nr. 1, S. 14426/1-11.

74) S. Elgazzar, I. Opahle, M. Richter, P.M. Oppeneer, Electronic structure and Fermi surface of PrMIn5 (M=Co, Rh, and Ir) compounds, Physical Review B 77 (2008) Nr. 12, S. 125105/1-7.

75) A. Elmali, S. Tekerek, I. Dincer, Y. Elerman, R. Theissmann, H. Ehrenberg, H. Fuess, Magnetic hardening of high-energy ball-milled nanocrystalline LaMn2Si2, Journal of Magnetism and Magnetic Materials 320 (2008) Nr. 3-4, S. 364-367.

76) M. Elmechaouri, B. Moenter, D. Kraemer, H. Pusch, W. Jasper, I. Erdman, R. Huehne, Microstructure and the grain boundaries evolution in sequential epitaxial buffer layers on RABiTS-Substrates, Journal of Physics: Conference Series 97 (2008) Nr. 1, S. 12042/1-9.

77) A. Elsner, H. Hermann, Computer simulation and optimization of properties of porous low-k dielectrics, Materials Science - Poland 25 (2007) Nr. 4, S. 1193-1202.

78) S. Engel, R. Huehne, K. Knoth, A. Chopra, N.H. Kumar, V.S. Sarma, P.N. Santhosh, L. Schultz, B. Holzapfel, Optimisation of single La2Zr2O7 buffer layers for YBCO coated conductors prepared by chemical solution deposition, Journal of Crystal Growth 310 (2008) Nr. 18, S. 4295-4300.

79) D.V. Evtushinsky, A.A. Kordyuk, V.B. Zabolotnyy, D.S. Inosov, B. Buechner, H. Berger, L. Patthey, R. Follath, S.V. Borisenko, Pseudogap-driven sign reversal of the hall effect, Physical Review Letters 100 (2008) Nr. 23, S. 236402/1-4.

80) S. Faehler, An introduction to actuation mechanisms of magnetic shape memory alloys, ECS Transactions 3 (2007) Nr. 25, S. 155-163.

81) J. Fassbender, J. McCord, Magnetic patterning by means of ion irradiation and implantation, Journal of Magnetism and Magnetic Materials 320 (2008) Nr. 3-4, S. 579-596.

82) K. Flatz, M. Grobosch, M. Knupfer, The dielectric function of potassium-doped zinc-phthalocyanine, Applied Physics A 90 (2008) Nr. 2, S. 243-246.

83) O. Frank, L. Kavan, A.A. Green, M.C. Hersam, L. Dunsch, In-situ Vis/NIR spectroelectrochemistry of single-walled carbon nanotubes enriched with (6,5) tubes, Physica Status Solidi B 245 (2008) Nr. 10, S. 2239-2242.

84) J. Freudenberger, E. Botcharova, A. Gaganov, J. Lyubimova, L. Schultz, H. Witte, H. Jones, T. Herrmannsdoerfer, S. Zherlitsyn, J. Wosnitza, D. Givord, V.M.T.S. Barthem, R.-D. Boettcher, K. Hannemann, Hochfeste Leitermaterialien auf Kupfer-Basis: quo vadis?, Metall 62 (2008), S. 126-128.

85) J. Freudenberger, H.-J. Klauss, K. Heinze, A. Gaganov, M. Schaper, L. Schultz, Fatigue of highly strengthened Cu–Ag alloys, International Journal of Fatigue 30 (2008) Nr. 3, S. 437-443.

86) D. Fritsch, K. Koepernik, M. Richter, H. Eschrig, Transition metal dimers as potential molecular magnets: A challenge to computational chemistry, Journal of Computational Chemistry 29 (2008) Nr. 13, S. 2210-2219.

87) D. Fritsch, H. Schmidt, R. Schmidt-Grund, M. Grundmann, Intensity of Optical Absorption Close to the Band Edge in Strained ZnO Films, Journal of the Korean Physical Society 53 (2008) Nr. 1, S. 123-126.

88) G. Fuchs, S.-L. Drechsler, N. Kozlova, G. Behr, A. Koehler, J. Werner, K. Nenkov, R. Klingeler, J. Hamann-Borrero, C. Hess, A. Kondrat, M. Grobosch, A. Narduzzo, M. Knupfer, J. Freudenberger, B. Buechner, L. Schultz, High-field pauli-limiting behavior and strongly enhanced upper critical magnetic fields near the transition temperature of an arsenic-deficient LaO0.9F0.1FeAs1- superconductor, Virtual Journal of Applications of Superconductivity 15 (2008) Nr. 12.

89) G. Fuchs, S.-L. Drechsler, N. Kozlova, G. Behr, A. Koehler, J. Werner, K. Nenkov, R. Klingeler, J. Hamann-Borrero, C. Hess, A. Kondrat, M. Grobosch, A. Narduzzo, M. Knupfer, J. Freudenberger, B. Buechner, L. Schultz, High-field pauli-limiting behavior and strongly enhanced upper critical magnetic fields near the transition temperature of an arsenic-deficient LaO0.9F0.1FeAs1- superconductor, Physical Review Letters 101 (2008) Nr. 23, S. 237003/1-4.

90) G. Fuchs, K. Nenkov, G. Krabbes, L. Shlyk, R. Weinstein, A. Gandini, R. Sawh, B. Mayes, D. Parks, Bulk YBCO with discontinuous irradiation defects: Bose-glass behaviour and very high critical current densities, Journal of Physics: Conference Series 97 (2008) Nr. 1, S. 12080/1-6.

91) J. Fuezer, J. Bednarcik, P. Kollar, S. Roth, Preparation and soft magnetic properties of bulk amorphous Co-rich alloys, Journal of Magnetism and Magnetic Materials 310 (2007), S. e852-e854.

92) B. Gao, C.B. Cai, Z.Y. Liu, J.L. Liu, L.L. Ying, S.X. Cao, J.C. Zhang, T. Thersleff, R. Huehne, B. Holzapfel, Single and binary rare earth REBa2Cu3O7-delta films prepared by chemical solution deposition, Journal of Physics: Conference Series 97 (2008) Nr. 1, S. 12245/1-5.

93) A. Gebert, V. Haehnel, E.S. Park, D.H. Kim, L. Schultz, Corrosion behaviour of Mg65Cu7.5Ni7.5Ag5Zn5Gd5Y5 bulk metallic glass in aqueous environments, Electrochimica Acta 53 (2008) Nr. 8, S. 3403-3411.

94) N. Ghosh, U.K. Roessler, K. Nenkov, C. Hucho, H.L. Bhat, K.-H. Mueller, Low temperature transport and specific heat studies of Nd1-xPbxMnO3 single crystals, Journal of Physics / Condensed Matter 20 (2008) Nr. 39, S. 395219/1-9.

95) A.A. Gippius, A.S. Moskvin, S.-L. Drechsler, Spin polarization of the magnetic spiral in NaCu2O2 as seen by nuclear magnetic resonance spectroscopy, Physical Review B 77 (2008) Nr. 18, S. 180403/1-4.

96) A. Goux, T. Pauporte, D. Lincot, L. Dunsch, In Situ ESR and UV/Vis Spectroelectrochemical Study of Eosin Y Upon Reduction with and without Zn(II) Ions, ChemPhysChem 8 (2007) Nr. 6, S. 926-931.

97) H.-J. Grafe, F. Hammerath, A. Vyalikh, G. Urbanik, V. Kataev, T. Wolf, G. Khaliullin, B. Buechner, Contrasting spin dynamics in Zn- and Ni-doped NdBa2Cu3O6+y single crystals from Cu nuclear quadrupole resonance: Evidence for correlations between antiferromagnetism and pseudogap effects, Physical Review B 77 (2008) Nr. 1, S. 14522/1-5.

98) H.-J. Grafe, D. Paar, G. Lang, N.J. Curro, G. Behr, J. Werner, J. Hamann-Borrero, C. Hess, N. Leps, R. Klingeler, B. Buechner, 75As NMR studies of superconducting LaFeAsO0.9F0.1, Physical Review Letters 101 (2008) Nr. 4, S. 47003/1-4.
99) M. Grobosch, K. Doerr, R.B. Gangineni, M. Knupfer, Energy level alignment and injection barriers at spin injection contacts between La0.7Sr0.3MnO3 and organic semiconductors, Applied Physics Letters 92 (2008) Nr. 2, S. 23302/1-3.
100) M. Grobosch, M. Knupfer, Electronic properties of the interface between the organic semiconductor alpha-sexithiophene and polycrystalline palladium, Organic Electronics 9 (2008) Nr. 5, S. 767-774.
101) M. Grobosch, M. Knupfer, K. Doerr, R.B. Gangineni, Alignment of the energy levels and charge injection barriers at interfaces for spin injection: La0.7Sr0.3MnO3 in contact with organic semiconductors, Physica Status Solidi B 245 (2008) Nr. 5, S. 799-803.
102) A. Grueneis, C. Attaccalite, T. Pichler, V. Zabolotnyy, H. Shiozawa, S.L. Molodtsov, D. Inosov, A. Koitzsch, M. Knupfer, J. Schiessling, R. Follath, R. Weber, P. Rudolf, L. Wirtz, A. Rubio, Electron-electron correlation in graphite: A combined angle-resolved photoemission and first-principles study, Physical Review Letters 100 (2008) Nr. 3, S. 37601/1-4.
103) A. Grueneis, C. Attaccalite, A. Rubio, S.L. Molodtsov, D.V. Vyalikh, J. Fink, R. Follath, T. Pichler, Preparation and electronic properties of potassium doped graphite single crystals, Physica Status Solidi B 245 (2008) Nr. 10, S. 2072-2076.
104) A. Grueneis, C. Attaccalite, L. Wirtz, H. Shiozawa, R. Saito, T. Pichler, A. Rubio, Tight-binding description of the quasiparticle dispersion of graphite and few-layer graphene, Physical Review B 78 (2008) Nr. 20, S. 205425/1-16.
105) A. Grueneis, D.V. Vyalikh, Tunable hybridization between electronic states of graphene and a metal surface, Physical Review B 77 (2008) Nr. 19, S. 193401/1-4.
106) A. Grueneis, T. Pichler, H. Shiozawa, C. Attaccalite, L. Wirtz, S.L. Molodtsov, R. Follath, R. Weber, A. Rubio, Low energy quasiparticle dispersion of graphite by angle-resolved photoemission spectroscopy, Physica Status Solidi B 244 (2007) Nr. 11, S. 4129-4133.
107) C. Gruenzweig, C. David, O. Bunk, M. Dierolf, G. Frei, G. Kuehne, J. Kohlbrecher, R. Schaefer, P. Lejcek, H.M.R. Ronnow, F. Pfeiffer, Neutron Decoherence Imaging for Visualizing Bulk Magnetic Domain Structures, Physical Review Letters 101 (2008) Nr. 2, S. 25504/1-4.
108) C. Gruenzweig, C. David, O. Bunk, M. Dierolf, G. Frei, G. Kuehne, R. Schaefer, S. Pofahl, H.M.R. Ronnow, F. Pfeiffer, Bulk magnetic domain structures visualized by neutron dark-field imaging, Applied Physics Letters 93 (2008) Nr. 11, S. 112504/1-3.
109) M.E. Gruner, P. Entel, I. Opahle, M. Richter, Ab initio investigation of twin boundary motion in the magnetic shape memory Heusler alloy Ni_2MnGa, Journal of Materials Science 43 (2008) Nr. 11, S. 3825-3831.
110) M. Haertel, J. Richter, D. Ihle, S.-L. Drechsler, Thermodynamics of a one-dimensional frustrated spin- 1/2 Heisenberg ferromagnet, Physical Review B 78 (2008) Nr. 17, S. 174412/1-6.
111) W. Haessler, M. Herrmann, C. Rodig, M. Schubert, K. Nenkov, B. Holzapfel, Further increase of the critical current density of MgB2 tapes with nanocarbon-doped mechanically alloyed precursor, Superconductor Science and Technology 21 (2008) Nr. 6, S. 62001-62003.
112) S. Haindl, M. Weisheit, T. Thersleff, L. Schultz, B. Holzapfel, Enhanced field compensation effect in superconducting/hard magnetic Nb/FePt bilayers, Superconductor Science and Technology 21 (2008) Nr. 4, S. 45017/1-6.
113) C. Hamann, I. Moench, R. Kaltofen, R. Schaefer, T. Gemming, L. Schultz, J. McCord, Size effects on the magnetization reversal behavior of exchange bias modulated thin films, Journal of Applied Physics 104 (2008) Nr. 1, S. 13926/1-7.
114) S. Hampel, D. Kunze, D. Haase, K. Kraemer, M. Rauschenbach, M. Ritschel, L. Leonhardt, J. Thomas, S. Oswald, V. Hoffmann, B. Buechner, Carbon nanotubes filled with a chemotherapeutic agent: a nanocarrier mediates inhibition of tumor cell growth, Nanomedicine 3 (2008) Nr. 2, S. 175-182.
115) J.H. Han, K.B. Kim, S. Yi, J.M. Park, D.H. Kim, S. Pauly, J. Eckert, Influence of a bimodal eutectic structure on the plasticity of a (Ti70.5Fe29.5)91Sn9 ultrafine composite, Applied Physics Letters 93 (2008) Nr. 20, S. 201906/1-3.
116) J.H. Han, K.B. Kim, S. Yi, J.M. Park, S.W. Sohn, T.E. Kim, D.H. Kim, J. Das, J. Eckert, Formation of a bimodal eutectic structure in Ti–Fe–Sn alloys with enhanced plasticity, Applied Physics Letters 93 (2008) Nr. 14, S. 141901/1-3.
117) S. Harikrishnan, C.M. Naveen Kumar, H.L. Bhat, S. Elizabeth, U.K. Roessler, K. Doerr, S. Roessler, S. Wirth, Investigations on the spin-glass state in Dy0.5Sr0.5MnO3 single crystals through structural, magnetic and thermal properties, Journal of Physics / Condensed Matter 20 (2008) Nr. 27, S. 275234/1-10.
118) H. Hartmann, P.K. Galenko, D. Holland-Moritz, M. Kolbe, D.M. Herlach, O. Shuleshova, Nonequilibrium solidification in undercooled Ti45Al55 melts, Journal of Applied Physics 103 (2008) Nr. 7, S. 73509/1-9.
119) O. Heczko, S. Faehler, T.M. Vasilchikova, T.N. Voloshok, K.V. Klimov, Y.I. Chumlyakov, A.N. Vasiliev, Thermodynamic, kinetic, and magnetic properties of a Ni54Fe19Ga27 magnetic shape-memory single crystal, Physical Review B 77 (2008) Nr. 17, S. 174402/1-7.
120) O. Heczko, M. Thomas, J. Buschbeck, L. Schultz, S. Faehler, Epitaxial Ni–Mn–Ga films deposited on SrTiO3 and evidence of magnetically induced reorientation of martensitic variants at room temperature, Applied Physics Letters 92 (2008) Nr. 7, S. 72502/1-3.
121) I. Hellmann, C. Taeschner, R. Klingeler, A. Leonhardt, B. Buechner, M. Knupfer, Structure and electronic properties of Li-doped vanadium oxide nanotubes, The Journal of Chemical Physics 128 (2008) Nr. 22, S. 224701/1-5.

122) A. Henssge, J. Acker, Chemical analysis of acidic silicon etch solutions: I. Titrimetric determination of HNO3, HF, and H2SiF6, Talanta 73 (2007) Nr. 2, S. 220-226.

123) R. Hermann, H. Vinzelberg, G. Behr, K. Woll, F. Muecklich, B. Buechner, Magnetic field controlled floating-zone crystal growth and properties of RuAl single crystal, Journal of Crystal Growth 310 (2008) Nr. 18, S. 4286-4289.

124) S.G. Hickey, C. Waurisch, B. Rellinghaus, A. Eychmueller, Size and shape control of colloidally synthesized IV-VI nanoparticulate tin(II) sulfide, Journal of the American Chemical Society 130 (2008), S. 14978-14980.

125) V.-D. Hodoroaba, D. Klemm, U. Reinholz, E. Strub, J. Roehrich, W. Bohne, V. Hoffmann, K. Wetzig, Potential candidates of certified reference material for determination of hydrogen concentration with glow discharge optical emission spectrometry (GD-OES)—a feasibility study, Journal of Analytical Atomic Spectrometry 23 (2008) Nr. 4, S. 460-462.

126) V. Hoffmann, V.V. Efimova, M.V. Voronov, P. Smid, E.B.M. Steers, J. Eckert, Measurement of voltage and current in continuous and pulsed rf and dc glow discharges, Journal of Physics: Conference Series 133 (2008), S. 12017/1-12.

127) R. Huehne, K. Gueth, M. Kidszun, R. Kaltofen, L. Schultz, B. Holzapfel, Metallic seed layers for ion-beam assisted pulsed laser deposition of highly textured transition metal nitride films, Journal of Physics / D 41 (2008) Nr. 24, S. 245404/1-5.

128) R. Huehne, D. Okai, K. Doerr, S. Trommler, A. Herklotz, B. Holzapfel, L. Schultz, Dynamic investigations on the influence of epitaxial strain on the superconducting transition in YBa2Cu3O7-x , Superconductor Science and Technology 21 (2008) Nr. 7, S. 75020/1-4.

129) K. Iketaki, K. Kanai, W. Fujita, K. Awaga, J. Tsutsumi, H. Yoshida, N. Sato, M. Knupfer, Y. Ouchi, K. Seki, Electronic structure of 1,3,5-trithia-2,4,6-triazapentalenyl on gold, Chemical Physics Letters 451 (2008) Nr. 1-3, S. 58-62.

130) D.S. Inosov, R. Schuster, A.A. Kordyuk, J. Fink, S.V. Borisenko, V.B. Zabolotnyy, D.V. Evtushinsky, M. Knupfer, B. Buechner, R. Follath, H. Berger, Excitation energy map of high-energy dispersion anomalies in cuprates, Physical Review B 77 (2008) Nr. 21, S. 212504/1-3.

131) D.S. Inosov, V.B. Zabolotnyy, D.V. Evtushinsky, A.A. Kordyuk, B. Buechner, R. Follath, H. Berger, S.V. Borisenko, Fermi surface nesting in several transition metal dichalcogenides, New Journal of Physics 10 (2008), S. 125027/1-10.

132) O. Isnard, M.D. Kuzmin, M. Richter, M. Loewenhaupt, R. Bewley, A high-energy inelastic neutron scattering investigation of the Gd–Co exchange interactions in GdCo4B: Comparison with density-functional calculations, Journal of Applied Physics 104 (2008) Nr. 1, S. 13922/1-6.

133) T. Ivek, T. Vuletic, B. Korin-Hamzic, O. Milat, S. Tomic, B. Gorshunov, M. Dressel, J. Akimitsu, Y. Sugiyama, C. Hess, B. Buechner, Crossover in charge transport from one-dimensional copper-oxygen chains to two-dimensional ladders in (La,Y)y(Sr,Ca)14-yCu24O41, Physical Review B 78 (2008) Nr. 20, S. 205105/1-8.

134) P. Jehanno, M. Heilmaier, H. Saage, M. Boening, H. Kestler, J. Freudenberger, S. Drawin, Assessment of the high temperature deformation behavior of molybdenum silicide alloys, Materials Science and Engineering A 463 (2007) Nr. 1-2, S. 216-223.

135) J.C.G. Jeynes, C. Jeynes, K.J. Kirkby, M. Ruemmeli, S.R.P. Silva, RBS/EBS/PIXE measurement of single-walled carbon nanotube modification by nitric acid purification treatment, Nuclear Instruments and Methods in Physics Research B 266 (2008) Nr. 8, S. 1569-1573.

136) H.-J. Jun, K.S. Lee, J. Eckert, Y.W. Chang, High-temperature deformation behavior and formability of a Zr-Cu-Al-Ni bulk metallic glass, Metallurgical and Materials Transactions A 39 (2008) Nr. 8, S. 1831-1837.

137) M. Kalbac, L. Kavan, L. Dunsch, M.S. Dresselhaus, Development of the tangential mode in the Raman spectra of SWCNT bundles during electrochemical charging, Nanoletters 8 (2008) Nr. 4, S. 1257-1264.

138) M. Kalbac, L. Kavan, M. Zukalova, L. Dunsch, Influence of an extended fullerene cage: Study of chemical and electrochemical doping of C-70 peapods by in situ Raman spectroelectrochemistry, The Journal of Physical Chemistry C 111 (2007) Nr. 3, S. 1079-1085.

139) M. Kalbac, O. Frank, L. Kavan, M. Zukalova, J. Prochazka, M. Klementova, L. Dunsch, Heterostructures from Single-Wall Carbon Nanotubes and TiO2 Nanocrystals, Journal of the Electrochemical Society 154 (2007) Nr. 8, S. K19-K24.

140) M. Kalbac, L. Kavan, M. Zukalova, L. Dunsch, An in situ Raman spectroelectrochemical study of the controlled doping of single walled carbon nanotubes in a conducting polymer matrix, Carbon 45 (2007) Nr. 7, S. 1463-1470.

141) M. Kalbac, L. Kavan, M. Zukalova, S.F. Yang, J. Chech, S. Roth, L. Dunsch, The change of the state of an endohedral fullerene by encapsulation into SWCNT: A Raman spectroelectrochemical study of Dy3N@C-80 peapods, Chemistry - A European Journal 13 (2007) Nr. 31, S. 8811-8817.

142) M. Kalbac, L. Kavan, L. Dunsch, In situ Raman spectroelectrochemistry as a tool for the differentiation of inner tubes of double-wall carbon nanotubes and thin single-wall carbon nanotubes, Analytical Chemistry 79 (2007) Nr. 23, S. 9074-9081.

143) M. Kalbacova, M. Kalbac, L. Dunsch, U. Hempel, Influence of single-walled carbon nanotube films on metabolic activity and adherence of human osteoblasts, Carbon 45 (2007) Nr. 11, S. 2266-2272.

144) G.M. Kalvius, D.R. Noakes, R. Waeppling, N. Marcano, E. Schreier, O. Hartmann, U.K. Roessler, K. Nenkov, K.-H. Mueller, B. Idzikowski, Study of magnetic clusters in granular CoxCu1- x, Physica Scripta 77 (2008) Nr. 2, S. 25705/1-15.

145) D. Kasinathan, K. Koepernik, H. Rosner, Quasi-one-dimensional magnetism driven by unusual orbital ordering in CuSb2O6, Physical Review Letters 100 (2008) Nr. 23, S. 237202/1-4.

146) D. Kasinathan, K. Koepernik, U. Nitzsche, H. Rosner, Ferromagnetism induced by orbital order in the charge-transfer insulator Cs2AgF4: An electronic structure study, Physical Review Letters 99 (2007) Nr. 24, S. 247210/1-4.
147) G. Katsaros, J. Tersoff, M. Stoffel, A. Rastelli, P. Acosta-Diaz, G.S. Kar, G. Costantini, O.G. Schmidt, K. Kern, Positioning of strained islands by interaction with surface nanogrooves, Physical Review Letters 101 (2008) Nr. 9, S. 96103/1-4.
148) F. Khelfaoui, M. Kohl, J. Buschbeck, O. Heczko, S. Faehler, L. Schultz, A fabrication technology for epitaxial Ni-Mn-Ga micro-actuators, The European Physical Journal - Special Topics 158 (2008) Nr. 1, S. 167-172.
149) B. Khorkounov, A. Gebert, C. Mickel, L. Schultz, Improving the performance of hydrogen storage electrodes based on mechanically alloyed Mg61Ni30Y9, Journal of Alloys and Compounds 458 (2008) Nr. 1-2, S. 479-486.
150) K.B. Kim, J. Das, M.H. Lee, D.H. Kim, Lee, W.H., J. Eckert, Formation of nano-scale omega-phase in arc-melted micron-scale dendrite reinforced Zr73.5Nb9Cu7Ni1Al9.5 ultrafine composite during heat treatment, Intermetallics 16 (2008) Nr. 4, S. 538-543.
151) K.B. Kim, X.F. Zhang, S. Yi, M.H. Lee, J. Das, J. Eckert, Effect of local chemistry, structure and length scale of heterogeneities on the mechanical properties of a Ti45Cu40Ni7.5Zr5Sn2.5 bulk metallic glass, Philosophical Magazine Letters 88 (2008) Nr. 1, S. 75-81.
152) K.T. Kim, S.I. Cha, T. Gemming, J. Eckert, S.H. Hong, The role of interfacial oxygen atoms in the enhanced mechanical properties of carbon-nanotube-reinforced metal matrix nanocomposites, Small 4 (2008) Nr. 11, S. 1936-1940.
153) K.T. Kim, J. Eckert, S.B. Menzel, T. Gemming, S.H. Hong, Grain refinement assisted strengthening of carbon nanotube reinforced copper matrix nanocomposites, Applied Physics Letters 92 (2008) Nr. 12, S. 121901/1-3.
154) S.A.J. Kimber, D.N. Argyriou, F. Yokaichiya, K. Habicht, S. Gerischer, T. Hansen, T. Chatterji, R. Klingeler, C. Hess, G. Behr, A. Kondrat, B. Buechner, Magnetic ordering and negative thermal expansion in PrFeAsO, Physical Review B 78 (2008) Nr. 14, S. 140503(R)/ 1-4.
155) S. Kiravittaya, M. Benyoucef, R. Zapf-Gottwick, A. Rastelli, O.G. Schmidt, Optical fine structure of single ordered GaAs quantum dots, Physica E 40 (2008) Nr. 6, S. 1909-1912.
156) S. Kiravittaya, O.G. Schmidt, Quantum-dot crystal defects, Applied Physics Letters 93 (2008) Nr. 17, S. 173109/1-3.
157) N.S. Kiselev, I.E. Dragunov, V. Neu, U.K. Roessler, A.N. Bogdanov, Theoretical analysis of magnetic force microscopy contrast in multidomain states of magnetic superlattices with perpendicular anisotropy, Journal of Applied Physics 103 (2008) Nr. 4, S. 43907/1-7.
158) N.S. Kiselev, I.E. Dragunov, A.T. Onisan, U.K. Roessler, A.N. Bogdanov, Theory of stripe domains in magnetic shape memory alloys, The European Physical Journal - Special Topics 158 (2008) Nr. 1, S. 119-124.
159) N.S. Kiselev, U.K. Roessler, A.N. Bogdanov, O. Hellwig, Topological defects in antiferromagnetically coupled multilayers with perpendicular anisotropy, Applied Physics Letters 93 (2008) Nr. 16, S. 162502/1-3.
160) N.S. Kiselev, I.E. Dragunov, U.K. Roessler, A.N. Bogdanov, Stripe domains in nanomagnetic superlattices, Technical Physics Letters (Original in russ.: Pisma v Zhurnal Technicheskoi Fiziki 33, 87) 33 (2007), S. 1028-1031.
161) H.-H. Klauss, H. Luetkens, R. Klingeler, C. Hess, F.J. Litterst, M. Kraken, M.M. Korshunov, I. Eremin, S.-L. Drechsler, R. Khasanov, A. Amato, J. Hamann-Borrero, N. Leps, A. Kondrat, G. Behr, J. Werner, B. Buechner, Commensurate spin density wave in LaFeAsO: A local probe study, Physical Review Letters 101 (2008) Nr. 7, S. 77005/1-4.
162) D. Klemm, M. Stangl, A. Peeva, V. Hoffmann, K. Wetzig, J. Eckert, Analysis of interface impurities in electroplated Cu layers by using GD-OES and TOF-SIMS, Surface and Interface Analysis 40 (2008) Nr. 3-4, S. 418-422.
163) R. Klingeler, S. Hampel, B. Buechner, Carbon nanotube based biomedical agents for heating, temperature sensoring and drug delivery, International Journal of Hyperthermia 24 (2008) Nr. 6, S. 496-505.
164) K. Knoth, R. Huehne, S. Oswald, L. Molina, O. Eibl, L. Schultz, B. Holzapfel, Growth of thick chemical solution derived pyrochlore La2Zr2O7 buffer layers for YBa2Cu3O7-x coated conductors, Thin Solid Films 516 (2008), S. 2099-2108.
165) V. Ko, K.L. Teo, T. Liew, T.C. Chong, T. Liu, A.T.S. Wee, A.Y. Du, M. Stoffel, O.G. Schmidt, Correlation of structural and magnetic properties of ferromagnetic Mn-implanted Si1-xGex films, Journal of Applied Physics 103 (2008) Nr. 5, S. 53912/1-7.
166) A. Koitzsch, S.V. Borisenko, D. Inosov, J. Geck, V.B. Zabolotnyy, H. Shiozawa, M. Knupfer, J. Fink, B. Buechner, E.D. Bauer, J.L. Sarrao, R. Follath, Hybridization effects in CeCoIn5 observed by angle-resolved photoemission, Physical Review B 77 (2008) Nr. 15, S. 155128/1-7.
167) A. Koitzsch, D. Inosov, J. Fink, M. Knupfer, H. Eschrig, V. Borisenko, G. Behr, A. Koehler, J. Werner, B. Buechner, R. Follath, H.A. Duerr, Valence-band and core-level photoemission spectroscopy of LaFeAsO1-xFx, Physical Review B 78 (2008) Nr. 18, S. 180506/1-4.
168) V. Kokotin, H. Hermann, Computational analysis of the atomic size effect in bulk metallic glasses and their liquid precursors, Acta Materialia 56 (2008) Nr. 18, S. 5058-5065.
169) P. Kollar, D. Oleksakova, J. Fuezer, J. Kovac, S. Roth, K. Polanski, The magnetic properties of powdered and compacted micro-crystalline permalloy, Journal of Magnetism and Magnetic Materials 310 (2007), S. 2609-2611.
170) D. Koudela, U. Schwarz, H. Rosner, U. Burkhardt, A. Handstein, M. Hanfland, M.D. Kuzmin, I. Opahle, K. Koepernik, K.-H. Mueller, M. Richter, Magnetic and elastic properties of YCo5 and LaCo5 under pressure, Physical Review B 77 (2008) Nr. 2, S. 24411/1-7.

171) J. Koza, M. Uhlemann, A. Gebert, L. Schultz, The effect of magnetic fields on the electrodeposition of iron, Journal of Solid State Electrochemistry 12 (2008) Nr. 2, S. 181-192.
172) J.A. Koza, M. Uhlemann, A. Gebert, L. Schultz, The effect of a magnetic field on the pH value in front of the electrode surface during the electrodeposition of Co, Fe and CoFe alloys, Journal of Electroanalytical Chemistry 617 (2008) Nr. 2, S. 194-202.
173) J.A. Koza, M. Uhlemann, A. Gebert, L. Schultz, The effect of magnetic fields on the electrodeposition of CoFe alloys, Electrochimica Acta 53 (2008) Nr. 16, S. 5344-5353.
174) J.A. Koza, M. Uhlemann, A. Gebert, L. Schultz, Nucleation and growth of the electrodeposited iron layers in the presence of an external magnetic field, Electrochimica Acta 53 (2008) Nr. 27, S. 7972-7980.
175) J.A. Koza, M. Uhlemann, A. Gebert, L. Schultz, Desorption of hydrogen from the electrode surface under influence of an external magnetic field, Electrochemistry Communications 10 (2008) Nr. 9, S. 1330-1333.
176) C. Kramberger, R. Hambach, C. Giorgetti, M.H. Ruemmeli, M. Knupfer, J. Fink, B. Buechner, L. Reining, E. Einarsson, S. Maruyama, F. Sottile, K. Hannewald, V. Olevano, A.G. Marinopoulos, T. Pichler, Linear plasmon dispersion in single-wall carbon nanotubes and the collective excitation spectrum of graphene, Physical Review Letters 100 (2008) Nr. 19, S. 196803/1-4.
177) C. Kramberger, M. Ruemmeli, M. Knupfer, J. Fink, B. Buechner, E. Einarsson, S. Maruyama, T. Pichler, Loss-spectroscopy on sparse arrays of aligned single-wall carbon nanotubes, Physica Status Solidi B 245 (2008) Nr. 10, S. 2284-2287.
178) M. Krishnan, Z. Petrasek, I. Moench, P. Schwille, Electrostatic self-assembly of charged colloids and macromolecules in a fluidic nanoslit, Small 4 (2008) Nr. 11, S. 1900-1906.
179) T. Kroll, S. Bonhommeau, T. Kachel, H.A. Duerr, J. Werner, G. Behr, A. Koitzsch, A.K. Ariffin, R. Manzke, F.M.F. de Groot, J. Fink, H. Eschrig, B. Buechner, M. Knupfer, On the electronic structure of electron doped LaFeAsO1-xFx, Journal of the Physical Society of Japan 77 (2008) Nr. Suppl. C, S. 117-181.
180) T. Kroll, S. Bonhommeau, T. Kachel, H.A. Duerr, J. Werner, G. Behr, A. Koitzsch, R. Huebel, S. Leger, R. Schoenfelder, A.K. Ariffin, R. Manzke, F.M.F. de Groot, J. Fink, H. Eschrig, B. Buechner, M. Knupfer, Electronic structure of LaFeAsO1-xFx from x-ray absorption spectroscopy, Physical Review B 78 (2008) Nr. 22, S. 220502/1-4.
181) S. Kudela jr., S. Oswald, S. Kudela, K. Wetzig, Application of FTIR spectra for evaluating interfacial reactions in metal matrix composites, Analytical and Bioanalytical Chemistry 390 (2008) Nr. 6, S. 1477-1486.
182) P. Kumar, K.G. Suresh, A.K. Nigam, O. Gutfleisch, Large reversible magnetocaloric effect in RNi compounds, Journal of Physics / D 41 (2008) Nr. 24, S. 245006/1-5.
183) D. Kunze, S. Hampel, K. Kraemer, D. Haase, S. Fuessel, A. Leonhardt, A. Meye, B. Buechner, M.O. Grimm, M.P. Wirth, Carbon nanotubes: A nanocontainer mediates transport of chemotherapeutics, European Urology Supplements 7 (2008) Nr. 3, S. 277 (823).
184) M.D. Kuzmin, Landau-type parametrization of the equation of state of a ferromagnet, Physical Review B 77 (2008) Nr. 18, S. 184431/1-13.
185) M.D. Kuzmin, Y. Skourski, K.P. Skokov, K.-H. Mueller, O. Gutfleisch, Determining anisotropy constants from a first-order magnetization process in Tb2Fe17, Physical Review B 77 (2008) Nr. 13, S. 132411/1-4.
186) Y.-W. Lai, R. Schaefer, L. Schultz, J. McCord, Direct observation of AC field-induced twin-boundary dynamics in bulk NiMnGa, Acta Materialia 56 (2008) Nr. 18, S. 5130-5137.
187) K.S. Lee, J. Eckert, Y.W. Chang, EXAFS and dilatometric analysis of structural rearrangement after annealing in a Zr-Based bulk metallic glass, Reviews on Advanced Materials Science 18 (2008) Nr. 1, S. 14-17.
188) M.H. Lee, D.H. Bae, D.H. Kim, W.T. Kim, D. J. Sordelet, B.K. Kim, J. Eckert, Nanocrystallization at shear bands in bulk metallic glass matrix composites, Scripta Materialia 58 (2008) Nr. 8, S. 651-654.
189) M.H. Lee, K.B. Kim, J.H. Han, J. Eckert, D.J. Sordelet, High strength porous Ti–6Al–4V foams synthesized by solid state powder processing, Journal of Physics/ D 41 (2008) Nr. 10, S. 105404/1-5.
190) Y.C. Lee, S.J. Lin, V. Buck, R. Kunze, H. Schmidt, C.Y. Lin, W.L. Fang, I.N. Lin, Surface acoustic wave properties of natural smooth ultra-nanocrystalline diamond characterized by laser-induced SAW pulse technique, Diamond and Related Materials 17 (2008) Nr. 4-5, S. 446-450.
191) K. Leistner, P. Schaaf, A. Voss, S. Faehler, L. Schultz, H. Schloerb, Interfacial Fe(III)-hydroxide formation during Fe–Pt alloy deposition, Electrochimica Acta 53 (2008) Nr. 23, S. 6973-6977.
192) K. Leistner, H. Schloerb, J. Thomas, L. Schultz, S. Faehler, Remanence enhancement in nanoscaled electrodeposited FePt films, Applied Physics Letters 92 (2008) Nr. 5, S. 52502/1-3.
193) A.A. Leonov, I.E. Dragunov, U.K. Roessler, A.N. Bogdanov, Phenomenological model of surface-induced anisotropy in magnetic nanostructures, Functional Materials 15 (2008) Nr. 1, S. 109-114.
194) A.A. Leonov, U.K. Roessler, A.N. Bogdanov, Phenomenological theory of magnetization reversal in nanosystems with competing anisotropies, Journal of Applied Physics 104 (2008) Nr. 8, S. 84304/1-13.
195) A.A. Levin, A.I. Pommrich, T. Weissbach, D.C. Meyer, O. Bilani-Zeneli, Reversible tuning of lattice strain in epitaxial SrTiO3/La0.7Sr0.3MnO3 thin films by converse piezoelectric effect of 0.72Pb(Mg1/3Nb2/3)O3-0.28 PbTiO3 substrate, Journal of Applied Physics 103 (2008) Nr. 5, S. 54102/1-5.

196) X. Li, Y.J. Wei, H. Ehrenberg, F. Du, C.Z. Wang, G. Chen, Characterizations on the structural and electrochemical properties of LiNi1/3Mn1/3Co1/302 prepared by a wet-chemical process, Solid State Ionics 178 (2008) Nr. 39-40, S. 1969-1974.
197) J. Liu, N. Scheerbaum, O. Gutfleisch, Comparative study of structural and magnetic properties of bulk and powder Ni52Fe17Ga27Co4 magnetic shape memory alloy, IEEE Transactions on Magnetics 44 (2008) Nr. 11, S. 3025-3027.
198) J. Liu, N. Scheerbaum, D. Hinz, O. Gutfleisch, Martensitic transformation and magnetic properties in Ni–Fe–Ga–Co magnetic shape memory alloys, Acta Materialia 56 (2008) Nr. 13, S. 3177-3186.
199) J. Liu, N. Scheerbaum, D. Hinz, O. Gutfleisch, Magnetostructural transformation in Ni–Mn–In–Co ribbons, Applied Physics Letters 92 (2008) Nr. 16, S. 162509/1-3.
200) J. Liu, N. Scheerbaum, D. Hinz, O. Gutfleisch, A high-temperature coupling of martensitic and magnetic transformations and magnetic entropy change in Ni–Fe–Ga–Co alloys, Scripta Materialia 59 (2008) Nr. 10, S. 1063-1066.
201) J. Liu, N. Scheerbaum, J. Lyubina, O. Gutfleisch, Reversibility of magnetostructural transition and associated magnetocaloric effect in Ni–Mn–In–Co, Applied Physics Letters 93 (2008) Nr. 10, S. 102512/1-3.
202) L. Liu, B. Gao, W. Chu, D. Chen, T. Hu, C. Wang, L. Dunsch, A. Marcelli, Y. Luo, Z. Wu, The structural determination of endohedral metallofullerene Gd@C82 by XANES, Chemical Communications 4 (2008), S. 474-476.
203) I. Llamas-Jansa, C. Rongeat, S. Doppiu, O. Gutfleisch, L. Schultz, Characterisation of complex hydrides synthesised or modified by ball milling, International Journal of Materials Research (Zeitschrift fuer Metallkunde) 99 (2008) Nr. 5, S. 553-556.
204) M. Loeffler, M.H. Ruemmeli, C. Kramberger, E. Borowiak-Palen, R. Klingeler, T. Gemming, B. Buechner, T. Pichler, On the formation of single-walled carbon nanotubes in pulsed-laser-assisted chemical vapor deposition, Chemical Materials 20 (2008), S. 128-134.
205) W. Loeser, R. Hermann, T.G. Woodcock, J. Fransaer, M. Krivilyov, L. Granasy, T. Pusztat, G.T. Toth, D.M. Herlach, D. Holland-Moritz, M. Kolbe, T. Volkmann, Nucleation and phase selection in undercooles melts: magnetic alloys of industrial relevance (MAGNEPHAS), Journal of the Japan Society of Microgravity Application 25 (2008) Nr. 3, S. 495-500.
206) H.B. Lu, L.C. Zhang, A. Gebert, L. Schultz, Pitting corrosion of Cu–Zr metallic glasses in hydrochloric acid solutions, Journal of Alloys and Compounds 462 (2008), S. 60-67.
207) H. Luetkens, H.-H. Klauss, R. Khasanov, A. Amato, R. Klingeler, I. Hellmann, N. Leps, A. Kondrat, C. Hess, A. Koehler, G. Behr, J. Werner, B. Buechner, Field and temperature dependence of the superfluid density in LaFeAsO1-xFx superconductors: A muon spin relaxation study, Physical Review Letters 101 (2008) Nr. 9, S. 97009/1-4.
208) V. Lukes, K. Matuszna, P. Rapta, R. Solc, L. Dunsch, A.J.A. Aquino, H. Lischka, Experimental and theoretical study of model ladder fluoranthenopyracylene with two-dimensional -conjugation upon charging: structure and optical properties, Journal of Physical Chemistry C 112 (2008) Nr. 10, S. 3949-3958.
209) V. Lukes, K. Matuszna, P. Rapta, L. Dunsch, A. Aquino, H. Lischka, Electronic excitations in a ladder type fluoranthenopyracylene in its neutral and charged states: A theoretical and experimental study, Zeitschrift fuer Physikalische Chemie 221 (2007) Nr. 7, S. 911-928.
210) T.T.A. Lummen, R.Y.N. Gengler, P. Rudolf, F. Lusitani, E.J.M. Vertelman, P.J. van Koningsbruggen, M. Knupfer, O. Molodtsova, J.-J. Pireaux, P.H.M. van Loosdrecht, Bulk and surface switching in Mn-Fe-based prussian blue analogues, Journal of Physical Chemistry C 112 (2008) Nr. 36, S. 14158-14167.
211) J. Luzon, M. Castro, E.J.M. Vertelman, R.Y.N. Gengler, P.J. van Koningsbruggen, O. Molodtsova, M. Knupfer, P. Rudolf, P.H.M. van Loosdrecht, R. Broer, Prediction of the equilibrium structures and photomagnetic properties of the prussian blue analogue RbMn[Fe(CN)6] by density functional theory, Journal of Physical Chemistry A 112 (2008), S. 5742-5748.
212) J. Lyubina, O. Gutfleisch, M.D. Kuzmin, M. Richter, La(Fe,Si)13-based magnetic refrigerants obtained by novel processing routes, Journal of Magnetism and Magnetic Materials 320 (2008) Nr. 18, S. 2252-2258.
213) J. Lyubina, K. Nenkov, L. Schultz, O. Gutfleisch, Multiple metamagnetic transitions in the magnetic refrigerant La(Fe,Si)13Hx, Physical Review Letters 101 (2008) Nr. 17, S. 177203/1-4.
214) D. Makarov, E. Bermudez-Urena, O.G. Schmidt, F. Liscio, M. Maret, C. Brombacher, S. Schulze, M. Hietschold, M. Albrecht, Nanopatterned CoPt alloys with perpendicular magnetic anisotropy, Applied Physics Letters 93 (2008) Nr. 15, S. 153112/1-3.
215) A. Malachias, Y. Mei, R.K. Annabattula, C. Deneke, P.R. Onck, O.G. Schmidt, Wrinkled-up nanochannel networks: Long-Range ordering, scalability, and X-ray investigation, ACS Nano 2 (2008) Nr. 8, S. 1715-1721.
216) J. Malek, S.-L. Drechsler, U. Nitzsche, H. Rosner, H. Eschrig, Temperature-dependent optical conductivity of undoped cuprates with weak exchange, Physical Review B 78 (2008) Nr. 6, S. 60508/1-4.
217) K. Mandal, D. Pal, N. Scheerbaum, J. Lyubina, O. Gutfleisch, Magnetocaloric effect in Ni–Mn–Ga alloys, IEEE Transactions on Magnetics 11, Part 1 (2008), S. 2993-2996.
218) L. Manosa, X. Moya, A. Planes, O. Gutfleisch, J. Lyubina, M. Barrio, J.-L. Tamarit, S. Aksoy, T. Krenke, M. Acet, Effects of hydrostatic pressure on the magnetism and martensitic transition of Ni–Mn–In magnetic superelastic alloys, Applied Physics Letters 92 (2008) Nr. 1, S. 12515/1-3.
219) G. Martin, R. Kunze, B. Wall, Temperature-stable double SAW resonators, IEEE Ultrasonics, Ferroelectrics and Frequency Control 55 (2008), S. 199-207.

220) N. Mattern, A. Schoeps, U. Kuehn, J. Acker, O. Khvostikova, J. Eckert, Structural behavior of CuxZr100-x metallic glass (x = 35-70), Journal of Non-Crystalline Solids 354 (2008) Nr. 10-11, S. 1054-1060.
221) N. Mattern, M. Zinkevich, W. Loeser, G. Behr, J. Acker, Experimental and Thermodynamic Assessment of the Nb-Ni-Y System, Journal of Phase Equilibria and Diffusion 29 (2008) Nr. 2, S. 141-155.
222) K. Matuszna, V. Lukes, P. Rapta, L. Dunsch, A.J.A. Aquino, H. Lischka, On the optical properties of fluoranthenopyracylene ladder type molecule series, Synthetic Metals 157 (2007), S. 214-221.
223) I. Mazilu, A. Teresiak, J. Werner, G. Behr, C.D. Cao, W. Loeser, J. Eckert, L. Schultz, Phase diagram studies on Er2PdSi3 and ErPd2Si2 intermetallic compounds, Journal of Alloys and Compounds 454 (2008) Nr. 1-2, S. 221-227.
224) I.I. Mazin, M.D. Johannes, L. Boeri, K. Koepernik, D.J. Singh, Problems with reconciling density functional theory calculations with experiment in ferropnictides, Physical Review B 78 (2008) Nr. 8, S. 85104/1-7.
225) J. McCord, C. Hamann, R. Schaefer, L. Schultz, R. Mattheis, Nonlinear exchange coupling and magnetic domain asymmetry in ferromagnetic/IrMn thin films, Physical Review B 78 (2008) Nr. 9, S. 94419/1-8.
226) J. McCord, Y. Henry, T. Hauet, F. Montaigne, E.E. Fullerton, S. Mangin, Mechanism of chirality reversal for planar interface domain walls in exchange-coupled hard/soft magnetic bilayers, Physical Review B 78 (2008) Nr. 9, S. 94417/1-5.
227) J. McCord, R. Kaltofen, O.G. Schmidt, L. Schultz, Tuning of magnetization dynamics by ultrathin antiferromagnetic layers, Applied Physics Letters 92 (2008) Nr. 16, S. 162506/1-3.
228) J. McCord, L. Schultz, J. Fassbender, Hybrid soft-magnetic lateral exchange spring films prepared by ion irradiation, Advanced Materials 20 (2008), S. 2090-2093.
229) Y. Mei, G. Huang, A.A. Solovev, E.B. Urena, I. Moench, F. Ding, T. Reindl, R.K.Y. Fu, P.K. Chu, O.G. Schmidt, Versatile approach for integrative and functionalized tubes by strain engineering of nanomembranes on polymers, Advanced Materials 20 (2008), S. 4085-4090.
230) D. Mikhailova, H. Ehrenberg, G. Miehe, D. Trots, C. Hess, R. Schneider, H. Fuess, ScRe2O6: A new ternary oxide with metallic Re–Re-bonds and a ferromagnetic component above room temperature, Journal of Solid State Chemistry 181 (2008), S. 190-198.
231) N.S. Mitrovic, S.N. Kane, P.V. Tyagi, S. Roth, Effect of dc-Joule-heating thermal processing on magnetoimpedance of Fe72Al5Ga2P11C6B4 amorphous alloy, Journal of Magnetism and Magnetic Materials 320 (2008), S. e792-e796.
232) N. Mitrovic, S. Roth, M. Stoica, Magnetic softening of bulk amorphous FeCrMoGaPCB rods by current annealing technique, Journal of Alloys and Compounds 434-435 (2007), S. 618-622.
233) A. Moebius, Indications for sharp continuous phase transitions at finite temperatures connected with the apparent metal-insulator transition in two-dimensional disordered systems, Physical Review B 77 (2008) Nr. 20, S. 205317/1-9.
234) L. Molina, S. Engel, K. Knoth, R. Huehne, B. Holzapfel, O. Eibl, Grain growth and biaxial texture of chemically deposited La2Zr2O7 buffer layers for YBCO-coated conductors, Journal of Physics: Conference Series 97 (2008) Nr. 1, S. 12108/1-6.
235) O.V. Molodtsova, M. Knupfer, V.Y. Aristov, D.V. Vyalikh, V.M. Zhilin, Y.A. Ossipyan, The unoccupied electronic structure of potassium doped copper phthalocyanine studied by near edge absorption fine structure, Journal of Applied Physics 103 (2008) Nr. 5, S. 53711/1-5.
236) O.V. Molodtsova, M. Knupfer, V.V. Maslyuk, D.V. Vyalikh, V.M. Zhilin, Y.A. Ossipyan, T. Bredow, I. Mertig, V.Y. Aristov, Unoccupied electronic states in an organic semiconductor probed with x-ray spectroscopy and first-principles calculations, The Journal of Chemical Physics 129 (2008) Nr. 15, S. 154705/1-4.
237) O.V. Molodtsova, M. Knupfer, Y.A. Ossipyan, V.Y. Aristov, Molecular orientation and ordering in CoPc and FePc thin films grown on Au(001)-5?20, Journal of Applied Physics 104 (2008) Nr. 8, S. 83704/1-5.
238) A.S. Moskvin, S.-L. Drechsler, Multiferroicity due to nonstoichiometry in the chain cuprate LiVCuO4, epl 81 (2008) Nr. 5, S. 57004/1-6.
239) A.S. Moskvin, S.-L. Drechsler, Microscopic mechanisms of spin-dependent electric polarization in 3d oxides, Physical Review B 78 (2008) Nr. 2, S. 24102/1-12.
240) T. Muehl, S. Myhra, Patterning of a-C DLC films: exploration of an aqueous electro-oxidative mechanism, Journal of Physics / D 40 (2007) Nr. 11, S. 3468-3477.
241) C. Mueller, D. Elefant, A. Leonhardt, B. Buechner, Incremental analysis of the magnetization behavior in iron-filled carbon nanotube arrays, Journal of Applied Physics 103 (2008) Nr. 3, S. 34302/1-5.
242) C. Mueller, D. Elefant, A. Leonhardt, B. Buechner, Incremental analysis of the magnetization behavior in iron-filled carbon nanotube arrays, Virtual Journal of Nanoscale Science and Technology 17 (2008) Nr. 7.
243) F.M. Muntyanu, A. Gilewski, K. Nenkov, A. Zaleski, V. Chistol, Superconducting crystallite interfaces with Tc up to 21 K in Bi and Bi-Sb bicrystals of inclination type, Solid State Communications 147 (2008), S. 183-185.
244) F. Muranyi, G. Urbanik, V. Kataev, B. Buechner, Electron spin dynamics of the superconductor CaC6 probed by ESR, Physical Review B 77 (2008) Nr. 2, S. 24507/1-5.
245) A. Narduzzo, M.S. Grbic, M. Pozek, A. Dulcic, D. Paar, A. Kondrat, C. Hess, I. Hellmann, R. Klingeler, J. Werner, A. Koehler, G. Behr, B. Buechner, Upper critical field, penetration depth, and depinning frequency of the high-temperature superconductor LaFeAsO0.9F0.1 studied by microwave surface impedance, Physical Review B 78 (2008) Nr. 1, S. 12507/1-4.

246) E.K. Nazarova, A.J. Zaleski, K.A. Nenkov, A.L. Zahariev, Intergranular flux pinning in underdoped and overdoped R1-xCaxBa2Cu3Oz (R = Y, Gd; x = 0, 0.2) samples, Physica C 468 (2008), S. 955-960.
247) A. Neudert, P.S. Keatley, V.V. Kruglyak, J. McCord, R.J. Hicken, Excitation and imaging of precessional modes in soft-magnetic squares, IEEE Transactions on Magnetics 44 (2008) Nr. 11, S. 3083-3086.
248) K. Nikolowski, N.N. Bramnik, H. Ehrenberg, Two-step process and fatigue in Li x CrMnO4 as positive electrode material for lithium ion batteries, Ionics 14 (2008) Nr. 2, S. 121-124.
249) A. Nilsson, W. Gruner, J. Acker, K. Wetzig, Critical aspects on preparation of Bi-2223 glassy precursor by melt-process, Journal of Non-Crystalline Solids 354 (2008) Nr. 10-11, S. 839-847.
250) L. Nyam-Ochir, H. Ehrenberg, A. Buchsteiner, A. Senyshyn, H. Fuess, D. Sangaa, The magnetic structures of double tungstates, NaM(WO4)2, M=Fe, Cr: Examples for superexchange couplings mediated by [NaO6]-octahedra, Journal of Magnetism and Magnetic Materials 320 (2008) Nr. 18, S. 3251-3255.
251) R.M. Oliveira, M. Ueda, B. Moreno, L. Hoshida, S. Oswald, E. Abramof, A novel process for plasma immersion ion implantation and deposition with ions from vaporization of solid targets, Physica Status Solidi C 5 (2008) Nr. 4, S. 893-896.
252) T. Ostapchuk, J. Petzelt, P. Kuzel, S. Veljko, A. Tkach, P. Vilarinho, I. Ponomareva, L. Bellaiche, E. Smirnova, V. Lemanov, A. Sotnikov, M. Weihnacht, Infrared and THz soft-mode spectroscopy of (Ba,Sr)TiO3 ceramics, Ferroelectrics 367 (2008), S. 139-148.
253) B. Oswald, K.-J. Best, M. Soell, E. Duffer, W. Gawalek, L.K. Kovalev, G. Krabbes, W. Prusseit, HTS motor program at OSWALD, present status, IEEE Transactions on Applied Superconductivity 17 (2007) Nr. 2, S. 1583-1586.
254) S. Oswald, Simulation of rough nanostructured surfaces for ARXPS, Surface Science 602 (2008), S. 291-299.
255) S. Oswald, F. Oswald, Modeling of complex surface structures for ARXPS, Surface and Interface Analysis 40 (2008), S. 700-705.
256) S. Oswald, D. Rittrich, W. Zahn, Initial growth of W-based films deposited on Si studied with ARXPS, Surface and Interface Analysis 40 (2008), S. 776-780.
257) G. Paasch, S. Scheinert, A. Herasimovich, I. Hoerselmann, T. Lindner, Characteristics and mechanisms of hysteresis in polymer field-effect transistors, Physica Status Solidi A 205 (2008) Nr. 3, S. 534-548.
258) E.S. Park, J.Y. Lee, D.H. Kim, A. Gebert, L. Schultz, Correlation between plasticity and fragility in Mg-based bulk metallic glasses with modulated heterogeneity, Journal of Applied Physics 104 (2008) Nr. 2, S. 23520/1-10.
259) J.M. Park, D.H. Kim, K.B. Kim, E. Fleury, M.H. Lee, W.T. Kim, J. Eckert, Enhancement of plasticity in Ti-rich Ti-Zr-Be-Cu-Ni-Ta bulk glassy alloy via introducing the structural inhomogeneity, Journal of Materials Research 23 (2008) Nr. 11, S. 2984-2989.
260) J.M. Park, D.H. Kim, K.B. Kim, M.H. Lee, W.T. Kim, J. Eckert, Influence of heterogeneities with different length scale on the plasticity of Fe-base ultrafine eutectic alloys, Journal of Materials Research 23 (2008) Nr. 7, S. 2003-2008.
261) J.M. Park, K.B. Kim, W.T. Kim, M.H. Lee, J. Eckert, D.H. Kim, High strength ultrafine eutectic Fe–Nb–Al composites with enhanced plasticity, Intermetallics 16 (2008) Nr. 5, S. 642-650.
262) J.M. Park, T.E. Kim, S.W. Sohn, D.H. Kim, K.B. Kim, W.T. Kim, J. Eckert, High strength Ni–Zr binary ultrafine eutectic-dendrite composite with large plastic deformability, Applied Physics Letters 93 (2008) Nr. 3, S. 31913/1-3.
263) J.M. Park, S.W. Sohn, D.H. Kim, K.B. Kim, W.T. Kim, J. Eckert, Propagation of shear bands and accommodation of shear strain in the Fe56Nb4Al40 ultrafine eutectic-dendrite composite, Applied Physics Letters 92 (2008) Nr. 9, S. 91910/1-3.
264) S. Pauly, J. Das, C. Duhamel, J. Eckert, Effect of titanium on microstructure and mechanical properties of Cu50Zr50- x Ti x (2.5 = x = 7.5) glass matrix composites, Metallurgical and Materials Transactions A 39 (2008) Nr. 8, S. 1868-1873.
265) V. Pavlyuk, G. Dmytriv, I. Tarasiuk, H. Pauly, H. Ehrenberg, Li8Cu12+xAl6-x (x = 1.16): a new structure type related to Laves phases, Acta Crystallographica C 64 (2008), S. i15-i17.
266) L. Peng, C. Cai, C. Chen, Z. Liu, R. Huehne, B. Holzapfel, Angular-dependent vortex pinning mechanism in YBa2Cu3O7-/YSZ quasi-multilayer, Journal of Applied Physics 104 (2008) Nr. 3, S. 33920/1-5.
267) A. Petr, D. Wei, C. Kvarnstroem, A. Ivaska, L. Dunsch, pi-dimer of an aniline dimer: An ESR-UV-Vis spectroelectrochemical study, The Journal of Physical Chemistry B 111 (2007) Nr. 43, S. 12395-12398.
268) R. Pfeiffer, H. Peterlik, H. Kuzmany, F. Simon, K. Pressl, P. Knoll, M.H. Ruemmeli, H. Shiozawa, H. Muramatsu, Y.A. Kim, T. Hayashi, M. Endo, A detailed comparison of CVD grown and precursor based DWCNTs, Physica Status Solidi B 245 (2008) Nr. 10, S. 1943-1946.
269) T. Pichler, C. Kramberger, P. Ayala, H. Shiozawa, M. Knupfer, M.H. Ruemmeli, D. Batcherlor, R. Kitaura, N. Imazu, K. Kobayashi, H. Shinohara, Bonding environment and electronic structure of Gd metallofullerene and Gd nanowire filled single-wall carbon nanotubes, Physica Status Solidi B 245 (2008) Nr. 10, S. 2038-2041.
270) T. Pieczonka, T. Schubert, S. Baunack, B. Kieback, Dimensional behaviour of aluminium sintered in different atmospheres, Materials Science and Engineering A 478 (2008) Nr. 1-2, S. 251-256.
271) P. Pieta, A. Petr, W. Kutner, L. Dunsch, In situ ESR spectroscopic evidence of the spin-trapped superoxide radical, O2-, electrochemically generated in DMSO at room temperature, Electrochimica Acta 53 (2008) Nr. 8, S. 3412-3415.
272) D. Placha, G.S. Martynkova, M.H. Ruemmeli, Preparation of organovermiculites using HDTMA: Structure and sorptive properties using naphthalene, Journal of Colloid and Interface Science 327 (2008) Nr. 2, S. 341-347.

273) M. Pletea, H. Wendrock, R. Kaltofen, O.G. Schmidt, R. Koch, Stress evolution during and after sputter deposition of thin Cu–Al alloy films, Journal of Physics / Condensed Matter 20 (2008) Nr. 25, S. 255215/1-6.

274) Y. Plevachuk, V. Sklyarchuk, R. Hermann, G. Gerbeth, Thermophysical properties of Nd-, Er-, YNi-alloys, International Journal of Materials Research (Zeitschrift fuer Metallkunde) 99 (2008) Nr. 3, S. 261-264.

275) A. Podlesnyak, M. Russina, A. Furrer, A. Alfonsov, E. Vavilova, V. Kataev, B. Buechner, T. Straessle, E. Pomjakushina, K. Conder, D.I. Khomskii, Spin-state polarons in lightly-hole-doped LaCoO3, Physical Review Letters 101 (2008) Nr. 24, S. 247603/1-4.

276) A.A. Popov, I.E. Kareev, N.B. Shustova, S.F. Lebedkin, S.H. Strauss, O.V. Boltalina, L. Dunsch, Synthesis, spectroscopic and electrochemical characterization, and DFT study of Seventeen C-70(CF3)(n) derivatives (n=2, 4, 6, 8, 10, 12), Chemistry - A European Journal 14 (2008) Nr. 1, S. 107-121.

277) A.A. Popov, N.B. Shustova, O.V. Boltalina, S.H. Strauss, L. Dunsch, ESR-Vis/NIR spectroelectrochemical study of C-70(CF3)(2)(-center dot) and C-70(C2F5)2(-center dot) radical anions, ChemPhysChem 9 (2008) Nr. 3, S. 431-438.

278) A.A. Popov, M. Krause, S. Yang, J. Wong, L. Dunsch, C-78 cage isomerism defined by trimetallic nitride cluster size: A computational and vibrational spectroscopic study, The Journal of Physical Chemistry B 111 (2007) Nr. 13, S. 3363-3369.

279) A.A. Popov, I.E. Kareev, N.B. Shustova, E.B. Stukalin, S.F. Lebedkin, K. Seppelt, S.H. Strauss, O.V. Boltalina, L. Dunsch, Electrochemical, spectroscopic, and DFT study of C-60(CF3)(n) frontier orbitals (n=2-18): The link between double bonds in pentagons and reduction potentials, Journal of the American Chemical Society 129 (2007) Nr. 37, S. 11551-11568.

280) A.A. Popov, L. Dunsch, Structure, stability, and cluster-cage interactions in nitride clusterfullerenes M3N@C-2n (M = Sc, Y; 2n=68-98): a density functional theory study, Journal of the American Chemical Society 129 (2007) Nr. 38, S. 11835-11849.

281) E.A. Popova, N. Tristan, A.N. Vasiliev, V.L. Temerov, L.N. Bezmaternykh, N. Leps, B. Buechner, R. Klingeler, Magnetization and specific heat of DyFe3(BO3)4 single crystal, The European Physical Journal B 62 (2008), S. 123-128.

282) U. Queitsch, E. Mohn, A. Blueher, B. Katzschner, M. Mertig, L. Schultz, B. Rellinghaus, Regular arrangement of gas phase prepared in-flight annealed FePt nanoparticles on S layers, IEEE Transactions on Magnetics 44 (2008) Nr. 11, S. 2756-2759.

283) U. Queitsch, D. Pohl, A. Blueher, M. Mertig, L. Schultz, B. Rellinghaus, Magnetic field induced improvement of the arrangement of nanomagnets from the gas phase on S layers, Journal of Physics / D 41 (2008) Nr. 13, S. 134019/1-5.

284) N. Qureshi, H. Fuess, H. Ehrenberg, T.C. Hansen, C. Ritter, P. Adelmann, C. Meingast, T. Wolf, Q. Zhang, W. Knafo, The magnetic composition–temperature phase diagram of the kagome mixed system (CoxNi1-x)3V2O8, Journal of Physics: Condensed Matter 20 (2008) Nr. 9, S. 95219/1-5.

285) N. Qureshi, H. Fuess, H. Ehrenberg, B. Ouladdiaf, J. Rodriguez-Carvajal, T.C. Hansen, T. Wolf, C. Meingast, Q. Zhang, W. Knafo, H. von Loehneysen, Magnetic structure of the kagome mixed compound (Co0.5Ni0.5)3V2O8 , Journal of Physics / Condensed Matter 20 (2008) Nr. 23, S. 235228/1-6.

286) K. Ramesh Kumar, N. Harish Kumar, G. Markandeyulu, J. Arout Chelvane, V. Neu, P.D. Babu, Structural, magnetic and transport properties of half-metallic ferrimagnet Mn2VGa, Journal of Magnetism and Magnetic Materials 320 (2008), S. 2737-2740.

287) P. Rapta, A. Tabet, H. Hartmann, L. Dunsch, New molecular materials for hole injection: the synthesis and in situ ESR-UV/Vis/NIR spectroelectrochemistry of 2-diarylaminothiophenebased starburst compounds, Journal of Materials Chemistry 17 (2007) Nr. 47, S. 4998-5007.

288) A. Rastelli, M. Stoffel, A. Malachias, T. Merdzhanova, G. Katsaros, K. Kern, T.H. Metzger, O.G. Schmidt, Three-dimensional composition profiles of single quantum dots determined by scanning-probe-microscopy-based nanotomography, Nanoletters 8 (2008) Nr. 5, S. 1404-1409.

289) A. Rastelli, M. Stoffel, T. Merdzhanova, O.G. Schmidt, Intermixing and composition profiles of strained SiGe islands on Si(001), Journal of Physics / Condensed Matter 20 (2008) Nr. 45, S. 454214/1-7.

290) A.D. Rata, A. Herklotz, K. Nenkov, L. Schultz, K. Doerr, Strain-induced insulator state and giant gauge factor of La0.7Sr0.3CoO3 films, Physical Review Letters 100 (2008) Nr. 7, S. 76401/1-4.

291) S. Rivoirard, J. Lyubina, E. Beaugnon, O. Gutfleisch, Magnetic field effect on the hydrogen desorption and recombination reaction in disproportionated Sm–Co-type alloys, Applied Physics Letters 93 (2008) Nr. 17, S. 172509/1-3.

292) D.T. Robb, Y.H. Xu, O. Hellwig, J. McCord, A. Berger, M.A. Novotny, P.A. Rikvold, Evidence for a dynamic phase transition in [Co/Pt]3 magnetic multilayers, Physical Review B 78 (2008) Nr. 13, S. 134422/1-11.

293) U.K. Roessler, A.N. Bogdanov, The structure of supercooled liquids and glasses as Skyrmionic texture, Journal of Non-Crystalline Solids 354 (2008) Nr. 35-39, S. 4198-4201.

294) H. Rosner, M.D. Johannes, S.-L. Drechsler, M. Schmitt, O. Janson, W. Schnelle, W. Liu, Y.-X. Huang, R. Kniep, Cu II materials—From crystal chemistry to magnetic model compounds, Science and Technology of Advanced Materials 8 (2007) Nr. 5, S. 352-356.

295) F. Roth, A. Koenig, R. Kraus, M. Knupfer, Potassium induced phase transition of FePc thin films, The Journal of Chemical Physics 128 (2008) Nr. 19, S. 194711/1-4.

296) S. Roth, U. Gaitzsch, M. Poetschke, L. Schultz, Magneto-mechanical behaviour of textured polycrystals of NiMnGa ferromagnetic shape memory alloys, Advanced Materials Research 52 (2008), S. 29-34.

297) M.H. Ruemmeli, F. Schaeffel, T. de los Arcos, D. Haberer, A. Bachmatiuk, C. Kramberger, P. Ayala, E. Borowiak-Palen, D. Adebimpe, T. Gemming, A. Leonhardt, B. Rellinghaus, L. Schultz, T. Pichler, B. Buechner, On the graphitisation role of oxide supports in carbon nanotube CVD synthesis, Physica Status Solidi B 245 (2008) Nr. 10, S. 1939-1942.

298) M.H. Ruemmeli, F. Schaeffel, M. Loeffler, C. Kramberger, D. Adebimpe, T. Gemming, P. Ayala, B. Rellinghaus, L. Schultz, B. Buechner, T. Pichler, Unifying catalyst size dependencies in floating catalyst and supported catalyst carbon nanotube synthesis, Physica Status Solidi A 205 (2008) Nr. 6, S. 1386-1390.

299) A. Rusydi, R. Rauer, G. Neuber, M. Bastjan, I. Mahns, S. Mueller, P. Saichu, B. Schulz, S.G. Singer, A.I. Lichtenstein, D. Qi, X. Gao, X. Yu, A.T.S. Wee, G. Stryganyuk, K. Doerr, G.A. Sawatzky, S.L. Cooper, M. Ruebhausen, Metal-insulator transition in manganites: Changes in optical conductivity up to 22 eV, Physical Review B 78 (2008) Nr. 12, S. 125110/1-5.

300) A. Sachse, G. Noel, S. Dechert, S. Demeshko, A. Honecker, A. Alfonsov, V. Kataev, F. Meyer, Bulky pyrazolate-based compartmental ligand scaffolds: Encapsulation of an edge-sharing Cu6O2 bitetrahedral core, European Journal of Inorganic Chemistry (2008) Nr. 34, S. 5390-5396.

301) E.V. Sampathkumaran, N. Mohapatra, K.K. Iyer, C.D. Cao, W. Loeser, G. Behr, Magnetic anomalies in single crystalline ErPd2Si2, Journal of Magnetism and Magnetic Materials 320 (2008), S. 1549-1552.

302) M. Samsel-Czekala, E. Talik, R. Troc, Electronic structure, magnetic, and electrical properties of single-crystalline magnetic fluctuator URuAl and comparison with reference systems, Physical Review B 78 (2008) Nr. 24, S. 245120/1-11.

303) M. Samsel-Czekala, E. Talik, R. Troc, J. Stepien-Damm, Electronic structure and bulk properties of the single-crystalline paramagnet URuGa, Physical Review B 77 (2008) Nr. 15, S. 155113/1-11.

304) V.S. Sarma, J. Eickemeyer, L. Schultz, B. Holzapfel, Rolling and recrystallisation textures in Cu–Al, Cu–Mn and Cu–Ni alloys, Journal of Materials Science 42 (2007) Nr. 17, S. 7586-7591.

305) F. Schaeffel, M.H. Ruemmeli, C. Kramberger, U. Queitsch, E. Mohn, R. Kaltofen, T. Pichler, B. Buechner, B. Rellinghaus, L. Schultz, Tailoring the diameter, density and number of walls of carbon nanotubes through predefined catalyst particles, Physica Status Solidi A 205 (2008) Nr. 6, S. 1382-1385.

306) F. Schaeffel, C. Schuenemann, M.H. Ruemmeli, C. Taeschner, D. Pohl, C. Kramberger, T. Gemming, A. Leonhardt, T. Pichler, B. Rellinghaus, B. Buechner, L. Schultz, Comparative study on thermal and plasma enhanced CVD grown carbon nanotubes from gas phase prepared elemental and binary catalyst particles, Physica Status Solidi B 245 (2008) Nr. 10, S. 1919-1922.

307) N. Scheerbaum, O. Heczko, J. Liu, D. Hinz, L. Schultz, O. Gutfleisch, Magnetic field-induced twin boundary motion in polycrystalline Ni–Mn–Ga fibres, New Journal of Physics 10 (2008), S. 73002/1-8.

308) R. Schmidt-Grund, B. Rheinlaender, E.M. Kaidashev, M. Lorenz, M. Grundmann, D. Fritsch, M.M. Schubert, H. Schmidt, C.M. Herzinger, Vacuum ultraviolet dielectric function and band structure of ZnO, Journal of the Korean Physical Society 53 (2008) Nr. 1, S. 88-93.

309) M. Schneider, A. Gladun, A. Kreyssig, J. Wosnitza, V. Petzold, H. Rosner, G. Behr, D. Souptel, K.-H. Mueller, S.-L. Drechsler, G. Fuchs, Heat and charge transport in YNi2B2C and HoNi2B2C single crystals, Journal of Physics / Condensed Matter 20 (2008) Nr. 17, S. 175221/1-7.

310) M. Schubert, W. Haessler, C. Rodig, M. Herrmann, K. Schroeder, B. Holzapfel, L. Schultz, Electron microscopic and metallographical investigations on superconducting MgB2 tapes with mechanically alloyed precursor powder, Praktische Metallographie 44 (2007) Nr. 12, S. 566-578.

311) B. Schwarz, H. Ehrenberg, H. Weitzel, A. Senyshyn, B. Thybusch, M. Knapp, G.J. McIntyre, H. Fuess, Crystal chemistry, structure and magnetic properties of the Cu(MoxW1-x)O4 solid solution series, Philosophical Magazine 88 (2008) Nr. 8, S. 1235-1258.

312) S. Scudino, M. Sakaliyska, M. Stoica, K.B. Surreddi, F. Ali, G. Vaughan, A.R. Yavari, J. Eckert, In-situ X-ray diffraction of mechanically milled - beta-Al3Mg2 powders, Physica Status Solidi (RRL) - Rapid Research Letters 2 (2008) Nr. 6, S. 272-274.

313) S. Scudino, D.J. Sordelet, J. Eckert, Devitrification of mechanically alloyed Zr-Ti-Nb-Cu-Ni-Al glassy powders studied by time-resolved X-ray diffraction, Reviews on Advanced Materials Science 18 (2008) Nr. 2, S. 221-224.

314) S. Scudino, S. Sperling, M. Sakaliyska, C. Thomas, M. Feuerbacher, K.B. Kim, H. Ehrenberg, J. Eckert, Phase transformations in mechanically milled and annealed single-phase beta-Al3Mg2, Acta Materialia 56 (2008) Nr. 5, S. 1136-1143.

315) S. Scudino, K.B. Surreddi, S. Sager, M. Sakaliyska, J.S. Kim, W. Loeser, J. Eckert, Production and mechanical properties of metallic glass-reinforced Al-based metal matrix composites, Journal of Materials Science 43 (2008) Nr. 13, S. 4518-4526.

316) S. Scudino, S. Venkataraman, J. Eckert, Thermal stability, microstructure and crystallization kinetics of melt-spun Zr-Ti-Cu-Ni metallic glass, Journal of Alloys and Compounds 460 (2008), S. 263-267.

317) S. Scudino, S. Venkataraman, M. Sakaliyska, J. Eckert, Crystallization behavior and consolidation of ball milled Zr60Ti5Ag5Cu12.5Ni10Al7.5 glassy powders, Journal of Alloys and Compounds 456 (2008) Nr. 1-2, S. 159-162.

318) A. Sebetci, Cobalt clusters (Con, n=6) and their anions, Chemical Physics 354 (2008), S. 196-201.

319) A. Sebetci, E. Mete, I. Boustani, Free standing double walled boron nanotubes, Journal of Physics and Chemistry of Solids 69 (2008) Nr. 8, S. 2004-2012.

320) D. Selbmann, B. Bendjemil, A. Leonhardt, T. Pichler, C. Taeschner, M. Ritschel, A parametric study of the synthesis and purification of single-walled carbon nanotubes using the high-pressure carbon monoxide proces, Applied Physics A 90 (2008) Nr. 4, S. 637-643.

321) T. Shapoval, S. Engel, M. Gruendlich, D. Meier, E. Backen, V. Neu, B. Holzapfel, L. Schultz, Nanoscale wedge polishing of superconducting thin films—an easy way to obtain depth dependent information by surface analysis techniques, Superconductor Science and Technology 21 (2008) Nr. 10, S. 105015/1-6.

322) V. Shatrov, G. Gerbeth, R. Hermann, An alternating magnetic field driven flow in a spinning cylindrical container, Journal of Fluids Engineering (ASME) 130 (2008) Nr. July, S. 71201/1-10.

323) V. Shatrov, G. Gerbeth, R. Hermann, Linear stability of an alternating-magnetic-field-driven flow in a spinning cylindrical container, Physical Review E 77 (2008) Nr. 4, S. 46307/1-11.

324) H. Shiozawa, T. Pichler, A. Grueneis, R. Pfeiffer, H. Kuzmany, Z. Liu, K. Suenaga, H. Kataura, A catalytic reaction inside a single-walled carbon nanotube, Advanced Materials 20 (2008) Nr. 8, S. 1443-1449.

325) H. Shiozawa, T. Pichler, C. Kramberger, A. Grueneis, M. Knupfer, B. Buechner, V. Zolyomi, J. Koltai, J. Kuerti, D. Batchelor, H. Kataura, Fine tuning the charge transfer in carbon nanotubes via the interconversion of encapsulated molecules, Physical Review B 77 (2008) Nr. 15, S. 153402/1-4.

326) T. Shirakawa, S. Nishimoto, Y. Ohta, Superconductivity in a model of two Hubbard chains coupled with ferromagnetic exchange interaction, Physical Review B 77 (2008) Nr. 22, S. 224510/1-10.

327) F. Simon, M. Galambos, D. Quintavalle, B. Nafradi, L. Forro, J. Koltai, V. Zolyomi, J. Kuerti, N.M. Nemes, M.H. Ruemmeli, H. Kuzmany, T. Pichler, Electron spin resonance in alkali doped SWCNTs, Physica Status Solidi B 245 (2008) Nr. 10, S. 1975-1978.

328) A. Singh, V. Neu, S. Faehler, K. Nenkov, L. Schultz, B. Holzapfel, Mechanism of coercivity in epitaxial SmCo5 thin films, Physical Review B 77 (2008) Nr. 10, S. 104443/1-6.

329) E.P. Smirnova, A.V. Sotnikov, S.I. Smirnov, M. Weihnacht, Ferroelastic transition and the relaxor state in SrTiO3-PbMg1/3Nb2/3O3, Physics of the Solid State 50 (2008) Nr. 11, S. 2145-2149.

330) E.P. Smirnova, A.V. Sotnikov, N.V. Zaitseva, M. Weihnacht, V.V. Lemanov, Relaxor behavior of SrTiO3-LiNbO3 solid solutions, Physics of the Solid State 50 (2008) Nr. 1, S. 122-125.

331) Z. Sniadecki, B. Idzikowski, J.-M. Greneche, P. Kerschl, U.K. Roessler, L. Schultz, Independence of magnetic behavior for different structural states in melt-spun DyMn6-xGe6-xFexAlx (0=x=6), Journal of Physics / Condensed Matter 20 (2008) Nr. 42, S. 425212/1-6.

332) J. Sort, N. Van Steenberge, A. Gimazov, A. Concustell, S. Surinach, A. Gebert, J. Eckert, M.D. Baro, Study of the mechanical behaviour of a Zr-based metallic glass rod using micro- and nano-indentation, The Open Materials Science Journal 2 (2008), S. 1-5.

333) D. Souptel, G. Behr, W. Loeser, A. Teresiak, Effect of B and C concentration on crystallization and properties of HoNi2B2C, Journal of Alloys and Compounds 455 (2008) Nr. 1-2, S. 60-66.

334) Y.I. Spichkin, A.V. Derkach, A.M. Tishin, M.D. Kuzmin, A.S. Chernyshov, jr. K.A. Gschneidner, V.K. Pecharsky, Thermodynamic features of magnetization and magnetocaloric effect near the magnetic ordering temperature of Gd, Journal of Magnetism and Magnetic Materials 316 (2007), S. e555-e557.

335) M. Spindler, S.B. Menzel, C. Eggs, J. Thomas, T. Gemming, J. Eckert, TEM investigation of Ti and Ti/Al bilayer as alternative diffusion barriers for Cu metallization for SAW device applications, Microelectronic Engineering 85 (2008) Nr. 10, S. 2055-2058.

336) M. Stangl, M. Liptak, A. Fletcher, J. Acker, J. Thomas, H. Wendrock, S. Oswald, K. Wetzig, Influence of initial microstructure and impurities on Cu room-temperature recrystallization (self-annealing), Microelectronic Engineering 85 (2008) Nr. 3, S. 534-541.

337) M. Stangl, M. Militzer, Modeling self-annealing kinetics in electroplated Cu thin films, Journal of Applied Physics 103 (2008) Nr. 11, S. 113521/1-7.

338) M. Stoffel, A. Malachias, T. Merdzhanova, F. Cavallo, G. Isella, D. Chrastina, H. von Kaenel, A. Rastelli, O.G. Schmidt, SiGe wet chemical etchants with high compositional selectivity and low strain sensitivity, Semiconductor Science and Technology 23 (2008) Nr. 8, S. 85021/1-6.

339) M. Stoica, J. Das, J. Bednarcik, H. Franz, N. Mattern, W.H. Wang, J. Eckert, Strain distribution in Zr64.13Cu15.75Ni10.12Al10 bulk metallic glass investigated by in situ tensile tests under synchrotron radiation, Journal of Applied Physics 104 (2008) Nr. 1, S. 13522/1-7.

340) M. Stoica, K. Hajlaoui, J. Das, J. Eckert, A.R. Yavari, FeNbB bulk metallic glass with high boron content, Reviews on Advanced Materials Science 18 (2008) Nr. 1, S. 61-65.

341) M. Taut, Jahn–Teller distortion of the Wigner molecule in a three-electron quantum dot and a magnetic field, Physica E 40 (2008) Nr. 5, S. 1062-1064.

342) A. Taylor, K. Kraemer, S. Hampel, S. Fuessel, R. Klingeler, M. Ritschel, B. Buechner, M.O. Grimm, M.P. Wirth, Carbon coated nanomagnets as potential hyperthermia agents, The Journal of Urology 179 (2008) Nr. 4, Supplement, S. 392-393.

343) M. Tekielak, P. Mazalski, A. Maziewski, R. Schaefer, J. McCord, B. Szymanski, M. Urbaniak, F. Stobiecki, Creation of out-of-plane magnetization ordering by increasing the repetitions number n in (Co/Au) n multilayers, IEEE Transactions on Magnetics 44 (2008) Nr. 11, S. 2850-2853.

344) I.S. Tereshina, N.L. Korenovskii, G.S. Burkhanov, M.D. Kuzmin, K.P. Skokov, J.J. Melero, Spin-reorientation transition in TbCo5, Journal of Experimental and Theoretical Physics 105 (2007) Nr. 6, S. 1230-1235.

345) K. Theis-Broehl, A. Westphalen, H. Zabel, U. Ruecker, J. McCord, V. Hoeink, J. Schmalhorst, G. Reiss, T. Weis, D. Engel, A. Ehresmann, B.P. Toperverg, Hyper-domains in exchange bias micro-stripe pattern, New Journal of Physics 10 (2008), S. 93021/1-21.

346) M. Thomas, O. Heczko, J. Buschbeck, U.K. Roessler, J. McCord, N. Scheerbaum, L. Schultz, S. Faehler, Magnetically induced reorientation of martensite variants in constrained epitaxial Ni–Mn–Ga films grown on MgO(001), New Journal of Physics 10 (2008), S. 23040/ 1-20.

347) M. Thomas, O. Heczko, J. Buschbeck, L. Schultz, S. Faehler, Stress induced martensite in epitaxial Ni–Mn–Ga films deposited on MgO(001), Applied Physics Letters 92 (2008) Nr. 19, S. 192515/1-3.

348) D.J. Thurmer, C. Deneke, O.G. Schmidt, In situ monitoring of the complex rolling behaviour of InGaAs/GaAs/Nb hybrid micro-tubes, Journal of Physics / D 41 (2008) Nr. 20, S. 205419/1-5.

349) J. Torrens-Serra, S. Roth, J. Rodriguez-Viejo, M.T. Clavaguera-Mora, Effect of Nb in the nanocrystallization and magnetic properties of FeNbBCu amorphous alloys, Journal of Non-Crystalline Solids 354 (2008) Nr. 47-51, S. 5110-5112.

350) J. Torrens-Serra, S. Roth, J. Rodriguez-Viejo, M.T. Clavaguera-Mora, Structure and thermomagnetic properties of powders produced from melt spun FeNbBCu ribbons, Journal of Non-Crystalline Solids 354 (2008), S. 3858-3863.

351) J.M. Tranquada, G.D. Gu, M. Huecker, Q. Jie, H.-J. Kang, R. Klingeler, Q. Li, N. Tristan, J.S. Wen, G.Y. Xu, Z.J. Xu, J. Zhou, M. von Zimmermann, Evidence for unusual superconducting correlations coexisting with stripe order in La1.875Ba0.125CuO4, Physical Review B 78 (2008) Nr. 17, S. 174529/1-13.

352) N. Tristan, V. Zestrea, G. Behr, R. Klingeler, B. Buechner, H.A. Krug von Nidda, A. Loidl, V. Tsurkan, Spin frustration and magnetic exchange in cobalt aluminum oxide spinels, Physical Review B 77 (2008) Nr. 9, S. 94412/1-10.

353) D. Tzankov, V. Skumryev, M. Aroyo, R. Puzniak, M.D. Kuzmin, M. Mikhov, Magnetic anisotropy of multiferroic HoMn2O5 single crystal, Solid State Communications 147 (2008) Nr. 5-6, S. 212-216.

354) N. Van Steenberge, A. Concustell, J. Sort, J. Das, N. Mattern, A. Gebert, S. Surinach, J. Eckert, M.D. Baro, Microstructural inhomogeneities introduced in a Zr-based bulk metallic glass upon low-temperature annealing, Materials Science and Engineering A 491 (2008) Nr. 1-2, S. 124-130.

355) A.N. Vasiliev, O.S. Volkova, L.S. Lobanovskii, I.O. Troyanchuk, Z. Hu, L.H. Tjeng, D.I. Khomskii, H.-J. Lin, C.T. Chen, N. Tristan, F. Kretzschmar, R. Klingeler, B. Buechner, Valence states and metamagnetic phase transition in partially B-site-disordered perovskite EuMn0.5Co0.5O3, Physical Review B 77 (2008) Nr. 10, S. 104442/1-5.

356) S. Venkataraman, H. Hermann, D.J. Sordelet, J. Eckert, Influence of sub-Tg annealing on the crystallization kinetics of Cu47Ti33Zr11Ni8Si1 metallic glass, Journal of Applied Physics 104 (2008) Nr. 6, S. 66107/1-3.

357) H. Vinzelberg, J. Schumann, D. Elefant, E. Arushanov, O.G. Schmidt, Transport and magnetic properties of Fe3Si epitaxial films, Journal of Applied Physics 104 (2008) Nr. 9, S. 93707/1-6.

358) H. Vinzelberg, J. Schumann, D. Elefant, R.B. Gangineni, J. Thomas, B. Buechner, Low temperature tunneling magnetoresistance on (La,Sr)MnO3/Co junctions with organic spacer layers, Virtual Journal of Nanoscale Science and Technology 17 (2008) Nr. 21.

359) H. Vinzelberg, J. Schumann, D. Elefant, R.B. Gangineni, J. Thomas, B. Buechner, Low temperature tunneling magnetoresistance on (La,Sr)MnO3/Co junctions with organic spacer layers, Journal of Applied Physics 103 (2008) Nr. 9, S. 93720/1-5.

360) A. Vyalikh, A. Wolter, S. Hampel, D. Haase, M. Ritschel, A. Leonhardt, H.-J. Grafe, A. Taylor, K. Kraemer, B. Buechner, R. Klingeler, A carbon-wrapped nanoscaled thermometer for temperature control in biological environments, Nanomedicine 3 (2008) Nr. 3, S. 321-327.

361) A. Vyalikh, T. Emmler, I. Shenderovich, Y. Zeng, G.H. Findenegg, G. Buntkowsky, 2H-solid state NMR and DSC study of isobutyric acid in mesoporous silica materials, Physical Chemistry Chemical Physics 9 (2007), S. 2249-2257.

362) J. Walowski, M. Djordjevic Kaufmann, B. Lenk, C. Hamann, J. McCord, M. Muenzenberg, Intrinsic and non-local Gilbert damping in polycrystalline nickel studied by Ti : sapphire laser fs spectroscopy, Journal of Physics / D 41 (2008) Nr. 16, S. 164016/1-10.

363) A. Walther, D. Givord, N.M. Dempsey, K. Khlopkov, O. Gutfleisch, Structural, magnetic, and mechanical properties of 5 μm thick SmCo films suitable for use in microelectromechanical systems, Journal of Applied Physics 103 (2008) Nr. 4, S. 43911/1-5.

364) L. Wang, A. Rastelli, S. Kiravittaya, P. Atkinson, F. Ding, C.C. Bof Bufon, C. Hermannstaedter, M. Witzany, G.J. Beirne, P. Michler, O.G. Schmidt, Towards deterministically controlled InGaAs/GaAs lateral quantum dot molecules, New Journal of Physics 10 (2008) Nr. 4, S. 45010.

365) W.-M. Wang, A. Gebert, S. Roth, U. Kuehn, L. Schultz, Effect of Si on the glass-forming ability, thermal stability and magnetic properties of Fe–Co–Zr–Mo–W–B alloys, Journal of Alloys and Compounds 459 (2008), S. 203-208.

366) W.-M. Wang, A. Gebert, S. Roth, U. Kuehn, L. Schultz, Glass formability and fragility of Fe61Co9-xZr8Mo5WxB17 (x = 0 and 2) bulk metallic glassy alloys, Intermetallics 16 (2008) Nr. 2, S. 267-272.

367) D. Wei, A. Petr, C. Kvarnstroem, L. Dunsch, A. Ivaska, Charge carrier transport and optical properties of poly[N-methyl(aniline)], The Journal of Physical Chemistry C 111 (2007) Nr. 44, S. 16571-16576.

368) W. Weinreich, J. Acker, I. Graeber, Determination of total fluoride in HF/HNO3/H2SiF6 etch solutions by new potentiometric titration methods, Talanta 71 (2007) Nr. 5, S. 1901-1905.

369) S. Widuch, Z. Celinski, K. Balin, R. Schaefer, L. Schultz, D. Skrzypek, J. McCord, Variation in ferromagnetic domain density and domain asymmetry in Fe/FeF2 exchange bias structures, Physical Review B 77 (2008) Nr. 18, S. 184433/1-6.

370) F. Wolny, U. Weissker, T. Muehl, A. Leonhardt, S. Menzel, A. Winkler, B. Buechner, Iron-filled carbon nanotubes as probes for magnetic force microscopy, Journal of Applied Physics 104 (2008) Nr. 6, S. 64908/1-5.

371) T.G. Woodcock, O. Shuleshova, B. Gehrmann, W. Loeser, Microstructural transitions in commercial Fe-Ni–Based soft-magnetic alloys quenched from undercooled liquid droplets, Metallurgical and Materials Transactions A 39 (2008) Nr. 12, S. 2906-2913.

372) F.-F. Wu, Z.-F. Zhang, B.-L. Shen, S.X.-Y. Mao, J. Eckert, Size effect on shear fracture and fragmentation of a Fe57.6Co14.4B19.2Si4.8Nb4 bulk metallic glass, Advanced Engineering Materials 10 (2008) Nr. 8, S. 727-730.

373) A. Yan, K.-H. Mueller, O. Gutfleisch, Magnetocaloric effect in LaFe11.8-xCoxSi1.2 melt-spun ribbons, Journal of Alloys and Compounds 450 (2008) Nr. 1-2, S. 18-21.

374) S. Yang, A.A. Popov, L. Dunsch, The role of an asymmetric nitride cluster on a fullerene cage: The Non-IPR endohedral DySC2N@C-76, The Journal of Physical Chemistry B 111 (2007) Nr. 49, S. 13659-13663.

375) X. Yang, K. Eckert, A. Heinze, M. Uhlemann, The concentration field during transient natural convection between vertical electrodes in a small-aspect-ratio cell, Journal of Electroanalytical Chemistry 613 (2008) Nr. 1, S. 97-107.

376) X. Yang, K. Eckert, K. Seidel, M. Uhlemann, The start-up of natural convection during copper electrolysis in the presence of an opposing Lorentz force, Electrochimica Acta 54 (2008), S. 352-359.

377) K. Zagorodniy, D. Chumakov, C. Taeschner, A. Lukowiak, H. Stegmann, D. Schmeisser, H. Geisler, H.-J. Engelmann, H. Hermann, E. Zschech, Novel carbon-cage-based ultralow- k materials: Modeling and first experiments, IEEE Transactions on Semiconductor Manufacturing 21 (2008) Nr. 4, S. 646-660.

378) K. Zagorodniy, H. Hermann, M. Taut, G. Seifert, E. Zschech, Structure analysis and property improvements of the computer-simulated fullerene-based ultralow-k dielectrics, Microelectronic Engineering 85 (2008), S. 2118-2122.

379) K. Zagorodniy, H. Hermann, M. Taut, Molecular design of ultralow-k insulator materials, Materials Science - Poland 25 (2007) Nr. 4, S. 1203-1211.

380) M. Zalibera, P. Rapta, L. Dunsch, In situ ESR–UV/VIS/NIR spectroelectrochemistry of an empty fullerene anion and cation: The C82:3 isomer, Electrochemistry Communications 9 (2007) Nr. 12, S. 2843-2847.

381) L.C. Zhang, M. Calin, M. Adam, J. Eckert, Crystallization kinetics and viscosity of Cu47Ti33Zr11Ni8X1 (X=Si, Sn) metallic glasses, Reviews on Advanced Materials Science 18 (2008) Nr. 5, S. 429-432.

382) S.-T. Zhang, A.B. Kounga, E. Aulbach, W. Jo, T. Granzow, H. Ehrenberg, J. Roedel, Lead-free piezoceramics with giant strain in the system Bi0.5Na0.5TiO3–BaTiO3–K0.5Na0.5NbO3. II. Temperature dependent properties, Journal of Applied Physics 103 (2008) Nr. 3, S. 34108/1-7.

383) W.Y. Zhang, M. Stoica, H.W. Chang, M. Calin, R. Schierholz, W.C. Chang, J. Eckert, The role of nonmagnetic phases in improving the magnetic properties of devitrified Pr2Fe14B-based nanocomposites, Materials Science and Engineering B 149 (2008) Nr. 1, S. 73-76.

384) W.Y. Zhang, M. Stoica, J. Eckert, H.W. Chang, W.C. Chang, H. Ehrenberg, The role of combined addition of Ti and B in magnetic hardening of devitrified Pr2Fe14B/(Fe3B,-Fe) nanocomposite magnets, Physica Status Solidi A 205 (2008) Nr. 5, S. 1207-1210.

385) W.Y. Zhang, M. Stoica, J. Eckert, P. Yu, J.Z. Jiang, Preparation of bulk Nd2Fe14B/Fe3B nanocomposite magnets with high rare earth content, Intermetallics 16 (2008) Nr. 3, S. 341-344.

386) W.Y. Zhang, B. Yang, M. Stoica, J., Shen, B.G. Shen, J. Eckert, Magnetic hardening mechanism of PrCo5-based ribbons with C addition prepared by melt spinning, International Journal of Materials Research (Zeitschrift fuer Metallkunde) 99 (2008) Nr. 1, S. 67-69.

387) C. Zhao, Y.H. Chen, B. Xu, C.G. Tang, Z.G. Wang, F. Ding, Study of the wetting layer of InAs/GaAs nanorings grown by droplet epitaxy, Applied Physics Letters 92 (2008) Nr. 6, S. 63122/1-3.

388) A.A. Zvyagin, S.-L. Drechsler, Magnetic ordering of weakly coupled frustrated quantum spin chains, Physical Review B 78 (2008) Nr. 1, S. 14429/1-6.

Contributions to Conference Proceedings and Monographs

1) S.V. Biryukov, H. Schmidt, M. Weihnacht, Ring waveguide resonator on SAW - quality factor vs electrode structure properties, 2008 IEEE International Ultrasonics Symposium, Beijing/ China, 2.-5.11.08, in: Proceedings, 6C-1 (2008).
2) S.V. Biryukov, M. Weihnacht, Zero LSAW propagation loss in a SiO2/periodic grating/LiTaO3 structure, 2008 IEEE International Ultrasonics Symposium, Beijing/ China, 2.-5.11.08, in: Proceedings, P3K100-01 (2008).
3) S.V. Biryukov, G. Martin, M. Weihnacht, Closed regular electrode structure for SAW resonators, 2007 IEEE International Frequency Control Symposium Jointly with the 21st European Frequency and Time Forum, (TimeNav'07), Genf/ Schweiz, 29.5.-1.6.07, in: Proceedings, 168-171 (2007).
4) R. Bruenig, M. Weihnacht, H. Schmidt, G. Guhr, More comprehensive model of quartz crystal microbalance response to viscoelastic loading, 2008 IEEE International Ultrasonics Symposium, Beijing/ China, 2.-5.11.08, in: Proceedings, 5C-5 (2008).
5) J. Buschbeck, L. Schultz, S. Faehler, Epitaxial Fe-Pd magnetic shape memory films - Issues for preparation and applications, Actuator 2008, 11th International Conference on New Actuators, Bremen, 9.-11.6.08, in: Proceedings, 750-753 (2008).
6) T.Y. Chemekova, A.V. Sotnikov, R. Kunze, H. Schmidt, M. Weihnacht, E.N. Mokhov, Y.N. Makarov, Investigation of SAW in sublimation aluminum nitride monocrystals, 6th All-Russian Conference "Gallium, aluminum and indium nitrides", St. Petersburg/ Russland, Juni 2008, in: Proceedings, 163-165 (2008).
7) A. Darinskii, M. Weihnacht, H. Schmidt, Acoustic waves in LiNbO3/SiO2/water/silicon rubber structures, 2008 IEEE International Ultrasonics Symposium, Beijing/ China, 2.-5.11.08, in: Proceedings, P1E070-02 (2008).
8) C. Duhamel, S. Venkataraman, S. Scudino, J. Eckert, Diffusionless transformations, in: Basics of Thermodynamics and Phase Transitions in Complex Intermetallics, Book Series on Complex Metallic Alloys, E. Bellin-Ferre (ed.), Singapur: World Scientific Publisher, 2008, Vol. 1, 119-146 (2008).
9) J. Eckert, S. Scudino, Crystallization of metallic glasses, in: Materials Processing Handbook, J.R.Groza; J.F. Schackelford; E.J. Lavernia M.T. Powers (eds.)Taylor and Francis, 2007, 6/1-27 (2007).
10) C. Edelmann, D. Klemm, V. Hoffmann, Evaluierung der Abpumpkurven einer Glimmentladungsquelle: Qualitaetskontrolle von Spektralanalysen, in: Transfer. Das Steinbeis Magazin, 9 (2008).
11) J. Eickemeyer, B. Holzapfel, Cube textured nickel-based substrates for buffer/YBCO coatings, in: YBCO Superconductor Research Progress, Liang, Li-Chun (ed.), Nova Science Publisher Inc., 2008, 93-126 (2008).
12) S. Faehler, Magnetic shape memory: Alloys achievements of the german SPP 1239, Actuator 2008, 11th International Conference on New Actuators, Bremen, 9.-11.6.08, in: Proceedings, 267-270 (2008).
13) S. Faehler, An introduction to actuation mechanisms of magnetic shape memory alloys, ECS Transactions 3 (2007) Nr. 25, S. 155-163.
14) S. Faehler, O. Heczko, M. Thomas, R. Niemann, J. Buschbeck, L. Schultz, Recent progress towards active epitaxial Ni-Mn-Ga magnetic shape memory films, Actuator 2008, 11th International Conference on New Actuators, Bremen, 9.-11.6.08, in: Proceedings, 754-757 (2008).
15) G. Guhr, R. Bruenig, M. Jaeger, R. Poll, H. Schmidt, M. Weihnacht, Akustische Thrombelastografie an Blut, 14. GMA/ ITG-Fachtagung, Ludwigsburg, 11.-12.3.08, in: Sensoren und Messsysteme 2008, VDI-Berichte 2011, 859-862 (2008).
16) G. Guhr, R. Bruenig, M. Jaeger, R. Poll, H. Schmidt, M. Weihnacht, A surface acoustic wave sensor for detection of cell adhesion, 2008 IEEE International Ultrasonics Symposium, Beijing/ China, 2.-5.11.08, in: Proceedings, P2P138-04 (2008).
17) G. Guhr, R. Bruenig, M. Jaeger, R. Poll, H. Schmidt, M. Weihnacht, Untersuchung zellulaerer Adhaesionsvorgaenge mittels akustischer Oberflaechenwellen, Dresdner Medizintechniksymposium 1.-3.12.08, in: Dresdner Beitraege zur Medizintechnik, 74-77 (2008).
18) O. Gutfleisch, N. Dempsey, High performance my-magnets for micro-electro-mechanical Systems (MEMS), in: Magnetic Nanostructures in Modern Technology, Springer-Verl., 2008, B. Azzerboni; G. Asti; L. Pareti; M. Ghidini (eds.), 167-194 (2008).
19) H. Hermann, A. Elsner, V. Kokotin, Computational optimization of multicomponent bernal`s liquids, in: Phase Transformations in Multicomponent Melts, D. M. Herlach (Ed), Weinheim: Wiley-VCH, 2008, 171-183 (2008).
20) R. Hermann, G. Gerbeth, K. Biswas, O. Filip, V. Shatrov, J. Priede, Effect of varying melt convection on microstructure evolution of Nd-Fe-B and Ti-Al peritectic alloys, in: Phase Transformations in Multicomponent Melts, D. M. Herlach (Ed), Weinheim: Wiley-VCH, 2008, 245-261 (2008).
21) L. Kavan, L. Dunsch, Electrochemistry of carbon nanotubes, Carbon Nanotubes, in: Topics in Applied Physics, Berlin: Springer-Verl., 2008, 111, 567-603 (2008).
22) M.S. Khatri, H. Schloerb, S. Faehler, L. Schultz, B. Nandan, M. Boehme, R. Krenek, M. Stamm, Electrodeposition of Co-Pt continuous films and nanowires, Euro-Interfinish Conference, Athen/ Griechenland, 18.-19.10.07, in: Proceedings, O 21 (2007).
23) J.A. Koza, M. Uhlemann, A. Gebert, S. Baunack, L. Schultz, The effect of magnetic fields on the eletrodeposition of CoFe alloys, 7th International Pamir Conference, Fundamental and Applied MHD, Presqu lle de Giens/ Frankreich, 8.-12.9.08, in: Proceedings, Vol. 1, 279-283 (2008).

24) J.A. Koza, M. Uhlemann, A. Gebert, L. Schultz, The effect of a magnetic field on the pH value in front of the electrode, 7th International pamir Conference, Fundamental and Applied MHD, Presqu lle de Giens/ Frankreich, 8.-12.9.08, in: Proceedings, Vol. 1, 339-343 (2008).

25) A. Krauze, J. Priede, R. Hermann, G. Gerbeth, Numerical modelling of the growth of small-diameter intermetallic compound crystals by a two-phase RF floating zone method, 7th PAMIR International Conference on Fundamental and Applied MHD, Giens/ Frankreich, 8.-12.9.08, in: Proceedings, 851-855 (2008).

26) K.S. Lee, H.-J. Jun, Y.W. Chang, J. Eckert, J.H. Lee, High temperature deformation and formability of Cu47.5Zr47.5Al5 bulk metallic glass, International Conference on Technology of Plasticity, Gyeongju/ Sued-Korea, 7.-11.9.08, in: Proceedings. Seoul: The Korean Society for Technology of Plasticity, CD-ROM, 570 (2008).

27) G. Martin, S.V. Biryukov, H. Schmidt, B. Steiner, B. Wall, Two-finger (TF) SPUDT cells, 2008 IEEE International Ultrasonics Symposium, Beijing/ China, 2.-5.11.08, in: Proceedings, 6C-4 (2008).

28) G. Martin, H. Schmidt, B. Wall, Improved temperature stability of one-port SAW resonators achieved without coils, 2007 IEEE International Ultrasonics Symposium, New York/ USA, 28.-31.10.07, in: Proceedings, 925-928 (2007).

29) P. Matteis, P. Russo Spena, C. Pozzi, D. Firrao, T.A. Baser, M. Baricco, J. Eckert, L. Battezzati, Fracture of Cu46.5Zr46.5Al7 and Cu46.5Zr41.5Al7Y5 bulk metallic glasss, 17th European Conference on Fracture (ECF 17). Multilevel Approach to Fracture of Materials, Components and Structures, in: Proceedings, J. Pokluda, P. Luká?, P. ?andera, I. Dlouhy, (eds.) VUTIUM Brno/ Tschechische Republik; CD-ROM, 1717 (2008).

30) J. McCord, Magnetization dynamics of coupled ferromagnetic-antiferromagnetic thin films, in: Advances in Solid State Physics, R. Haug (ed.), Springer (2008), 48, 157-168 (2008).

31) C. Mennerich, H. -H. Klauss, A. U. B. Wolter, S. Suellow, F. J. Litterst, C. Golze, R. Klingeler, V. Kataev, B. Buechner, M. Goiran, H. Rakoto, J. -M. Broto, O. Kataeva, D. J Price, High field level crossing studies on spin dimers in the low dimensional quantum spin system Na2T2(C2O4)(3)(H2O)(2) with T = Ni, Co, Fe, Mn, Pacific-Institute-of-Theoretical-Physics Summer School on Quantum Magnetism, Les Houches, France, Juni 2006, in: NATO Science for Peace and Security Series B - Physics and Biophysics, B. Barbara; Y. Imry; G. Sawatzky; P.C.E. Stamp (eds.), 97-124 (2008).

32) C. Mueller, S. Hampel, D. Haase, D. Elefant, T. Muehl, A. Vyalikh, R. Klingeler, D. Golberg, A. Leonhardt, B. Buechner, Selected synthesis methods for nanowires encapsulated inside carbon nanostructures and their fascinating properties, in: Nanorods, Nanotubes and Nanomaterials Research Progress; W. V. Prescott and A. I. Schwartz (eds.), Nova Science Publishers, 2008 (2008).

33) K.-H. Mueller, M. Schneider, G. Fuchs, S.-L. Drechsler, Rare-Earth nickel borocarbides, in: Handbook on the Physics and Chemistry of Rare Earths, K.A. Gscheidner, Jr., J.-C.G. Buenzli, V.K. Pecharsky (eds.), Elsevier, 2008, 38, 175-336 (2008).

34) O. Perroud, A. Wiedemann, M. Stoica, J. Eckert, Nanosized megnetization density profiles in hard magnetic Nd-Fe-Co-Al-glasses, in: Phase Transformations in Multicomponent Melts, D. M. Herlach (ed), Weinheim: Wiley-VCH, 2008, 263-276 (2008).

35) A. Rastelli, S. Kiravittaya, M. Benyoucef, Y.F. Mei, O.G. Schmidt, In situ tuning of optical modes in single semiconductor micro-cavities by laser heating, The 9th International Conference on Transparent Optical Networks, in: Proceedings, 3, 58-60 (2007).

36) M. Richter, K. Koepernik, H. Eschrig, Full-potential local-orbital approach to the electronic structure of solids and molecules, 43rd Karpacz Winter School of Theoretical Physics, Ladek Zdroj/ Polen, 5.-11.2.07, in: Lecture Notes of 43rd Karpacz Winter School of Theoretical Physics, 271-291 (2008).

37) M. Seifert, V. Neu, K. Nenkov, L. Schultz, Epitaxial growth, thickness and temperature dependent properties of thin SmCo5 films with perpendicular anisotropy, 20th International Workshop on Rare Earth Permanent Magnets and their Applications, Knossos/ Griechenland, 8.-10.9.08, in: Proceedings, D. Niarchos (ed.), 233-237 (2008).

38) E.P. Smirnova, A.V. Sotnikov, N.V. Zaitseva, M. Weihnacht, V.V. Lemanov, Phase transitions evolution in solid solutions on the base of strontium titanate (SrTiO3-PMN, SrTiO3-BiFeO3), 18th All-Russian Conference on Ferroelectricity, St. Petersburg/ Russland, Juni 2008, in: Proceedings (2008).

39) A. Sotnikov, H. Schmidt, K. Suschke, M. Weihnacht, M. Hengst, J. Goetze, Piezoelectric and elastic properties of SNGS and STGS single crystals at elevated temperatures, 2008 IEEE International Ultrasonics Symposium, Beijing/ China, 2.-5.11.08, in: Proceedings, P3K102-02 (2008).

40) A.V. Sotnikov, V.V. Lemanov, B.T. Melekh, M. Weihnacht, Dielectric properties of barium zirconate (BaZrO3): single crystals and ceramics, 18th All-Russian Conference on Ferroelectricity, St. Petersburg/ Russland, Juni 2008, in: Proceedings (2008).

41) A.V. Sotnikov, E.P. Smirnova, M. Weihnacht, V.V. Lemanov, Dielectric and acoustic properties of SrTiO3-PMN solid solutions, 17th International Symposium on the Applications of Ferroelectrics, Santa Fe/ USA, February 2008, in: Proceedings, 145-147 (2008).

42) A. Sotnikov, R. Kunze, H. Schmidt, M. Weihnacht, M. Hengst, J. Goetze, K. Jaenicke-Roessler, Temperature dependent material parameters of Sr3NbGa3Si2O14 (SNGS) single crystal, 2007 IEEE International Frequency Control Symposium Jointly with the 21st European Frequency and Time Forum, (TimeNav'07), Genf/ Schweiz, 29.5.-1.6.07, in: Proceedings, 719-723 (2007).

43) M. Stangl, J. Acker, V. Hoffmann, K. Wetzig, U. Kuenzelmann, J.W. Bartha, Application of the copper damascene process for the preparation of electromigration test structures, in: Proceedings, ICPT, Berlin: VDE-Verl., 2008, 331-335 (2008).

44) M. Stangl, M. Liptak, V. Hoffmann, K. Wetzig, J. Acker, Thermoelektrische Schaedigungsmechanismen an elektrochemisch abgeschiedenen Kupfer-Damaszen-Leitbahnen, in: Jahrbuch Oberflaechentechnik; Richard Suchentrunk (ed.) ; Leuze-Verl.; 2008, 64, 287-292 (2008).
45) M. Stoica, G. Kumar, M. Emmi, O. Perroud, A. Wiedemann, A. Gebert, S. Ram, L. Schultz, J. Eckert, Microstructure and magnetic properties of rapidly quenched (Nd100-xGax)80Fe20 (x = 0, 5, 10, 15 at.%) alloys, in: Phase Transformations in Multicomponent Melts, D. M. Herlach (Ed), Weinheim: Wiley-VCH, 2008, 277-295 (2008).
46) M. Stoica, S. Roth, J. Eckert, G. Vaughan, Crystallization behavior and magnetic properties of Fe-Based bulk metallic glasses, in: Intermetallics Research Progress, Y.N. Berdovsky (ed.) Hauppauge: Nova Science Publisher, 2008, 261-277 (2008).
47) M. Uhlemann, J.A. Koza, A. Krause, S. Muehlenhoff, K. Eckert, J.P. Chopart, The effect of high magnetic fields on electrodeposition, 7th International Pamir Conference, Fundamental and Applied MHD, Presqu lle de Giens/ Frankreich, 8.-12.9.08, in: Proceedings, Vol. 1, 23-27 (2008).
48) E. Vavilova, Y. Arango, A. Sotnikov, V. Kataev, S.-L. Drechsler, A. Moskvin, A. Vasiliev, B. Buechner, Interplay of magnetism and paraelectricity in the quantum spin-chain compound Li2CuZrO4 probed by magnetic resonance and dielectric spectroscopy, 25th International Conference on Low Temperature Physics, Amsterdam/ Niederlande, 6.-13.8.08, in: Proceedings (2008).
49) M. Weihnacht, R. Bruenig, H. Schmidt, More accurate simulation of quartz crystal microbalance (QCM) response to viscoelastic loading, 2007 IEEE International Ultrasonics Symposium, New York/ USA, 28.-31.10.07, in: Proceedings, 377-380 (2007).
50) K. Werniewicz, U. Kuehn, N. Mattern, B. Bartusch, J. Eckert, U. Siegel, L. Schultz, T. Kulik, Fe-Based composite materials with improved mechanical properties, in: Glass Materials Research Progres, J.C. Wolf; L. Lange (eds.), Hauppauge: Nova Science Publisher, 2008, 259-274 (2008).
51) X. Yang, K. Eckert, P.A. Nikrityuk, K. Seidel, M. Uhlemann, The start-up process of natural convection in presence of a counteracting Lorentz Force-driven convection, 7th International pamir Conference, Fundamental and Applied MHD, Presqu lle de Giens/ Frankreich, 8.-12.9.08, in: Proceedings, Vol. 1, 297-301 (2008).
52) K. Zagorodniy, H. Hermann, M. Taut, Y. Wang, G. Seifert, E. Zschech, Structure and physical properties of computer-simulated fullerene-based ultralow k dielectric materials, in: Stress-induced Phenomena in Metallization, AIP Conference Proceedings, 945, 162-169 (2007).

Invited Talks

1) J. Acker, S. Buecker, V. Hoffmann, Flammen-Molekuelabsorptionsspektrometrie zweiatomiger Molekuele - Zum Mechanismus der Bildung von AlF in der Acetylen-Lachgas-Flamme, 2nd International Symposium on CSAAS, Berlin, 7.-8.10.08 (2008).
2) P. Atkinson, O.G. Schmidt, Site control of quantum dots, Photonics Seminar Series, Tyndall National Institute, Cork/ Irland, 13.5.08 (2008).
3) E. Backen, S. Haindl, T. Niemeier, J. Freudenberg, R. Huehne, J. Werner, G. Behr, L. Schultz, B. Holzapfel, Superconductivity in FeAs-based compounds - Thin film growth and anisotropy, Shanghai University, Physics Department, Group Meeting, Shanghai/ China, 2.11.08 (2008).
4) G. Behr, J. Werner, A. Koehler, C. Hess, A.-J. Kondrat, R. Klingeler, N. Leps, J.E. Hamann-Borrero, B. Buechner, Preparation, characterization and selected physical properties of new superconductors RO1-xFxFeAs (R=La, Ce, Pr, Nd, Sm, Gd), 4th International Conference on Materials Science and Condensed Matter Physics, Chisinau/ Moldawien, 23.-26.9.08 (2008).
5) M. Benyoucef, Quantum dots for quantum optics, Seminar am Max Planck Institut fuer Physik komplexer Systeme, Dresden, 15.7.08 (2008).
6) M. Benyoucef, Single dot spectroscopy, Seminar, Forschungszentrum Dresden-Rossendorf, 11.7.08 (2008).
7) A. Bernardi, S. Kiravittaya, O.G. Schmidt, Glucose detection on the femtoliter scale, Analyses of chemical and biological processes causing adhesion of macromolecules, cells to materials surfaces, Politecnico di Milano/ Italien, 13.-15.11.08 (2008).
8) S. Borisenko, (pi, pi)-electronic order in iron arsenide superconductors, International Conference on "FeAs High Tc Superconducting Multilayers and Related Phenomena", Rom/ Italien, 9.-13.12.08 (2008).
9) S. Borisenko, Superconductivity and CDW in 2D: the ARPES view, Solid State Physics Seminar, ETH Zuerich/ Schweiz, 17.-19.3.08 (2008).
10) S. Borisenko, (pi, pi)-electronic order in iron arsenide superconductors, International Workshop Properties of Cuprate Superconductors III, Schloss Ringberg, 3.-7.11.08 (2008).
11) S. Borisenko, ARPES - ein Werkzeug zur Erforschung der Natur, Solid State Physics Seminar, Universitaet Wuerzburg, 21.12.08 (2008).
12) S. Borisenko, Superconductivity and CDW in 2D: the ARPES view, Condensed Matter Physics Seminar, Masaryk, University, Brno/ Tschechische Republik, 18.11.08 (2008).
13) S. Borisenko, ARPES - a tool to study nature, Condensed Matter Physics Seminar, Masaryk, University Brno/ Tschechische Republik, 18.11.08 (2008).

14) S. Borisenko, A struggle for the Fermi surface: density waves vs. superconductivity, International Conference Stripes'08, Erice, Sizilien/ Italien, 26.7.-1.8.08 (2008).
15) S. Borisenko, Competing orders in two-dimensional superconductors: the ARPES view, International Workshop on Competing Orders, Dresden, 30.6.-4.7.08 (2008).
16) S. Borisenko, A struggle for the Fermi surface: density waves vs. superconductivity, International Seminar and Workshop, Dresden, 2.-27.6.08 (2008).
17) S. Borisenko, 1-cubed ARPES at BESSY, Workshop on Advanced Photoemission, University of Madrid/ Spanien, 4.-6.6.08 (2008).
18) S. Borisenko, CDW and Superconductivity in 2D: the ARPES view, DPG-Fruehjahrstagung, Berlin, 25.-29.2.08 (2008).
19) S. Borisenko, ARPES - a tool to study nature, Seminar an der Oxford University, Oxford/ GB, 15.2.08 (2008).
20) B. Buechner, Supraleitung und Magnetismus in FeAs-Systemen, Physikalisches Kolloquium der Johannes Gutenberg-Universitaet und der Max-Planck-Institute fuer Polymerforschung und Chemie, Mainz, 18.11.08 (2008).
21) B. Buechner, Anomalous low energy excitations in one dimensional cuprates, Konferenz Schloss Ringberg, 28.9.-1.10.08 (2008).
22) B. Buechner, Magnetism and superconductivity in FeAs based superconductors, 4th International Conference on Materials Science and Condensed Matter Physics, Chisinau/ Moldawien, 23.-26.9.08 (2008).
23) B. Buechner, Superconductivity and magnetism in iron arsenides, Physical Technical Seminar, Russian Academy of Sciences, RAS Kasan/ Russland, 24.9.08 (2008).
24) B. Buechner, Research on correlated electron systems: From basic science to applications, Workshop for young scientists in Kasan / Russland, 26.9.08 (2008).
25) B. Buechner, Superconductivity in FeAs compounds, Kick-off Meeting FOR 912, Dresden, 24.-26.10.08 (2008).
26) B. Buechner, Superconductivity and magnetism in FeAs compounds, Physikalisches Kolloquium der MPIs und der Universitaet Stuttgart, 16.6.08 (2008).
27) B. Buechner, Magnetism and superconductivity in FeAs superconductors, International Symposium/Summer School, Rathen, 11.-15.8.08 (2008).
28) B. Buechner, Magnetism and superconductivity in FeAs superconductors, Seminarvortrag, FZ Karlsruhe, 10.7.08 (2008).
29) B. Buechner, Anomalous low energy excitations in cuprates, MISM 2008, Moscow International Symposium on Magnetism, Moskau/ Russland, 20.-25.6.08 (2008).
30) B. Buechner, Superconductivity and magnetism in FeAs compounds, Physikalisches Kolloquium an der Universitaet Bielefeld, 1.12.08 (2008).
31) B. Buechner, Magnetissm and superconductivity in FeAs superconductors, Properties of High Tc Superconductors III, Schloss Ringberg, 3.-7.11.08 (2008).
32) B. Buechner, Superconductivity and magnetism in LaO1-xFxFeAs, DPG Fruehjahrstagung, Dresden, 22.-27.3.08 (2008).
33) B. Buechner, Nanoscale electronic inhomogeneities in oxides, Seminarvortrag, MPI Halle, 13.5.08 (2008).
34) B. Buechner, Properties of the novel FeAs superconductors, International Seminar on Unconventional Phases, MPI PkS, Dresden, 12.6.08 (2008).
35) B. Buechner, Novel FeAs-based superconductors, Kolloquium, Universitaet Frankfurt, 22.5.08 (2008).
36) J. Buschbeck, I. Opahle, L. Schultz, S. Faehler, Control of structure and modification of magnetic properties in disordered, epitaxial Fe70-xPd30+x films, Sonderseminar des Insitutes für Physik, Universitaet Mainz, 25.8.08 (2008).
37) J. Buschbeck, M. Weisheit, L. Schultz, S. Faehler, Fe-Pt permanent magnet films – L10 ordering, growth and magnetic properties, Seminar am Institut fuer Physik, TU Chemnitz, 21.10.08 (2008).
38) K. Doerr, Reversible strain experiments in strongly correlated magnetic oxide films, Seminar, Unite-Mixte Thales-CNRS, Manuel Bibes, Orsay/ Frankreich, 7.4.08 (2008).
39) K. Doerr, Reversible strain tuning of magnetism and electrical conductivity, EMRS Fall Meeting, Warschau/ Polen, 17.9.08 (2008).
40) K. Doerr, Reversible strain experiments in strongly correlated magnetic oxide films, Seminar an der Universitaet Tuebingen, Prof. R. Kleiner, 30.5.08 (2008).
41) K. Doerr, Strain effects in perovskite cobaltites, Orlando, Villa Conference on Complex Oxide Heterostructures, Orlando/ USA, 3.11.08 (2008).
42) K. Doerr, Reversible strain experiments in strongly correlated magnetic oxide films, Vortrag an der Cambridge University, Neil Mathur, Cambridge/ GB, 6.3.08 (2008).
43) K. Doerr, Piezoelectric strain control of thin film magnetism, TMS 2008, New Orleans/ USA, 10.3.08 (2008).
44) K. Doerr, Reversible strain experiments on strongly correlated oxide films, International Workshop on Computational Magnetism and Spintronics, Dresden, 7.11.08 (2008).
45) J. Eckert, Complex metallic alloys in confined geometries: Processing, structure and mechanical properties, International Workshop on Multiscale Phenomena in Materials, Wien/ Oesterreich, 10.9.08 (2008).
46) H. Ehrenberg, Lithium ion batteries: Challenges for materials science and perspectives, Jilin University, Changchun/ China, 27.6-4.7.08 (2008).

47) H. Ehrenberg, Synchrotron: in situ studies of electrochemical reactions, Inorganic Complex Materials, Puerto Escondido/ Mexiko, 2.-4.9.08 (2008).
48) H. Ehrenberg, Crystallographic aspects in Li-ion batteries: The effect of structural changes and microstructure on fatigue of cathode materials, Electrochemistry - Crossing boundaries, Vortrag an der Universitaet Giessen, 6.-8.10.08 (2008).
49) H. Ehrenberg, N. N. Bramnik, W. Jaegermann, S. Bhuvaneswari, Phosphoolivine LiMPO4 (M=Mn,Fe,Co) cathodes in Li-ion batteries: properties, mechanism and new composite concepts, Jilin University, Changchun/ China, 27.6.-4.7.08 (2008).
50) H. Ehrenberg, N.N. Bramnik, W. Jaegermann, S. Bhuvaneswari, Phosphoolivine LiMPO4 (M=Mn,Fe,Co) cathodes in Li-ion batteries: properties, mechanism and new composite concepts, International Conference on Advanced Ceramics and Composites, ACERS 32, Daytona Beach, Florida/ USA, 28.1.-2.2.08 (2008).
51) H. Ehrenberg, N.N. Bramnik, K. Nikolowski, Degradation mechanisms as guides to new electrode materials for Li-ion batteries, International Conference on Advanced Materials, ICAM 2008, Kerala/ Indien, 18.-21.2.08 (2008).
52) H. Ehrenberg, D. Mikhailova, N. Narayanan, A. Senyshyn, W. Gruner, S. Oswald, A. Voss, D. Trots, C. Ritter, H. Fuess, The effect of structural and compositional details on physical properties of new double-perovskites, International Union of Crystallography Meeting, Osaka/ Japan, 23.-31.8.08 (2008).
53) J. Eickemeyer, Textured nickel-based substrate tapes for YBCO-coated conductors, 3. Braunschweiger Supraleiter-Seminar, TU Braunschweig, 26.5.08 (2008).
54) H. Eschrig, Half-metals - a new materials class, SFB/TR21 - Kolloquium, FB Physik, Universitaet Ulm, 8.2.08 (2008).
55) H. Eschrig, Die BCS-Beschreibung des supraleitenden Zustands, Seminar, Korrelation BCS-Zustand und Bose-Einstein, Bad Honnef, 6.-8.2.08 (2008).
56) S. Faehler, Magnetic shape memory alloy films: What is different to bulk materials?, DPG-Fruehjahrstagung, Berlin, 25.-29.2.08 (2008).
57) S. Faehler, Ueber die Kontrolle von Struktur und Gefuege durch Magnetfelder: Was aendert sich, wenn man bei magnetischen Formgedaechtnislegierungen von Massivmaterial zu duennen Schichten uebergeht?, 3-Professoren Seminar, TU Chemnitz, 3.6.08 (2008).
58) J. Fink, Spin- and angle-resoved photoemission, V. International School on Synchrotron Radiation and Magnetismus, Mittelwihr, Colmar/ Frankreich, 19.-24.10.08 (2008).
59) J. Fink, ARPES, a many-body spectroscopy, applied to conventional and unconvetional superconductors, Vortrag an der FU Berlin, 14.11.08 (2008).
60) J. Fink, Many-body properties of solids studied by high-energy spectroscopies, SFB Seminar, Koeln, 11.6.08 (2008).
61) J. Fink, ARPES, a many-body spectroscopy of solids, applied to conventional and unconventional superconductors, SFB Kolloquium, Mainz, Frankfurt, 27.11.08 (2008).
62) J. Fink, Charge order in La1.8_xEu0.2SrxCuO4 studied by resonant soft X-ray diffraction, 6th International Confernece of the Stripes Series, Stripes08 Quantum Phenomena in Complex Matter, Erice/ Italien, 26.7. - 1.8.08 (2008).
63) J. Fink, Stripes in high-Tc superconductors as detected by soft resonant X-ray scattering, Properties of High Tc Superconductors III, Schloss Ringberg, 3.-7.11.08 (2008).
64) J. Fink, Many-body properties of solids studied by angle-resolved photoemission spectroscopy (ARPES): application to conventional and unconventional superconductors, Colloquium, Universitaet Groningen/ Niederlande, 11.9.08 (2008).
65) J. Fink, Stripes in high-Tc superconductors as detected by resonant soft X-ray scattering, van der Vaals-Zeeman Colloquium, Universitaet Amsterdam/ Niederlande, 9.9.08 (2008).
66) J. Fink, Recent studies of the electronic structure of high-Tc superconductors, Vortrag am Hahn-Meitner-Institut, Berlin, 3.4.08 (2008).
67) J. Fink, Stripes in high-Tc superconductors as detected by resonant soft X-ray scattering, Seminarvortrag, Universitaet Leipzig, 5.9.08 (2008).
68) J. Freudenberger, J. Lyubimova, E. Bocharova, A. Gaganov, L. Schultz, Hochfeste Leitermaterialien auf Kupfer-Basis, Materialphysikalisches Kolloquium, Universitaet Goettingen, 13.5.08 (2008).
69) J. Freudenberger, J. Lyubimova, A. Gaganov, E. Bocharova, L. Schultz, High strength Cu-based conductor materials, Werkstoff-seminar des Institutes fuer Werkstoffkunde I der Universitaet Karlsruhe, Adelboden/ Schweiz, 1.-8.3.08 (2008).
70) G. Fuchs, N. Kozlova, S.-L. Drechsler, A. Kairo, W. Haessler, M.M. Hermann, K. Nenkov, J. Freudenberger, Upper critical fields in carbon doped MgB2, Eingeladener Vortrag im Internationalen Labor fuer Hohe Magnetfelder und Tiefe Temperaturen Wroclaw/ Polen, 8.-9.5.08 (2008).
71) R.B. Gangineni, Reversible strain effects in polycrystalline and structured manganite tunnel junctions, Seminar an der Universitaet Goettingen, 2.6.08 (2008).
72) R.B. Gangineni, Reversible strain effects in polycrystalline and structured manganite tunnel junctions, SPINTEC, Grenoble/ Frankreich, 23.6.08 (2008).
73) R.B. Gangineni, Reversible strain effects in polycrystalline and structured manganite tunnel junctions, Seminar, Max-Planck-Institut fuer Mikrostrukturphysik Halle, 19.5.08 (2008).

74) A. Gebert, Effect of mechanical and structural defects on the corrosion behaviour of Zr-based bulk metallic glasses and composites, PRIME 2008 ECS Conference, Honolulu/ Hawaii, 12.-17.10.08 (2008).
75) A. Gebert, A. Teresiak, B. Khorkounov, M. Uhlemann, L. Schultz, Amorphous- nanocrystalline Mg-Ni-RE alloys for room temperature hydrogen storage, 19. Edgar-Luescher Seminar, Klosters/ Schweiz, 16.-21.2.08 (2008).
76) H.-J. Grafe, F. Hammerath, D. Paar, G. Urbanik, V. Kataev, T. Wolf, G. Khaliullin, B. Buechner, Nuclear magnetic resonance evidence for correlations between antiferromagnetism and pseudogap effects in Zn- and Ni-doped (Eu,Nd)Ba2Cu3O6+y single crystals, International Conference Stripes'08, Erice, Sizilien/ Italien, 26.7.-1.8.08 (2008).
77) D. Grimm, D. Haberer, B. Buechner, A. Latge, M. Terrones, An experimental and theoretical study of the electronic properties of low-dimensional carbon nanotube structures, Seminar im Institut fuer Physik, Universitaet Regensburg, 24.6.08 (2008).
78) D. Grimm, D. Haberer, B. Buechner, A. Latge, M. Terrones, Interference effects in the electronic properties of low dimensional carbon nanotube structures, Seminar im Institut fuer Physik, Universitaet Basel/ Schweiz, 19.6.08 (2008).
79) O. Gutfleisch, Advanced energy efficient materials - application to solid state magnetic cooling, Kolloquium: Physik der Nanostrukturen, Forschungszentrum Dresden Rossendorf, 19.12.08 (2008).
80) O. Gutfleisch, Complex hydrides: potential hydrogen storage materials for mobile applications, Edgar-Luescher Seminar, Klosters/ Schweiz, 18.2.08 (2008).
81) O. Gutfleisch, Magnetic materials for energy-related applications, IEEE Magnetics Society Technical Committee Meeting, Intermag, Madrid/ Spanien, 4.-8.5.08 (2008).
82) O. Gutfleisch, J. Lyubina, S. Rivoirard, E. Beaugnon, Magnetic-field assisted processing: a route to superior nano-composites?, Workshop on Rare Earth Permanent Magnets, Kreta/ Griechenland, 8.-10.9.08 (2008).
83) O. Gutfleisch, J. Lyubina, N. Scheerbaum, J. Liu, Novel functional materials based on magnetostructural transitions, International Workshop, NIMS, Tsukuba/ Japan, 27.10.08 (2008).
84) O. Gutfleisch, J. Lyubina, L. Schultz, Novel magnetocaloric materials, Research Trends in Novel Magnetic Materials, Santorini/ Griechenland, 3.-5.9.08 (2008).
85) O. Gutfleisch, C. Rongeat, Thermodynamics and kinetics of complex hydrides for solid state storage of hydrogen, COSY International Workshop, Universitaet Autonoma de Barcelona/ Spanien, 8.-10.12.08 (2008).
86) W. Haessler, Nanocrystalline precursor powders for MgB2wires and tapes, 21th International Symposium on Superconductivity, Tsukuba/ Japan, 27.-29.10.08 (2008).
87) V. Hoffmann, RF and pulsed glow discharges,and crater formation in glow discharges, FA CSS 2008, Reno/ USA, 28.9.-2.10.08 (2008).
88) V. Hoffmann, V. Efimova, D. Klemm, M. Voronov, J. Eckert, Pulsed glow discharges – from fundamentals to applications, 2008 Third Asia Pacific Winter Conference, Tsukuba/ Japan, 16.-21.11.08 (2008).
89) V. Hoffmann, V. Efimova, M. Voronov, P. Smid, E. Steers, J. Eckert, Measurement of voltage and current in continuous and pulsed rf and dc glow discharges, 24th SPIG, Novi Sad/ Serbien, 25.-29.8.08 (2008).
90) V. Hoffmann, D. Klemm, K. Wetzig, Progress at thin film analysis by glow discharge spectrometry, Nordic Conference on Plasma Spectrochemistry, Loen/ Norwegen, 15.-18.6.08 (2008).
91) R. Huehne, Development of coated conductor architectures for high temperature superconductors, Institutsseminar, Physics Department, Shanghai University, Shanghai/ China, 7.11.08 (2008).
92) D. Inosov, ARPES studies of the many-body effects in the electronic structure of high-Tc cuprates, IMPRS evaluation, MPI - PkS Dresden, 4.7.08 (2008).
93) D. Inosov, High-energy anomalies in the electronic spectra of high-Tc superconductors, Vortrag am Max-Planck-Institut fuer Festkoerperforschung, Stuttgart, 4.4.08 (2008).
94) D. Inosov, High-energy anomalies in the electronic spectra of high-Tc superconductors, Vortrag am Paul Scherrer Institut, Villigen/ Schweiz, 18.3.08 (2008).
95) V. Kataev, Heavy fermion magnetic resonance in the dense Kondo lattice system YbRh2Si2 probed by high field ESR, International Zavoisky Workshop "Modern developments of magnetic resonance", Kasan/ Russland, 29.9.-3.10.08 (2008).
96) V. Kataev, Tunable electron spin resonance spectroscopy of multi-center paramagnetic molecular complexes in strong magnetic fields, DPG-Fruehjahrstagung, Berlin, 25.-29.2.08 (2008).
97) J.-W. Kim, Growth and characterization of Hexagonal multiferroic HoMnO3 films, Seminar an der Universitaet Leipzig, M. Grundmann, 10.7.08 (2008).
98) J.-W. Kim, Multiferroic hexagonal HoMnO3 films, Seminar, Max-Planck-Institut fuer Mikrostrukturphysik Halle, 20.6.08 (2008).
99) R. Klingeler, Magnetism meets Nanotechnology: Biomedical and technological applications of carbon nanotubes, SFB Seminar, Bielefeld, 29.7.08 (2008).
100) R. Klingeler, Magnetic and electronic properties of FeAs-based superconductors, Seminar, University of Birmingham/ GB, 21.11.08 (2008).
101) R. Klingeler, Magnetic, thermodynamic and structural properties of FeAs-based superconductors, International Conference on FeAs High Tc Superconducting Multilayers and Related Phenomena, Rom/ Italien, 9.-13.12.08 (2008).

102) R. Klingeler, Magnetic and electronic properties of doped oxide nanotubes, Moscow International Symposium on Magnetism, Moskau/ Russland, 23.-26.6.08 (2008).
103) R. Klingeler, Biomedical applications of functionalised carbon nanotubes, Hyperthemia and Nanomedicine: International Workshop, Winston-Salem, NC/ USA, 7.-9.4.08 (2008).
104) M. Knupfer, Elektronische Eigenschaften von Grenzflaechen organischer Halbleiter mit Metallen, Physikalisches Kolloquium, TU Bergakademie Freiberg, 21.5.08 (2008).
105) M. Knupfer, Orbital and spin ground state of transition metal phthalocyanines, Workshop DFT meets Experiment, Dresden, 25.-28.8.08 (2008).
106) A. Kordyuk, Persistent pseudo-gap and density ordering in 2D metals (plenary talk), 3rd International Conference "Fundamental Problems of High Temperature Superconductivity" (FPS'08), Moskau/ Russland, 13.-17.10.08 (2008).
107) C. Kramberger, Confined collective electronic excitations in quantum wires (aka nanotubes), Seminarvortrag, Palaiseau/ Frankreich 25.4.08 (2008).
108) C. Kramberger, Angle resolved dielecetric response in carbon nanotubes, Seminarvortrag, Wien/ Oesterreich 14.3.08 (2008).
109) K. Lipert, Y. Krupskaya, C. Mahn, D. Haase, S. Hampel, F. Wolny, A. Leonhardt, M. Ritschel, A. Wolter, T. Muehl, R. Klingeler, B. Buechner, Magnetic properties of carbon nanotubes and their possible applications, Seminar an der Universitaet Regensburg, 12.3.08 (2008).
110) J. Lyubina, O. Gutfleisch, Novel magnetocaloric materials, Delft Days on Magnetocalorics, University of Delft/ Niederlande, 30.-31.10.08 (2008).
111) J. Lyubina, O. Gutfleisch, L. Schultz, Nanocrystalline L10 FePt-based alloys: phase transformations, structure and magnetism, JEMS 2008, Dublin/ Irland, 14.-19.9.08 (2008).
112) N. Mattern, T. Gemming, J. Thomas, G. Goeringk, H. Franz, J. Eckert, Phase separation in Ni-Nb-Y metallic glasses, ISMANAM2008, Buenos Aires/ Argentinien, 6.-10.7.08 (2008).
113) J. McCord, Magnetic domain reorganization and twin boundary dynamics in magnetic shape memory alloys, Intermag 2008, Madrid/ Spanien, 4.-8.5.08 (2008).
114) J. McCord, Magnetization dynamics of ferromagnetic-antiferromagnetic systems, Workshop on High Temporal and Spatial Resolution, Augustow/ Polen, 27.6.08 (2008).
115) J. McCord, Influence of antiferromagnetic layers on the magnetization dynamics of exchange coupled thin films, DPG-Fruehjahrstagung, Berlin, 25.-29.2.08 (2008).
116) J. McCord, Magnetization dynamics of coupled ferromagnetic-antiferromagnetic thin films, Seminaire LPM Magnetization dynamics of coupled ferromagnetism, Nancy/ Frankreich, 15.4.08 (2008).
117) J. McCord, Control of magnetization dynamics by magnetic domain engineering, Seminaire CNRS Institut Neel, Grenoble/ Frankreich, 17.3.08 (2008).
118) J. McCord, Aspects of magnetic heterostructures - influencing effective magnetic properties, Kolloquium der Werkstoffwissenschaften, TU Dresden, 3.12.08 (2008).
119) J. McCord, Magnetization dynamics of magnetic heterostructures, MISM, Moskau/ Russland, 20.-25.6.08 (2008).
120) Y.F. Mei, Nanomembrane releasing technology for novel applications, Seminar, School of Material Science and Engineering, University of Science and Technology Beijing/ China, 22.4.08 (2008).
121) Y.F. Mei, Rolled-up Nanotech and ALD: More Choices, GerALD Workshop, Halle, 22.-23.9.08 (2008).
122) Y.F. Mei, Strain engineered micro-/nanotubes on polymers, Seminar, Universitaet Hamburg, 17.12.08 (2008).
123) Y.F. Mei, Nanomembrane technology - towards applications in biology and chemistry, Seminar, University of Southampton, Southampton/ GB, 2.12.08 (2008).
124) Y.F. Mei, Shaping single crystalline nanomembranes as fluidic micro-/nanochannels, Seminar, Key Laboratory of Molecular Nanostructure and Nanotechnology, Institute of Chemistry, Chinese Academy of Sciences, Beijing/ China, 21.4.08 (2008).
125) Y.F. Mei, Strained epitaxial layers: Rolling and wrinkling, Key Lab of Semiconductor Materials, Institute of Semiconductors, Chinese Academy of Sciences, Beijing/ China. 22.4.08 (2008).
126) L. Menoza, A. Planes, M. Acet, J. Lyubina, O. Gutfleisch, Effects of pressure and magnetic field on the magnetic properties and martensitic transition in Ni-Mn-X magnetic shape memory alloys, International Conference on Martensitic Transformations, Santa Fe/ USA, 29.6.-5.7.08 (2008).
127) S. Menzel, T. Gemming, Study and application of individual multiwall carbon nanotubes, Nanotechnik User Meeting, Kusterdingen, 16.-17.4.08 (2008).
128) T. Muehl, Magnetic nanowires inside carbon nanotubes - magnetic force microscopy sensors using iron-filled carbon nanotubes, SFB-Seminar, Universitaet Duisburg-Essen, 6.11.08 (2008).
129) T. Muehl, Magnetic force microscopy sensors using iron-filled carbon nanotubes, Vortrag zum SFB-Seminar, Universitaet Bielefeld, 22.4.08 (2008).
130) T. Muehl, Magnetic nanowires inside carbon nanotubes, Seminar, Institut fuer Werkstoffwissenschaften, TU Dresden, 27.11.08 (2008).

131) F. Muranyi, Electron spin resonance, a tool to study superconductors, Seminar an der Universitaet Zuerich/ Schweiz, 3 0.4.08 (2008).
132) V. Neu, Nanoskalige Domaenenstrukturen und Magnetisierungsprozesse in duennen Schichten, Physikalisches Kolloquium der TU Dresden, 17.6.08 (2008).
133) V. Neu, C. Bran, F. Fleischhauer, A. Singh, U. Wolff, L. Schultz, Nanoscaled domain structures and magnetization processes in thin films, DPG-Fruehjahrstagung, Berlin, 25.-29.2.08 (2008).
134) R. Pfrengle, Informationsbuendelung als Antrieb der wirtschaftlichen Entwicklung in den Regionen, Internationale Konferenz "Wirtschaft und Raum" des Bundesministeriums fuer Verkehr, Bau und Stadtentwicklung, Leipzig, 27.10.08 (2008).
135) R. Pfrengle, M. Calin, F. Wasserscheidt, Frauenfoerderung als Personalfuehrung, Wissenschaftsmanagement als Berufs- und Karrierefeld fuer Frauen, Gemeinsame Veranstaltung des Deutschen Forschungsinstituts fuer Oeffentliche Verwaltung und des Zentrums fuer Wissenschaftsmanagement, Speyer, 9.-10.10.08 (2008).
136) U. Queitsch, I. Lindemann, B. Rellinghaus, L. Schultz, Selforganization of gas phase deposited FePt nanoparticles on bacterial S layer templates, Kolloquium des SFB 445, Universitaet Duisburg-Essen, 8.12.2008 (2008).
137) U. Queitsch, B. Rellinghaus, L. Schultz, Towards ultra-high-density magnetic data storage media, Jahrestreffen der CNV Stiftung, Tuebingen, 6.-7.9.08 (2008).
138) A. Rastelli, Scalable quantum dot systems: current challenges, International Material Research Conference 2008, Chongqing/ China, 8.-12.6.08 (2008).
139) A. Rastelli, Optically active lateral quantum dot molecules, 15th International Conference on Superlattices, Nanostructures and Nanodevices (ICSNN08) Natal/ Brasilien, 3.-8.8.08 (2008).
140) A. Rastelli, Towards position- and wavelength-controlled quantum dots for single dot based devices, UK Compound Semiconductors Conference 2008, Sheffield/ GB, 3.7.08 (2008).
141) A. Rastelli, Growth and control of self-assembled quantum dot structures , Key Lab of Semiconductor Materials, Institute of Semiconductors, Chinese Academy of Sciences, Beijing/ China, 13.6.08 (2008).
142) A. Rastelli, Optically active lateral quantum dot molecules, 15th International Conference on Superlattices, Nanostructures and Nanodevices (ICSNN08), Natal/ Brasilien, 3.-8.8.08 (2008).
143) A. Rastelli, Quantum dots and microcavities, EU-ProMiNaS Training course on "Electrical and optical characterization of nanodevices", Rom/ Italien, 9.-20.6.08 (2008).
144) A. Rastelli, Towards position- and wavelength-controlled quantum dots for single dot based devices, UK Compound semiconductors Conference 2008, Sheffield/ GB, 2.-3.7.08 (2008).
145) A. Rastelli, Quantum dots with perfectly resonant emission energies, International Workshop on Optical Properties of Coupled Semiconductor and Metallic Nanoparticles (OPCSMN08), Dresden, 21.-25.7.08 (2008).
146) A. Rastelli, Self-assembled quantum dots: composition profiles and emission energy tuning, Seminar, Tyndall National Institute, Cork/ Irland, 16.12.08 (2008).
147) B. Rellinghaus, Magnetische Nanostrukturen, Luescher Lectures – Magnetismus, Akademie fuer Lehrerfortbildung, Dillingen, 15.-17.10.08 (2008).
148) B. Rellinghaus, E. Mohn, U. Queitsch, L. Schultz, FePt nanomagnets from the gas phase, DPG-Fruehjahrstagung, Berlin, 25.-29.2.08 (2008).
149) B. Rellinghaus, E. Mohn, U. Queitsch, M. Sparing, B. Holzapfel, L. Schultz, Tailoring the properties of magnetic nanoparticles from the gas phase, Physics of Magnetism 2008 - PM08, Poznan/ Polen, 23.-27.6.08 (2008).
150) B. Rellinghaus, D. Pohl, E. Mohn, L. Schultz, T. Jaervi, J. Fassbender, K. Albe, Irradiation-induced structural modifications of binary metal nanoparticles, Towards Reality in Nanoscale Materials - TRNM08, Levi/ Finnland, 3.-5.12.08 (2008).
151) M.H. Ruemmeli, Opportunities with nanostructured thermoelectric materials, Seminar talk at the ITT Friction, Barge, Piemont/ Italien, 8.2.08 (2008).
152) M.H. Ruemmeli, F. Schaeffel, M. Bystrejewski, M. Loeffler, R. Schoenfelder, B. Buechner, Advances in understand carbon nanotube nucleation and growth, Invited talk at the University of Alabama, Birmingham/ USA, 22.8.08 (2008).
153) M.H. Ruemmeli, F. Schaeffel, M. Bystrejewski, M. Loeffler, R. Schoenfelder, J. Warner, B. Rellinghaus, L. Schultz, B. Buechner, On the advantages of gas phase prepared catalyst particles in understanding carbon nanotube growth, Conference, Ostrava/ Tschechien, 1.-4.8.08 (2008).
154) M.H. Ruemmeli, F. Schaeffel, M. Bystrejewski, R. Schoenfelder, B. Buechner, Advanced in understanding carbon nanotube nucleation and growth, Invited talk at the Fisk University/ USA, 20.8.08 (2008).
155) M.H. Ruemmeli, F. Schaeffel, M. Bystrejewski, R. Schoenfelder, B. Buechner, Advances in understanding carbon nanotube nucleation and growth, Invited talk at the Vanderbilt University, Nashville/ USA, 20.8.08 (2008).
156) M.H. Ruemmeli, F. Schaeffel, M. Bystrejewski, R. Schoenfelder, B. Buechner, Advanced in understanding carbon nanotube nucleation and growth, Invited talk at the US Air Force Research Laboratories/ USA, 18.8.08 (2008).
157) R. Schaefer, Kerr microscopy, Seminarvortrag, Institut fuer Ferrous, Postech, Pohang/ Suedkorea, 3.11.08 (2008).
158) R. Schaefer, Vom Barkhausenrauschen zur Spindynamik, Seminarvortrag am Fraunhofer IZFP, Saarbruecken, 19.5.08 (2008).

159) R. Schaefer, Magnetische Werkstoffe, Vorlesungsreihe, Polytechnische Universitaet Bucharest/ Rumaenien, 24.-27.11.08 (2008).
160) R. Schaefer, Kerrmikroskopie: Grundlagen, Entwicklungen und Anwendungen, Innovent Kolloquium, Jena, 6.2.08 (2008).
161) R. Schaefer, The magnetic microstructure of amorphous and nanocrystallien materials, Seminarvortrag, Institut fuer Physik, Postech, Pohang/ Suedkorea, 3.11.08 (2008).
162) R. Schaefer, Magnetische Mikrostrukturen, Luescher Lectures, Akademie fuer Lehrerfortbildung, Dillingen, 15.10.08 (2008).
163) R. Schaefer, Magnetic domain analysis in bulk ferromagnets, SLS Seminar, Paul Scherrer Institut, Villingen, 20.6.08 (2008).
164) R. Schaefer, The magnetic microstructure of soft magnetic materials, Vorlesungsreihe, Institut fuer Ferrous, Postech, Pohang/ Suedkorea, 27.-31.10.08 (2008).
165) F. Schaeffel, M.H. Ruemmeli, C. Kramberger, T. Pichler, T. Gemming, B. Buechner, B. Rellinghaus, L. Schultz, Microscopic studies on the tailored growth of carbon nanotubes from pre-defined catalyst particles, 19. Edgar-Luescher Seminar, Klosters/ Schweiz, 16.-21.2.08 (2008).
166) O.G. Schmidt, Shaped nanomembranes for interdisciplinary research, 4th International Conference on Materials Science and Condensed Matter Physics Chisinau/ Moldavien, 23.-26.9.08 (2008).
167) O.G. Schmidt, Spatial and spectral control of individual quantum dots, International Workshop on Nonequilibrium Nanostructures, Dresden, 1.-6.12.08 (2008).
168) O.G. Schmidt, Nanomembrane technologies, Summer School on the Physics and Chemistry of Nano Materials, Cluj-Napoca/ Rumaenien, 17.-30.8.08 (2008).
169) O.G. Schmidt, Self-assembled SiGe islands: From fundamental perception to ultra large scale integration, JST-DFG Workshop on Nanoelectronics, Aachen, 5.-7.3.08 (2008).
170) O.G. Schmidt, Shaped nanomembranes, Seminar an der Karls-Universitaet, Prag/ Tschechien, 17.1.08 (2008).
171) O.G. Schmidt, Semiconductor quantum dots, Summer School on the Physics and Chemistry of Nano Materials, Cluj-Napoca/ Rumaenien, 17.-30.8.08 (2008).
172) O.G. Schmidt, Hybrid heterostructures and interfaces in radial geometries, Summer School on Modern Concepts for Creating and Analyzing Surfaces and Nanoscale Materials, Sant Feliu de Guixols, Costa Brava/ Spanien, 12.-16.5.08 (2008).
173) O.G. Schmidt, Shaped nanomembranes for interdisciplinary research, Kolloquium, Forschungszentrum Dresden-Rossendorf, 26.6.08 (2008).
174) O.G. Schmidt, General introduction to nanomaerials, Summer School on the Physics and Chemistry of Nano Materials, Cluj-Napoca/ Rumaenien, 17.-30.8.08 (2008).
175) O.G. Schmidt, Rolled-up Si nanomembranes for on-chip photonic applications, The 5th International Conference on Group IV Photonics, Sorrento/ Italien, 17.-19.9.08 (2008).
176) O.G. Schmidt, Vom Loewenzahn zum Mikro-U-Boot: Stress und Entspannung in Materialien, 125. Versammlung der Gesellschaft Deutscher Naturforscher und Aerzte e.V., Tuebingen, 19.-22.9.08 (2008).
177) O.G. Schmidt, Island formation during lattice mismatched heteroepitaxy: Experimental observations, Summer School on Modern Concepts for Creating and Analyzing Surfaces and Nanoscale Materials, Sant Feliu de Guixols, Costa Brava/ Spanien, 12.-16.5.08 (2008).
178) O.G. Schmidt, Efforts towards a deterministic quantum dot technology, The 5th International Conference on Semiconductor Quantum Dots, Gyeongju/ Korea, 11.-16.5.08 (2008).
179) O.G. Schmidt, Quantum dots und smart tubes, Kolloquium, Technische Universitaet Ilmenau, 16.12.08 (2008).
180) L. Schultz, Vom Schweben auf Magnetfeldern: die wundersame Welt der Supraleitung, Vortrag am Anne-Augustum-Gymnasium Goerlitz, 15.10.08 (2008).
181) L. Schultz, Vom Schweben auf Magnetfeldern: die wundersame Welt der Supraleiter, Physikalisches Kolloquium der Universitaet Duisburg, 12.11.08 (2008).
182) L. Schultz, Nanostructured high temperature superconductor materials for new applications, ISMANAM 2008, Buenos Aires/ Argentinien, 9.7.08 (2008).
183) L. Schultz, Riding on magnetic fields, Research Trends in Novel Magnets for Electromagnetic Applications, Santorini/ Griechenland, 5.9.08 (2008).
184) L. Schultz, Riding on magnetic fields - The miraculous world of magnetism and superconductivity, REPM 2008, Kreta/ Griechenland, 9.9.08 (2008).
185) L. Schultz, Vom Schweben auf Magnetfeldern: die wundersame Welt der Supraleiter, Kolloquium zum Gedaechtnis an Prof. Dr. H. J. Engell, Duesseldorf, 2.7.08 (2008).
186) L. Schultz, Riding on magnetic fields: The miraculous world of superconductors, 1st Dresden-Karlsruhe Seminar on Materials and Applications of Superconductivity, Bad Liebenzell, 28.5.08 (2008).
187) L. Schultz, Riding on magnetic fields: The miraculous world of superconductors, Kolloquium, Universitaet Leuven/ Belgien, 26.5.08 (2008).
188) L. Schultz, Riding on magnetic fields: Macroscopic interaction of ferromagnetic and superconducting permanent magnets, INTERMAG 2008, Madrid/ Spanien, 7.5.08 (2008).

189) L. Schultz, Vom Schweben auf Magnetfeldern: die wundersame Welt der Supraleitung, Vortrag am Werner-Heisenberg-Gymnasium Riesa, 17.4.08 (2008).
190) L. Schultz, High temperature superconductors for energy and traffic technologies, APNFN, Dresden, 23.-25.1.08 (2008).
191) O. Shuleshova, Solidification kinetics and metastable phase formation in undercooled melts of Ti-Al-Nb turbine blade alloys, Seminar im Institut fuer Raumsimulation, DLR Koeln, 12.12.08 (2008).
192) O. Shuleshova, Equilibrium and metastable solidification of Ti-Al-Nb and Ni-Al intermetallic alloys, Seminar im Institut fuer Strukturphysik, TU Dresden, 9.12.08 (2008).
193) O. Shuleshova, In situ real-time observation of solidification process, On-line lecture within IMPRESS project lecture series, Dresden, 21.5.08 (2008).
194) E. Steers, P. Smid, V. Hoffmann, Effects of traces of molecular gases (hydrogen, nitrogen) in glow discharges in noble gases, 24th SPIG, Novi Sad/ Serbien, 25.-29.8.08 (2008).
195) R. Sueptitz, J.A. Koza, M. Uhlemann, A. Gebert, L. Schultz, Korrosion von Eisenelektroden im Magnetfeld, Institutsseminar, TU Dresden, Institut fuer Stroemungsmechanik, 5.11.08 (2008).
196) A. Teresiak, A. Gebert, M. Uhlemann, Untersuchungen an neuen Mg-Ni-La Legierungen als Elektrodenmaterial fuer wiederaufladbare Batterien, PANalytical-Industrie-Symposium, Kassel, 11.-12.6.08 (2008).
197) T. Thersleff, L. Molina, E. Backen, S. Engel, C. Mickel, S. Menzel, B. Schlobach, O. Eibl, L. Schultz, B. Holzapfel, Focused Ion Beam preparation of YBCO thin film TEM lamellae, Invited Scientist at the Univeristy of Cambridge, Cambridge/ GB, 26.9.-2.10.08 (2008).
198) T. Thersleff, L. Molina, E. Backen, S. Engel, C. Mickel, S. Menzel, B. Schlobach, O. Eibl, L. Schultz, B. Holzapfel, Focused Ion Beam preparation of YBCO thin film TEM lamellae, NESPA TEM Workshop, Barcelona/ Spanien, 5.-9.5.08 (2008).
199) T. Thersleff, L. Molina, E. Backen, S. Engel, C. Mickel, S. Menzel, B. Schlobach, O. Eibl, L. Schultz, B. Holzapfel, Focused Ion Beam preparation of YBCO thin film TEM lamellae, Invited Scientist at Shanghai University, Shanghai/ China, 24.10.-7.11.08 (2008).
200) M. Uhlemann, Electrodeposition in high magnetic fields, Institutsseminar, Grenoble HMFL - CNRS, Grenoble/ Frankreich, 5.11.08 (2008).
201) M. Uhlemann, J.A. Koza, A. Krause, The effect of high magnetic field on the electrodeposition, 7th PAMIR International Conference on Fundamental and Applied MHD, Presqu´île de Giens / Frankreich, 8.-12.9.08 (2008).
202) E. Vavilova, Interplay between charge doping and magnetism in vanadium-oxide nanotubes, Physical Seminar, High Magnetic Field Laboratory (HLD) Dresden, 23.1.08 (2008).
203) F. Wasserscheidt, R. Pfrengle, Zertifizierung "berufundfamilie", Verwaltungsausschuss der Leibniz-Gemeinschaft, Magdeburg, 27.11.08 (2008).
204) H. Wendrock, Anwendungen der EBSD-Technik in der Werkstoffforschung, Kolloquium "Neue Entwicklungen in der EDX-Analyse", Berlin, 3.-4.6.08 (2008).
205) U. Wolff, C. Bran, L. Schultz, V. Neu, Imaging of topographic and magnetic structures on a nanometer scale by AFM and MFM, Winter School, Kranjska Gora/ Slowenien, 7.-9.2.08 (2008).
206) F. Wolny, T. Muehl, U. Weissker, Iron filled carbon nanotubes as probes in magnetic force microscopy, Eingeladener Vortrag im FZ Dresden-Rossendorf, 9.4.08 (2008).
207) T.G. Woodcock, K. Khlopkov, T. Gemming, A. Walther, N.M. Dempsey, D. Givord, O. Gutfleisch, Interaction domains in high performance NdFeB thick films for applications in micro-electro-mechanical systems (MEMS), International Workshop, NIMS, Tsukuba/ Japan, 27.10.08 (2008).

Patents

Issues of Patents 2008

DE 10 2004 006 234 Verfahren zur Herstellung oxidischer Supraleiter
Inventors: W. Gruner, W. Häßler

DE 10 2005 036 682 Verfahren zu Herstellung eines Schicht-Substrat-Verbundes und Schicht-Substrat-Verbund
Inventors: S. Fähler, K. Leistner, V. Neu

DE 10 2005 026 548 Metallstangen mit magnetischen Bitmustern sowie Verfahren und Einrichtung zum Erzeugen der Bitmuster
Inventor: S. Fähler

DE 10 2006 027 880 Isolationsschichtmaterial für die Mikroelektronik
Inventors: H. Hermann, Ch. Täschner et al.

DE 10 2006 042 616 Wellenleiterbauelemente auf der Grundlage akustischer Oberflächenwellen und deren Verwendung
Inventors: S. Biryukov, G. Martin, M. Weihnacht

DE 10 2006 041 515 Verfahren zur Herstellung von ein- oder mehrwandigen, mit einem oder mehreren Übergangsmetallen beschichteten Kohlenstoff-Nanoröhren
Inventors: A. Leonhardt, S. Hampel, B. Büchner

EP 1 143 531 Permanentmagnet aus einem supraleitenden keramischen Material
Inventors: G. Krabbes, G. Fuchs, G. Stöver, P. Verges, L. Shlyk

Patent Applications 2008

10715 Verfahren und Vorrichtung zur Erzeugung eines räumlich frei orinetierbaren Magnetfeldes mittels supraleitender Dauermagneten
Inventors: D. Lindackers, A. Horst, B. Büchner

10722 Formkörper aus einem magnesiumhaltigen Verbundwerkstoff und Verfahren zu seiner Herstellung
Inventors: M. Sakaliyska, S. Scudino, K. Surreddi, J. Eckert

10723 Formkörper aus einem aluminiumhaltigen Verbundwerkstoff und Verfahren zu seiner Herstellung
Inventors: M. Sakaliyska, S. Scudino, K. Surreddi, J. Eckert

10802 Thermoelektrisches Bauelement und Verfahren zu seiner Herstellung
Inventors: T. Dienel, J. Schumann, A. Rastelli, O.G. Schmidt

10804 Röhrenförmiger Multifunktionssensor in Flüssigkeiten, Verfahren zu seiner Herstellung und Verwendung
Inventors: E. Bermudez, Y. Mei, O. G. Schmidt

10806 Verfahren zur Herstellung eines Schichtverbundes mit epitaktisch gewachsenen Schichten aus einem magnetischen Formgedächtnismaterial und Schichtverbund mit epitaktisch gewachsenen Schichten aus einem magnetischen Formgedächtnismaterial, sowie deren Verwendung
Inventors: F. Khelfaoni, J. Buschbeck, S. Fähler, et al.

10807 Temperaturstabiler Doppelresonator
Inventor: G. Martin

10809 Schichtsystem für Elektroden
Inventor: S. Menzel

10810	Strangförmiges Kompositleitermaterial *Inventor:* S. Menzel
10811	Schicht oder Schichtsystem für Interdigitalwandler für SAW- Bauelemente für Hochleistungs- und/oder Hochtemperaturanwendungen und/oder mit hohem Reflexionsfaktor *Inventors:* S. Menzel, A. Winkler, H. Schmidt
10812	Verfahren zur Herstellung von dotierten Vanadium-Nanoröhren *Inventors:* G. Zakharova, C. Täschner, V. Volkov, A. Leonhardt
10814	Elektisch leitfähiger Hochtemperatur-Supraleiter-Schichtaufbau und Verfahren zu seiner Herstellung *Inventors:* R. Hühne, K. Güth, R. Kaltofen
10815	Verfahren zur Anwendung eines Bauelementes aus mindestens einem ferromagnetischen Formgedächtnis-Material, Bauelement und dessen Verwendung *Inventors:* S. Fähler, M. Thomas, O. Heczko, J. Buschbeck, J. Mc Cord
10816	Verfahren zur Bestimmung der Viskosität und Elastizität von viskoelastischen Medien *Inventors:* R. Brünig, M. Weihnacht, H. Schmidt, G. Martin
10817	Verfahren zur Bestimmung der Viskosität und Elastizität von viskoelastischen Medien *Inventors:* R. Brünig, M. Weihnacht, H. Schmidt
10818	Diagnostisches und/oder therapeutisches Agens, Verfahren zu seiner Herstellung und Verwendung *Inventors:* L. Dunsch et al.
10826	Verfahren zur Herstellung von großen Vesikeln aus selbstorganisierenden, membranbildenden Molekülen *Inventors:* L. Steller, H. Schmidt, et al.
10832	Beschichtetes magnetisches Legierungsmaterial und Verfahren zu seiner Herstellung *Inventors:* J. Lyubina, M. Buschbeck, O. Gutfleisch

PhD Theses 2008

Gangineni Ramesh Babu	Extrinsic Magnetotransport in Manganites and its Dependence on Mechanical Strain
Kaushik Biswas	Effect of melt convection on microstructure evolution of peritectic Nd-Fe-B and Ti-Al alloys.
Jayanta Das	Heterostructured copper- and titanium-base ultrafine and glassy alloys
Denny Deutsch	Nanostructurierte Fullerenschichten für organische Bauelemente
Uwe Gaitzsch	Struktureinstellung und magnetische Dehnung in polykristallinen magnetischen Ni-Mn-Ga – Formgedächtnislegierungen
Christian Golze	Tunable High-Field/High-Frequency ESR and High-Field Magnetization on Single-Molecule Clusters
Daniel Grimm	A combined experimental and theoretical approach towards the understanding of transport in one-dimensional molecular nanostructures
Dmytro Inosov	Many-Body Effects in the Electronic Structure of High-Tc Cuprates
Christian Kramberger	Angle-resolved dielectric response in carbon nanotubes
Christian Müller	Grundlegende Untersuchungen zum CVD-Wachstum Fe-gefüllter Kohlenstoff-Nanoröhren
Ajit Kumar Patra	Crystal Structure, anisotropy and spin reorientation transition of highly coercive, epitaxial Pr-Co films
Patrick Riberio	One-dimensional quantum magnets in cuprates: Single crystal growth and magnetic heat transport studies
Thomas Riedl	$La_{0,7}Sr_{0,3}MnO_3$-Dünnschichten auf $SrTiO_3$(0 0 1)-Substrat: Struktur und Mn-Wertigkeit
Nicolle Seifert	Mikrostruktur und mechanisches Verhalten von teilamorphen und kristallinen Materialien auf Zirkon-Basis
Venkataraman Shankar	Studies on microstructural transformations in $Cu_{47}Ti_{33}Zr_{11}Ni_8Si_1$ metallic glass
Marcel Stangl	Charakterisierung und Optimierung elektrochemisch abgeschiedener Kupferdünnschichtmetallisierungen für Leitbahnen höchstintegrierter Schaltkreise
Volodymyr Zabolotny	Investigation of renormalization effects in high temperature cuprate superconductors
Wenxu Zhang	Magnetism, Structure and their Interactions

Diploma and Master Theses 2008

Ioana-Ruxandrs Balan	Einführung von Programmbudgets in die Leibniz-Gemeinschaft am Beispiel des IFW Dresden (Univ. Politehnica Bukarest)
Anja Backen	Statisches und dynamisches Magnetisierungsverhalten austauschgekoppelter magnetischer Mikrodrähte (TU Dresden)
Mathias Bayer	Spin Density Wave Chromium (TU Dresden)
Martin Engel	Synthese von stickstoffhaltigen Kohlenstoff-Nanotubes mittels plasmagestützter chemischer Gasphasenabscheidung (TU Bergakademie Freiberg)
Andreea C. Ghinea	Structure and mechanical properties of ßTi-Nb and TiNbIn alloys with potential biomedical applications (Univ. Politehnica Bukarest)
Konrad Güth	Entwicklung leitfähiger Pufferarchitekturen auf der Basis von IBAD-TiN (TU Dresden)
Andreas Herklotz	PMN-PT als Dünnschichtsubstrat (TU Dresden)
René Illgen	Herstellen, Öffnen, Kürzen, Füllen und Wiederverschließen von Kohlenstoffnanoröhren (FH Zittau-Görlitz)
Christian Kästner	Synthese und Charakterisierung von Mono- und Dimetallofullerenen (TU Ilmenau)
Florian Kretzschmar	Magnetische Untersuchungen geometrisch frustrierter Spinmagnete (TU Dresden)
Christopher Mahn	Aufbau einer Messzelle für medizinische Anwendung von Nanomagneten (TU Dresden)
Claudia Patschureck	Untersuchung der Anisotropieabhängigkeit der magnetischen Domänenstruktur und des dynamischen Magnetisierungsverhaltens in magnetischen Dünnschichtelementen (TU Dresden)
Maik Peschel	Hydrothermale Synthese von eisenhaltigen Nanostrukturen (FHS Jena)
Darius Pohl	Einfluss von Ionenbestrahlung auf die Morphologie und Kristallstruktur von Übergangsmetall-Nanopartikeln (TU Dresden)
Paul Saß	STM-Untersuchungen an Übergangsmetalloxiden (TU Dresden)
Antje Schlieter	Mikrostrukturelle sowie mechanische und thermische Charakterisierung von $Fe_{84.3}Cr_{4.3}Mo_{4.6}V_{2.2}C_{4.6}$ (TU Bergakademie Freiberg)
Christoph Schlosser	Erarbeitung einer Lösung zur Realisierung und zum Einsatz von Videokonferenzen im IFW (BA Dresden)
Marietta Seifert	Dünne epitaktische $SmCo_5$-Schichten mit senkrechter magnetischer Anisotropie (TU Dresden)
Konrad Suschke	Charakterisierung neuer piezoelektrischer Materialien (TU Dresden)
Juliane Thielsch	Kerrmikroskopische Untersuchung von Magnetisierungsprozessen in kornorientiertem Elektroblech (TU Dresden)
Sven Thierbach	Membrandomänen - Manipulation und Charakterisierung durch akustische Oberflächenwellen (TU Dresden)
Franziska Thoss	Ni-Mn-Ga: Gefügeeinstellung durch Wärmebehandlung (TU Dresden)
Dirk Rittrich	Grenzflächen- und Wachstumsuntersuchungen an dünnen Wolfram- und Wolframnitridschichten auf Silizium mittels winkelaufgelöster Photoelektronenspektroskopie (WHZ Zickau)

Calls and Awards 2008

Calls on Professorships

Dr. Yuanfu Chen	Univ. of Electronic Science and Technology China (UESC)

Awards

Prof. Dr. Jürgen Eckert	Gottfried-Wilhelm-Leibniz-Preis 2009 of the DFG (announced Dec. 2008, awarded March 2009)
Team Megalloys	FutureSax Award
Olga Shuleshova	IMPRESS Prize for Young Researchers
Dr. Anja Wolter	Heinrich-Büssing-Preis 2008
Dr. Alexander Grüneis	Apart-Stipendium der Österreichischen Akademie der Wissenschaften
Kristina Tschulik	Lohrmann-Medaille der TU Dresden
Uwe Neu	Gustav-von-Lauenstein-Erfinderpreis

Publication and Poster Awards

Jong-Woo Kim	Young Scientist Award for the best paper at EMRS 2008
Franziska Schäffel	Best Poster Award at „Trends in Nanotechnology“ in Oviedo
Alexander Grüneis	Best Poster Award at 9th Int. Conf. on the Science and Application of Nanotubes in Montpellier June 29 – July 4, 2008
Jörg Buschbeck	Best Oral Presentation Award JEMS 08 in Dublin
Christine Hamann	Best Oral Presentation Award JEMS 08 in Dublin
Jacub Koza	Best Oral Presentation Award JEMS 08 in Dublin
Vyacheslav Khavrus et al.	Best Poster Award of the 3rd International Symposium on Carbon for Catalysis conference 2008

IFW Awards

Dr. Kathrin Dörr	IFW Research Award 2008
Dr. Jayanta Das	Deutsche Bank Junior Award 2008 for the best PhD thesis
Dr. Rüdiger Klingeler	IFF Research Award 2008
Dr. Wolfgang Häßler	IMW Research Award 2008
Dr. Helmut Ehrenberg	IKM Research Award 2008
Dr. Yongfeng Mei	IIN Research Award 2008

Conferences and colloquia 2008

Conferences

Final European Workshop "Strengthening the role of women scientists in Nano-Science"
March 6-8, 2008 in Dresden, Germany
Chairperson: Dr. Annett Gebert (IFW Dresden)

GLADNET Spring Meeting
April 21–25, 2008 in Dresden, Germany
Chairperson: Dr. Volker Hoffmann (IFW Dresden)

RQ13: 13th International Conference on Rapidly Quenched & Metastable Materials
August 24 - 29, 2008 in Dresden, Germany
Chairmen: Prof. L. Schultz, Prof. J. Eckert (IFW Dresden)

Hand-on-FPLO: DFT meets Experiment & 7th Tutorial Hands-on-FPLO
August 25 - 28, 2008 in Dresden, Germany
Chairmen: Prof. H. Eschrig, Dr. M. Richter (IFW Dresden)

Global Research Laboratory Workshop on Bulk Metallic Glasses
August 30, 2008 in Dresden, Germany
Chairmen: Prof. J. Eckert (IFW Dresden), Do Hyang Kim (Yonsei Univ. Seoul)

21. ICP-MS Anwendertreffen und 8. Symposium über Massenspektrometrische Verfahren der Elementspurenanalyse
September 17 – 19, 2008 in Dresden, Germany
Chairman: Dr. Volker Hoffmann (IFW Dresden)

International Workshop "Physics and Chemistry of FeAs-based Superconductors"
1st German-Russian workshop on Quantum Ground States
October 27 - 29, 2008 in Dresden, Germany
Chairman: Prof. B. Büchner (IFW Dresden)

3rd International Workshop „European Activities in Hydrogen Technology Research"
November 18th, 2008 in Dresden, Germany
Organized by the Helmholtz Initiative FuncHy and IFW Dresden

IFW Colloquia

Prof. Josep Fontcuberta, Institut de Ciència de Materials de Barcelona, Multifunctional oxide heterostructures for spintronics, 10.01.2008

Prof. Dr. Reinhold Kleiner, Univ. Tübingen, Splitting flux quanta in superconductors, 31.01.2008

Prof. Dr. Peter Gumbsch, Fraunhofer IWM Freiburg, A Multiscale Modelling Approach to Structure and Properties of Diamond Like Carbon Coatings, 07.02.2008

Prof. Klaus Capelle, Univ. of Sao Paulo, Crystals made of light, 24.04.2008

Prof. Steven Hayden, Univ. of Bristol, New Structures in the Spin Excitations of LaSrCuO and their possible relationship to High Temperature Superconductivity, 22.05.2008

Prof. Josef Michl, Univ. of Colorado at Boulder, USA, From Molecular Rotors to Molecular Bubbles, 29.05.2008

Prof. Ulrich Gösele, MPI für Mikrostrukturphysik Halle, Reactions at the nanoscale, 09.06.2008

Prof. Manfred Bayer, Univ. Dortmund, All-Optical Control of Electron Spins in Quantum Dot Ensembles, 12.06.2008

Prof. Paul Heitjans, Univ. Hannover, Mobile Lithium Ions in Solids, 26.06.2008

Prof. Cynthia A. Volkert, Univ. Göttingen, Deformation of nanostructured metals: How dislocations behave in small spaces, 03.07.2008

Prof. Markus Winterer, Univ. Duisburg-Essen, Synthesis and Characterization of Complex Nanocrystalline Oxides, 10.07.2008

Prof. Yasutomo J. Uemura, Columbia Univ., Energy-scale Phenomenology and Spin-mediated Pairing for FeAs, CuO, heavy-fermion and other exotic superconductors, 30.10.2008

Prof. Alexander Lichtenstein, Univ. Hamburg, Magnetism of correlated systems, 20.11.2008

Prof. Dr. Claudia Felser, Univ. Mainz, Ferrimagnetic Heusler compounds, 11.12.2008

IFW Winterschool on Magnetism in Oberwiesenthal, January 13-16, 2008

Honorary colloquium on the occasion of the 70th anniversary of Prof. Fink, 29.04.2008

Workshop Magnetic Heat Transport 10.07.2008

Opening of the IFW-Colloquium in the winter terms with talks of the prizewinners of the Research-Awards 2008 of the IFW´s Institutes, Oct. 16, 2008

Heyrovsky-Ilkovic-Nernst-Lecture 2008 of the GDCh 17.10.2008
Prof. RNDr. Jiri Barek, Karlsuniversität Prag: Possibilities and Limitations of Modern Electrochemical Techniques

Seminars of the IFW's Institutes

Joint Seminars

Dr. Isabella Gallino, Univ. des Saarlandes, Kinetics of relaxation and corrosion of bulk metallic glasses, 30.01.2008, IMW-IKM Seminar

Prof. Ralf Busch, Univ. des Saarlandes, Melt rheology of bulk metallic glass forming liquides, 30.01.2008, IMW- IKM Seminar

Dr. Giles Allison and Dr. Oleg Makarovsky, Univ. of Nottingham
Magnetic field studies of the electronic states of diluted semiconductors: GaMnAs and GaAsN, 23.05.2008, IMW-IIN Seminar

IFF Seminars

Prof. Adam Pron, CEA Grenoble, Composites of semiconductor AIIBVI nanocrystals and conjugated polymers via molecular recognition, 04.02.2008

Prof. Bella Lake, HMI Berlin, Neutron scattering studies of spin ladders, 11.02.2008

Prof. Claudia Felser, Univ. Mainz, Heusler Compounds - Multifunctional Materials, 22.02.2008

Dr. Lubomir Pospisil, J. Heyrovsky Institute Prague, Nitrogen fixation mediated by fullerenes, 31.03.2008

Prof. Ladislav Kavan, J. Heyrovsky Institute Prague, Electrochemistry of Ti(IV)-oxides, 14.04.2008

Prof. Markus Braden, Univ.Köln, Charge and spin ordering in layered perovskites, 21.04.2008

Prof. Emil Roduner, Univ. Stuttgart, Anwendungen der ESR-Spektroskopie in der Materialforschung, 28.04.2008

Dr. Norbert Koch, Humboldt-Univ. Berlin,Functional interfaces with conjugated organic materials for electronic devices, 19.05.2008

Dr. Revaz Ramazashvili, Univ. Paris-Sud, Electron magnetism of antiferromagnetic conductors: giant Zeeman electric-dipole spin resonance and more, 02.06.2008

Prof. Sasha Chernyshev, Univ. of California Irvine, Spin-mediated thermal transport in low-dimensional magnets, 03.07.2008

Dr. Paul Goddard, Univ. of Oxford, Isotope shifts and magnetic breakdown: aspects of organic molecular magnets and metals, 07.07.2008

Prof. Masayoshi Tabata, Muroran Institute of Technology, Pi-conjugated helical nano-columnar polyacetylenes as novel color-controllable materials, 15.09.2008

Prof. Karel Stulik, Charles Univ. Prague, Some aspects of the recent progress in electrochemical sensors and detectors, 22.09.2008

Prof. Miroslav Pozek, Univ. of Zagreb, Microwave response of small superconducting samples, 20.10.2008

Prof. David Singh, Oak Ridge National Lab, Electronic Structure of Fe-based Superconductors, 21.10.2008

Dr. Frank Ludwig, TU Braunschweig, Magnetorelaxometry: Fundamentals, Practical Realization and Applications, 17.11.2008

Dr. Sabine Wurmehl, Eindhoven Univ. of Technology, NMR studies of spin polarized Heusler compounds, 24.11.2008

IMW Seminars

Dr. Dietrich Hinz, IFW Dresden, Design von Magnetkreisen, 04.02.2008

Prof. Fernando Audebert, Univ. of Buenos Aires, Icosahedral order at liquid and undercooled liquid in Al based Alloys, 10.03.2008

Prof. Manfred Albrecht, TU Chemnitz, Magnetische Filme auf Partikeloberflächen, 18.04.2008

Prof. Ludwig Gauckler, ETH Zürich, Innovations in Materials Science Based on Colloidal Chemistry, 22.05.2008

Prof. Michael Farle, Univ. Duisburg-Essen, Magnetism and crystalline structure of FePt nanocubes and icosahedra, 05.06.2008

Dr. Nicole Grobert, Univ. Oxford, Carbon nanotubes: Controlling structure property relationships through nitrogen doping? 17.07.2008

Dr. Christian Kisielowski, National Center for Electron Microscopy, Berkeley, The Team 0.5 microscope: Single atom detection across the Periodic Table of Element, 08.09.2008

Dr. Udo Weigelt, Patent- und Rechtanwaltskanzlei München, Wie schützt man geistiges Eigentum, 18.12.2008

IKM Seminars

Dr. Hartmut Wiggers, Univ. Duisburg-Essen, Synthese von Nanopartikeln, 09.01.2008

Kumar Babu Surreddi, IFW Dresden, Consolidation and mechanical properties of high strength Aluminum based alloys, 18.01.2008

Dr. Frank Haaß, BASF Ludwigshafen, Halbleiterentwicklung für thermoelektrische Materialien, 23.01.2008

Dr. Isabella Gallino, Univ. des Saarlandes, Kinetics of relaxation and corrosion of bulk metallic glasses, 30.01.2008

Andreas Nilsson, IFW Dresden, Glass-ceramic route of BSCCO Superconductors – Part II: Crystallization of glassy-precursors, 01.02.2008

Dr. Jürgen Ramm, Balzers AG Lichtenstein, Highly Ionized Pulsed Cathodic Arc Evaporation and the Synthesis of Corundum-type Al-Cr-O Solid Solutions, 15.02.2008

Dr. Marina Galano, Univ. of Oxford, Nanoquasicrystalline Al-Fe-Cr-based Alloys, 10.03.2008

Prof. Dr. Lutz Krüger, TU Bergakademie Freiberg, Werkstoffverhalten von hochfesten Fe-Mn-Al-Si-Leichtbaustählen, 09.04.2008

PD Dr. Astrid Pundt, Univ. Göttingen, Wasserstoff in nanoskaligen Metallen, 21.05.2008

Prof. Zhongyun Fan, Brunel Univ., Melt Conditoning by Advanced Shear Technology (MCAST) for Refining Solidification Microstructures, 04.06.2008

Prof. Dr. Martin Lerch, TU Berlin, Anionensubstitution als Weg zu neuen Materialien, 25.06.2008

Prof. Dr. Jozef Janovec, TU Bratislava, Transport and transformation phenomena in selected metallic systems, 02.07.2008

Prof. Jan Schroers, Yale Univ., New Haven, Processing of bulk metallic glass, 16.07.2008

Dr. M. Elena Arroyo-de Dompablo, Univ. Complutense de Madrid, High-pressure materials for lithium batteries, 01.10.2008

Dr. Sylvio Indris, FZ Karlsruhe, Li Dynamics in Solids: From a Single Crystal to Li Ion Batteries, 26.11.2008

IIN-Seminars

Dr. César Bof Bufon, Towards hybrid rolled-up electronic devices, 24.04.2008

Dr. Yang Yang, MPI Halle, Template-Directed Fabrication of Binary and Ternary Oxide Nanotubes, 08.05.2008

Shadi Yasin, Univ. Stuttgart, Electron spin reesonance on low dimensional organic conductors: Anion order transition in (TMTTF)2 REO4, 29.05.2008

Angelo Malachias, MPI Stuttgart, Nanoscience in the reciprocal space: the use of x-ray techniques to probe structural properties of nanostructures in thin films, 05.06.2008

Dr. Petra S. Dittrich, ISAS, Dortmund, Lab-on-Chip-Technology for Living Cell Analysis, 12.06.2008

Prof. Ulrike Diebold, Tulane Univ. New Orleans, Surfaces of Metal Oxide Materials, 17.06.2008

Dr. Stephan Reizenstein, Univ. Würzburg, Cavity quantum electrodynamics in single quantum dot-micropillar Systems, 26.06.2008

Dr. Stefan Diez , MPI Dresden, Motor Proteins at work: Molecular transport in cell biology and nanotechnology, 03.07.20008

Jianjun Zhang, Univ. Linz, Growth and characterization of ordered SiGe islands on patterned Si (001) substrates, 10.07.2008

Dr. Frank Bertram, Univ. Magdeburg, Kinetics of capture, relaxation and recombination in ZnO, 21.08.2008

Prof. Paul K. Chu, City Univ. of Hong Kong, Plasma-Based Technology in Microelectronics, Nanotechnology and Biomedical Engineering, 03.09.2008

Prof. Francois Peeters, Univ. Antwerpen, Excitons in self-assembled quantum dots and molecules, 15.10.2008

Prof. Vladimir M. Fomin, Univ. Antwerpen, Electronic and Optical Properties of Self-Assembled Seminconductor Quantum Rings, 28.11.08

Dr. Harald Schneider, FZ Dresden-Rossendorf, Ultrafast infrared and THZ spectroscopy of semiconductor quantum structures, 12.12.2008

ITF Seminars

Prof. Dr. Friedhelm Bechstedt, Univ. Jena, Parameterfree calculations of material properties: Fiction or reality? 24.01.2008

Prof. Alexander Moskvin, Ural State Univ. Ekaterinburg, Magnetoelectric coupling and multiferroicity in chain cuprates, 19.02.2008

Prof. Dr. Gotthard Seifert, TU Dresden, Hydrogen in nanostructures - Quantum Liquid DFT simulations, 08.04.2008

Andrei A. Leonov, Donetsk Inst. for Physics and Techn. and Ulrich Rößler, IFW Dresden, Picturing supercooled and glass-forming liquids as Skyrmionic textures of a frustrated continuum, 22.04.2008

Igor Popov, TU Dresden, Mo6S6 nanowire as a unique building block of future nanometer-sized electronic devices, 29.04.2008

Dr. György Vankó, KFKI Budapest, Hard X-ray spectroscopy studies of spin state and intersite mixing in cobalt oxides, 14.07.2008

Dr. Gustav Bihlmayer, FZ Jülich, Spin-orbit induced spin-spirals in low dimensional magnetic systems, 10.06.2008

Prof. Adri Lodder, Univ. of Amsterdam, Electromigration force on a proton with a bound state, 18.09.2008

Dr. Emmanuele Cappelluti, SMC Research Center, Univ. La Sapienza Roma, Spectroscopic signatures of massless gap opening in grapheme, 30.10.2008

Guests and Scholarships

Guest scientists (stay of 4 weeks and more)

Name	Home Institute	Home country
Dr. Umut Adem		Turkey
Prof. Dr. Vladimir Aleshin	Moscow State Univ.	Russia
Prof. Dr. Victor Aristov	Inst. of Solid State Physics Moscow	Russia
Prof. Dr. Ernest Arusanov	Inst. for Appl. Physics Kishinev	Rep. Moldova
Bhanu L. Aryasomayajula	Univ. of Arkansas, Fayetteville, USA	India
Alicja Bachmatiuk	Szczecin Univ. of Technology	Poland
Dr. Ashna Bajpai	Tata Inst. of Fund. Res. Colaba, Mumbai	India
Dr. Larisa Balsanova	Buryat State Univ.	Russia
Simona Bejan	Polytechnic Univ. of Bucharest	Romania
Dr. Natalya Bramnik		Russia
Ganna Butenko	Donetsk Inst. for Physics and Technology	Ukraine
Michal Bystrzejewski	Univ. Warszawa	Poland
Prof. Dr. Chuanbing Cai	Shanghai Univ.	China
Prof. Dr. Mariana Calin	Polytechnic Univ. of Bucharest	Romania
Dr. Igor Chaplygin		Russia
Dr. Yuanfu Chen		China
Sasha Chernyshev	Univ. of California	Russia
Dr. Ihor Chumak	Univ. Lvov	Ukraine
Dr. Roman Cicka	Slovak Univ. of Technology Bratislava	Slovakia
Dr. Jacek Cwik		Poland
Dr. Alexander Darinskiy	Inst. for Crystallography Moscow	Russia
Dr. Jayanta Das		India
Dr. Evgenia Dmitrieva	GmbH "Algorithm" St. Petersburg	Russia
Hryhoriy	Dmytriv Lvov National Univ.	Ukraine
Dr. Otakar Frank	Charles Univ. Prague	Tschechien
Prof. Dr. Ilgiz Garifullin	Zavoisky Physical Technical Inst. Kazan	Russia
Prof. Dr. Alexander Germanenko	Ural State Univ.	Russia
Peter Gogola	Slovak Univ. of Technology Trnava	Slovakia
Dr. Vadim Grinenko	Inst. Supercond. and Solid State Phys. Moscow	Russia
Prof. Dr. Volodymyr Gvozdikov	Kharkov National Univ.	Ukraine
Dr. Silvia Haindl	TU Wien	Austria
Prof. Dr. Bothina A. H. Hamad	Univ. of Jordan	Jordan
Dr. Oleg Heczko	Helsinki Univ. of Technology	Czech Rep.
Dr. Bogdan Idzikowski	Inst. for Molecular Physics Poznan	Poland
Dr. Kazumasa Iida	Univ. of Cambridge, Dept. of Engineering	Japan
Dr. Deepa Kasinathan	MPI CPFS Dresden	India
Dr. Olga Kataeva	Inst. of Organic and Phys. Chem. Kazan	Russia
Dr. Vyacheslav Khavrus	Inst. of Physical Chemistry	Ukraine
Dr. Kyung Tae Kim	Samsung Electronics Co ltd., Yongin-City	Rep. Korea
Dr. Timur Kim		Russia
Dr. Xianghua Kong	Inst. of Chemistry, Chinese Ac. of Sc.	China
Dr. Alexander Kordyuk	Inst. of Metal Physics Kiev	Ukraine
Prof. Yuriy Kucherenko	Inst. of Metal Physics Kiev	Ukraine
Miloslav Kulich	Inst. of Electrical Engineering, Bratislava	Slovakia
Dr. Pramod Kumar	Indian Inst. of Technology Bombay	India
Dr. Roman Kuzian	Inst. for Materials Sc. Kiev	Ukraine
Dr. Min Ha Lee	Iowa State Univ., USA	Rep. Korea
Dr. Isabel Llamas Jansa		Spain
Dr. Yuming Lu	Shanghai Univ.	China
Dr. Vladimir Lukes	Slovak Univ. of Technology Bratislava	Slovakia
Dr. Jiri Malek	Inst. of Physics, Univ. Prague	Czech Rep.

Dr. Daria Mikhailova	TU Darmstadt	Russia
Prof. Noboru Miura	Japan Sc. and Techn. Agency, Tokyo	Japan
Dr. Igor Morozov	Moscow State Univ.	Russia
Prof. Alexander Moskvin	Ural State Univ. Yekaterinburg	Russia
Eduardo Motta	Federal Univ. of Rio de Janeiro	Brasilia
Prof. Dr. Nilay K. Mukhopadhyay	Banaras Hindu Univ. Varanasi	India
Jong H. Na	Yonsei Univ. Seoul	Rep. Korea
Dr. Satoshi Nishimoto		Japan
Anton Nosenko	Taras Shevchenko Univ. Kiev	Ukraine
Dr. Alim Ormeci		Turkey
Dr. Jérome Paillier		France
Dr. Jin Man Park	Yonsei Univ. Seoul	Rep. Korea
Prof. Amalia Patane	Univ. Nottingham, GB	Italia
Prof. Dr. Volodymyr Pavlyuk	Ivan Franko Lvov National Univ.	Ukraine
Benjamin Podmiljsak	Jozef Stefan Inst. Ljubljana	Slovenia
Dr. Kheira L. Rabah	Univ. Reims, France	Algeria
Dr. Ines Rabelo de Moraes		Brasilia
Prof. Peter Rapta	Slovak. Tech. Univ. Bratislava	Slovakia
Dr. Malgorzata A. Samsel-Czekala		Poland
Angelina Sarapulova	Baikal Inst. of Nature Management, Ulan-Ude	Russia
Dr. Ali Sebetci	Cankaya Univ. Ankara	Turkey
Dr. Shivakumara Sekharappa	Indian Inst. of Science, Bangalore	India
Oleg Slukhovskyy	Inst. of Metal Physics Kiev	Ukraine
Dr. Elena Smirnova	A.F. Ioffe Phys. Techn. Inst. St. Petersburg	Russia
Maciej Szorcz	Inst. of Molecular Physics	Poland
Dr. Jan Tarabek	J. Heyrovsky Inst. for Phys. Chem. Prague	Czech Rep.
Andrea Vargova	Slovak Univ. of Technology, Bratislava	Slovakia
Tatyana Vasilchikova	Moscow State Univ.	Russia
Prof. Alexander Vasiliev	Moscow State Univ.	Russia
Dr. Evgeniya Vavilova	Kazan Physical Technical Inst.	Russia
Dr. Olga Volkova	Moscow State Univ.	Russia
Dr. Yingjin Wei	Yonsei Univ. Seoul, Korea	China
Miroslaw Werwinski	IFM PAN, Poznan	Poland
Dr. Xuegeng Yang	Shandong Univ. Jinan	China
Dr. Galina Zakharova	Inst. of Solid State Chemistry Yekaterinburg	Russia
Wenxu Zhang	Univ. of Electronic Sc. and Technology	China
Agnieszka Zlotorowicz	Univ. St. Petersburg	Poland
Prof. Andriy Zvyagin	Inst. for Low Temp. Physics & Eng. Kharkov	Ukraine

Scholarships

Name	Home country	Donor
Alexey Alfonsov	Russia	Int. Max-Planck Research School
Fahad Ali	Pakistan	PIEAS Islamabad
Alphons A. Antonysamy	India	DAAD (IIT-Master-Sandwich-Prog.)
Yulieth Arango	Columbia	EU (AlBan Fellow)
Orkidia Bilani-Zeneli	Albania	Int. Max-Planck Research School
Cristina Bran	Romania	Int. Max-Planck Research School
Prof. Dr. Mihai Branzei	Romania	Univ. Bucharest (EU)
Giuseppe Cirillo	Italia	Univ. Calabria
Mohammed Y. T. El Bahrawy	Egypt	DAAD
Ahmed A. M. Elgendy	Egypt	Egyptian Government
Fedor Fedorov	Russia	DAAD
Ping Feng	China	Alexander von Humboldt Stiftung
Dr. Ahmed Hashem	Egypt	DAAD

Dr. Eslam M. Ibrahim	Egypt	Egyptian Government
Jayaraj Jayamani	India	Alexander von Humboldt Stiftung
Trisha Karan	India	DAAD (IIT-Master-Sandwich-Prog.)
Jong-Woo Kim	Korea	DAAD
Dr. Kyung Tae Kim	Korea	Korea Research Foundation
Dr. Igor Korsakov	Russia	DAAD
Christian Kramberger	Austria	Int. Max-Planck Research School
Ram B. Kumar	India	DAAD (IIT-Master-Sandwich-Prog.)
Marcia C. Kutz	Brazil	CAPES Brazil
Dr. Oksana Kvitnytska	Ukraine	Alexander von Humboldt Stiftung
Yiu Wai Lai	China	Int. Max-Planck Research School
Dr. Guillaume M. Lang	France	Alexander von Humboldt Stiftung
Dr. Hong Seok Lee	Rep. Korea	Korea Research Foundation
Ran Li	China	Alexander von Humboldt Stiftung
Prof. Dr. Gang Liu	China	Alexander von Humboldt Stiftung
Dr. Kalobaran Maiti	India	Alexander von Humboldt Stiftung
Dr. Ferenc Muranyi	Hungary	Alexander von Humboldt Stiftung
Dr. Yuri Naidyuk	Ukraine	Alexander von Humboldt Stiftung
Daniel H. Nogueira Dias	Brazil	DAAD
Dr. Dalibor Paar	Croatia	DFG
Anupama Parameswaran	India	Int. Max-Planck Research School
Martin Philipp	Germany	Sant-Gobain-Recherche France
Andreia I. Popa	Romania	Int. Max-Planck Research School
Dr. Alexey Popov	Romania	Alexander von Humboldt Stiftung
Konda G.s Prashanth	India	DAAD (IIT-Master-Sandwich-Prog.)
Franziska Schäffel	Germany	Cusanuswerk
Marietta Seifert	Germany	Studienstiftung des deutschen Volkes
Dr. Konstantin Skokov	Russia	DAAD
Roland Solc	Slovakia	Alexander von Humboldt Stiftung
Maria Sparing	Germany	Studienstiftung des deutschen Volkes
Kumar B. Surreddi	India	DAAD
Ivan Tarasiuk	Ukraine	DAAD
Grzegorz Urbanik	Poland	Int. Max-Planck Research School
Silvia Vock	Germany	Cusanuswerk
Dr. Gang Wang	China	Alexander von Humboldt Stiftung
Liran Wang	China	Int. Max-Planck Research School
Yiku Xu	China	China Scholarship Council
Lin Zhang	China	China Scholarship Council
Prof. Dr. Zhe-Feng Zhang	China	Alexander von Humboldt Stiftung
Na Zheng	China	China Scholarship Council

Guest stays of IFW members at other institutes

Dr. Kathrin Dörr	Oak Ridge National Laboratory, Tennessee, USA 14 April - 18 May 2008
Dr. Jochen Geck	Univ. of British Columbia, Vancouver, Canada, 01 Jan. – 15 Aug. 2008
Daniel Grimm	Institute of Physics of the Univ. Federal Fluminense Rio de Janeiro, Brazil, 6 weeks
Anja Kießling	Department of Materials Science and Metallurgy, Univ. of Cambridge, 14 Oct. – 8 Dec. 2008
Dr. Michael Kuzmin	Univ. d'Aix-Marseille, 02 -26 May 2008, 13 Sept. – 4 Oct. 2008
Lars Kühn	Univ. Federal do Rio de Janeiro UFRJ, Brazil, 27 Feb. 2008 - 27 April 2008
Darius Pohl	FZ Jülich / ER-C, 1 June – 1 Aug. 2008
Darius Pohl	NCEM, Berkeley, California, 4 Nov. 2008 – 31 Jan 2009
Lorenz Wolfram	Institut Laue-Langevin (ILL) Grenoble, France, 1 month

The Institute by numbers

Personnel

In 2008 the Leibniz Institute for Solid State Material Research Dresden employed 500 staff members in average, including 94 doctarate students, 32 post docs, 29 guest scientists and 20 apprentices. The quote of female staff is 40 %. Furthermore, in 2008 the IFW hosted 53 fellows, that came with their own money to work at the institute. 42 diploma students worked at the IFW and 23 trainees did a practical course at the institute in 2008. The total number of guest scientist, above all was 200.

Financing

Total budget	32,234.6 k€
thereof	
Federal States of Germany	11,720.4 k€
Free State of Saxony	11,720.4 k€
Third party funding spent	8,537.8 k€
Return on infrastructure, interest, royalties	256.0 k€
Third party funding	
by the DFG	2,640 k€
by the EC	2,335 k€
by the Federal States of Germany	2,236 k€
by Free State of Saxony	31 k€
by industry	982 k€
by DAAD	32 k€
by foundations / others	282 k€
Total	8,538 k€

Expenditures

Remuneration costs	18,542.6 k€
Equipment, infrastructure and consumables	8,009.0 k€
Investment	5,683.0 k€
Total	32,234.6 k€

Patents

By 31 Dec. 2008 the institute can boast of total of 117 German and 163 patents registered abroad. In 2008 a total of 18 patent applications were registered.

Board of trustees

Dr. Petra Karl, Saxon Ministry of Science and Art - Head -
Liane Horst, Federal Ministry of Education and Research
Prof. Dr. Konrad Samwer, Univ. Göttingen
Dr. Hans Rainer Hilzinger, Vacuumschmelze GmbH & Co Hanau

Scientific Advisory Board

Prof. Dr. Reiner Kirchheim, Univ. Göttingen, Germany -Head-
Prof. Dr. Gertrud Zwicknagl, TU Braunschweig, Germany
Dr. Hans Deppe, AMD Saxony Ltd & Co. KG Dresden, Germany
Prof. Dr. Dominique Givord, Laboratoire Louis Néel, Grenoble, France
Prof. Dr. Alan Lindsay Greer, Univ. of Cambridge, U.K.
Dr. Giselher Herzer, Vacuumschmelze GmbH & Co Hanau, Germany
Prof. Dr. Max Lagally, Univ. of Wisconsin-Madison, U.S.A.
Prof. Dr. Xavier Obradors Berenguer, Univ. Autònoma de Barcelona, Spain
Prof. Dr. George Sawatzky, Univ. of British Columbia Vancouver, Canada

IFW's Research Program 2009

1. Superconductivity and superconductors
1.1 Electronic structure and fundamentals
1.2 Superconducting materials
1 P1 Superconducting transport systems and bearings
1 P2 YBCO tapes
1 P3 Pact 2009: Nanoscaled inhomogeneities in superconductors
1 P4 New FeAsREO superconductors

2. Magnetism and magnetic materials
2.1 Theoretical and experimental fundamentals
2.2 Magnetic materials
2.3 Magnetic microstructures
2.4 Phase equilibria and single crystal growth
2 P1 High pulsed magnetic fields
2 P2 Magnetic shape memory alloys

3. Molecular nanostructures and molecular solids
3.1 Nanotubes and fullerenes
3.2 Conducting polymers and organic molecular solids
3.3 Molecular Magnets
3 P1 Pact 2007: Manipulation of nanoscaled magnets

4. Metastable alloys
4.1 Solidification and crystallization
4.2 Corrosion and hydrogen
4.3 Materials for sports
4.4 Bulk amorphous metals and composite materials
4.5 Lithium-ion batteries
4 P1 Pact 2008: Cluster materials with competing properties

5. Stress-driven architectures and phenomena
5.1 Heterogeneous multiferroica
5.2 3D micro/nanoarchitectures
5.3 Quantum dots
5.4 SAW systems
5 P1 New multiferroic oxides (continuation of Pact 2006)